

1 **Desorption Lifetimes and Activation Energies Influencing Gas-Surface Interactions and**
2 **Multiphase Chemical Kinetics**

3

4 *Daniel A. Knopf^{1,2,*}, Markus Ammann³, Thomas Berkemeier⁴, Ulrich Pöschl⁴, Manabu Shiraiwa^{5,*}*

5 1. School of Marine and Atmospheric Sciences, Stony Brook University, Stony Brook, New York,
6 USA.

7 2. Department of Chemistry, Stony Brook University, Stony Brook, New York, USA.

8 3. Laboratory of Environmental Chemistry, Paul Scherrer Institute, Villigen, Switzerland

9 4. Multiphase Chemistry Department, Max Planck Institute for Chemistry, Mainz, Germany

10 5. Department of Chemistry, University of California Irvine, California, USA

11 *Correspondence to:* *daniel.knopf@stonybrook.edu; m.shiraiwa@uci.edu

12 **Abstract**

13 Adsorption and desorption of gases on liquid or solid substrates are involved in multiphase
14 processes and heterogeneous chemical reactions. The desorption energy (E_{des}^0), which depends on
15 the intermolecular forces between adsorbate and substrate, determines the residence time of
16 chemical species at interfaces. We show how E_{des}^0 and temperature influence the net uptake or
17 release of gas species, the rates of surface-bulk exchange and surface or bulk reactions, and the
18 equilibration timescales of gas-particle partitioning. Using literature data, we derive a
19 parameterization to estimate E_{des}^0 for a wide range of chemical species based on the molecular
20 mass, polarizability, and oxygen to carbon ratio of the desorbing species independent of substrate-
21 specific properties, which is possible because of the dominant role of the desorbing species'
22 properties. Correlations between E_{des}^0 and the enthalpies of vaporization and solvation are rooted
23 in molecular interactions. The relation between E_{des}^0 and desorption kinetics reflects the key role
24 of interfacial exchange in multiphase processes. For small molecules and semi-volatile organics
25 (VOC, IVOC, SVOC), E_{des}^0 values around 10 - 100 kJ mol⁻¹ correspond to desorption lifetimes
26 around nanoseconds to days at room temperature. Even higher values up to years are obtained at
27 low temperatures and for low volatile organic compounds (LVOC, ELVOC/ULVOC) relevant for
28 secondary organic aerosols (SOA). Implications are discussed for SOA formation, gas-particle
29 partitioning, organic phase changes, and indoor surface chemistry. We expect these insights to
30 advance the mechanistic and kinetic understanding of multiphase processes in atmospheric and
31 environmental physical chemistry, aerosol science, materials science, and chemical engineering.

32

33

34 **1. Introduction**

35 The interaction of gases with condensed phase matter via heterogeneous or multiphase reactions
36 is of importance for a variety of disciplines such as chemical engineering, catalysis, materials
37 science, and environmental and atmospheric chemistry (Cussler, 2009; Chorkendorff and
38 Niemantsverdriet, 2007; Finlayson-Pitts and Pitts, 2000; Ravishankara, 1997; Solomon, 1999;
39 Hoffmann et al., 1995; Beller et al., 2012; Hanefeld and Lefferts, 2018). In the atmosphere, gas-
40 particle interactions and multiphase chemical processes involve gaseous and condensed-phase
41 species manifesting in condensation, gas-particle partitioning, and alteration in the
42 physicochemical properties of aerosol particles and cloud droplets (Pöschl et al., 2007; Kolb et al.,
43 2010; Rudich et al., 2007; George and Abbatt, 2010; Pöschl and Shiraiwa, 2015; Moise et al.,
44 2015; Ammann et al., 2013; Crowley et al., 2013; Kroll et al., 2011; Donahue et al., 2011; Jimenez
45 et al., 2009; Abbatt and Ravishankara, 2023; Ravishankara, 1997; Penkett et al., 1979; Hoffmann
46 and Edwards, 1975; Davidovits et al., 2006). The dramatic effects of multiphase reactions in the
47 atmosphere are most impressively demonstrated by the large-scale stratospheric ozone depletion
48 (ozone hole) over the south pole during Antarctic winter and spring, where inactive gaseous
49 chlorine species are converted to active gas species on cloud particles (Solomon, 1999; Rowland,
50 1991; Peter, 1997; Koop et al., 1997; Muller et al., 1997; Carslaw et al., 1997).

51 Atmospheric aerosol particles and environmental interfaces are often chemically complex
52 systems comprising multiple components in multiple phases. The large compositional variety of
53 airborne particulate matter and gas species including reactive radicals, oxidants, and volatile
54 inorganic and volatile organic compounds (VOCs), in addition to the wide temperature and
55 humidity range present in the atmosphere, poses challenges to resolve multiphase chemical
56 kinetics on a molecular level. The underlying molecular processes are important for the scientific

57 understanding and reliable description of gas uptake and chemical transformation of aerosols
58 (Shiraiwa et al., 2011a; Berkemeier et al., 2013; Zhou et al., 2013; Abbatt et al., 2012; Kolb et al.,
59 2010; Schwartz, 1986; Hanson and Lovejoy, 1995; Hanson et al., 1996; Shen et al., 2022; Willis
60 and Wilson, 2022), the chemical evolution of secondary organic aerosol (SOA) including the
61 partitioning of semivolatile species (Shiraiwa and Seinfeld, 2012; Shiraiwa et al., 2013b; Perraud
62 et al., 2012; Donahue et al., 2011; Ingram et al., 2021), and the impact of multiphase reactions on
63 the particles' activation as cloud condensation nuclei (CCN) or ice-nucleating particles (INPs)
64 (Slade et al., 2015; Slade et al., 2017; Petters et al., 2006; Wang et al., 2012; Wang and Knopf,
65 2011; Knopf et al., 2018; Knopf and Alpert, 2023).

66 Atmospheric multiphase reactions usually involve an adsorbed state of gas species at the surface
67 of a liquid or solid material (Langmuir, 1918, 1916, 1915; Iupac, 1997), which can be regarded as
68 physisorption or chemisorption depending on the nature and intensity of the surface interaction.
69 Physisorption is caused by weak intermolecular interactions (van der Waals, hydrogen bond, ionic
70 and hydrophobic interactions, Table 1) with energies up to $\sim 50 \text{ kJ mol}^{-1}$, whereas chemisorption
71 involves changes of chemical bonds with higher interaction energies (Desjonqueres and Spanjaard,
72 1996; Masel, 1996; Pöschl et al., 2007). The phenomenon of reversible adsorption is easiest to
73 depict on solid surfaces but applies also to liquid surfaces, where it is coupled to the exchange with
74 the bulk liquid (Langmuir, 1918, 1916, 1915; Nathanson, 2004; Ringeisen et al., 2002a, b; Behr et
75 al., 2001; Morris et al., 2000; Masel, 1996; Nathanson et al., 1996; Rettner et al., 1996; Donaldson
76 and Anderson, 1999; Donaldson et al., 1995; Donaldson, 1999; Pöschl et al., 2007).

77 According to the Frenkel equation, the desorption lifetime (τ_{des}) of a surface-adsorbed chemical
78 species (adsorbate) follows an Arrhenius-type behavior (Arrhenius, 1889b; Arrhenius, 1889a;
79 Laidler, 1949; Frenkel, 1924; Laidler et al., 1940):

80
$$\tau_{\text{des}} = \frac{1}{k_{\text{des}}} = \frac{1}{A_{\text{des}}} e^{\left(E_{\text{des}}^0 / (RT) \right)}, \quad (1)$$

81 where k_{des} is a first-order desorption rate coefficient, A_{des} is a pre-exponential factor, in more
82 detail discussed below, R is the gas constant, and T is the temperature. E_{des}^0 is the desorption
83 energy with the energy reference of the gas molecule at rest at $T = 0$ K. E_{des}^0 is referred to as the
84 activation energy of desorption. In terms of the theory of the kinetics of desorption, desorption is
85 always considered an activated process, independent of whether E_{des}^0 corresponds to just the
86 energy difference between gas and adsorbed state or also include an energy barrier on top of that
87 (Knopf and Ammann, 2021). In case of physisorption, E_{des}^0 is equal to the negative value of the
88 enthalpy of adsorption with a correction for the change in degree of freedom between gas and
89 adsorbed phase (see below and Knopf and Ammann, 2021; Kolasinski, 2012). In turn, in the other
90 direction, for the kinetics of the process from the gas phase to the adsorbed state, the adsorption
91 rate normalized to the gas kinetic collision rate is often expressed as the surface accommodation
92 coefficient as discussed below.

93 Atmospheric trace gases and water vapor adopt reversibly adsorbed states on aerosol, cloud, and
94 ground surfaces over a wide range of temperatures from below 200 to above 300 K. The rate of
95 interfacial processes, which may involve reversible, reactive and catalytic steps, generally depends
96 on the concentration of surface-adsorbed reactants and hence on τ_{des} . Especially at low
97 temperatures, high values of τ_{des} can (over)compensate for the low rates of thermally activated
98 chemical reactions and diffusion and thereby enhance the overall gas uptake (Ammann et al., 2013;
99 Crowley et al., 2013; Kolb et al., 2010; Pöschl et al., 2007).

100 Factors influencing gas uptake are competitive co-adsorption of other species (Pöschl et al.,
101 2001; Pöschl et al., 2007; Slade and Knopf, 2014; Kaiser et al., 2011; Springmann et al., 2009;

102 Shiraiwa et al., 2009), solvent dynamics and polarization effects (Ringeisen et al., 2002b; Morris
103 et al., 2000; Klassen et al., 1997; Nathanson et al., 1996; Jungwirth et al., 2006), thermodynamics
104 and kinetics of surface – bulk exchange and bulk diffusivity in viscous liquids (Lakey et al., 2016;
105 Berkemeier et al., 2016; Steimer et al., 2015; Shiraiwa et al., 2014; Shiraiwa et al., 2013a; Houle
106 et al., 2018; Wiegel et al., 2017; Davies and Wilson, 2015; Marshall et al., 2016; Marshall et al.,
107 2018), and phase separations or heterogeneous structures in the condensed phase (You and
108 Bertram, 2015; You et al., 2014; You et al., 2012; Bertram et al., 2011; Huang et al., 2021).

109 Apart from adsorption and desorption, further processes influencing gas-particle interactions and
110 multiphase chemical kinetics include mass transport to the condensed phase by gas-phase diffusion
111 and accommodation at the interface; chemical reactions at the surface following Langmuir-
112 Hinshelwood or Eley-Rideal type mechanisms; dissolution, diffusion, and chemical reactions in
113 the bulk. Together with desorption, these processes may proceed sequentially or in parallel for
114 multiple chemical species, which can be described by appropriate differential equations and
115 numerical models (Shiraiwa et al., 2010; Shiraiwa et al., 2009; Ammann and Pöschl, 2007; Pöschl
116 et al., 2007; Shiraiwa et al., 2012; Wilson et al., 2022).

117 Traditionally, the uptake of trace gases by solid and liquid particles or substrates has often been
118 analyzed by the so-called resistor model, treating each of the above processes in analogy to parallel
119 or serial resistors in an electrical circuit (Schwartz, 1986; Worsnop et al., 2002; Hanson and
120 Lovejoy, 1995; Hanson et al., 1994; Ammann et al., 2013; Crowley et al., 2010). Despite
121 constraints and limitations such as the required approximations regarding steady state and mixing,
122 and a limited capability to describe multicomponent systems, the resistor model has proven to be
123 useful for the investigation and characterization of various processes and substrates, including
124 mineral dust, ice, sulfuric acid, and organic and inorganic particles (Pöschl et al., 2007; Hanson,

125 1997; Davidovits et al., 2006; Crowley et al., 2010; Kolb et al., 2010; Hanson et al., 1994; Ammann
 126 et al., 2013; Ammann et al., 2003; Knopf et al., 2005; Li and Knopf, 2021; Schwartz, 1986). In the
 127 resistor model approach, the uptake of a gas species with reaction at the surface and in the bulk is
 128 described by the following or equivalent equations (Pöschl et al., 2007):

$$129 \quad \frac{1}{\gamma} = \frac{1}{\alpha_s} + \frac{1}{\Gamma_s + \frac{1}{\frac{1}{\Gamma_{sb}} + \frac{1}{\Gamma_b}}} . \quad (2)$$

130 Here, γ is the uptake coefficient, defined as the overall loss rate from the gas phase normalized to
 131 the gas kinetic collision rate, and α_s is the surface accommodation coefficient, which represents
 132 the probability for a gas molecule colliding with the surface to be accommodated at the surface for
 133 period longer than the duration of an elastic scattering process (Pöschl et al., 2007). This parameter
 134 thus represents the adsorption rate normalized to the gas kinetic collision rate. The term Γ_s
 135 represents the normalized loss rate due to surface reaction, Γ_{sb} is the normalized rate of surface to
 136 bulk transfer, and Γ_b is the normalized loss rate in the bulk-phase induced by solubility, diffusion
 137 and reaction (Hanson et al., 1994; Ammann et al., 2013; Crowley et al., 2013; Kolb et al., 2010;
 138 Ammann and Pöschl, 2007; Pöschl et al., 2007; Wilson et al., 2022; Shiraiwa and Pöschl, 2021).
 139 By virtue of the coupled nature of the involved elementary processes, the desorption rate
 140 coefficient can influence the rates of all other surface and bulk processes involving this species,
 141 i.e., k_{des} can influence Γ_s , Γ_{sb} , and Γ_b (Pöschl et al., 2007). For example, the terms Γ_s , Γ_{sb} and Γ_b
 142 governed by the competition between desorption and surface reaction, between desorption and
 143 surface to bulk transfer, or between desorption and surface to bulk transfer coupled to reaction and
 144 diffusion, respectively, are inversely proportional to k_{des} and can be expressed as follows:

$$145 \quad \Gamma_s = \alpha_s \frac{k_s}{k_{des}} , \quad (3)$$

$$146 \quad \Gamma_{sb} = \alpha_s \frac{k_{sb}}{k_{des}} , \quad (4)$$

$$\Gamma_b = \alpha_s \frac{k_{sb} \sqrt{k_b D_b}}{k_{des} k_{bs}} . \quad (5)$$

Here, k_s is a first-order rate coefficient of chemical reaction at the surface; k_{sb} is a first-order rate coefficient for the transfer of molecules from the surface into the bulk (solvation); k_b is a first-order rate coefficient of chemical reaction in the bulk; D_b is the diffusion coefficient of the trace gas in the bulk; k_{bs} is a first-order rate coefficient for the transfer of molecules from the bulk to the surface. Even though the rate coefficients for these elementary processes are independent of k_{des} , the overall normalized rates of Γ_s , Γ_{sb} , and Γ_b are. Similarly, the overall rate of transfer of a gas molecule into the bulk of a liquid or (semi)solid particle (independent of whether diffusion and reaction therein contributes to loss) also depends on k_{des} and can be expressed by the bulk accommodation coefficient, α_b (Pöschl et al., 2007; Edwards et al., 2022):

$$\alpha_b = \alpha_s \frac{k_{sb}}{k_{sb} + k_s + k_{des}} . \quad (6)$$

Hence, the desorption rate coefficient is a critical parameter influencing all processes overall rates involved in the uptake of a gas species by condensed matter (Li and Knopf, 2021).

The role of reversible adsorption and desorption has been addressed in many studies of gas uptake and heterogeneous chemistry in particular for the decoupling of mass transport and chemical reaction (Kolb et al., 1995; Hanson and Ravishankara, 1991; Kolb et al., 2010; Ammann et al., 2013; Crowley et al., 2013; Pöschl and Shiraiwa, 2015; Tabazadeh et al., 1994; Peter, 1997; Carslaw et al., 1997; Hanson et al., 1994; Hanson and Lovejoy, 1995). More recently, kinetic multilayer model analyses of measured uptake coefficients for OH radicals on levoglucosan substrates (Arangio et al., 2015) and the heterogeneous reaction of ozone with shikimic acid (Berkemeier et al., 2016; Steimer et al., 2015) and oleic acid aerosol (Berkemeier et al., 2021) demonstrated the complex dependency of the reactive uptake coefficient on the elementary steps, such as surface accommodation, desorption, surface reaction and bulk diffusion by virtue of Eq.

170 (3-5). The range of experimental conditions was not sufficient to constrain the associated
171 coefficients unambiguously. To determine a best estimate for the surface reaction rate coefficient,
172 it was thus necessary to assume a realistic value for α_s and τ_{des} derived from molecular dynamics
173 simulations (Vieceli et al., 2005; Von Domaros et al., 2020). *Li and Knopf* (2021) made use of the
174 temperature-dependent measurement of OH uptake to decouple τ_{des} from surface reactivity. The
175 intimate coupling of adsorption and desorption with other multiphase processes has also been
176 discussed in the context of many other reaction systems. Ground-breaking work driving much of
177 the developments of the kinetic concepts introduced above was directed at halogen activation on
178 stratospheric aerosol and polar stratospheric clouds (Tabazadeh et al., 1994; Peter, 1997; Carslaw
179 et al., 1997; Hanson et al., 1994; Hanson and Lovejoy, 1995). ~~These~~ Others include the uptake of
180 SO₂ into sulfuric acid (Jayne et al., 1990; Ammann and Pöschl, 2007), adsorption of acetone on
181 ice and HNO₃ on mineral dust (Bartels-Rausch et al., 2005; Vlasenko et al., 2009; Cwiertny et al.,
182 2008; Usher et al., 2003), ozonolysis in liquid, viscous, and solid particles (Knopf et al., 2005;
183 Berkemeier et al., 2016; Steimer et al., 2015; Shiraiwa et al., 2011a; Hearn and Smith, 2007; Pöschl
184 et al., 2001; Shiraiwa et al., 2009; Zhou et al., 2013; Kahan et al., 2006; Kwamena et al., 2004;
185 Mu et al., 2018; Knopf et al., 2011; Willis and Wilson, 2022), and gas-particle partitioning of SOA
186 (Shiraiwa et al., 2013a; Ingram et al., 2021; Schervish and Shiraiwa, 2023). Accordingly, the
187 design and interpretation of heterogeneous and multiphase reaction rate measurements should
188 include a careful assessment whether reversible adsorption is an important or even rate-limiting
189 step, whereby the applicable kinetic regime, may vary with reaction time and conditions
190 (Berkemeier et al., 2013; Berkemeier et al., 2016; Shiraiwa et al., 2014; Ingram et al., 2021; Willis
191 and Wilson, 2022). Hence, desorption lifetimes and related activation energies are important for
192 describing the interaction of gas phase and condensed phase species.

193 To address and elucidate these issues, the remainder of this article is structured as follows: In
194 Section 2, we discuss the molecular interactions underlying adsorption and desorption, and we
195 outline the relevant thermodynamic and kinetic equations and parameters. In Section 3, we compile
196 and present a comprehensive set of desorption energies and thermodynamic parameters for
197 environmentally and atmospherically relevant gas species and substrates. In Section 4, we evaluate
198 the role of the desorption energy in reactive and non-reactive gas uptake by solid and liquid
199 substrates considering characteristic tropospheric temperatures by exploratory kinetic flux model
200 simulations. In Section 5, we develop and present a simplified parameterization for estimating E_{des}^0
201 based on the gas species' polarizability and oxygen to carbon (*O:C*) ratio. Section 6 outlines the
202 role of E_{des}^0 in selected atmospheric implications including the formation and properties of viscous
203 secondary organic aerosol (SOA). We conclude the document with a summary and open questions.

204

205 **2. Thermodynamic Relations**

206 A detailed discussion of the microscopic and thermodynamic treatments of adsorption and
207 desorption and implications for uncertainties in E_{des}^0 is given in *Knopf and Ammann (2021)*. Here
208 we provide the key relationships and concepts needed to follow our assumptions when applying
209 literature obtained E_{des}^0 values for derivation of a parameterization.

210 Typically, the adsorption rate is a measure of the amount of gas molecules that adsorb on the
211 surface as a consequence of gas kinetic collisions. As mentioned above, in the atmospheric
212 sciences this is often expressed with the surface accommodation coefficient α_s (Kolb et al., 2010),
213 operationally defined as the probability that a gas kinetic collision leads to adsorption. The
214 adsorbed molecules may be considered an ideal 2D gas, meaning that the molecules have
215 equilibrated with the surface in terms of the degrees of freedom perpendicular to the surface but

216 may still retain some kinetic energy parallel to the surface. Alternatively, the adsorbed molecules
 217 may be considered an ideal 2D lattice gas, where the degrees of freedom in the horizontal plane
 218 are restricted to vibrations. Also, other models describing intermediate situations have been
 219 suggested (Savara et al., 2009; Campbell et al., 2016; Kisliuk, 1957). Here, we use α_s to describe
 220 the rate of adsorption into either adsorbed state. The term thermal accommodation coefficient, α_t ,
 221 is commonly used for the case where the adsorbed molecule is fully thermally equilibrated with
 222 the substrate, thus close to the case of the ideal 2D lattice gas. Adsorption can be considered a non-
 223 activated process, though in presence of an energy barrier, adsorption has to be treated as an
 224 activated process (Knopf and Ammann, 2021). The corresponding energy barrier directly impacts
 225 α_s (Knopf and Ammann, 2021). In contrast, desorption is always treated as an activated process,
 226 even in the absence of an energy barrier. The explicit treatment of an additional energy barrier
 227 when deriving adsorption and desorption rates is given in *Knopf and Ammann (2021)*. Here we
 228 solely consider E_{des}^0 as reported in the literature, independent of whether an additional activation
 229 barrier was included in the analysis. As discussed below, the choice of adsorbate model and
 230 standard state will impact the value and uncertainties in E_{des}^0 (Knopf and Ammann, 2021; Savara,
 231 2013; Campbell et al., 2016).

232 Adsorption proceeds spontaneously and this implies an exergonic process with the
 233 thermodynamic condition (Bolis, 2013):

$$234 \quad \Delta G_{\text{ads}}^0 = \Delta H_{\text{ads}}^0 - T\Delta S_{\text{ads}}^0 < 0, \quad (6)$$

235 where ΔG_{ads}^0 represents the standard Gibbs free energy change of adsorption, ΔH_{ads}^0 is the
 236 standard enthalpy change of adsorption (in this case negatively defined), ΔS_{ads}^0 is the standard
 237 entropy change of adsorption, and T is temperature. Adsorption of a gas on a substrate results in
 238 an increase of order, thus, $\Delta S_{\text{ads}}^0 < 0$. This is because the degrees of freedom of the adsorbed

239 molecules are more constrained than in the gas phase. Often, the adsorbed molecule may be
240 considered a 2D ideal gas, a 2D ideal lattice gas, or an ideal hindered translator on the surface,
241 with the motion perpendicular to the surface strongly constrained but with varying freedom parallel
242 to the surface (Hill, 1986; Campbell et al., 2016; Savara et al., 2009; Sprowl et al., 2016). Since
243 $\Delta S_{\text{ads}}^0 < 0$, the change in enthalpy ΔH_{ads}^0 has to be negative. The adsorption enthalpy is determined
244 by the binding energy of a gas on the surface, thus on the molecular interactions between gas
245 species and substrates, including hydrogen bonds and van der Waals forces (Poe et al., 1988;
246 Valsaraj and Thibodeaux, 1988; Valsaraj, 1988a, b; Goss and Eisenreich, 1995b; Goss, 1993,
247 1994b; Valsaraj, 1994; Valsaraj et al., 1993). The van der Waals forces comprise London
248 dispersion forces between instantaneously induced dipoles, Debye forces between permanent and
249 induced dipoles, and Keesom forces between permanent dipoles (Iupac, 1997). For organic
250 molecules, the strength of both van der Waals and hydrogen bonds depends on the polarity of
251 functional groups and commonly follows the order (Jeffrey, 1997; Jeffrey and Saenger, 1991;
252 Vinogradov and Linnell, 1971):

253 Amide > Acid > Alcohol > Ketone \approx Aldehyde > Amine > Ester > Ether > Alkane .

254 Table 1 gives an overview of intermolecular forces active among functional groups present in
255 typical gas- and condensed-phase atmospheric species. While all molecules exhibit van der Waals
256 forces, their thermodynamic properties are largely determined by the number and type of hydrogen
257 bonds they can form. The presence of charged groups, e.g., due to a dipole moment, can
258 significantly increase binding energy. The hydrogen bond strength in liquid water is around 10-19
259 kJ mol⁻¹ (Hakem et al., 2007), and with a few exceptions, usually involving fluorine, the energies
260 associated with hydrogen bonding are typically less than 20-25 kJ mol⁻¹ per hydrogen bond
261 (Steiner, 2002; Jeffrey, 1997; Jeffrey and Saenger, 1991; Brini et al., 2017; Iupac, 1997).

262 The complexity of the interaction between adsorbate and substrate can go beyond the 2D ideal
263 gas, 2D ideal lattice gas, and hindered translator model depending on how physisorption and
264 chemisorption are considered. For example, the Kisliuk precursor mechanism allows for more
265 complex configurations of the adsorbate that could include adsorbate-adsorbate interactions
266 (Kisliuk, 1957; Tully, 1994; Campbell et al., 2016; Kisliuk, 1958). Hence, the overall adsorbate-
267 substrate binding energy may involve contributions from adsorbate-surface as well as adsorbate-
268 adsorbate interactions (see e.g. Meyer et al., 2001). Moreover, the binding energy may vary
269 between different types of adsorption sites co-existing on real surfaces, depending on the
270 morphology and chemical heterogeneities of the substrate (Kolasinski, 2012). In view of the
271 complex mixture of substances present in the atmosphere, such effects and variations are not
272 explicitly resolved in this study. Instead, we assume that the energetics of reversible adsorption on
273 atmospheric surfaces can be approximated by effective average values characterizing the binding
274 energy to the substrate. The assumption of reversible adsorption has been crucial in studies of gas
275 uptake and heterogeneous or multiphase chemical reactions when decoupling mass transport and
276 chemical reaction (Kolb et al., 2010; Hanson and Ravishankara, 1991; Ammann et al., 2013;
277 Crowley et al., 2013; Pöschl and Shiraiwa, 2015; Li and Knopf, 2021). The assumption of
278 reversible adsorption directly leads to $\Delta H_{\text{ads}}^0 = -\Delta H_{\text{des}}^0$ and $\Delta S_{\text{ads}}^0 = -\Delta S_{\text{des}}^0$, where ΔH_{des}^0 and
279 ΔS_{des}^0 represent the changes in the desorption enthalpy and entropy, respectively.

280 The free energy change is the driving force for desorption from the thermodynamic point of
281 view. The Frenkel equation, given by Eq. (1), is usually applied to describe the kinetics of
282 desorption. By itself it does not differentiate between physisorption and chemisorption. For the
283 description and understanding of atmospheric heterogeneous and multiphase kinetics, it is useful
284 to treat chemisorption as a chemical reaction following physisorption (Pöschl et al., 2007; Hanson

285 et al., 1994; George and Abbatt, 2010), as expressed in Eqs. (2) to (5). We note that the energy
 286 range of 50 kJ mol⁻¹ mentioned above to distinguish between physisorption and chemisorption is
 287 not necessarily appropriate, if chemisorption is reflecting the fact that chemical bonds are formed
 288 or disrupted. Large molecules may undergo a multitude of van der Waals and hydrogen bonds
 289 adding up to large interaction energies, which would still be considered physisorption. As outlined
 290 above, for these cases we regard the adsorption process to be reversible.

291 *Knopf and Ammann* (2021) have provided the thermodynamic and microscopic equations, the
 292 latter based on conventional transition state (TS) theory, that are implicitly included in the Frenkel
 293 equation, while accounting for the choice of standard states. For example, for the case of a 2D
 294 ideal gas as adsorbate model, the desorption rate expressed in thermodynamic quantities is

$$295 \quad k_{\text{des}} = \kappa \left(\frac{k_{\text{B}}T}{h} \right) \frac{(N_{\text{TS}}/\mathcal{A})^0}{(N_{\text{ads}}/\mathcal{A})^0} e^{-\Delta G_{\text{des}}^0/RT} = \kappa \left(\frac{k_{\text{B}}T}{h} \right) e^{-\Delta G_{\text{des}}^0/RT}, \quad (7)$$

296 where κ is a transmission coefficient giving the probability with which an activated complex
 297 proceeds to desorption (Kolasinski, 2012), k_{B} is the Boltzmann constant, and h is the Planck
 298 constant. Furthermore, we assume the standard concentration of molecules in the TS, $(N_{\text{TS}}/\mathcal{A})^0$,
 299 is equal to the standard concentration of adsorbed molecules, $(N_{\text{ads}}/\mathcal{A})^0$, i.e., $\frac{(N_{\text{TS}}/\mathcal{A})^0}{(N_{\text{ads}}/\mathcal{A})^0} = 1$.

300 In microscopic quantities, k_{des} is derived as

$$301 \quad k_{\text{des}} = \kappa \left(\frac{k_{\text{B}}T}{h} \right) \left(\frac{q_{\text{TS}}^{0'}}{q_{\text{ads}}^0} \right) \frac{(N_{\text{TS}}/\mathcal{A})^0}{(N_{\text{ads}}/\mathcal{A})^0} e^{-\frac{(E_{\text{des}}^0)}{RT}}, \quad (8)$$

302 where $q_{\text{TS}}^{0'}$ and q_{ads}^0 are the standard partition functions for the TS and adsorbate, respectively,
 303 evaluated using standard molar volume and area. Equations (7) and (8) clearly demonstrate the
 304 importance of the choice of standard state when comparing measured k_{des} and evaluated E_{des}^0 .

305 Looking at the equations for k_{des} allows to derive the pre-exponential factor of the Frenkel
 306 equation as (Knopf and Ammann, 2021)

$$A_{\text{des}} = \kappa \left(\frac{k_{\text{B}}T}{h} \right) \left(\frac{q'_{\text{TS}}}{q_{\text{ads}}} \right) = \kappa \left(\frac{k_{\text{B}}T}{h} \right) \frac{(N_{\text{TS}}/\mathcal{A})^0}{(N_{\text{ads}}/\mathcal{A})^0} e^{\Delta S_{\text{des}}^0/R}, \quad (9)$$

where q'_{TS} and $q_{\text{ads},2\text{D}}$ are the partition functions for the TS and adsorbate, respectively. The microscopic interpretation of A_{des} shows that A_{des} depends on temperature and the choice of adsorbate model, expressed as partition functions. The thermodynamic interpretation of A_{des} demonstrates its dependency on standard concentrations and the change in entropy when desorbing from the substrate surface into the activated TS.

We can now interpret A_{des} for the case of a 2D ideal gas adsorbate model. If we assume $\kappa \approx 1$, and adsorbate and TS are 2D ideal gases with similar degrees of freedom (neglecting vibrations), i.e., $\frac{q'_{\text{TS}}}{q_{\text{ads}}} = 1$, then we obtain $A_{\text{des}} \approx \frac{k_{\text{B}}T}{h} = 6 \times 10^{12} \approx 10^{13} \text{ s}^{-1}$ at room temperature (298 K). This is the commonly applied value for the pre-exponential factor. In this case, Eq. (9) demonstrates that the change in ΔS_{des}^0 must be negligible. However, significant deviations from this benchmark factor can occur. For example, if going from the adsorbate state to the activated TS coincides with $\Delta S_{\text{des}}^0 > 0$, and thus $\frac{q'_{\text{TS}}}{q_{\text{ads}}} > 1$, implying more degrees of freedom in the TS, then $A_{\text{des}} > 10^{13} \text{ s}^{-1}$. In contrast, if the TS is more constrained, e.g., only a limited number of molecular orientations are allowed, then $\Delta S_{\text{des}}^0 < 0$, and thus $\frac{q'_{\text{TS}}}{q_{\text{ads}}} < 1$, then $A_{\text{des}} < 10^{13} \text{ s}^{-1}$. A similar analysis has been provided for the 2D ideal lattice gas adsorbate model (Knopf and Ammann, 2021). A_{des} varies between 180 and 300 K for a 2D ideal gas and 2D ideal lattice gas adsorbate model by about a factor of 2 and 3, respectively, indicating minor temperature effects (Knopf and Ammann, 2021). However, A_{des} can differ by about 3 orders of magnitude between the 2D ideal gas and 2D ideal lattice gas adsorbate models.

Experimental studies usually yield pre-exponential factors in the range between 1×10^{11} to $1 \times 10^{12} \text{ s}^{-1}$ for smaller molecules such as methane and $1 \times 10^{13} \text{ s}^{-1}$ for larger alkanes (Fichthorn and

329 Miron, 2002). For large adsorbates, A_{des} can be several orders of magnitude larger (Fichthorn and
330 Miron, 2002). For example, adsorption of benzene and toluene by graphite surfaces exhibit A_{des}
331 of about 10^{15} and 10^{19} s^{-1} , respectively (Ulbricht et al., 2006). In general, the larger the adsorbate
332 molecule, the larger A_{des} (Ulbricht et al., 2006).

333 Nevertheless, for this study and the compilation of literature data of E_{des}^0 , we have assumed a
334 constant pre-exponential factor $A_{\text{des}} = 1 \times 10^{13} \text{ s}^{-1}$, being aware of the underlying assumptions
335 discussed above. We justify this approach by noting that our aim is to derive E_{des}^0 estimates for
336 complex substrate systems, including multicomponent and multiphase aerosol particles, which will
337 impose additional uncertainties in E_{des}^0 . Due to the involvement of entropic contributions to the
338 pre-exponential factor, experimentally derived A_{des} values often contain not well-documented
339 implicit standard state assumptions (related to experimental surface to volume ratios) (Donaldson
340 et al., 2012a; Campbell et al., 2016; Savara, 2013) and thus carry more uncertainty than the E_{des}^0
341 obtained from the slope of temperature dependent data.

342 Figure 1 displays the dependency of τ_{des} on E_{des}^0 and temperature using the Eq. (1). As
343 illustrated in Fig. 1a, the temperature dependency of τ_{des} increases with increasing E_{des}^0 .
344 Calculations have been performed with $A_{\text{des}} = 10^{13} \text{ s}^{-1}$, while the shading represents the
345 application of A_{des} being one order of magnitude greater or smaller, thereby covering the typical
346 temperature dependency of A_{des} . Clearly, temperature can significantly increase the residence time
347 of a molecule on the substrate surface, by several orders of magnitude, thereby, potentially,
348 allowing different reaction pathways. It is also evident that uncertainties in A_{des} directly translate
349 into corresponding uncertainties in τ_{des} . Hence, assuming $A_{\text{des}} = 10^{13} \text{ s}^{-1}$ in the analysis of
350 literature data will yield uncertainties in E_{des}^0 values. For example, one order of magnitude
351 uncertainty in A_{des} , changes E_{des}^0 by $\sim 4\text{-}6 \text{ kJ mol}^{-1}$ over a temperature range of 210 to 300 K.

352 Conversely, an uncertainty of E_{des}^0 by 5 kJ mol^{-1} imposes an uncertainty in τ_{des} of about a factor
353 of ~ 7 - 17 for a similar temperature range. These interdependencies are further outlined in Fig. 1b
354 showing typical τ_{des} for given temperatures and E_{des}^0 , again derived assuming $A_{\text{des}} = 10^{13} \text{ s}^{-1}$.
355 This discussion implies an uncertainty in our E_{des}^0 values of about $\pm 5 \text{ kJ mol}^{-1}$. However, as
356 outlined in detail in *Knopf and Ammann (2021)*, additional uncertainties in E_{des}^0 can arise when
357 the appropriate adsorbate model is not known and if the surface coverage of the adsorbate is
358 uncertain. For example, for a given τ_{des} , E_{des}^0 can differ by 10 - 15 kJ mol^{-1} when assuming either
359 a 2D ideal gas or 2D ideal lattice gas adsorbate model. If a surface is assumed to be pristine but
360 actual coverage is about 20% , E_{des}^0 may be uncertain by 10 - 20 kJ mol^{-1} . In summary, literature
361 E_{des}^0 values applied in this analysis, assuming a conservative estimate, may be uncertain by up to
362 $\sim \pm 15 \text{ kJ mol}^{-1}$.

363 In the formulation of the kinetic and thermodynamic concepts and expressions, we have not
364 made an explicit assumption about the physical state of the condensed phase - solid, liquid,
365 crystalline or amorphous. Lattice gas statistics can be applied generally in different dimensions
366 and has been used for liquids, sorption of ions to proteins or polymer wires (Hill, 1986). In spite
367 of the simplifying assumptions, we use the equations summarized above and derived in more detail
368 in (Knopf and Ammann, 2021) for all substrates, including liquids. This is straightforward for
369 poorly soluble gases. For soluble gases, however, the full thermochemical cycle also involves the
370 dissolved state (Donaldson, 1999). We also note that the system free energy change upon
371 adsorption of a gas on a liquid manifests in a surface tension change, with the Gibbs adsorption
372 isotherm relating the surface tension change to surface excess (Kolasinski, 2012; Donaldson,
373 1999). The manifestation of the change in surface tension convolutes the complex response of
374 structure and dynamics at a liquid interface to an adsorbing molecule (Brini et al., 2017).

375 Depending on the polarity of the adsorbate, the structural features of the interface may then also
376 deviate significantly from that of an adsorbate on a solid surface, as exemplified in recent theory
377 work by Cruzeiro et al. (2022) and Galib and Limmer (2021) for the interaction of N_2O_5 with
378 water.

379 **3. Compilation of Desorption Energies for Solid and Liquid Substrates**

380 To derive a parameterization of E_{des}^0 applicable to typical gas-aerosol particle systems,
381 literature values of E_{des}^0 reflecting typical atmospheric constituents or serving as aerosol surrogates
382 have been compiled. If available, E_{des}^0 reflects values derived from lowest surface coverage,
383 preferentially below one monolayer. Tables A1-A7, A8, and A9-A15 provide thermodynamic and
384 physicochemical literature values for gas-to-solid, gas-to-ice, and gas-to-liquid substrate
385 interactions, respectively. For derivation of E_{des}^0 and τ_{des} values, we use Eq. (1) and assume
386 $A_{des} = 10^{13} \text{ s}^{-1}$, if not otherwise noted. We assume the temperature effect on A_{des} (proportional
387 to T , see Eq. (9)) and changes in the desorption entropy to be negligible compared to the Arrhenius
388 factor (Eq. (8)). The tables include the parameters E_{des}^0 , τ_{des} , and for the gas species the molar
389 mass (M), enthalpy of vaporization (ΔH_{vap}), polarizability (α), dipole moment (μ), $O:C$, and
390 enthalpy of solvation (ΔH_{sol}). Lastly, the dielectric constant or relative permittivity of the substrate
391 (ϵ_r) is given. E_{des}^0 values are obtained from different experimental techniques and theoretical
392 studies described briefly below.

393

394 **3.1 Experimental and theoretical techniques yielding desorption energies**

395 Temperature programmed desorption (TPD), sometimes also termed thermal desorption
396 spectroscopy (TDS), is an experimental technique where the flux of desorbing molecules is
397 observed as the surface temperature is increased. TDS can yield coverages, activation energies,

398 and pre-exponential factors for desorption (Ulbricht et al., 2006). Thermal gravimetry with
399 differential scanning calorimetry (TG-DSC) determines the amount and rate (velocity) of change
400 in the mass of a sample as a function of temperature or time in a controlled atmosphere in addition
401 to thermophysical and thermoplastic properties derived by DSC (Giraudet et al., 2006). In general,
402 if heats of adsorption are measured experimentally by, e.g., calorimetric methods, the accurate
403 thermodynamic definitions have to be applied since heat is not a state function (Bolis, 2013). In
404 Knudsen cells and diffusion tubes coupled to mass spectrometric detection (KN) the rate of
405 molecules desorbing from a substrate can be selectively measured (Caloz et al., 1997; Koch and
406 Rossi, 1998b; Tolbert et al., 1987; Alcalá-Jornod et al., 2000). Scattering experiments of molecular
407 beams (MB) are applied to directly measure desorption from and adsorption of gas species to solid
408 or liquid substrates (Thomson et al., 2011; Morris et al., 2000; Nathanson et al., 1996). While
409 straightforward in use and interpretation for solid surfaces in high vacuum, the developments
410 around using MB techniques for atmospherically relevant volatile liquids is experimentally
411 challenging and also data interpretation with respect to desorption is less straightforward
412 (Nathanson, 2004; Ringeisen et al., 2002b; Morris et al., 2000; Klassen et al., 1997; Nathanson et
413 al., 1996; Gao and Nathanson, 2022), as discussed below. Inverse gas chromatography (IGC)
414 applies the solid of interest as the chromatographic sorbent (stationary phase) and yields sorption
415 coefficients of gas species (Mader et al., 1997). Vacuum microbalance (VM) determines the
416 change in weight due to adsorbed gases (Rouquerol and Davy, 1978; Thomas and Williams, 1965).
417 The desorption rate can be determined by measuring the time evolution of the adsorbed phase by
418 using diffuse reflectance infrared Fourier transform spectroscopy (DRIFT), while the gas phase is
419 monitored by selected-ion flow-tube mass spectrometry (SIFT-MS) and long path transmission
420 Fourier transform infrared spectroscopy (FTIR) (Romanias et al., 2016). Since measurement of the

421 desorption rate requires pressures in the molecular flow regime, this is only straightforward for
422 low vapor pressure materials, such as mineral dust or dry salts. For high vapor pressure materials
423 (aqueous or organic liquids and ice) or materials featuring complex microstructure (mineral dust,
424 soot), complications arise from the convolutions of pore space (Woodill et al., 2013; Keyser et al.,
425 1991), bulk liquid diffusion (Koop et al., 2011b; Pöschl et al., 2007), gas phase diffusion (Knopf
426 et al., 2015; Fuchs and Sutugin, 1971; Fuchs, 1964; Seinfeld and Pandis, 1998; Pöschl et al., 2007)
427 and other coupled processes, making the determination of desorption life time an indirect and often
428 difficult task. Kinetic uptake (KU) experiments operated in the molecular flow regime can yield
429 estimates of species' surface residence times (Alcala-Jornod et al., 2000; Koch and Rossi, 1998a;
430 Koch et al., 1997). KU experiments using laminar flow tube reactors can also yield estimates of
431 the residence time of adsorbed species via determination of the Langmuir equilibrium constant
432 (Pöschl et al., 2001; Von Hessberg et al., 2008; Slade and Knopf, 2013). Vibrational spectroscopy
433 (VS) is used to study the interaction of molecules with, e.g., ice surfaces, by examining the shifted
434 dangling hydrogen bond of ice in presence of an adsorbed molecule (Silva and Devlin, 1994).
435 Surface tension (ST) measurements of adsorbing gases on liquid substrates can yield directly the
436 thermodynamic parameters describing adsorption (Hauxwell and Ottewill, 1968; Donaldson,
437 1999), and the molecular level relationship between surface excess and surface coverage can be
438 assessed by direct spectroscopy (Lee et al., 2016).

439 IGC derives sorption coefficients which can yield estimates of E_{des}^0 via the van't Hoff equation
440 (Goss and Eisenreich, 1996). For experimental TPD and TDS desorption data analysis usually the
441 Redhead equation (Redhead, 1962) is applied that considers the heating rate and gas species
442 surface coverage. k_{des} derived from DRIFT studies yields τ_{des} which allows derivation of E_{des}^0
443 according to Eq. (1), with similar constraints with respect to effusion times from packed powder

444 samples (Woodill et al., 2013; Keyser et al., 1991). MB methods allow to uniquely differentiate
445 thermal desorption of molecules from those undergoing elastic or inelastic scattering, or from those
446 undergoing exchange with the bulk and/or reaction. For solid surfaces the interpretation is
447 straightforward, and corresponding desorption lifetimes can directly be observed. For liquid
448 surfaces, this is less straightforward, since the trajectory of a desorbing molecule may involve
449 diffusion into and out of the near-surface bulk layers (Faust et al., 2013), so that the ‘surface
450 residence time’ is not strictly a true desorption lifetime. Equilibrium measurements of surface
451 tension as a function of partial pressure of the trace gas allows to determine ΔG_{ads}^0 and ΔH_{ads}^0 , if
452 the latter is assumed to be independent of temperature (Donaldson, 1999).

453 The choice of standard states can impact data interpretation. Standard free energies of formation
454 are typically referenced to 1 bar or 1 mol L⁻¹ (at 298 K) (Donaldson et al., 2012a). Commonly it
455 can be assumed that standard enthalpy values are not strongly dependent on the choice of standard
456 state, because the dependence of enthalpy on pressure is weak (Donaldson et al., 2012a). However,
457 the standard entropies of phase transfer will depend on the choice of the standard-state (Donaldson
458 et al., 2012a; Knopf and Ammann, 2021; Campbell et al., 2016; Savara, 2013). Further
459 complications arise when choosing standard states for different adsorbate-surface interactions
460 (Campbell et al., 2016). This can impact standard state surface concentrations, equilibrium
461 constants and rate constants, and renders the adsorbate chemical potential dependent on surface
462 coverage (Campbell et al., 2016; Savara, 2013).

463 Molecular dynamics (MD) simulations can provide estimates of the residence time of gas
464 species at a surface or interface (Vieceli et al., 2005; Von Domaros et al., 2020). MD simulations
465 can yield residence times at the interface or substrate surface and as such an estimate of τ_{des} . Then,
466 for given A_{des} and temperature, E_{des}^0 can be estimated using Eq. (1). Density functional theory

467 (DFT) represents a computational quantum mechanical modelling method to compute the
468 electronic structure of matter (Meng et al., 2004). Monte Carlo (MC) methods based on
469 computational algorithms rely on repeated random sampling to obtain numerical results (Remorov
470 and Bardwell, 2005). Grand canonical Monte Carlo (GCMC) simulations account for density
471 fluctuations at fixed volume and temperature and represents the preferred choice for the
472 investigation of interfacial phenomena (Croteau et al., 2009; Collignon et al., 2005). A theoretical
473 approach to the description of the electronic structure of molecules adsorbed on solid surfaces and
474 surface reactions is the embedded cluster theory (ECT) (Whitten, 1993). This allows ab initio
475 calculations of molecular properties of the lattice-adsorbate system. The dipped adcluster model
476 (DAM) is applied to study chemisorption and surface reactions in which an adcluster (admolecule
477 + cluster) is dipped onto the electron bath of a solid metal (Nakatsuji, 1987). This treatment allows
478 to derive adsorption energies (Hu and Nakatsuji, 1999).

479

480 **3.2 Atmospherically Relevant Gas-Substrate Systems**

481 **Gas Adsorption by Solid Substrates.** Gas adsorption and desorption is important when
482 describing the reactivity between trace gases and solid interfaces in terms of removal rates and
483 gas-particle partitioning (Kolb et al., 2010; Pöschl et al., 2007). It also constitutes a significant
484 removal process of gaseous organic compounds by partitioning between gas and solid phases
485 (Goss and Eisenreich, 1996, 1995a; Goss, 1993). Mineral dust particles are the most abundant
486 aerosol particles globally by mass, providing ample solid surface area for adsorption of gaseous
487 species (Usher et al., 2003; Tang et al., 2016). Atmospheric soot particles also represent a solid
488 surface which allows for multiphase chemistry involving adsorption and reaction of atmospheric
489 oxidants (Pöschl et al., 2001; Shiraiwa et al., 2009; Kaiser et al., 2011; Springmann et al., 2009),

490 though soot can be complex consisting of solid graphite structures coated by organic carbon, the
491 latter being amorphous or soft in nature (Bond et al., 2013; China et al., 2013; Cappa et al., 2012).
492 Also, amorphous solid organic particles (Virtanen et al., 2010; Koop et al., 2011b; Shiraiwa et al.,
493 2017a) provide solid substrates that serve as adsorption and reactive sites for trace gas species
494 (Knopf et al., 2018; Slade et al., 2017; Slade and Knopf, 2014, 2013; Houle et al., 2018; Hearn
495 and Smith, 2007; Lakey et al., 2016; Berkemeier et al., 2016; Steimer et al., 2015; Shiraiwa et al.,
496 2011a; Li and Knopf, 2021; Li et al., 2020).

497 In the atmosphere, adsorbing trace gases including oxidants, radicals, and VOCs compete with
498 adsorbing water for substrate surface sites. A mineral dust surface is usually hydroxylated and
499 covered by a monolayer of water at about 20-30% relative humidity (Usher et al., 2003; Tang et
500 al., 2016; Goss, 1994a). Adsorption of water by mineral dust is also crucial for our understanding
501 of the ability of dust particles to serve as CCN (Tang et al., 2016) and INPs (Kanji et al., 2017;
502 Knopf et al., 2018; Knopf and Koop, 2006; Hoose and Möhler, 2012; Knopf and Alpert, 2023).
503 Since water vapor is abundant in our environment, adsorption of a reactive or non-reactive gas
504 species will likely always proceed in competition with co-adsorbing water molecules (Kaiser et
505 al., 2011; Springmann et al., 2009). Reactive uptake of O₃ and OH radicals by insoluble organic
506 aerosol surfaces has been shown to decrease as humidity increases, following a Langmuir-
507 Hinshelwood mechanism, where water vapor co-adsorbs and competes for surface sites (Pöschl et
508 al., 2001; Slade and Knopf, 2014). Condensation of water may lead to dissolution of soluble gas
509 species and coating material on top of solid substrates, e.g., present as an aqueous organic coating
510 on soot (Charnawskas et al., 2017). Those cases should then be considered as a solid substrate
511 covered by a liquid layer and adsorption or uptake processes should be treated as proceeding on a
512 liquid substrate. Tables A1-A7 present a compilation of E_{des}^0 and other molecular parameters for

513 a selection of atmospherically relevant reactive and non-reactive trace gases interacting with
514 various solid substrates serving as surrogates of aerosol particles.

515

516 **Gas Adsorption by Ice.** Ice is among the most abundant solid materials on the Earth's surface.
517 Roughly 50% of the northern hemisphere landmass is covered by ice and snow in winter (Bartels-
518 Rausch, 2013). Adsorption and desorption of trace gases on ice impact gas-phase chemistry in the
519 stratosphere and upper troposphere (Solomon, 1999; Borrmann et al., 1996; Voigt et al., 2006;
520 Huthwelker et al., 2006), snow chemistry and boundary layer gas-phase chemistry over perennial
521 and permanent snowpacks and gas-phase chemistry above sea-ice (Bartels-Rausch et al., 2014;
522 Artiglia et al., 2017; Raso et al., 2017; George et al., 2015; McNeill et al., 2012; Abbatt et al., 2012;
523 Jeong et al., 2022; Mcnamara et al., 2021). Partitioning of gases to ice in polar and high-alpine
524 snow also result in signals in ice cores used to reconstruct past climates and environmental
525 conditions (Vega et al., 2015). In comparison to other solid materials, ice is a high-temperature
526 material existing in the environment at temperatures relatively close to its melting point. As in
527 other molecular solids this leads to surface premelting and thus a disordered interface, also referred
528 to as quasi-liquid layer, the properties of which are a matter of ongoing debate (Bartels-Rausch et
529 al., 2014; Asakawa et al., 2016; Cho et al., 2002; Slater and Michaelides, 2019). Since this layer
530 is the interface with which adsorbing gases interact, the mutual interplay between the properties
531 of the disordered interface and the nature of the interaction of gases have spurred speculations
532 about whether it should be treated as a thin aqueous solution layer or a purely solid surface. Recent
533 spectroscopic evidence indicates that soluble gases form solvation shells similar as in liquid water
534 without, however, modifying the remaining ice structure significantly (Bartels-Rausch et al.,
535 2017). Thus under typical atmospherically relevant conditions with low coverages of volatile

536 gases, the surface remains dominated by the properties of ice. A template for this may be the case
537 of HCl adsorption on ice (Huthwelker et al., 2006), for which singly hydrogen bonded HCl is
538 adsorbed at the outermost surface (Kong et al., 2017), while upon hydration and dissociation,
539 chloride enters deeper into the interface (Zimmermann et al., 2016; Mcneill et al., 2007; Mcneill
540 et al., 2006). This is in accord with a low desorption energy and thus low coverage with molecular
541 HCl (Table A8). This behavior can mask the weak temperature dependence of the total coverage
542 by HCl (molecular and dissociated). Similar conclusions come from MB experiments, e.g., with
543 NO_y compounds, where the desorption kinetics are characterized directly (Lejonthun et al., 2014).
544 An exception may be the case of H₂O itself, where the MB experiments may not have been able
545 to resolve singly hydrogen bonded H₂O desorbing, but only completely hydrated ones desorbing
546 more slowly (Kong et al., 2014b; Kong et al., 2014a). Therefore, adsorption on ice may well be
547 considered as adsorption within the simplified scheme adopted in this work even for very soluble
548 and more straightforwardly for less soluble molecules. Table A8 summarizes the thermodynamic
549 literature data on gas species adsorption by ice substrates applied in this study.

550

551 **Gas Adsorption by Water and Aqueous Solutions.** Liquid water and aqueous solutions are a
552 dominant form of condensed matter in the environment including aerosol particles, clouds, or
553 ocean surfaces. In aerosol particles, aqueous solutions may range from dilute solutions at very high
554 humidity and at or close to the point of activation into a cloud droplet to very concentrated
555 supersaturated solutions at low relative humidity. High solute strength solutions may yield highly
556 viscous, semi-solid and glassy particle phase states occurring throughout the atmosphere (Shiraiwa
557 et al., 2017a; Koop et al., 2011b; Mikhailov et al., 2009; Zobrist et al., 2008; Klassen et al., 1998).
558 Decreasing bulk diffusivity in these viscous phases increases the relative importance of the

559 desorption lifetime as exchange with the bulk is retarded (Behr et al., 2009; Knox and Phillips,
560 1998; Li and Knopf, 2021) (see Eq. (4)).

561 The notion that adsorbed molecules on liquid surfaces represent a distinct feature comes from
562 both spectroscopic and kinetic evidence. MB experiments of HCl on deuterated sulfuric acid
563 clearly identified collision-, adsorption-, and desorption trajectories (Behr et al., 2001; Morris et
564 al., 2000; Gao and Nathanson, 2022), as a direct and unique manifestation of Langmuir's view of
565 adsorption (Langmuir, 1918). The time the HCl molecule spends on the surface is directly related
566 to E_{des}^0 and A_{des} . In other cases studied by the MB technique, the picosecond scale hydrogen bond
567 exchange dynamics and fast diffusion (nanoseconds – microseconds for diffusion into and out of
568 depths of several nanometers) prevented unambiguous separation of pure desorption from
569 trajectories including entry into the liquid (Ringeisen et al., 2002a, b; Brastad et al., 2009; Faust
570 and Nathanson, 2016; Faust et al., 2016; Faust et al., 2013). A comparable situation as for HCl has
571 been documented through the MB technique for N_2O_5 (Shaloski et al., 2017). Later high-level
572 theory work established the interaction of this important trace gas with the hydrogen bonding
573 network of water that then subsequently controls hydrolysis (Cruzeiro et al., 2022; Galib and
574 Limmer, 2021). Similar conclusions about adsorption – desorption trajectories in the case of
575 $\text{H}_2\text{O}(\text{g})$ on liquid water may be drawn from different isotope exchange kinetics for HDO with H_2O
576 and H_2^{18}O with H_2O that require different degrees of hydration on the water surface (Davidovits
577 et al., 2011, 2006). The suggestion that a distinct population of H_2O molecules exists that is singly
578 hydrogen bonded at the liquid water surface comes from detailed interpretation of IR spectra in
579 line with theory (Devlin et al., 2000). The high vapor pressure of environmentally relevant liquids
580 and other difficulties (including those related to fast exchange with the bulk liquid) prevent direct
581 determination of desorption kinetics for many relevant trace gas – substrate pairs. In spite of this

582 situation, we suggest to apply the same concept of converting desorption energies (derived from
583 partitioning or chromatographic methods) into desorption lifetimes as for solid surfaces.

584 The fact that molecules at the aqueous solution or liquid water – air interface experience a
585 different environment than in the bulk liquid is straightforward. The density drops over molecular
586 length scales and the hydrogen bond dynamics and orientation in water and aqueous solutions on
587 average lead to a strongly asymmetric environment at the interface (Brini et al., 2017; Ahmed et
588 al., 2021; Hao et al., 2022). The extension of the interface depends on the type of solutes and
589 adsorbates present, as molecules with larger hydrophobic moieties or when charges are present at
590 the adsorbate interacting with solute ions, which may establish a larger interfacial thickness (Brini
591 et al., 2017; Zhao et al., 2020). The asymmetric environment at the interface leads to specific
592 molecular interaction options (as described above) and in turn to specific binding energies as result
593 of these. Changes to the equilibrium surface tension of aqueous solutions in response to adsorption
594 of gases is the consequence of the changes in the surface free energy. Its temperature dependence
595 is reflecting the energy gain as a result of the sum of these interactions. Tables A9 to A15 are a
596 compilation of E_{des}^0 for a range of inorganic and organic trace gases on pure water or on aqueous
597 solutions. The simplest case $\text{H}_2\text{O}(\text{g})$ on $\text{H}_2\text{O}(\text{l})$, exhibits a single hydrogen bond and a
598 corresponding low E_{des}^0 value. Among the given families of species, interaction energies scale with
599 molar mass or the degree of substitution with functional groups that alter the amount of weak or
600 strong molecular interactions. The degree of substitution may be represented by the dipole moment
601 (μ) and $O:C$ for organic molecules as outlined in the discussion of parameterized E_{des}^0 . The
602 presence of hydrophilic functional groups with strong hydrogen bonding interaction options leads
603 to correspondingly larger E_{des}^0 . Since these groups also interact with the hydrogen bonding

604 network of water, these interactions are sensitive to the presence of other solutes or, especially,
 605 ions (Demou and Donaldson, 2002; Lee et al., 2019; Ohrwall et al., 2015; Ekholm et al., 2018).

606

607 **4. Impact of Desorption Lifetime on Gas Uptake**

608 To assess the impact of τ_{des} on multiphase chemical kinetics, the kinetic multi-layer models of
 609 aerosol surface and bulk chemistry (K2-SURF, KM-SUB) are applied (Shiraiwa et al., 2010;
 610 Shiraiwa et al., 2009). These models are based on the PRA framework (Ammann and Pöschl, 2007;
 611 Pöschl et al., 2007) and describe the gas-particle interface by implementation of several model
 612 compartments and molecular layers in which species can undergo mass transport and chemical
 613 reactions. Here, the compartments included are: gas phase, near-surface gas phase, sorption layer,
 614 quasi-static surface layer, and a number of bulk layers.

615 Gas-phase diffusion of a species X from the gas phase to the near-surface gas-phase surrounding
 616 the particle is treated by the net flux of gas-phase diffusion:

$$617 \quad J_{\text{g,X}} = 2\pi(d_p + 2\lambda D_g)([X]_{\text{g}} - [X]_{\text{gs}}), \quad (10)$$

618 where d_p is the particle diameter, λ is the mean free path, D_g is the gas diffusivity and $[X]_{\text{g}}$ and
 619 $[X]_{\text{gs}}$ are concentrations of X in the gas and near-surface gas phases, respectively (Pöschl et al.,
 620 2007; Knopf et al., 2015; Li et al., 2018). The mass balance and rate equation for X in the near-
 621 surface gas phase can be described as:

$$622 \quad \frac{d[X]_{\text{gs}}}{dt} = \frac{J_{\text{g,X}} - (J_{\text{ads,X}} - J_{\text{des,X}})A_s}{V_{\text{gs}}}, \quad (11)$$

623 where A_s is the particle surface area and V_{gs} is the volume of the near-surface gas phase. $J_{\text{des,X}}$ is
 624 the desorption flux defined as $J_{\text{des,X}} = k_{\text{des,X}}[X]_{\text{s}} = \tau_{\text{des,X}}^{-1}[X]_{\text{s}}$. $J_{\text{ads,X}}$ is the adsorption flux defined

625 as $J_{\text{ads},X} = \alpha_{s,X} J_{\text{coll},X}$, where $\alpha_{s,X}$ represents the surface accommodation coefficient, and the
 626 collision flux is defined as $J_{\text{coll},X} = \frac{1}{4} \omega_X [X]_{\text{gs}}$ with ω_X being the mean thermal velocity of X.

627 The surface-layer reaction (SLR), involving only the adsorbed species, X(s), or components of
 628 the quasi-static layer, Y(ss), such as $X(s) + Y(ss) \rightarrow \text{products}$, is described by the second-order
 629 rate coefficient k_{SLR} . The surface reaction rate is described as $L_s = k_{\text{SLR}} [X]_s [Y]_{\text{ss}}$. The mass
 630 balance and rate equations for X in the near-surface gas phase and at the surface can be described
 631 as below:

$$632 \frac{d[X]_s}{dt} = J_{\text{ads},X} - J_{\text{des},X} - L_s - J_{s,b,X} + J_{b,s,X}, \quad (12)$$

633 where $J_{s,b,X}$ and $J_{b,s,X}$ are the fluxes from the surface to the near-surface bulk and from the near-
 634 surface bulk to the surface of X, respectively ($J_{s,b,X} = J_{b,s,X} = 0$ in the absence of bulk diffusion),
 635 and treated as a function of the bulk diffusion coefficient. The reactive uptake coefficient, γ , is
 636 usually the experimentally accessible parameter and the one used in atmospheric modeling studies.
 637 γ of a gas species X is defined as

$$638 \gamma_X = \frac{J_{\text{ads},X} - J_{\text{des},X}}{J_{\text{coll},X}}. \quad (13)$$

639
 640 **Simulation of reactive gas uptake by solid substrates.** We apply the kinetic double-layer model
 641 of aerosol surface chemistry (K2-SURF; (Shiraiwa et al., 2009)) to investigate the sensitivity of γ
 642 to the desorption lifetime for a solid substrate. The surface reaction of an adsorbed species X with
 643 condensed species Y is considered, while surface-bulk exchange and bulk diffusion and reaction
 644 are not considered for simplicity. The α_s on an adsorbate-free substrate is assumed to be one for
 645 all simulations. Figure 2 shows the dependence of γ on τ_{des} and k_{SLR} at constant temperature. γ
 646 values represent steady-state values. Higher k_{SLR} leads to higher γ at fixed τ_{des} due to faster

647 surface reaction rates. At fixed k_{SLR} , longer τ_{des} leads to higher surface concentrations of X, and
648 consequently to higher surface reaction rates and γ . In turn, with sufficiently long residence times
649 of the adsorbed gas species, low k_{SLR} can still lead to high values of γ . It is evident that different
650 pairs of τ_{des} and k_{SLR} can yield the same γ value. Furthermore, when k_{SLR} is known, uncertainties
651 in τ_{des} can result in large differences in γ . This exercise demonstrates that experimentally derived
652 γ values do not sufficiently constrain the heterogeneous reaction process to yield unambiguous
653 τ_{des} and k_{SLR} values, unless a significant parameter space is covered by the experiment to constrain
654 them individually. For instance, at large enough gas phase partial pressure the surface gets
655 saturated (fully covered by the adsorbate), which leads to decoupling of τ_{des} and k_{SLR} (Knopf et
656 al., 2011; Artiglia et al., 2017; Berkemeier et al., 2016; Steimer et al., 2015). However, this is often
657 not possible due to technical constraints. Therefore, constraining τ_{des} by application of E_{des}^0 , or
658 best estimates of E_{des}^0 , can significantly improve our molecular understanding of the underlying
659 processes in multiphase chemical kinetics and support the development of parameterizations for
660 modelling purposes.

661 Figure 3 displays the temperature dependence of γ with E_{des}^0 of 30 – 50 kJ mol⁻¹. The pre-
662 exponential frequency factor A_{des} was set to 10¹³ s⁻¹ and k_{SLR} was set to (a) 10⁻¹² and (b) 10⁻⁹ cm²
663 s⁻¹. Temperature dependence of k_{SLR} was not considered in these simulations to evaluate only the
664 effects of temperature-dependent τ_{des} on γ . The modeling results suggest that γ depends strongly
665 on temperature, where lower temperatures yield higher γ values. This is because lower
666 temperatures lead to longer τ_{des} and hence higher surface concentrations of X and reaction rates.
667 Generally, γ is more temperature-dependent at higher values of E_{des}^0 . However, if E_{des}^0 is close to
668 values typical for chemisorption (~50 kJ mol⁻¹), γ is close to 1 in this calculation. Further away
669 from this special case and natural cap of $\gamma = 1$, γ increases by about two orders of magnitude over

670 a temperature range of 80 K. These modeling results indicate that extrapolating multiphase
671 chemical kinetics acquired at room temperature to lower temperatures, can result in significantly
672 different reactive uptake coefficients. Clearly, a detailed understanding of the molecular processes
673 is necessary when applying multiphase reaction kinetics to environmental and atmospheric
674 conditions.

675 Even though the above simulations clearly suggest potentially large effects of the temperature
676 dependence of τ_{des} on γ , surface reaction rate coefficients are also temperature dependent which
677 in turn affect γ as well (Li and Knopf, 2021; Li et al., 2020). To further investigate the role of
678 temperature on heterogeneous reaction kinetics, we apply the K2-SURF model to heterogeneous
679 reactions between O_3 and polycyclic aromatic hydrocarbons (PAHs) adsorbed on soot. This
680 reaction proceeds with a multi-step Langmuir-Hinshelwood mechanism that includes I) O_3
681 physisorption, II) decomposition of O_3 into long-lived reactive oxygen intermediates (ROIs, O
682 atoms), and III) reactions of O atoms with PAHs (Shiraiwa et al., 2011b):



686 The activation energy for physisorbed O_3 to dissociated into chemisorbed O ($E_{\text{a,pc}}$) is $\sim 40 \text{ kJ mol}^{-1}$
687 and the activation energy for O reacting to oxidation products (E_{ox}) is $\sim 80 \text{ kJ mol}^{-1}$ (Berkemeier
688 et al., 2016; Shiraiwa et al., 2011b). Temperature dependence of the reaction rate coefficients of
689 reactions II and III are considered using an Arrhenius equation. We examine the response of this
690 reaction system to changes in initial E_{des}^0 of O_3 (reaction I) and temperature.

691 Figure 4 shows the results of such simulations. Higher E_{des}^0 yields higher surface concentrations
692 of physisorbed O_3 , and hence higher concentrations of O and reaction rates, yielding higher γ

693 values. γ decreases as temperature decreases, which is in contrast to above sensitivity studies
694 shown in Fig. 3. This is because the overall temperature dependency of the gas uptake is mostly
695 determined by the temperature dependency of the rate-limiting reaction III and also influenced by
696 thermally-activated chemical reaction II. Although physisorbed O_3 molecules can reside
697 significantly longer on the PAH surface at lower temperatures, the decrease in the formation rate
698 of ROIs and subsequent oxidation reaction rate govern γ , suggesting lower γ values at lower
699 temperatures.

700 Clearly, E_{des}^0 and activation energies for chemical reactions are crucial parameters to predict
701 multiphase chemical kinetic processes under tropospheric conditions. Conducting temperature-
702 dependent reactive uptake experiments of known reaction systems can be used to determine
703 coupled desorption lifetimes and reaction rates (e.g., Kerbrat et al., 2010; Li and Knopf, 2021).
704 For example, *Li and Knopf* (2021) measured the reactive uptake of OH radicals by triacontane for
705 temperatures between 213 and 293 K. By having a temperature-dependent multiphase kinetics data
706 set, E_{des}^0 and k_{SLR} could be decoupled and individually assessed.

707
708 **Non-reactive gas uptake into liquids.** To demonstrate the effect of τ_{des} on the equilibration
709 timescale of non-reactive gas uptake by a liquid substrate, the kinetic multi-layer model for aerosol
710 surface and bulk chemistry (KM-SUB) (Shiraiwa et al., 2010) was applied (Fig. 5). We simulate
711 non-reactive uptake of species X with a constant gas-phase concentration of 1 ppb into a particle
712 with 100 nm diameter that initially contains no amount of X. The Henry's law constant of X was
713 set to be $1 \times 10^{-5} \text{ mol cm}^{-3} \text{ atm}^{-1}$ at 298 K and its temperature dependence was considered using the
714 van't Hoff equation with a solvation enthalpy of 20 kJ mol^{-1} ; these values are chosen to be
715 comparable with ozone solvation into water (Sander, 2015, 2023). The temperature dependence of

716 the Henry's law constant is shown in Fig. S1. The particle is assumed to be liquid with a
717 temperature-dependent bulk diffusion coefficient following the parameterization of Zobrist *et al.*
718 (2011) for pure water, which varies from $2 \times 10^{-5} - 2 \times 10^{-6} \text{ cm}^2 \text{ s}^{-1}$ in this temperature range. E_{des}^0
719 values in the range of $10 - 80 \text{ kJ mol}^{-1}$ were used, and the temperature dependence of τ_{des} was
720 considered using the Frenkel equation (see Eq. (1) and Fig. 1). Here, X can be regarded as a small
721 molecule with moderate water solubility such as ozone for the simulations at low E_{des}^0 , or a
722 carboxylic acid with similar water solubility (e.g., nonanoic acid) for the simulations at high E_{des}^0 .
723 The equilibration time is defined as the time after which the surface and particle bulk
724 concentrations deviate by less than a factor of 1/e from their equilibrium or steady-state value.

725 The simulations show that equilibration times can vary over many orders of magnitude in the
726 investigated range of E_{des}^0 (Fig. 5). For $E_{\text{des}}^0 < 30 \text{ kJ mol}^{-1}$, the timescales of surface equilibration
727 (black solid lines) are shorter than the timescale of bulk equilibration (blue dashed lines). The
728 convergence of the blue lines at low E_{des}^0 ($< 30 \text{ kJ mol}^{-1}$) reflects the kinetic limitation of gas-
729 particle equilibration by diffusion inside the particle bulk ($2 \times 10^{-7} \text{ s}^{-1}$; (Shiraiwa *et al.*, 2011a)). At
730 higher E_{des}^0 , the increase of desorption lifetime leads to the increase of the equilibration times, as
731 a larger amount of X is needed to saturate the surface; in fact, at $E_{\text{des}}^0 \geq 15 \text{ kJ mol}^{-1}$, the majority
732 of molecules reside on the surface and the partitioning is governed by the surface processes in this
733 simulation.

734 In the range of E_{des}^0 around 40 to 60 kJ mol^{-1} , surface and bulk equilibration times coincide, as
735 the simulated 100 nm particles are well-mixed and non-reactive uptake is limited by interfacial
736 transport from the gas phase. The flattening and convergence of the black lines at $E_{\text{des}}^0 > 60 \text{ kJ}$
737 mol^{-1} reflects the kinetic limitation of gas-particle equilibration by interfacial transport (surface
738 adsorption and surface-bulk exchange) if the surface gets fully covered by the adsorbate. The bulk

739 equilibration (blue lines) and thus also the overall gas-particle equilibration time still increase for
740 $E_{\text{des}}^0 > 60 \text{ kJ mol}^{-1}$ with decreasing temperature, because interfacial transport is slowed by the high
741 surface propensity of X and its full surface coverage. Note that the slowing of bulk equilibration
742 time as a consequence of sorption layer coverage is a direct consequence of using a Langmuir
743 adsorption model. In case of multilayer adsorption and bulk condensation, especially at high E_{des}^0 ,
744 results may differ, which will be explored in follow-up studies (see also Sect. “Gas-particle
745 Partitioning of Secondary Organic Aerosol”). Also note that the increased surface propensity of X
746 with increasing E_{des}^0 is not a general rule, but a consequence of the fixed Henry’s law solubility
747 coefficient in this sensitivity study.

748 The calculations for Fig. 5 represent an open system in which the gas-phase concentration of X
749 is held constant. *Wilson et al. (2021)* investigated equilibration timescales for gas uptake of PAHs
750 on soot surfaces in the closed system, i.e., where a fixed amount of X is distributed between the
751 gas and particulate phases. In that study, equilibration timescales were either controlled by the
752 adsorption or by the desorption process, depending on whether the particle surface was under- or
753 oversaturated with X at the start of the model simulations, respectively. Temperature strongly
754 influenced equilibration timescales in the desorption-controlled regime, whereas particle number
755 concentrations influenced adsorption-controlled systems. Note that in the presence of chemical
756 reactions in the gas phase or on the surface, the partitioning equilibrium can be perturbed and adopt
757 a quasi-stationary state that differs from thermodynamic equilibrium.

758 For reactions occurring in liquids, the same features apply as for the case of surface reactions on
759 solids, i.e., the temperature dependence of an activated reaction may counteract the temperature
760 dependencies of desorption and solubility, e.g., for the reactions on sulfuric acid aerosol of HCl
761 with HONO (Longfellow et al., 1998; Ammann et al., 2013) or with ClONO₂ (Shi et al., 2001).

762 These cold and viscous sulfuric acid aerosols, but also viscous aqueous organic aerosols are also
763 at the same time high solute strength systems. The situation then is very complex since viscosity
764 is modulated by temperature and humidity, thereby impacting diffusion and salting out effects, and
765 thus, ultimately, solubility and kinetics (Edebeli et al., 2019; Li and Knopf, 2021; Li and Shiraiwa,
766 2019).

767

768 **5. Derivation of a Parameterization of the Desorption Energy**

769 Thermodynamic and chemical parameters given in Tables A1-A15 provide the basis to derive
770 E_{des}^0 estimates for application in multiphase chemical kinetics involving atmospheric gas species
771 and aerosol particles. This analysis includes over 500 gas species-substrate systems. As discussed
772 above, we note the underlying caveats in this analysis. The pre-exponential factor is set to 10^{13} s^{-1} .
773 ¹. The dependence of E_{des}^0 on adsorbate model and surface coverage is neglected. Thus, a highly
774 accurate prediction of E_{des}^0 is not possible. However, the goal here is to provide a best estimate of
775 E_{des}^0 in agreement with this training data set (Tables A1-A15) to enable improved analyses of
776 environmental multiphase chemical kinetics under the wide range of thermodynamic conditions
777 encountered in the Earth's environment. Furthermore, it would be desirable to predict E_{des}^0 from
778 commonly measured and accessible parameters, e.g., derived by mass spectroscopy, such as molar
779 mass, molecular structure, and oxidation state.

780 Following our previous discussion on the intermolecular bonding between adsorbate and
781 substrate, gas species polarizability, α , should serve as predictor of E_{des}^0 . Larger α should, in
782 general, coincide with an increase in E_{des}^0 . The oxidation state of an organic gas species,
783 represented in a simplified way by the ratio $O:C$, reflects the number of oxygenated functional
784 groups, typically monitored by mass spectrometry (Isaacman-Vanwertz et al., 2018). An increase

785 in the gas species' oxidation state should also yield an increase in E_{des}^0 . Figure 6 displays a
 786 multilinear regression analysis using all available data including solid, ice, and liquid substrates
 787 (Tables A1-A15) to derive a relationship between E_{des}^0 , α , and $O:C$. Figure S2 depicts the same
 788 data in more detail as two separate plots. Figure 6 indicates that E_{des}^0 increases with increasing α
 789 and $O:C$, as one would expect from considerations of intermolecular bonding discussed above.
 790 This is also corroborated by a principal component analysis given in Fig. S3, showing significant
 791 correlation between E_{des}^0 and α . The regression analysis yields the following model (with an $R^2 =$
 792 0.559 and a root mean squared error (RMSE) = 25.4):

$$793 \quad E_{\text{des}}^0(\alpha, O:C) = 25.895 + 2.330\alpha + 12.367(O:C) , \quad (14)$$

794 where E_{des}^0 is in units kJ mol^{-1} and α is in units 10^{-24} cm^3 .

795 Figure 7 shows α as a function of molar mass and $O:C \leq 1$. Note that the few data for the three
 796 gas species with $O:C \geq 1$, namely CO_2 (Table A3), formic acid (Table A7), and, peroxyacetyl
 797 nitrate, PAN (Table A8) are colored as $O:C = 1$ for better visibility of the overall training set.
 798 Figure 6 shows the few data points for $O:C > 1$. The data show a strong linear correlation between
 799 α and M , where $O:C$ appears to play a less significant role. This can be understood by realizing
 800 that a carbon atom in a molecule contributes three times more to α than an oxygen atom (Bosque
 801 and Sales, 2002), discussed in more detail below. Hence, the number of methylene groups can
 802 dominate α for larger molecules. Thus, the polarizability can be described, applying regression
 803 analysis, as a linear function of molar mass ($R^2 = 0.952$ and RMSE = 2.765):

$$804 \quad \alpha(M) = -0.837 + 0.128M , \quad (15)$$

805 where M is in units g mol^{-1} . The linear regression is shown as a red line in Fig. 7.

806 We can now combine Eqs. (14) and (15) to obtain a parameterization to calculate E_{des}^0 from
 807 knowledge of the gas species' molar mass and $O:C$:

$$E_{\text{des}}^0(M, O:C) = 25.895 + 2.330(-0.837 + 0.128M) + 12.367(O:C) . \quad (16)$$

Figure 8 shows E_{des}^0 values derived from Eq. (16) using M and $O:C$ values given by the training datasets as input. Similarly to Fig. 7, we have color-coded $O:C$ for values up to one for better data visibility. Figure S4 shows E_{des}^0 values derived from the training data set separated by different substrate types corroborating the correlation displayed in Fig. 8. Figure S5 shows E_{des}^0 values derived from Eq. (16) using arbitrary M and $O:C$ values. For application of inorganic gas species with $C = 0$, $O:C$ should be set to zero. E_{des}^0 shows a linear relationship with M where deviation from linearity is only found at $M < 250 \text{ g mol}^{-1}$. Figure 8B demonstrates that gas species with larger $O:C$ show larger E_{des}^0 . To understand this trend in the data, we have to address the role of the gas species' dipole moment and substrate in the derivation of the E_{des}^0 values. Equation (16) provides estimates of E_{des}^0 without specifically addressing substrate properties. As discussed, its dependency solely on M and $O:C$ is advantageous for application to complex gas species-particle composition data. Considering the underlying uncertainties due to unknown applied standard states, absorbate model, and assumed pre-factor, this parameterization is accurate within those limits. However, one would expect that gas species' μ and the substrate's ϵ_r impact E_{des}^0 .

We recommend application of this parameterization (Eq. (16)) for gas species with $O:C \lesssim 1$. Due to the few data points at $O:C \gtrsim 1$, E_{des}^0 could be significantly under- or overestimated in this range. For example, for CO_2 (Table A3), tabulated $E_{\text{des}}^0 = 16.4 \text{ kJ mol}^{-1}$, while the parameterization yields 61.8 kJ mol^{-1} . In the case of formic acid (Table A7), the tabulated $E_{\text{des}}^0 = 94.6 \text{ kJ mol}^{-1}$, while the parameterization yields 62.4 kJ mol^{-1} . Hence, when applying Eq. (16) to gas species with $O:C \gtrsim 1$, considering additional information or constraints is recommended.

For our data set, the principal component analysis in Fig. S3 indicates no strong correlation between ϵ_r and E_{des}^0 . Fig. 9 corroborates the negligible dependence of E_{des}^0 on ϵ_r . However, one

831 would expect that greater μ , α , and ϵ_r result in larger E_{des}^0 due to enhanced molecular interactions.
832 The derivation of our parameterization exploited the strong dependency of E_{des}^0 on α . We suggest
833 that the underlying reason for this dependency is the competing effects of μ and α on E_{des}^0 as
834 outlined below.

835 Small molecules with polar groups can exert significant dipole moments while the polarizability
836 is still small. As depicted in Fig. S6, smaller molecules exert greater μ while $O:C$ values are high
837 and α is low (see also Fig. 7). Note that alkanes and PAHs in the data set, following common
838 convention, have zero dipole moments. Gas species with greater μ may interact more strongly with
839 polarizable substrates expressed by ϵ_r , yielding larger E_{des}^0 . However, as the gas molecules become
840 larger, their α increases, e.g., by the addition of methylene groups (Bosque and Sales, 2002),
841 thereby dominating over the impact of μ on E_{des}^0 . Figure S2 supports this trend where molecules
842 with largest α have low $O:C$ and small μ . Hence, this data set yields a negative correlation between
843 μ and α . As a consequence, for larger molecules the role of the molecule's μ interacting with the
844 substrate becomes less important. Thus, in a way, the range of available desorption data could be
845 responsible for the negligible correlation between E_{des}^0 and substrate ϵ_r (Fig. 9). In other words,
846 polarizability α , which is strongest for molecules with small μ and low $O:C$, compensates and
847 dominates the impact of the dipole moment on E_{des}^0 and, in turn, renders the substrate of less
848 importance for parameterizing E_{des}^0 . This is also evident in Fig. 10, where the scatter of
849 parameterization-derived E_{des}^0 values is largest for molecules with lower M and lower α . We can
850 attribute the scatter in E_{des}^0 at lower M to the competing contributions of the gas species' μ , here
851 accounted by $O:C$ and α . These may be the reasons why E_{des}^0 can be reasonably parameterized
852 from our data set without accounting for the substrate's ϵ_r and gas species' μ . Though, we would

853 expect with more available data, the role of gas species' μ and substrate's ε_r to likely be resolved
854 in a parameterization.

855 Considering the significant number of data and omission of substrate specific properties in the
856 parameterization, the scatter in E_{des}^0 is not very large. This suggests that this parameterization can
857 serve as a reasonable first estimate of E_{des}^0 for a complex environmental substrate such as an
858 aerosol particle. We would expect that with increasing number of desorption data that include
859 larger molecules with larger $O:C$ or μ and applied known standard states and adsorbate models,
860 the scatter in E_{des}^0 at lower molar masses can be resolved.

861

862 **Relationship Between Desorption Energy and Enthalpy of Vaporization.** To examine the
863 relationship between E_{des}^0 and ΔH_{vap} , we have plotted the data given in supplemental tables (not
864 the parameterized values) separated for the different substrate types in Fig. 11. Our data supports
865 a positive correlation between E_{des}^0 and ΔH_{vap} , where E_{des}^0 for most instances is larger than ΔH_{vap} .
866 The role of $O:C$ in the relationship between E_{des}^0 and ΔH_{vap} is not clearly identifiable for the cases
867 that include all, solid, and ice substrates data. However, for liquid substrates, the data suggest that
868 for given ΔH_{vap} , larger $O:C$ yields larger E_{des}^0 . Figure S7 provides a linear regression model for
869 the case of liquid substrates. As shown above, larger $O:C$ correlates with a larger μ , which may
870 exert a greater impact on E_{des}^0 in the case of a liquid substrate. In fact, the interaction strength at
871 the surface often exceeds the enthalpy of condensation between gas and its condensed liquid for
872 the same species family, e.g., in the case of methyl-substituted benzenes (Raja et al., 2002; Bruant
873 and Conklin, 2002), but also for other species like alcohols, acids, amines and ketones (Mmerek
874 et al., 2000) and alkanes (Goss, 2009) and halogenated alkanes (Bruant and Conklin, 2001). This
875 indicates that the aqueous solution – air interface allows for a two-dimensional environment in

876 which the intermolecular interactions are as important as in the **bulk** condensed phase of the
877 adsorbate alone (Valsaraj, 1988a, 2009).

878

879 **Relationship Between Desorption Energy and Enthalpy of Solvation for Aqueous**

880 **Substrates.** To examine the relationship between E_{des}^0 and ΔH_{solv} , we have plotted the data for
881 liquid substrates, consisting mostly of water and few aqueous solutions (Tables A9 to A15) in Fig.
882 12. Despite the scatter in the data, a positive correlation between E_{des}^0 and ΔH_{solv} can be identified.
883 The data falls symmetrically around the 1:1 line, indicating no strong bias. In the case of liquid
884 substrates, the correlation between E_{des}^0 and ΔH_{solv} is comparable to that observed between E_{des}^0
885 and ΔH_{vap} (Fig. 11c). Figure S8 provides a linear regression model for the data shown in Fig. 12.

886 The relationship between E_{des}^0 and ΔH_{solv} shown in Fig. 12 can be understood in the following
887 way. For large non-polar molecules, the free energy cost of entering the aqueous solution is mostly
888 driven by enthalpic changes, because hydrogen bonds need to be disrupted to form a cavity around
889 the molecule (Kronberg, 2016; Valsaraj, 1988a; Brini et al., 2017). The surface energy in that
890 cavity is then driven by the surface energy of pure water and the hydrophobic interactions with the
891 solute (Chandler, 2005). This is then somewhat similar to the situation when the same molecule is
892 adsorbed at the aqueous solution – air interface. Thus, for the larger non-polar molecules, the
893 contribution of the enthalpy of cavity formation can be identified as a dominating factor of the
894 solvation process, which in turn depends on the intermolecular strength between adsorbing
895 molecule and liquid. This, hence, can explain the correlation between E_{des}^0 and ΔH_{solv} for the case
896 of the non-polar molecules.

897 For small non-polar molecules, the transfer to the aqueous phase is mostly entropy-driven,
898 because the hydrogen bonds do not need to be disrupted but need to reorganize around the solute

899 (Kronberg, 2016; Shinoda, 1992, 1977; Hvidt, 1983; Brini et al., 2017). Polar molecules would be
900 comparable to ions, but also in this case, the size and charge distribution determine the cost of
901 solvation through the number and strength of hydrogen bonds to water, which lead to a correlation
902 of and ΔH_{solv} with the number of hydrophilic groups. The latter also determine E_{des}^0 (i.e., $O:C$
903 correlates with μ). Among the small organic molecules contained in Fig. 12, with the increasing
904 presence of hydrophilic functional groups, the larger $O:C$ ratios lead to larger E_{des}^0 . For these
905 reasons, the relationship between E_{des}^0 and ΔH_{solv} shown in Fig. 12 supports the specific and
906 physical interaction model at the aqueous solution – air interface mentioned above: E_{des}^0 scales
907 with the magnitude of hydrophobic interactions for non-polar molecules and with the presence of
908 hydrophilic functional groups (i.e., $O:C$ correlates with μ) for polar molecules, and thus the
909 correlation with ΔH_{solv} is a logical consequence.

910 Note that since both E_{des}^0 and ΔH_{solv} are correlated, and are mostly independent of temperature
911 (Hildebrand and Scott, 1964) within the idealized concept presented here, the temperature
912 dependence of τ_{des} may apparently dominate the temperature dependence of solvation when
913 $E_{\text{des}}^0 > \Delta H_{\text{solv}}$. This idea of parallel behavior of desorption and solvation is also supported by a
914 very recent experimental study that provides in situ measurements of the uptake of gas-phase water
915 into ionic liquids at the gas-liquid interface using ambient pressure X-ray photoelectron
916 spectroscopy (Broderick et al., 2019). These measurements indicate that, dependent on water mole
917 fraction and temperature, solvation is governed by similar thermodynamics as relevant for crossing
918 the gas-liquid interface during the mass-transfer process (Broderick et al., 2019). The positive
919 correlation between the E_{des}^0 and ΔH_{solv} values displayed in Fig. 12 supports this notion, ascribing
920 the molecular interactions controlling τ_{des} and solvation an important role in the molecular
921 understanding of gas-substrate interactions.

922

923 **6. Atmospheric Implications**

924 The discussion in the above sections demonstrated the importance of accurate knowledge of E_{des}^0
925 for the representation of multiphase chemical reactions across various environmental interfaces
926 and phase states including aerosol particles. Analyses of experimentally conducted multiphase
927 chemical kinetics studies as well modeling the detailed processes that lead to the physicochemical
928 transformation of particles and define their atmospheric fate will greatly benefit from improved
929 estimates of E_{des}^0 (Su et al., 2020; Zheng et al., 2020; Shiraiwa et al., 2017a; Shiraiwa et al., 2017b;
930 Shrivastava et al., 2017b; Shrivastava et al., 2017a; Li and Knopf, 2021; Kaiser et al., 2011;
931 Springmann et al., 2009; Mu et al., 2018; Hems et al., 2021; Laskin et al., 2015). Below we discuss
932 further relevant atmospheric chemistry processes that connect to and/or make use of E_{des}^0 including
933 gas-particle partitioning, secondary organic aerosol (SOA) formation, indoor air chemistry, and
934 glass transition of OA particles.

935 **Gas-Particle Partitioning of Secondary Organic Aerosol.** Organic aerosol is ubiquitous,
936 consists of numerous chemical species, and represents a large mass fraction (20–90%) of the total
937 submicron particles in the troposphere (Nizkorodov et al., 2011; Jimenez et al., 2009; Hallquist et
938 al., 2009; Kanakidou et al., 2005). The formation of SOA proceeds by complex pathways including
939 reaction and mass transport in the gas and condensed phases. The equilibration timescale for gas-
940 particle partitioning for SOA particles and particle-particle mixing of varying viscosity has been
941 evaluated (Shiraiwa and Seinfeld, 2012; Berkemeier et al., 2020; Schervish and Shiraiwa, 2023;
942 Li and Shiraiwa, 2019; Schervish et al., 2023). In some of those modeling studies a fixed $\tau_{\text{des}} =$
943 10^{-9} s, which corresponds to about $E_{\text{des}}^0 = 22$ kJ mol⁻¹ at 293 K, was applied. The simulation results
944 shown in Fig. 5, however, demonstrated that we can expect significant changes in condensed phase

945 equilibration times for gas-particle partitioning when E_{des}^0 and temperature change. Our tabulated
946 data suggests that oxygenated VOCs will exert larger E_{des}^0 and, as such, longer τ_{des} .

947 It has been shown that SOA oxidation products with a variety of functional groups fall into
948 molecular corridors characterized by a tight inverse correlation between volatility (or saturation
949 mass concentration, C_0) and molar mass as depicted in Fig. 13 (Li et al., 2016; Shiraiwa et al.,
950 2014). They are constrained by two boundary lines corresponding to the volatility of n-alkanes
951 C_nH_{2n+2} and sugar alcohols $C_nH_{2n+2}O_n$, which we now identify as “van der Waals” and “hydrogen-
952 bonding” dominated boundaries. This interpretation can be understood by the governing
953 intermolecular forces. For example, using the EVAPORATION model (Compernelle et al., 2011),
954 the vapor pressures for alkane, ketone, alcohol, and acid with a molecular weight of about 142 g
955 mol^{-1} at 298 K yield: $p^0(C_{10}H_{22}) = 1.73$ hPa, $p^0(H_7C_3C(O)C_5H_{11}) = 0.084$ hPa, $p^0(C_9H_{19}OH) =$
956 0.023 hPa, and $p^0(C_7H_{15}COOH) = 1.62 \times 10^{-3}$ hPa, respectively. The decrease of about three orders
957 of magnitude in the vapor pressure between the alkane and the carboxylic acid is mainly due to
958 two carboxylic acid molecules forming hydrogen bonds, resulting in a dimer. A highly-oxidized
959 amide having ketone and alcohol groups such as $N=CC(O)C(O)C(O)CO$ and $M = 149.146$ g mol^{-1}
960 has $p^0 = 8.93 \times 10^{-7}$ hPa. This is due to the fact that this molecule not only establishes the van der
961 Waals forces such as London dispersion and Keesom forces but also hydrogen bonding with three
962 hydrogen bond donors and multiple hydrogen bond acceptors. As can be seen in Fig. 13, the change
963 in C_0 derived from decane to C_0 of the highly-oxidized amide spans the identified molecular
964 corridor around $M = 145$ g mol^{-1} , indicating that the van der Waals forces and the number of
965 hydrogen bonds that can be established by a particular molecule may fundamentally describe the
966 volatility range of the organic species.

967 Keeping this approach in mind, we can ask: what are the extreme limits of the saturation mass
968 concentration? The smallest organic molecule is methane, only prone to London dispersion forces.
969 $p^0(\text{CH}_4) = 46000 \text{ hPa}$ with $\log_{10}(C_0) = 10.5$, which corresponds to the upper bound of the
970 molecular corridor. Ammonia (NH_3) has a similar molar mass as CH_4 but has lower vapor pressure,
971 because NH_3 can establish two hydrogen bonds. N_2O_5 does not form hydrogen bonds and locates
972 above the alkane line. The lower bound of the molecular corridor is mainly defined by the
973 molecule's permanent dipole moments and number of hydrogen bonds it can entertain. Clearly,
974 these attributes are likely to be found in larger and highly-oxidized compounds. Water constitutes
975 a peculiarity when looking at its position in the $C_0 - M$ framework depicted in Fig. 13. There is no
976 other molecule with this small size that can form four hydrogen bonds. Sulfuric acid (H_2SO_4) can
977 also form four hydrogen bonds and locates close to the lower bound of the molecular corridor. As
978 molecules become larger, there are steric hindrances that likely inhibit stronger intermolecular
979 bonding, whereas water with its small size is ideal. This reason may ultimately limit the lower
980 bound of the molecular corridor and thus the lowest volatilities experienced by OA species.

981 As we have discussed above, E_{des}^0 and ΔH_{vap} are positively correlated and E_{des}^0 in most cases
982 is larger than ΔH_{vap} (Fig. 11). Also, we found that gas species with higher $O:C$, and thus larger μ ,
983 exhibit larger E_{des}^0 values. This indicates that intermolecular interactions at the interface are as
984 important as in the condensed phase of the adsorbate alone (Valsaraj, 2009, 1988a). We expect
985 this also to hold for the case of SOA formation. It is generally observed that the composition of
986 the organic matrix, barring any mass-transport limitations, has little influence on the gas-particle
987 partitioning equilibrium (Donahue et al., 2012; Donahue et al., 2011). Oxygenated VOCs have
988 higher $O:C$ and larger μ . Saturation vapor pressure or volatility provides guidance in this regard
989 (Epstein et al., 2010), however, our study suggests that considering desorption, i.e., E_{des}^0 values,

990 can impact equilibrium times of gas-particle partitioning as outlined in the gas uptake multilayer
991 model simulations discussed in section 4.

992 Figure 13A shows that the compiled data sets fall within the $C_0 - M$ framework. In comparison,
993 Fig. 13B shows the distribution of SOA oxidation products (916 different species) in the $C_0 - M$
994 space evaluated previously by Shiraiwa *et al.* (2014). Since the gas species discussed in this work
995 cover a similar C_0 and M range as the SOA oxidation products, we can apply the parameterization
996 of E_{des}^0 to provide estimates of E_{des}^0 for gas species typically involved in SOA gas-particle
997 partitioning. This will allow a more detailed understanding and prediction of SOA formation, in
998 particular for temperatures typically encountered in the troposphere during transport.

999 We derive E_{des}^0 of SOA oxidation products by application of Eq. (14). Since we know the
1000 molecular structure of the SOA oxidation products, we can calculate polarizability using the
1001 equation provided by Bosque and Sales (2002), instead of using Eq. (15):

$$\begin{aligned} 1002 \quad \alpha = & 1.51\#C + 0.17\#H + 0.57\#O + 1.05\#N + 2.99\#S + 2.48\#P + 0.22\#F + \\ 1003 \quad & 2.16\#Cl + 3.29\#Br + 5.45\#I + 0.32, \end{aligned} \quad (20)$$

1004 where $\#C$, $\#H$, $\#O$, $\#N$, $\#S$, $\#P$, $\#F$, $\#Cl$, $\#Br$, and $\#I$ represent the respective numbers of atoms in
1005 the molecule.

1006 Figure 14 displays E_{des}^0 values for the molecular corridor data of SOA precursors gases and
1007 oxidation products from Fig. 13 as a function of molar mass and its dependence on $O:C$ and
1008 polarizability, following the molecular corridor approach using molar mass as the primary
1009 parameter characterizing a the physicochemical properties of a molecule (Shiraiwa *et al.*, 2014).
1010 Figures S9 provides the same analysis using parameterization Eq. (16). For the majority of data
1011 points the predicted E_{des}^0 values are within $\pm 10\%$ of the values shown in Fig. 14 and within the
1012 expected general uncertainty of E_{des}^0 as discussed above. Figure 14A demonstrates the impact of

1013 $O:C$ on E_{des}^0 , where alkanes, constituting the upper bound in the molecular corridor, have the
1014 lowest E_{des}^0 for a given molar mass. With increasing molecule $O:C$, E_{des}^0 increases as expected
1015 from our previous analyses and discussions. The largest impact of molecule $O:C$ is at smallest
1016 molar masses. Figure 14B corroborates the strong correlation between molar mass and
1017 polarizability. Figure S9 depicts a tighter correlation of E_{des}^0 with molar mass and polarizability
1018 due to the linear representation of polarizability (Eq. (15)). Estimates of E_{des}^0 for these SOA
1019 oxidation products will allow refinement of gas-particle partitioning timescales, specifically when
1020 temperature changes are considered as outlined in our example shown in Fig. 5.

1021 Figure 15 relates saturation vapor pressures (p^0) at 298 K, estimated using the
1022 EVAPORATION model (Compernelle et al., 2011), to estimated E_{des}^0 , derived using Eq. 14, for
1023 selected compounds relevant for atmospheric chemistry and SOA molecular corridor data from
1024 Figs. 13 (Shiraiwa et al., 2014). The top axis of Fig. 15 shows the corresponding desorption
1025 lifetimes τ_{des} at 298 K using the Frenkel equation (Eq. 1) with a pre-exponential factor A_{des} of
1026 10^{13} s^{-1} . The linear behavior in semi-logarithmic space (black solid line) reflects an exponential
1027 relation between p^0 and E_{des}^0 and a linear relation between p^0 and τ_{des} . Similar relationships are
1028 known for p^0 and ΔH_{vap} (Epstein et al., 2010), which underscores the correlation of these two
1029 quantities as observed in Fig. 11. We find, however, a steeper slope of p^0 with E_{des}^0 than previously
1030 found for p^0 and ΔH_{vap} , which suggests $E_{\text{des}}^0 < \Delta H_{\text{vap}}$ for large, oxygenated molecules with low
1031 vapor pressures. Note, however, that those gas species are lacking in our datasets. The relation of
1032 E_{des}^0 and ΔH_{vap} and its consequences for gas-particle partitioning of SOA will be further
1033 investigated in follow-up studies.

1034 Table 2 summarizes characteristic values of p^0 , E_{des}^0 , and τ_{des} for the categories of a volatility
1035 basis set (VBS) widely used for the description of SOA: intermediate volatility organic compounds

1036 (IVOC), semi-volatile organic compounds (SVOC), low volatility compounds (LVOC), extremely
1037 low volatility compounds (ELVOC), and ultra-low volatility compounds (ULVOC) (Schervish
1038 and Donahue, 2020; Donahue et al., 2009). We obtain characteristic desorption lifetimes of
1039 nanoseconds to milliseconds for VOC, milliseconds to hours for IVOC, and seconds to months for
1040 SVOC, respectively. For LVOC, ELVOC, and ULVOC we obtain τ_{des} values in the range of
1041 minutes to years and millennia. The latter, however, have to be considered as rough estimates,
1042 because the amounts of data available for parameterizing p^0 and E_{des}^0 at low volatility are very
1043 sparse. Note that these VBS categories were originally defined in terms of saturation mass
1044 concentration C^0 . To express the categories in terms of p^0 , we applied a constant conversion factor
1045 of $10^{-10} \text{ atm m}^3 \mu\text{g}^{-1}$, i.e., assuming a molar mass of 244 g mol^{-1} , for general orientation. For
1046 applications in which keeping the exact definition is required, a more nuanced conversion to vapor
1047 pressures could be achieved by parameterizing typical values of molar mass as a function of vapor
1048 pressure along the SOA molecular corridor. We provide an analogous figure displaying saturation
1049 mass concentrations in the Supplement (Fig. S10).

1050 Gas-particle partitioning plays an important role in chemical transport models, which describe
1051 the long-distance transport and chemical degradation of atmospheric constituents. In these models,
1052 gas-particle partitioning is often treated with instantaneous-equilibration approaches. Desorption
1053 lifetimes crucially determine the position of partitioning steady states and thus affect chemical
1054 degradation rates. Moreover, they have a significant influence on the validity of the instantaneous-
1055 equilibration assumption (Wilson et al., 2021; Stolzenburg et al., 2018).

1056 Adsorption and desorption processes of semi-volatile species are important in indoor
1057 environments, as large surface area-to-volume ratios indoors favor heterogeneous interactions. The
1058 deposition of semi-volatile organic compounds on impermeable indoor surfaces can lead to the

1059 formation of thin organic films (Weschler and Nazaroff, 2017). The desorption lifetime is a critical
1060 parameter for the initial film formation via multi-layer adsorption and the subsequent film growth
1061 (Lakey et al., 2021). These surface films act as reservoirs of semivolatile compounds and also
1062 serve as reaction media, affecting indoor air composition (Wang et al., 2020; Lakey et al., 2023).

1063

1064 **Summary and Conclusions**

1065 We have compiled computationally and experimentally derived desorption energy data to
1066 provide estimates of E_{des}^0 for a variety of gas species and solid, liquid, and ice substrates, thereby
1067 covering a range of relevant aerosol particle systems. The desorption energies have been placed in
1068 context with intermolecular forces. We were able to express E_{des}^0 as a function of molecular weight
1069 and $O:C$ ratio only, facilitating the application of the proposed parameterization. The important
1070 role of gas species' polarizability and dipole moment governing E_{des}^0 have been recognized. We
1071 demonstrated the importance of correct E_{des}^0 values for interpretation of multiphase chemical
1072 reactions and gas-particle partitioning, especially when extrapolating laboratory findings to
1073 atmospherically relevant temperature ranges. For example, assessment of chemical aging of
1074 aerosol particles during transport relies on E_{des}^0 values for various atmospheric oxidants.

1075 The compiled literature data allowed us to correlate E_{des}^0 with the enthalpy of vaporization and
1076 solvation, thereby evaluating the role of desorption in these interfacial processes. We identified a
1077 positive correlation between E_{des}^0 and ΔH_{vap} , where E_{des}^0 values are often larger than ΔH_{vap} . For
1078 liquid substrates, we observe a correlation with molecule oxidation state as well, indicating the
1079 importance of intermolecular interactions when looking at interfacial processes.

1080 A positive correlation has been observed between E_{des}^0 and ΔH_{soln} in liquid substrates. This
1081 trend could be related to the gas species' dipole moment and the interfacial interactions among the
1082 adsorbed gas species and molecules in the liquid phase.

1083 We demonstrated the relevance of E_{des}^0 in gas-particle partitioning and its relationship to the
1084 concept of molecular corridors. E_{des}^0 values for many SOA components were derived allowing for
1085 in detail simulation of SOA formation and growth processes. Accurate representation of particle
1086 growth and SOA formation processes requires E_{des}^0 for typically oxygenated VOCs. The relevance
1087 of E_{des}^0 for application in indoor air chemistry has been highlighted. Furthermore, in the Appendix
1088 A1 we outline the correlation of glass transition points with E_{des}^0 which adds another layer of
1089 complexity when modeling multiphase chemical reactions (through the potential of viscous phase
1090 states). Our findings identify the following areas of further research needs:

- 1091 - More adsorption and desorption data for environmentally-relevant interfaces, including
1092 multicomponent aerosol particle surfaces, are needed. Experimental and computational
1093 approaches can yield necessary E_{des}^0 values.
- 1094 - Reporting and application of adsorption and/or desorption data should consider applied
1095 standard states and adsorption models to better constrain E_{des}^0 (Donaldson et al., 2012b;
1096 Savara, 2013; Campbell et al., 2016; Knopf and Ammann, 2021).
- 1097 - Desorption kinetic measurements involving liquids with high vapor pressure are needed.
1098 Furthermore, the role of solutes in aqueous solutions on the hydrogen bonding network and
1099 in turn on the desorption process is not well understood. For example, adsorbates with
1100 hydrophilic functional groups exert greater E_{des}^0 . Systematic examination of desorption
1101 kinetics as a function of varying solute concentration and gas species $O:C$ and dipole

1102 moment are needed to improve our understanding of adsorption and desorption processes
1103 on liquid surfaces.

1104 - Experimental and theoretical multiphase chemical kinetics studies should aim to represent
1105 the typical atmospheric temperature range. This can add to further complications with
1106 regard to the underlying thermodynamics and kinetics in addition to possibly phase state
1107 changes of the substrate (Li and Knopf, 2021; Li et al., 2020; Slade et al., 2017; Knopf et
1108 al., 2005; Davies and Wilson, 2015; Chan et al., 2014; Hearn and Smith, 2007).

1109 - Advancing our understanding of the interfacial processes that govern mass
1110 accommodation, solvation, and vaporization is needed. Adsorption and desorption can play
1111 a role in these processes. However, the degree of how much impact E_{des}^0 has on gas species'
1112 solvation or vaporization depends on its relationship with ΔH_{vap} and ΔH_{solv} . Considering
1113 that aerosol particles are chemically complex and exhibit multiple phases and phase states,
1114 these advances will improve representation of gas-particle partitioning.

1115

1116 **Appendix**

1117 This appendix provides a discussion of observed correlation between E_{des}^0 and T_g , nomenclature
1118 used in this study, and lists the applied data sets to develop the E_{des}^0 parameterization and to
1119 produce correlation plots. The parameters given in Tables are also available electronically (Knopf
1120 et al., 2023).

1121

1122 **A1. Glass Transition**

1123 Molecular corridors yield also significant insight into particle phase state and viscosity. The
1124 glass transition temperature (T_g) characterizes the non-equilibrium phase change from a glassy
1125 solid state to a more pliable semi-solid state upon an increase of temperature or humidity (Koop et
1126 al., 2011b). T_g depends primarily on the molar mass and secondarily on the $O:C$ (Koop et al.,
1127 2011a; Shiraiwa et al., 2017a). Organic compounds with greater molar mass and lower volatility
1128 have higher T_g , indicating that these compounds adopt an amorphous (semi-) solid phase with
1129 higher viscosity. For weakly functionalized compounds, viscosity and T_g are sensitive to addition
1130 of carboxylic acid (COOH) and hydroxyl (OH) groups compared to carbonyl (CO) and methylene
1131 (CH_2) (Rothfuss and Petters, 2017; Galeazzo and Shiraiwa, 2022). It has been demonstrated that
1132 on average the addition of one OH group increases the viscosity by a factor of approximately 22
1133 to 45 (Grayson et al., 2017). These studies imply that hydrogen bonding may play an important
1134 role in determining viscosity, which is consistent with its role in influencing glass transition
1135 temperatures (Nakanishi and Nozaki, 2011; Van Der Sman, 2013).

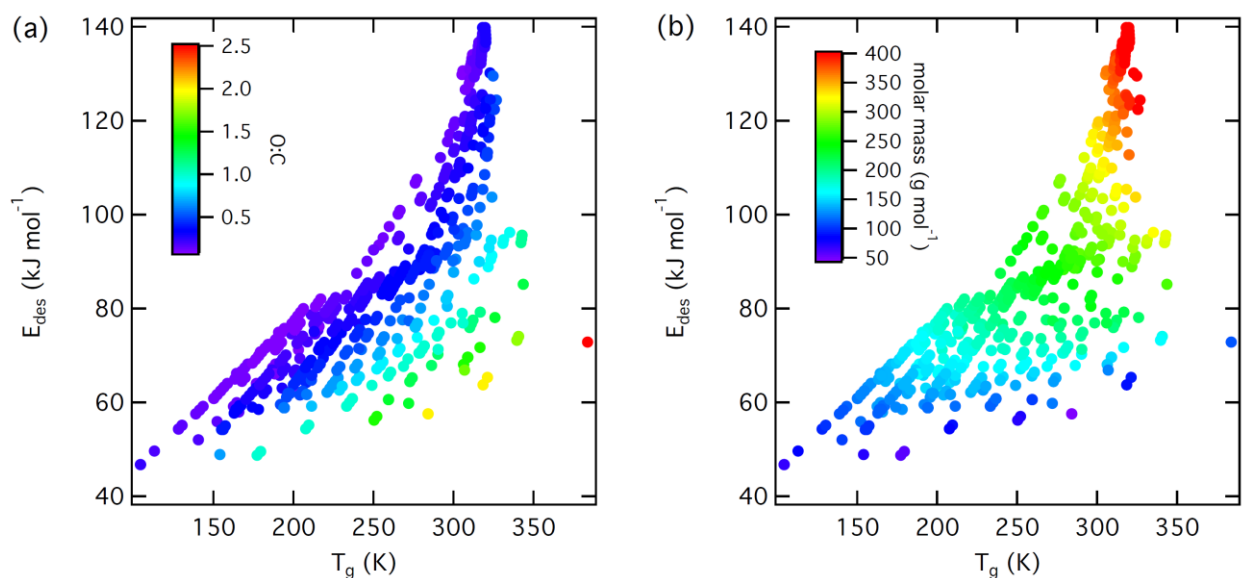
1136 Recent studies have shown that a glassy surface can be much more dynamic with lower
1137 viscosity than anticipated based on T_g and bulk viscosity (Tian et al., 2022; Zhang and Fakhraai,
1138 2017; Sikorski et al., 2010). The enhanced surface mobility, however, is mostly shown by two

1139 typical amorphous polymers of polystyrene and poly(methyl methacrylate) (Tian et al., 2022).
1140 Though it is likely that also enhanced mobility on the surface compared to the bulk is relevant for
1141 atmospheric organic matter, further studies are necessary to assess if this is applicable to
1142 atmospheric glassy SOA particles, which are highly complex multicomponent mixtures that are
1143 very different from polymers.

1144 Application of our parameterization of E_{des}^0 , we can now construct a relationship between E_{des}^0
1145 and T_g of the SOA oxidation products shown in Fig. 1. T_g was derived applying the
1146 parameterization presented in (Shiraiwa et al., 2017a) using molar mass and $O:C$ as input
1147 variables. E_{des}^0 was derived applying Eqs. (14) and (20). Since both of our parameterizations of
1148 E_{des}^0 and T_g depend on molar mass and $O:C$ ratio, it is reasonable to expect we can now construct
1149 a positive relationship between E_{des}^0 and T_g of the SOA oxidation products. Figure A1 shows that
1150 gas species with lower E_{des}^0 have lower T_g and vice versa. Figure A1A demonstrates that for gas
1151 species with same E_{des}^0 , an increase in $O:C$ results in a significant increase of T_g pointing to
1152 enhanced molecular interactions. Hence, alkanes represent species with lowest T_g at given E_{des}^0 .
1153 Figure A1B further corroborates this fact. T_g has a strong dependency on molar mass. However,
1154 for the same molar mass, T_g can vary by 100 K (which coincides with only small changes in E_{des}^0),
1155 which can now be attributed to the impact of $O:C$. In other words, increased molecular interactions
1156 can significantly increase T_g , when other parameters remain the same. Similar trends hold for E_{des}^0 ,
1157 thereby allowing to recognize that comparable molecular interactions control the properties of the
1158 amorphous phase state of a system and its E_{des}^0 . In absence of knowing the molecular structure,
1159 Fig. S11 provides the same analysis of the relationship between E_{des}^0 and T_g of the SOA oxidation
1160 products using parameterization Eq. (16) for comparison. We see that without knowing the
1161 molecular structure, a tighter correlation between E_{des}^0 and T_g is observed due to the linearization

1162 of the gas species' polarizability. Similarly to Figs. 14 and S6, the predicted E_{des}^0 values in Fig.
1163 S11 are within $\pm 10\%$ of the values shown in Fig. A1 and within the expected general uncertainty
1164 of E_{des}^0 .

1165 The correlation between E_{des}^0 and T_g serves as empirical and observational evidence. The
1166 theoretical and physical basis are yet to be established. It does not account for the potentially
1167 enhanced mobility on the surface of glassy matter (Tian et al., 2022; Zhang and Fakhraai, 2017;
1168 Sikorski et al., 2010). One would expect that surface mobility would similarly scale with the
1169 strength of intermolecular interactions. Molecules with high E_{des}^0 interact strongly with molecules
1170 of the same kind at the surface and in the bulk, are expected to also exhibit reduced dynamics in
1171 their own condensed phase (or in a mixture of similar molecules) and thus high viscosity. The
1172 presented correlation observed is meaningful for advancing our understanding of interfacial
1173 processes and supports further investigations.



1174
1175 **Figure A1.** Relationship between calculated desorption energies (E_{des}^0) of SOA precursor gases
1176 from Shiraiwa et al. (2014) and species' glass transition temperature (T_g) and its dependence on
1177 O:C (a) and molar mass (b). This analysis applies parameterizations given in Eqs. (14) and (20).

1178

τ_{des}	desorption lifetime
k_{des}	first-order desorption rate coefficient
A_{des}	pre-exponential factor
E_{des}^0	desorption energy with the energy reference of the gas molecule at rest at $T = 0$ K
γ	uptake coefficient
α_s	surface accommodation coefficient
Γ_b	normalized loss rate in the bulk-phase induced by solubility, diffusion and reaction
Γ_{sb}	normalized rate of surface to bulk transfer
Γ_s	normalized loss rate due to surface reaction
k_s	first-order rate coefficient of chemical reaction at the surface
k_{sb}	first-order rate coefficient for the transfer of molecules from the surface into the bulk (solvation)
k_{bs}	first-order rate coefficient for the transfer of molecules from the bulk to the surface
α_b	bulk accommodation coefficient
ΔG_{ads}^0	Gibbs free energy change of adsorption
ΔH_{ads}^0	standard enthalpy change of adsorption
ΔS_{ads}^0	standard entropy change of adsorption
κ	transmission coefficient
$(N_{\text{TS}}/\mathcal{A})^0$	standard concentration of molecules in the TS
$(N_{\text{ads}}/\mathcal{A})^0$	standard concentration of adsorbed molecules
$q_{\text{TS}}^{0'}$	standard partition functions for the TS
q_{ads}^0	standard partition functions for the adsorbate
q'_{TS}	partition functions for the TS
q_{ads}	partition functions for the adsorbate

M	molar mass
ΔH_{vap}	enthalpy of vaporization
α	polarizability
μ	dipole moment
$O:C$	oxygen to carbon ratio
ΔH_{sol}	enthalpy of solvation
ϵ_r	relative permittivity of the substrate
TPD	temperature programmed desorption
TDS	thermal desorption spectroscopy
TG-DSC	thermal gravimetry with differential scanning calorimetry
KN	Knudsen cell
MB	molecular beams
IGC	inverse gas chromatography
VM	vacuum microbalance
DRIFT	diffuse reflectance infrared fourier transform spectroscopy
FTIR	Fourier transform infrared spectroscopy
KU	kinetic uptake
VS	vibrational spectroscopy
ST	surface tension
MD	molecular dynamics
DFT	density functional theory
MC	Monte Carlo
GCMC	grand canonical Monte Carlo
ECT	embedded cluster theory
DAM	dipped adcluster model

1180

1181

1182 **Table A1.** Compiled adsorbate-substrate data for water vapor and heavy water vapor adsorbed on
 1183 various mineral and clay substrates, inorganics, organics, and carbonaceous substrates. Gas
 1184 species, gas species' molar mass, substrate, experimental or theoretical method, desorption energy
 1185 (E_{des}^0), and desorption lifetimes (τ_{des}) evaluated at 293 K using $A_{des} = 10^{13} \text{ s}^{-1}$, enthalpy of
 1186 vaporization (ΔH_{vap}), gas species' polarizability (α), gas species' dipole moment (μ), substrate's
 1187 relative permittivity (ϵ_r), and gas species' oxygen to carbon ratio ($O:C$) are given.

Gas Species	Molar Mass / g mol ⁻¹	Substrate	Method	E_{des}^0 / kJ mol ⁻¹	$\tau_{des}^{293 K}$ / s	ΔH_{vap} (T) / kJ mol ⁻¹	α / 10 ⁻²⁴ cm ³	μ / D	ϵ_r	O:C
H ₂ O	18.02	clay: orthic luvisol	VM	9.7 (Sokolowska et al., 1993)	5.4×10 ⁻¹²	44 (Chickos and Acree, 2003)	1.45 (Lide, 2008)	1.85 (Lide, 2008)	2 (Daniels, 2004)	0
H ₂ O	18.02	clay: mollic gleysol	VM	11.2 (Sokolowska et al., 1993)	1.0×10 ⁻¹¹	44 (Chickos and Acree, 2003)	1.45 (Lide, 2008)	1.85 (Lide, 2008)	2 (Daniels, 2004)	0
H ₂ O	18.02	clay: eutric cambisol	VM	13.2 (Sokolowska et al., 1993)	2.3×10 ⁻¹¹	44 (Chickos and Acree, 2003)	1.45 (Lide, 2008)	1.85 (Lide, 2008)	2 (Daniels, 2004)	0
H ₂ O	18.02	clay: stagn. phaeozem	VM	12.8 (Sokolowska et al., 1993)	1.9×10 ⁻¹¹	44 (Chickos and Acree, 2003)	1.45 (Lide, 2008)	1.85 (Lide, 2008)	2 (Daniels, 2004)	0
H ₂ O	18.02	clay: eutric cambisol	VM	12.6 (Sokolowska et al., 1993)	1.7×10 ⁻¹¹	44 (Chickos and Acree, 2003)	1.45 (Lide, 2008)	1.85 (Lide, 2008)	2 (Daniels, 2004)	0
H ₂ O	18.02	kaolinite, si, spc/e	GCMC	21.6 (Croteau et al., 2009)	7.1×10 ⁻¹⁰	44 (Chickos and Acree, 2003)	1.45 (Lide, 2008)	1.85 (Lide, 2008)	5.10 (Leluk et al., 2010)	0
H ₂ O	18.02	kaolinite, al, spc/e	GCMC	46.4 (Croteau et al., 2009)	1.9×10 ⁻⁵	44 (Chickos and Acree, 2003)	1.45 (Lide, 2008)	1.85 (Lide, 2008)	5.10 (Leluk et al., 2010)	0
H ₂ O	18.02	kaolinite, unprotonated edge, spc/e	GCMC	73.5 (Croteau et al., 2009)	1.3	44 (Chickos and Acree, 2003)	1.45 (Lide, 2008)	1.85 (Lide, 2008)	5.10 (Leluk et al., 2010)	0
H ₂ O	18.02	kaolinite, protonated edge, spc/e	GCMC	94.1 (Croteau et al., 2009)	6.0×10 ³	44 (Chickos and Acree, 2003)	1.45 (Lide, 2008)	1.85 (Lide, 2008)	5.10 (Leluk et al., 2010)	0
H ₂ O	18.02	kaolinite (Al)	DRIFTS	56.0 (Budi et al., 2018)	9.6×10 ⁻⁴	44 (Chickos and Acree, 2003)	1.45 (Lide, 2008)	1.85 (Lide, 2008)	5.10 (Leluk et al., 2010)	0
H ₂ O	18.02	kaolinite (Si)	DRIFTS	21.2 (Budi et al., 2018)	6.0×10 ⁻¹⁰	44 (Chickos and Acree, 2003)	1.45 (Lide, 2008)	1.85 (Lide, 2008)	5.10 (Leluk et al., 2010)	0
H ₂ O	18.02	Arizona test dust (0-3 μm)	DRIFTS	53.6	3.6×10 ⁻⁴	44 (Chickos and Acree, 2003)	1.45 (Lide, 2008)	1.85 (Lide, 2008)	5.00 (Sharif, 1995)	0
H ₂ O	18.02	Arizona test dust particles (5-10 μm)	DRIFTS	50.5 (Ibrahim et al., 2018)	1.0×10 ⁻⁴	44 (Chickos and Acree, 2003)	1.45 (Lide, 2008)	1.85 (Lide, 2008)	5.00 (Sharif, 1995)	0
H ₂ O	18.02	Arizona test dust particles (10-20 μm)	DRIFTS	49.5 (Ibrahim et al., 2018)	6.7×10 ⁻⁵	44 (Chickos and Acree, 2003)	1.45 (Lide, 2008)	1.85 (Lide, 2008)	5.00 (Sharif, 1995)	0
H ₂ O	18.02	Arizona test dust particles (20-40 μm)	DRIFTS	48.9 (Ibrahim et al., 2018)	5.2×10 ⁻⁵	44 (Chickos and Acree, 2003)	1.45 (Lide, 2008)	1.85 (Lide, 2008)	5.00 (Sharif, 1995)	0

H ₂ O	18.02	Arizona test dust particles (40-80 μm)	DRIFTS	48.3 (Ibrahim et al., 2018)	4.1×10 ⁻⁵	44 (Chickos and Acree, 2003)	1.45 (Lide, 2008)	1.85 (Lide, 2008)	5.00 (Sharif, 1995)	0
H ₂ O	18.02	NaCl (100)	DFT	40.6 (Meyer et al., 2001)	1.7×10 ⁻⁶	44 (Chickos and Acree, 2003)	1.45 (Lide, 2008)	1.85 (Lide, 2008)	5.9 (Lide, 2008)	0
H ₂ O	18.02	KCl (100)	DFT	32.3 (Meyer et al., 2001)	5.7×10 ⁻⁸	44 (Chickos and Acree, 2003)	1.45 (Lide, 2008)	1.85 (Lide, 2008)	4.86 (Lide, 2008)	0
H ₂ O	18.02	NaCl(001)	FTIR	48.0 (Foster and Ewing, 2000)	3.6×10 ⁻⁵	44 (Chickos and Acree, 2003)	1.45 (Lide, 2008)	1.85 (Lide, 2008)	5.9 (Lide, 2008)	0
H ₂ O	18.02	Al(111)	DFT	56 (Hai et al., 2023)	9.6×10 ⁻⁴	44 (Chickos and Acree, 2003)	1.45 (Lide, 2008)	1.85 (Lide, 2008)		0
H ₂ O	18.02	α-Al ₂ O ₃ (0001, hydroxylated)	TPD	134 (Nelson et al., 1998)	7.7×10 ¹⁰	44 (Chickos and Acree, 2003)	1.45 (Lide, 2008)	1.85 (Lide, 2008)	9.34 (Lide, 2008)	0
H ₂ O	18.02	α-Al ₂ O ₃	FTIR	52.0 (Goodman et al., 2001)	1.9×10 ⁻⁴	44 (Chickos and Acree, 2003)	1.45 (Lide, 2008)	1.85 (Lide, 2008)	9.34 (Lide, 2008)	0
H ₂ O	18.02	SiO ₂	FTIR	50.3(Goodman et al., 2001)	9.3×10 ⁻⁵	44 (Chickos and Acree, 2003)	1.45 (Lide, 2008)	1.85 (Lide, 2008)	4.42 (Lide, 2008)	0
H ₂ O	18.02	TiO ₂	FTIR	54.6(Goodman et al., 2001)	5.4×10 ⁻⁴	44 (Chickos and Acree, 2003)	1.45 (Lide, 2008)	1.85 (Lide, 2008)	86 (Lide, 2008)	0
H ₂ O	18.02	γ-Fe ₂ O ₃	FTIR	53.7(Goodman et al., 2001)	3.7×10 ⁻⁴	44 (Chickos and Acree, 2003)	1.45 (Lide, 2008)	1.85 (Lide, 2008)	4.5 (Lide, 2008)	0
H ₂ O	18.02	CaO	FTIR	49.2(Goodman et al., 2001)	5.9×10 ⁻⁵	44 (Chickos and Acree, 2003)	1.45 (Lide, 2008)	1.85 (Lide, 2008)	11.8 (Lide, 2008)	0
H ₂ O	18.02	MgO	FTIR	50.2(Goodman et al., 2001)	8.9×10 ⁻⁵	44 (Chickos and Acree, 2003)	1.45 (Lide, 2008)	1.85 (Lide, 2008)	9.65 (Lide, 2008)	0
H ₂ O	18.02	NaCl powder	DRIFTS	51.7 (Woodill et al., 2013)	1.6×10 ⁻⁴	44 (Chickos and Acree, 2003)	1.45 (Lide, 2008)	1.85 (Lide, 2008)	5.9 (Lide, 2008)	0
H ₂ O	18.02	catechol coated NaCl	DRIFTS	49.0 (Woodill et al., 2013)	5.4×10 ⁻⁵	44 (Chickos and Acree, 2003)	1.45 (Lide, 2008)	1.85 (Lide, 2008)	~3.52(Kronberger and Weiss, 1944)	0
H ₂ O	18.02	catechol coated NaCl + O ₃	DRIFTS	50.1 (Woodill et al., 2013)	8.4×10 ⁻⁵	44 (Chickos and Acree, 2003)	1.45 (Lide, 2008)	1.85 (Lide, 2008)	~3.52(Kronberger and Weiss, 1944)	0
H ₂ O	18.02	Al ₂ O ₃ powder	DRIFTS	55.1 (Woodill et al., 2013)	6.6×10 ⁻⁴	44 (Chickos and Acree, 2003)	1.45 (Lide, 2008)	1.85 (Lide, 2008)	9.34 (Lide, 2008)	0
H ₂ O	18.02	catechol coated Al ₂ O ₃	DRIFTS	49.8 (Woodill et al., 2013)	7.5×10 ⁻⁵	44 (Chickos and Acree, 2003)	1.45 (Lide, 2008)	1.85 (Lide, 2008)	~3.52(Kronberger and Weiss, 1944)	0
H ₂ O	18.02	Catechol coated Al ₂ O ₃ + O ₃	DRIFTS	49.8 (Woodill et al., 2013)	7.5×10 ⁻⁵	44 (Chickos and Acree, 2003)	1.45 (Lide, 2008)	1.85 (Lide, 2008)	~3.52(Kronberger and	0

									Weiss, 1944)	
H ₂ O	18.02	CaCO ₃	DFT	80.0 (Budi et al., 2018)	18	44 (Chickos and Acree, 2003)	1.45 (Lide, 2008)	1.85 (Lide, 2008)	8.67 (Lide, 2008)	0
H ₂ O	18.02	CaCO ₃	TPD	79.1 (Dickbreder et al., 2023)	13	44 (Chickos and Acree, 2003)	1.45 (Lide, 2008)	1.85 (Lide, 2008)	8.67 (Lide, 2008)	0
H ₂ O	18.02	CaCO ₃	TPD	106.1 (Dickbreder et al., 2023)	8.2×10 ⁵	44 (Chickos and Acree, 2003)	1.45 (Lide, 2008)	1.85 (Lide, 2008)	8.67 (Lide, 2008)	0
H ₂ O	18.02	SiO ₂	DFT	53.1 (Budi et al., 2018)	2.9×10 ⁻⁴	44 (Chickos and Acree, 2003)	1.45 (Lide, 2008)	1.85 (Lide, 2008)	4.42 (Lide, 2008)	0
H ₂ O	18.02	Au(111)	DFT	10.1 (Meng et al., 2004)	6.3×10 ⁻¹²	44 (Chickos and Acree, 2003)	1.45 (Lide, 2008)	1.85 (Lide, 2008)	6.9 (Shklyare vskii and Pakhomo v, 1973)	0
H ₂ O	18.02	Pt(111)	DFT	28.1 (Meng et al., 2004)	1.0×10 ⁻⁸	44 (Chickos and Acree, 2003)	1.45 (Lide, 2008)	1.85 (Lide, 2008)		0
H ₂ O	18.02	Pd(111)	DFT	29.3 (Meng et al., 2004)	1.7×10 ⁻⁸	44 (Chickos and Acree, 2003)	1.45 (Lide, 2008)	1.85 (Lide, 2008)		0
H ₂ O	18.02	Ru(0001)	DFT	39.5 (Meng et al., 2004)	1.1×10 ⁻⁶	44 (Chickos and Acree, 2003)	1.45 (Lide, 2008)	1.85 (Lide, 2008)		0
H ₂ O	18.02	Rh(111)	DFT	39.4 (Meng et al., 2004)	1.1×10 ⁻⁶	44 (Chickos and Acree, 2003)	1.45 (Lide, 2008)	1.85 (Lide, 2008)		0
H ₂ O	18.02	steel	KU	60.4 (Koch et al., 1997)	5.9×10 ⁻³	44 (Chickos and Acree, 2003)	1.45 (Lide, 2008)	1.85 (Lide, 2008)		0
H ₂ O	18.02	pyrex Glass	KU	56.1 (Koch et al., 1997)	1.0×10 ⁻³	44 (Chickos and Acree, 2003)	1.45 (Lide, 2008)	1.85 (Lide, 2008)	5.0 (Lide, 2008)	0
H ₂ O	18.02	SAM-acid	TPD	45.2 (Dubois et al., 1990)	1.1×10 ⁻⁵	44 (Chickos and Acree, 2003)	1.45 (Lide, 2008)	1.85 (Lide, 2008)	4.1 (Millany and Jonscher , 1980)	0
H ₂ O	18.02	SAM-methyl	TPD	35.1 (Dubois et al., 1990)	1.8×10 ⁻⁷	44 (Chickos and Acree, 2003)	1.45 (Lide, 2008)	1.85 (Lide, 2008)	2.1 (Akkerma n et al., 2007; Rampi et al., 1998)	0
H ₂ O	18.02	SAM-alcohol	TPD	39.3 (Dubois et al., 1990)	1.0×10 ⁻⁶	44 (Chickos and Acree, 2003)	1.45 (Lide, 2008)	1.85 (Lide, 2008)		0
H ₂ O	18.02	SAM-amide	TPD	38.5 (Dubois et al., 1990)	7.3×10 ⁻⁷	44 (Chickos and Acree, 2003)	1.45 (Lide, 2008)	1.85 (Lide, 2008)	2 (Romane r et al., 2008)	0
H ₂ O	18.02	SAM-ester	TPD	37.2 (Dubois et al., 1990)	4.3×10 ⁻⁷	44 (Chickos and Acree, 2003)	1.45 (Lide, 2008)	1.85 (Lide, 2008)		0
H ₂ O	18.02	HOPG	TDS	37.2 (Ulbricht et al., 2006)	4.3×10 ⁻⁷	44 (Chickos and Acree, 2003)	1.45 (Lide, 2008)	1.85 (Lide, 2008)	13 (Dovbesh	0

									ko et al., 2015)	
H ₂ O	18.02	graphene	CCSD(T)	13.0 (Voloshina et al., 2011)	1.6×10 ⁻⁵	44 (Chickos and Acree, 2003)	1.45 (Lide, 2008)	1.85 (Lide, 2008)	13 (Dovbeshko et al., 2015)	0
H ₂ O	18.02	graphene	DFT	12.5 (Liang et al., 2021)	1.7×10 ⁻¹¹	44 (Chickos and Acree, 2003)	1.45 (Lide, 2008)	1.85 (Lide, 2008)	13 (Dovbeshko et al., 2015)	0
H ₂ O	18.02	graphene, Stone-Wales	DFT	13.5 (Liang et al., 2021)	2.6×10 ⁻¹¹	44 (Chickos and Acree, 2003)	1.45 (Lide, 2008)	1.85 (Lide, 2008)	13 (Dovbeshko et al., 2015)	0
H ₂ O	18.02	graphene, single vacancy defect	DFT	51.1 (Liang et al., 2021)	1.3×10 ⁻⁴	44 (Chickos and Acree, 2003)	1.45 (Lide, 2008)	1.85 (Lide, 2008)	13 (Dovbeshko et al., 2015)	0
H ₂ O	18.02	graphene, double vacancy defect	DFT	15.4 (Liang et al., 2021)	5.6×10 ⁻¹¹	44 (Chickos and Acree, 2003)	1.45 (Lide, 2008)	1.85 (Lide, 2008)	13 (Dovbeshko et al., 2015)	0
H ₂ O	18.02	grey Soot	KU	29.3 (Alcala-Jornod et al., 2002)	1.7×10 ⁻⁸	44 (Chickos and Acree, 2003)	1.45 (Lide, 2008)	1.85 (Lide, 2008)	13 (Dovbeshko et al., 2015)	0
H ₂ O	18.02	black Soot	KU	37.7 (Alcala-Jornod et al., 2002)	5.3×10 ⁻⁷	44 (Chickos and Acree, 2003)	1.45 (Lide, 2008)	1.85 (Lide, 2008)	13 (Dovbeshko et al., 2015)	0
H ₂ O	18.02	soot-OH	DFT	18.0 (Collignon et al., 2005)	1.6×10 ⁻¹⁰	44 (Chickos and Acree, 2003)	1.45 (Lide, 2008)	1.85 (Lide, 2008)	~13 (Dovbeshko et al., 2015)	0
H ₂ O	18.02	soot-COOH	DFT	38.4 (Collignon et al., 2005)	7.0×10 ⁻⁷	44 (Chickos and Acree, 2003)	1.45 (Lide, 2008)	1.85 (Lide, 2008)	~13 (Dovbeshko et al., 2015)	0
H ₂ O	18.02	benzo[a]pyrene/soot	KU	50.0 (Pöschl et al., 2001)	8.2×10 ⁻⁵	44 (Chickos and Acree, 2003)	1.45 (Lide, 2008)	1.87 (Townes and Schawlow, 1975)	3.52 (Kronberger and Weiss, 1944)	0
D ₂ O	20.03	SAM-methyl	TPD	34.0 (Grimm et al., 2008)	1.2×10 ⁻⁷	45.14 (Crabtree and Simantov, 1993)	1.26 (Lide, 2008)	1.87 (Townes and Schawlow, 1975)	2.1 (Akkerman et al., 2007; Rampi et al., 1998)	0
D ₂ O	20.03	SAM-COOH	TPD	50.0 (Grimm et al., 2008)	8.2×10 ⁻⁵	45.14 (Crabtree and Simantov, 1993)	1.26 (Lide, 2008)	1.87 (Townes and Schawlow, 1975)	4.1 (Millany and Jonscher, 1980)	0
D ₂ O	20.03	uncoated glass	TPD	50.0 (Moussa et al., 2009)	8.2×10 ⁻⁵	45.14 (Crabtree and Simantov, 1993)	1.26 (Lide, 2008)	1.87 (Townes and Schawlow, 1975)	4.42 (Lide, 2008)	0

								ow, 1975)		
D ₂ O	20.03	C18-SAM	TPD	36.0 (Moussa et al., 2009)	2.6×10^{-7}	45.14 (Crabtree and Simantov, 1993)	1.26 (Lide, 2008)	1.87 (Townes and Schawlow, 1975)	2.1 (Akkerman et al., 2007; Rampi et al., 1998)	0
D ₂ O	20.03	C8-SAM	TPD	40.0 (Moussa et al., 2009)	1.4×10^{-6}	45.14 (Crabtree and Simantov, 1993)	1.26 (Lide, 2008)	1.87 (Townes and Schawlow, 1975)	2.03 (Crossley, 1973)	0
D ₂ O	20.03	KMnO ₄ , O ₃ oxidized SAM	TPD	44.0 (Moussa et al., 2009)	7.0×10^{-6}	45.14 (Crabtree and Simantov, 1993)	1.26 (Lide, 2008)	1.87 (Townes and Schawlow, 1975)	-4.1 (Millany and Jonscher, 1980)	0
D ₂ O	20.03	methanol on HOPG	MB	45.3 (Thomson et al., 2011)	1.2×10^{-5}	45.14 (Crabtree and Simantov, 1993)	1.26 (Lide, 2008)	1.87 (Townes and Schawlow, 1975)		0
D ₂ O	20.03	solid butanol	MB	27.0 (Johansson et al., 2019)	6.5×10^{-9}	45.14 (Crabtree and Simantov, 1993)	1.26 (Lide, 2008)	1.87 (Townes and Schawlow, 1975)	17.84* (Lide, 2008)	0
D ₂ O	20.03	solid acetic acid	DFT	19.0 (Allouche and Bahr, 2006)	2.4×10^{-10}	45.14 (Crabtree and Simantov, 1993)	1.26 (Lide, 2008)	1.87 (Townes and Schawlow, 1975)	6.2* (Lide, 2008)	0
D ₂ O	20.03	solid nopinone	MB	26.0 (Johansson et al., 2020)	4.3×10^{-9}	45.14 (Crabtree and Simantov, 1993)	1.26 (Lide, 2008)	1.87 (Townes and Schawlow, 1975)		0
D ₂ O	20.03	nitric acid monolayer	MB	49.2 (Thomson et al., 2015)	5.9×10^{-5}	45.14 (Crabtree and Simantov, 1993)	1.26 (Lide, 2008)	1.87 (Townes and Schawlow, 1975)		0

1188 *Applied the value for liquid phase of substrate species.

1189

1190 **Table A2.** Compiled adsorbate-substrate interaction energies for reactive gases on solid substrates.
1191 Gas species, gas species' molar mass, substrate, experimental or theoretical method, desorption
1192 energy (E_{des}^0), and desorption lifetimes (τ_{des}) evaluated at 293 K using $A_{des} = 10^{13} \text{ s}^{-1}$, enthalpy
1193 of vaporization (ΔH_{vap}), gas species' polarizability (α), gas species' dipole moment (μ),
1194 substrate's relative permittivity (ϵ_r), and gas species' oxygen to carbon ration ($O:C$) are given.

Gas Species	Molar Mass / g mol ⁻¹	Substrate	Method	E_{des}^0 / kJ mol ⁻¹	$\tau_{des}^{293 K}$ / s	$\Delta H_{vap}(T)$ / kJ mol ⁻¹	α / 10 ⁻²⁴ cm ³	μ / D	ϵ_r	O:C
OH	17.01	Al ₂ O ₃	MC	47.5 (Remorov and Bardwell, 2005)	2.9×10 ⁻⁵		7.11 (Zen et al., 2014)	1.65 (Lide, 2008)	9.34 (Lide, 2008)	0
OH	17.01	NaCl	MC	42.7 (Remorov and Bardwell, 2005)	4.1×10 ⁻⁶		7.11 (Zen et al., 2014)	1.65 (Lide, 2008)	5.90 (Lide, 2008)	0
OH	17.01	NH ₄ NO ₃	MC	42.7 (Remorov and Bardwell, 2005)	4.1×10 ⁻⁶		7.11 (Zen et al., 2014)	1.65 (Lide, 2008)	10.70 (Lide, 2008)	0
OH	17.01	NH ₄ HSO ₄	MC	41 (Remorov and Bardwell, 2005)	2.0×10 ⁻⁶		7.11 (Zen et al., 2014)	1.65 (Lide, 2008)	165 (Lide, 2008)	0
OH	17.01	(NH ₄) ₂ SO ₄	MC	43.1 (Remorov and Bardwell, 2005)	4.8×10 ⁻⁶		7.11 (Zen et al., 2014)	1.65 (Lide, 2008)	10 (Lide, 2008)	0
OH	17.01	Ni(100)	ECT	292.9 ^s (Yang and Whitten, 1997)	1.6×10 ³⁹		7.11 (Zen et al., 2014)	1.65 (Lide, 2008)		0
OH	17.01	Ni(111)	ECT	309.6 ^s (Yang and Whitten, 1997)	1.6×10 ⁴²		7.11 (Zen et al., 2014)	1.65 (Lide, 2008)		0
OH	17.01	Fe(110)	ECT	284.5 ^s (Yang and Whitten, 1997)	5.3×10 ³⁷		7.11 (Zen et al., 2014)	1.65 (Lide, 2008)		0
OH	17.01	Ag(110)	DAM	415.9 ^s (Hu and Nakatsuji, 1999)	1.4×10 ⁶¹		7.11 (Zen et al., 2014)	1.65 (Lide, 2008)		0
OH	17.01	Triacontane (solid)	KU	12.7 (Li and Knopf, 2021)	1.8×10 ⁻¹¹		7.11 (Zen et al., 2014)	1.65 (Lide, 2008)	1.91* (Lide, 2008)	0
NO ₃	62.00	oleic acid (monolayer)	K2-SURF	27.8 (Sebastiani et al., 2018)	9.0×10 ⁻⁹		5.15 (Alkorta et al., 2022)		2.34 (Lide, 2008)	0
NO ₃	62.00	palmitoleic acid (monolayer)	K2-SURF	29.5 (Sebastiani et al., 2018)	1.8×10 ⁻⁸		5.15 (Alkorta et al., 2022)		2.34 (Lide, 2008)	0
NO ₃	62.00	methyl oleate (monolayer)	K2-SURF	27.8 (Sebastiani et al., 2018)	9.0×10 ⁻⁹		5.15 (Alkorta et al., 2022)		3.21 (Lide, 2008)	0

				ni et al., 2018)						
NO ₃	62.00	stearic acid (monolayer)	K2-SURF	29.8 (Sebastiani et al., 2018)	2.1×10 ⁻⁸		5.15 (Alkorta et al., 2022)		2.31 (Lide, 2008)	0
O ₃	48.00	BaP/soot	KU	85 (Pöschl et al., 2001)	1.4×10 ²	12.2 (Stull, 1947)	3.21 (Lide, 2008)	0.53 (Mack and Muentner, 1977)	3.52 (Kronberger and Weiss, 1944)	0
O ₃	48.00	graphene, physisorption	DFT	24.1 (Lee et al., 2009)	2.0×10 ⁻⁹	12.2 (Stull, 1947)	3.21 (Lide, 2008)	0.53 (Mack and Muentner, 1977)	13 (Dovbeshko et al., 2015)	0
O ₃	48.00	graphene, chemisorption	DFT	31.8 (Lee et al., 2009)	4.7×10 ⁻⁸	12.2 (Stull, 1947)	3.21 (Lide, 2008)	0.53 (Mack and Muentner, 1977)	13 (Dovbeshko et al., 2015)	0
O, ROI	16.00	BaP/soot	K2-SURF	40 (Shiraiwa et al., 2011b)	1.4×10 ⁻⁶		0.79 (Van Duijnen and Swart, 1998; Cambi et al., 1991)		3.52 (Kronberger and Weiss, 1944)	0
O ₂	32.00	Ir(100)	DFT	187 [§] (Cao et al., 2022)	2.2×10 ²⁰					0

1195

1196 §Not applied in analysis.

1197 *Applied value for the liquid phase of substrate species.

1198

1199 **Table A3.** Compiled adsorbate-substrate interaction energies for reactive and non-reactive gases
1200 on soot of light duty vehicle (LDV) and heavy-duty vehicle (HDV), pyrex glass, steel, salt, mineral,
1201 clay, and highly oriented pyrolyzed graphite (HOPG). Gas species, gas species' molar mass,
1202 substrate, experimental or theoretical method, desorption energy (E_{des}^0), and desorption lifetimes
1203 (τ_{des}) evaluated at 293 K using $A_{des} = 10^{13} \text{ s}^{-1}$, enthalpy of vaporization (ΔH_{vap}), gas species'
1204 polarizability (α), gas species' dipole moment (μ), substrate's relative permittivity (ϵ_r), and gas
1205 species' oxygen to carbon ration ($O:C$) are given.

Gas Species	Molar Mass / g mol ⁻¹	Substrate	Method	E_{des}^0 / kJ mol ⁻¹	$\tau_{des}^{293 K}$ / s	$\Delta H_{vap} (T)$ / kJ mol ⁻¹	α / 10 ⁻²⁴ cm ³	μ / D	ϵ_r	O:C
NO ₂	46.01	soot LDV	KU	54.7 (Messere et al., 2006)	5.6×10 ⁻⁴	18.89	3.02 (Lide, 2008)	0.316 (Lide, 2008)	~13.00 (Dovbeshko et al., 2015)	0
NO ₂	46.01	soot HDV	KU	37.6 (Messere et al., 2006)	5.0×10 ⁻⁷	18.89	3.02 (Lide, 2008)	0.316 (Lide, 2008)	~13.00 (Dovbeshko et al., 2015)	0

				r et al., 2007)					ko et al., 2015)	
NO ₂	46.01	NH ₄ Cl	KU	34 (Takenaka and Rossi, 2005)	1.2×10 ⁻⁷	18.89	3.02 (Lide, 2008)	0.316 (Lide, 2008)	6.90 (Lide, 2008)	0
NO ₂	46.01	HOPG	TDS	37 (Ulbricht et al., 2006)	3.9×10 ⁻⁷	18.89	3.02 (Lide, 2008)	0.316 (Lide, 2008)	13.00 (Dovbeshko et al., 2015)	0
NO ₂	46.01	HOPG	TDS	33 (Ulbricht et al., 2006)	7.6×10 ⁻⁸	18.89	3.02 (Lide, 2008)	0.316 (Lide, 2008)	13.00 (Dovbeshko et al., 2015)	0
NO ₂	46.01	Model coal surface	DFT	12.04 (Wang et al., 2021)	1.4×10 ⁻¹¹	18.89	3.02 (Lide, 2008)	0.316 (Lide, 2008)	13.00 (Dovbeshko et al., 2015)	0
HCl	36.46	pyrex glass	KU	56.7 (Koch et al., 1997)	1.3×10 ⁻³	16.15 (Lide, 2008)	2.7 (Lide, 2008)	1.11 (Lide, 2008)	5.00 (Lide, 2008)	0
HCl	36.46	steel	KU	57.4 (Koch et al., 1997)	1.7×10 ⁻³	16.15 (Lide, 2008)	2.7 (Lide, 2008)	1.11 (Lide, 2008)		0
HCl	36.46	α-Al ₂ O ₃ (0001)	TPD	105 (Nelson et al., 2001)	5.2×10 ⁵	16.15 (Lide, 2008)	2.63 (Lide, 2008)	1.11 (Lide, 2008)	9.34 (Lide, 2008)	0
CO ₂	44.01	graphene	TPD	26.1 (Smith and Kay, 2019)	4.5×10 ⁻⁹	16.4 (Chickos and Acree, 2003)	2.91 (Lide, 2008)	0.0001 (Kolomiitsova et al., 2000)	13.00 (Dovbeshko et al., 2015)	2
CO ₂	44.01	HOPG	TDS	24 (Ulbricht et al., 2006)	1.9×10 ⁻⁹	16.4 (Chickos and Acree, 2003)	2.91 (Lide, 2008)	0.0001 (Kolomiitsova et al., 2000)	13.00 (Dovbeshko et al., 2015)	2
CO ₂	44.01	HOPG	TDS	23 (Ulbricht et al., 2006)	1.3×10 ⁻⁹	16.4 (Chickos and Acree, 2003)	2.91 (Lide, 2008)	0.0001 (Kolomiitsova et al., 2000)	13.00 (Dovbeshko et al., 2015)	2
CO ₂	44.01	Calcite	DFT	29.9 (Budi et al., 2018)	2.1×10 ⁻⁸	16.4 (Chickos and Acree, 2003)	2.91 (Lide, 2008)	0.0001 (Kolomiitsova et al., 2000)	8.67 (Lide, 2008)	2
CO ₂	44.01	Quartz	DFT	6.8 (Budi et al., 2018)	1.6×10 ⁻¹²	16.4 (Chickos and Acree, 2003)	2.91 (Lide, 2008)	0.0001 (Kolomiitsova et al., 2000)	4.42 (Lide, 2008)	2
CO ₂	44.01	kaolinte (Al)	DFT	28.9 (Budi et al., 2018)	1.4×10 ⁻⁸	16.4 (Chickos and Acree, 2003)	2.91 (Lide, 2008)	0.0001 (Kolomiitsova et al., 2000)	5.00 (Robinson et al., 2002)	2
CO ₂	44.01	kaolinite (si)	DFT	9.6 (Budi et al., 2018)	5.1×10 ⁻¹²	16.4 (Chickos and Acree, 2003)	2.91 (Lide, 2008)	0.0001 (Kolomiitsova et al., 2000)	5.00 (Robinson et al., 2002)	2
CO	28.01	HOPG	TDS	13 (Ulbricht et al., 2006)	2.1×10 ⁻¹¹	6.0 (Chickos and Acree, 2003)	1.95 (Lide, 2008)	0.122 (Lide, 2008)	13.00 (Dovbeshko et al., 2015)	1

CO	28.01	Au(111)	MB	11.7 (Borodin et al., 2020)	1.2×10^{-11}	6.0 (Chickos and Acree, 2003)	1.95 (Lide, 2008)	0.122 (Lide, 2008)		1
N ₂	28.01	HOPG	TDS	13 (Ulbricht et al., 2006)	2.1×10^{-11}	5.57 (Lide, 2008)	1.74 (Lide, 2008)	0.001 (Gustafsson and Andersson, 2006)	13.00 (Dovbeshko et al., 2015)	0
SF ₆	146.06	HOPG	TDS	31 (Ulbricht et al., 2006)	3.4×10^{-8}	8.99 (Lide, 2008)	6.54 (Lide, 2008)	0.08 (Bruska and Piechota, 2008)	13.00 (Dovbeshko et al., 2015)	0
SF ₆	146.06	HOPG	TDS	25 (Ulbricht et al., 2006)	2.9×10^{-9}	8.99 (Lide, 2008)	6.54 (Lide, 2008)	0.08 (Bruska and Piechota, 2008)	13.00 (Dovbeshko et al., 2015)	0
O ₂	32.00	HOPG	TDS	12 (Ulbricht et al., 2006)	1.4×10^{-11}	6.82 (Lide, 2008)	1.57 (Lide, 2008)	0.002 (on metal) (Gustafsson and Andersson, 2006)	13.00 (Dovbeshko et al., 2015)	0
O ₂	32.00	HOPG	TDS	9 (Ulbricht et al., 2006)	4.0×10^{-12}	6.82 (Lide, 2008)	1.57 (Lide, 2008)	0.002 (on metal) (Gustafsson and Andersson, 2006)	13.00 (Dovbeshko et al., 2015)	0
Xenon	131.29	HOPG	TD	24 (Ulbricht et al., 2006)	1.9×10^{-9}	12.57 (Lide, 2008)	4.04 (Cambi et al., 1991)	0	13.00 (Dovbeshko et al., 2015)	0
Xenon	131.29	HOPG	TD	18 (Ulbricht et al., 2006)	1.6×10^{-10}	12.57 (Lide, 2008)	4.04 (Cambi et al., 1991)	0	13.00 (Dovbeshko et al., 2015)	0

1206

1207 **Table A4.** Compiled adsorbate-substrate interaction energies for organic gases on self-assembled
1208 monolayers, salt, fly ash, and urban aerosol. Gas species, gas species' molar mass, substrate,
1209 experimental or theoretical method, desorption energy (E_{des}^0), and desorption lifetimes (τ_{des})
1210 evaluated at 293 K using $A_{des} = 10^{13} \text{ s}^{-1}$, enthalpy of vaporization (ΔH_{vap}), gas species'
1211 polarizability (α), gas species' dipole moment (μ), substrate's relative permittivity (ϵ_r), and gas
1212 species' oxygen to carbon ration ($O:C$) are given.

Gas Species	Molar Mass / g mol ⁻¹	Substrate	Method	E_{des}^0 / kJ mol ⁻¹	$\tau_{des}^{293 K}$ / s	$\Delta H_{vap} (T)$ / kJ mol ⁻¹	α / 10 ⁻²⁴ cm ³	μ / D	ϵ_r	O:C
methanol	32.04	thin nopinone	MB	17.4 (Kong et al., 2021)	1.3×10^{-10}	37.8 (Chickos and Acree, 2003)	3.28 (Lide, 2008)	1.7 (Lide, 2008)		1
methanol	32.04	multilayer nopinone	MB	17.4 (Kong et al., 2021)	1.3×10^{-10}	37.8 (Chickos and Acree, 2003)	3.28 (Lide, 2008)	1.7 (Lide, 2008)		1

methanol	32.04	SAM-methyl	TPD	47.7 (Dubois et al., 1990)	3.2×10^{-5}	37.8 (Chickos and Acree, 2003)	3.28 (Lide, 2008)	1.7 (Lide, 2008)	4.1 (Milla ny and Jonsc her, 1980)	1
methanol	32.04	SAM-acid	TPD	35.1 (Dubois et al., 1990)	1.8×10^{-7}	37.8 (Chickos and Acree, 2003)	3.28 (Lide, 2008)	1.7 (Lide, 2008)	2.1 (Akke rman et al., 2007)	1
methanol	32.04	SAM-amide	TPD	41.0 (Dubois et al., 1990)	2.0×10^{-6}	37.8 (Chickos and Acree, 2003)	3.28 (Lide, 2008)	1.7 (Lide, 2008)		1
n-hexane	86.18	SAM-methyl	TPD	38.5 (Dubois et al., 1990)	7.3×10^{-7}	31.5 (Chickos and Acree, 2003)	11.9 (Lide, 2008)	0 (Yaws, 2014)	4.1 (Milla ny and Jonsc her, 1980)	0
n-hexane	86.18	SAM-acid	TPD	33.9 (Dubois et al., 1990)	1.1×10^{-7}	31.5 (Chickos and Acree, 2003)	11.9 (Lide, 2008)	0 (Yaws, 2014)	2.1 (Akke rman et al., 2007)	0
anthracene	178.23	NaCl	TD	18 (Chu et al., 2010)	1.6×10^{-10}	79.6 (Chickos and Acree, 2003)	25.665 (Lide, 2008)	0 (Yaws, 2014)	5.9 (Lide, 2008)	0
pyrene	202.26	NaCl	TD	19.6 (Chu et al., 2010)	3.1×10^{-10}	78.6 (Chickos and Acree, 2003)	28.22 (Lide, 2008)	0 (Yaws, 2014)	5.9 (Lide, 2008)	0
benzo(a)pyrene	252.32	NaCl	TD	22.8 (Chu et al., 2010)	1.2×10^{-9}	91 (Chickos and Acree, 2003)	35.8 (Mceachran et al., 2018)	0 (Yaws, 2014)	5.9 (Lide, 2008)	0
perylene		NaCl	TD	123.5 (Steiner and Burtscher, 1994)	1.0×10^9	78.6 (Chickos and Acree, 2003)	35.8 (Mceachran et al., 2018)	0 (Yaws, 2014)	5.9 (Lide, 2008)	0
phenanthrene	178.23	fly ash	GC	24.3 (Lee and Chen, 1995)	2.2×10^{-9}	78.7 (Chickos and Acree, 2003)	30.75 (Lide, 2008)	0 (Yaws, 2014)	~5 (Shari f, 1995)	0
pyrene	202.26	fly ash	GC	26.6 (Lee and Chen, 1995)	5.5×10^{-9}	78.6 (Chickos and Acree, 2003)	28.22 (Lide, 2008)	0 (Yaws, 2014)	~5 (Shari f, 1995)	0
benzo(a)pyrene	252.33	fly ash	TD	31.2 (Chu et al., 2010)	3.7×10^{-8}	91 (Chickos and Acree, 2003)	35.8 (Mceachran et al., 2018)	0 (Yaws, 2014)	~5 (Shari f, 1995)	0
phenanthrene/ anthracene		urban aerosol	TD	18.9 (Yamasaki et al., 1982; Pankow, 1991)	2.3×10^{-10}			0 (Yaws, 2014)		0

pyrene	202.26	urban aerosol	TD	20.4 (Yamasaki et al., 1982; Pankow, 1991)	4.3×10^{-10}	78.6 (Chickos and Acree, 2003)	28.22 (Lide, 2008)	0 (Yaws, 2014)		0
benzo(a)pyrene/benzo(e)pyrene		urban aerosol	TD	22.3 (Yamasaki et al., 1982; Pankow, 1991)	9.5×10^{-10}			0 (Yaws, 2014)		0
perylene	252.32	carbon	TD	136.5 (Steiner and Burtscher, 1994)	2.2×10^{11}	123.1 (Chickos and Acree, 2003)	35.8 (Mceachran et al., 2018)	0 (Yaws, 2014)	13 (Dovbeshko et al., 2015)	0
perylene	252.32	diesel soot	TD	139 (Steiner and Burtscher, 1994)	6.0×10^{11}	123.1 (Chickos and Acree, 2003)	35.8 (Mceachran et al., 2018)	0 (Yaws, 2014)	13 (Dovbeshko et al., 2015)	0
perylene	252.32	oil burner soot	TD	140 (Steiner and Burtscher, 1994)	9.1×10^{11}	123.1 (Chickos and Acree, 2003)	35.8 (Mceachran et al., 2018)	0 (Yaws, 2014)	13 (Dovbeshko et al., 2015)	0

1213

1214 **Table A5.** Compiled adsorbate-substrate interaction energies of volatile organic compounds
1215 (VOCs) on graphite (C(0001)), highly oriented pyrolytic graphite (HOPG), granular activated
1216 carbon (GAC), and soot from combustion of kerosene. Gas species, gas species' molar mass,
1217 substrate, experimental or theoretical method, desorption energy (E_{des}^0), and desorption lifetimes
1218 (τ_{des}) evaluated at 293 K using $A_{des} = 10^{13} \text{ s}^{-1}$, enthalpy of vaporization (ΔH_{vap}), gas species'
1219 polarizability (α), gas species' dipole moment (μ), substrate's relative permittivity (ϵ_r), and gas
1220 species' oxygen to carbon ration ($O:C$) are given.

Gas Species	Molar Mass / g mol^{-1}	Substrate	Method	E_{des}^0 / kJ mol^{-1}	$\tau_{des}^{293 \text{ K}}$ / s	ΔH_{vap} (T) / kJ mol^{-1}	α / 10^{-24} cm^3	μ / D	ϵ_r	O:C
methane	16.04	graphite	TPD	14.1 (Tait et al., 2006)	3.3×10^{-11}	8.5 (Chickos and Acree, 2003)	2.59 (Lide, 2008)	0 (Yaws, 2014)	13.0 (Dovbeshko et al., 2015)	0
ethane	30.07	graphite	TPD	24.6 (Tait et al., 2006)	2.4×10^{-9}	15.3 (Chickos and Acree, 2003)	4.45 (Lide, 2008)	0 (Yaws, 2014)	13.0 (Dovbeshko et al., 2015)	0
propane	44.10	graphite	TPD	32.1 (Tait et al., 2006)	5.3×10^{-8}	18.8 (Chickos and Acree, 2003)	6.33 (Lide, 2008)	0 (Yaws, 2014)	13.0 (Dovbeshko et al., 2015)	0
butane	58.12	graphite	TPD	40.8 (Tait et al., 2006)	1.9×10^{-6}	22.4 (Chickos and Acree, 2003)	8.2 (Lide, 2008)	0 (Yaws, 2014)	13.0 (Dovbeshko et al., 2015)	0
pentane	72.15	graphite	TPD	65 (Paserba and	3.9×10^{-2}	25 (Chickos and Acree, 2003)	9.99 (Lide, 2008)	0 (Yaws, 2014)	13.0 (Dovbeshko	0

				Gellman, 2001)					o et al., 2015)	
hexane	86.18	graphite	TPD	63 (Tait et al., 2006)	1.7×10^{-2}	31.5 (Chickos and Acree, 2003)	11.9 (Lide, 2008)	0 (Yaws, 2014)	13.0 (Dovbeshko et al., 2015)	0
hexane	86.18	graphite	TPD	73.6 (Paserba and Gellman, 2001)	1.3	31.5 (Chickos and Acree, 2003)	11.9 (Lide, 2008)	0 (Yaws, 2014)	13.0 (Dovbeshko et al., 2015)	0
heptane	100.21	graphite	TPD	81.5 (Paserba and Gellman, 2001)	3.4×10^1	36.6 (Chickos and Acree, 2003)	13.61 (Lide, 2008)	0 (Yaws, 2014)	13.0 (Dovbeshko et al., 2015)	0
octane	114.23	graphite	TPD	72.6 (Tait et al., 2006)	8.8×10^{-1}	41.6 (Chickos and Acree, 2003)	15.9 (Lide, 2008)	0 (Yaws, 2014)	13.0 (Dovbeshko et al., 2015)	0
octane	114.23	graphite	TPD	88.2 (Paserba and Gellman, 2001)	5.3×10^2	41.6 (Chickos and Acree, 2003)	15.9 (Lide, 2008)	0 (Yaws, 2014)	13.0 (Dovbeshko et al., 2015)	0
decane	142.29	graphite	TPD	91.4 (Tait et al., 2006)	2.0×10^3	51.4 (Chickos and Acree, 2003)	19.1 (Lide, 2008)	0 (Yaws, 2014)	13.0 (Dovbeshko et al., 2015)	0
decane	142.29	graphite	TPD	101 (Paserba and Gellman, 2001)	1.0×10^5	51.4 (Chickos and Acree, 2003)	19.1 (Lide, 2008)	0 (Yaws, 2014)	13.0 (Dovbeshko et al., 2015)	0
dodecane	170.33	graphite	TPD	114.8 (Paserba and Gellman, 2001)	2.9×10^7	62.1 (Chickos and Acree, 2003)	22.75 (Lide, 2008)	0 (Yaws, 2014)	13.0 (Dovbeshko et al., 2015)	0
tetradecane	198.39	graphite	TPD	124.7 (Paserba and Gellman, 2001)	1.7×10^9	72.1 (Chickos and Acree, 2003)	26.22 (Laib and Mittleman, 2010)	0 (Yaws, 2014)	13.0 (Dovbeshko et al., 2015)	0
hexadecane	226.41	graphite	TPD	134.3 (Paserba and Gellman, 2001)	8.7×10^{10}	81.4 (Chickos and Acree, 2003)	29.84 (Laib and Mittleman, 2010)	0 (Yaws, 2014)	13.0 (Dovbeshko et al., 2015)	0
octadecane	254.50	graphite	TPD	146.7 (Paserba and Gellman, 2001)	1.4×10^{13}	91.8 (Chickos and Acree, 2003)	33.46 (Laib and Mittleman, 2010)	0 (Yaws, 2014)	13.0 (Dovbeshko et al., 2015)	0
icosane	282.55	graphite	TPD	156.2 (Paserba and Gellman, 2001)	7.0×10^{14}	100 (Chickos and Acree, 2003)	37.08 (Laib and Mittleman, 2010)	0 (Yaws, 2014)	13.0 (Dovbeshko et al., 2015)	0

docosane	310.61	graphite	TPD	166.2 (Paserba and Gellman, 2001)	4.3×10^{16}	115.6 (Chickos and Acree, 2003)	40.7 (Laib and Mittleman, 2010)	0 (Yaws, 2014)	13.0 (Dovbeshk o et al., 2015)	0
tetracosane	338.65	graphite	TPD	174.2 (Paserba and Gellman, 2001)	1.1×10^{18}	126.8 (Chickos and Acree, 2003)	44.32 (Laib and Mittleman, 2010)	0 (Yaws, 2014)	13.0 (Dovbeshk o et al., 2015)	0
hexacosane	366.71	graphite	TPD	182.3 (Paserba and Gellman, 2001)	3.2×10^{19}	106.1 (Chickos and Acree, 2003)	47.94 (Laib and Mittleman, 2010)	0 (Yaws, 2014)	13.0 (Dovbeshk o et al., 2015)	0
octacosane	396.79	graphite	TPD	190.7 (Paserba and Gellman, 2001)	9.9×10^{20}	150.8 (Chickos and Acree, 2003)	51.56 (Laib and Mittleman, 2010)	0 (Yaws, 2014)	13.0 (Dovbeshk o et al., 2015)	0
dotriacontane	452.88	graphite	TPD	205.5 (Paserba and Gellman, 2001)	4.3×10^{23}	130.5 (Chickos and Acree, 2003)	58.8 (Laib and Mittleman, 2010)	0 (Yaws, 2014)	13.0 (Dovbeshk o et al., 2015)	0
hexatriacontane	506.97	graphite	TPD	219.6 (Paserba and Gellman, 2001)	1.4×10^{26}	157 (Chickos and Acree, 2003)	66.04 (Laib and Mittleman, 2010)	0 (Yaws, 2014)	13.0 (Dovbeshk o et al., 2015)	0
tetracontane	563.08	graphite	TPD	232.9 (Paserba and Gellman, 2001)	3.3×10^{28}	132.2 (Chickos and Acree, 2003)	73.28 (Laib and Mittleman, 2010)	0 (Yaws, 2014)	13.0 (Dovbeshk o et al., 2015)	0
tetratetracontane	619.19	graphite	TPD	246.2 (Paserba and Gellman, 2001)	7.8×10^{30}	140.1 (Chickos and Acree, 2003)	80.52 (Laib and Mittleman, 2010)	0 (Yaws, 2014)	13.0 (Dovbeshk o et al., 2015)	0
octatetracontane	677.31	graphite	TPD	256.7 (Paserba and Gellman, 2001)	5.8×10^{32}	145.9 (Chickos and Acree, 2003)	87.76 (Laib and Mittleman, 2010)	0 (Yaws, 2014)	13.0 (Dovbeshk o et al., 2015)	0
hexapentacontane	787.50	graphite	TPD	280.5 (Paserba and Gellman, 2001)	1.0×10^{37}	157.8 (Chickos and Acree, 2003)	102.24 (Laib and Mittleman, 2010)	0 (Yaws, 2014)	13.0 (Dovbeshk o et al., 2015)	0
hexacontane	843.61	graphite	TPD	289 (Paserba and Gellman, 2001)	3.3×10^{38}	163 (Chickos and Acree, 2003)	109.48 (Laib and Mittleman, 2010)	0 (Yaws, 2014)	13.0 (Dovbeshk o et al., 2015)	0
methanol (monomer)	32.04	graphite	MB	17.4 (Kong et al., 2021)	1.3×10^{-10}	37.8 (Chickos and Acree, 2003)	3.28 (Laib and Mittleman, 2010)	1.7 (Lide, 2008)	13.0 (Dovbeshk o et al., 2015)	1

methanol (clusters)	32.04	graphite	MB	34.7 (Kong et al., 2019)	1.5×10^{-7}	37.8 (Chickos and Acree, 2003)	3.28 (Laib and Mittleman, 2010)	1.7 (Lide, 2008)	13.0 (Dovbeshko et al., 2015)	1
methanol (monomer)	32.04	graphene	DFT	20.6 (Schroder, 2013)	4.7×10^{-10}	37.8 (Chickos and Acree, 2003)	3.28 (Laib and Mittleman, 2010)	1.7 (Lide, 2008)	13.0 (Dovbeshko et al., 2015)	1
methanol (3 cluster)	32.04	graphene	DFT	30.4 (Schroder, 2013)	2.6×10^{-8}	37.8 (Chickos and Acree, 2003)	3.28 (Laib and Mittleman, 2010)	1.7 (Lide, 2008)	13.0 (Dovbeshko et al., 2015)	1
methanol (5 cluster)	32.04	graphene	DFT	34.9 (Schroder, 2013)	1.7×10^{-7}	37.8 (Chickos and Acree, 2003)	3.28 (Laib and Mittleman, 2010)	1.7 (Lide, 2008)	13.0 (Dovbeshko et al., 2015)	1
methane	16.04	HOPG	TDS	17 (Ulbricht et al., 2006)	1.1×10^{-10}	8.5 (Chickos and Acree, 2003)	2.59 (Laib and Mittleman, 2010)	0 (Yaws, 2014)	13.0 (Dovbeshko et al., 2015)	0
methanol	32.04	HOPG	TDS	48 (Ulbricht et al., 2006)	3.6×10^{-5}	37.8 (Chickos and Acree, 2003)	3.28 (Laib and Mittleman, 2010)	1.7 (Lide, 2008)	13.0 (Dovbeshko et al., 2015)	1
ethanol	46.07	HOPG	TDS	50 (Ulbricht et al., 2006)	8.2×10^{-5}	42.4 (Chickos and Acree, 2003)	5.26 (Laib and Mittleman, 2010)	1.69 (Lide, 2008)	13.0 (Dovbeshko et al., 2015)	0.5
1,1-dichloroethane	98.96	HOPG	TDS	51 (Ulbricht et al., 2006)	1.2×10^{-4}	33.5 (Chickos and Acree, 2003)	8.64 (Laib and Mittleman, 2010)	2.06 (Lide, 2008)	13.0 (Dovbeshko et al., 2015)	0
trichloromethane	119.38	HOPG	TDS	54 (Ulbricht et al., 2006)	4.2×10^{-4}	31.1 (Chickos and Acree, 2003)	8.87 (Laib and Mittleman, 2010)	1.04 (Lide, 2008)	13.0 (Dovbeshko et al., 2015)	0
benzene	78.11	HOPG	TDS	48 (Ulbricht et al., 2006)	3.6×10^{-5}	42.3 (Chickos and Acree, 2003)	10.53 (Laib and Mittleman, 2010)	0 (Yaws, 2014)	13.0 (Dovbeshko et al., 2015)	0
n,n-dimethylformamide	73.09	HOPG	TDS	53 (Ulbricht et al., 2006)	2.8×10^{-4}	46.9 (Chickos and Acree, 2003)	7.93 (Bosque and Sales, 2002)	3.82 (Lide, 2008)	13.0 (Dovbeshko et al., 2015)	0
ethylbenzene	106.17	HOPG	TDS	79 (Ulbricht et al., 2006)	1.2×10^1	42.3 (Chickos and Acree, 2003)	14.2 (Laib and Mittleman, 2010)	0.59 (Lide, 2008)	13.0 (Dovbeshko et al., 2015)	0
toluene	92.14	HOPG	TDS	68 (Ulbricht et al., 2006)	1.3×10^{-1}	38.9 (Chickos and Acree, 2003)	12.12 (Laib and Mittleman, 2010)	0.375 (Lide, 2008)	13.0 (Dovbeshko et al., 2015)	0
sigma-dichlorobenzene	147.01	HOPG	TDS	69 (Ulbricht et al., 2006)	2.0×10^{-1}	50.9 (Chickos and Acree, 2003)	14.3 (Mceachran et al., 2018)	2.5 (Lide, 2008)	13.0 (Dovbeshko et al., 2015)	0
naphthalene	128.17	HOPG	TDS	77 (Ulbricht et al., 2006)	5.3	53.4 (Chickos and Acree, 2003)	17 (Laib and Mittleman, 2010)	0 (Yaws, 2014)	13.0 (Dovbeshko et al., 2015)	0

coronene	300.35	HOPG	TDS	127 (Ulbricht et al., 2006)	4.4×10^9	148 (Chickos and Acree, 2003)	42.5 (Laib and Mittleman, 2010)	0 (Yaws, 2014)	13.0 (Dovbeshko et al., 2015)	0
fullerene	720.66	HOPG	TDS	163 (Ulbricht et al., 2006)	1.1×10^{16}	42.4 (Chickos and Acree, 2003)	76.5	0 (Yaws, 2014)	13.0 (Dovbeshko et al., 2015)	0
ovalene	398.45	HOPG	TDS	230 (Ulbricht et al., 2006)	1.0×10^{28}	31.6 (Chickos and Acree, 2003)	45.8	0 (Yaws, 2014)	13.0 (Dovbeshko et al., 2015)	0
ethanol	46.07	GAC	TG-DSC	56.8 (Giraudet et al., 2006)	1.3×10^{-3}	31.3 (Chickos and Acree, 2003)	5.26 (Lide, 2008)	1.69 (Lide, 2008)	13.0 (Dovbeshko et al., 2015)	0.5
acrylnitrile	53.06	GAC	TG-DSC	49 (Giraudet et al., 2006)	5.4×10^{-5}	28.8 (Chickos and Acree, 2003)	8.05 (Lide, 2008)	3.87 (Lide, 2008)	13.0 (Dovbeshko et al., 2015)	0
acetone	58.08	GAC	TG-DSC	51.1 (Giraudet et al., 2006)	1.3×10^{-4}	47.45 (Chickos and Acree, 2003)	6.37 (Lide, 2008)	2.88 (Lide, 2008)	13.0 (Dovbeshko et al., 2015)	0.33
dichloromethane	84.93	GAC	TG-DSC	45.6 (Giraudet et al., 2006)	1.3×10^{-5}	31.6 (Chickos and Acree, 2003)	7.21 (Lide, 2008)	1.6 (Lide, 2008)	13.0 (Dovbeshko et al., 2015)	0
propanol	60.09	GAC	TG-DSC	52.6 (Giraudet et al., 2006)	2.4×10^{-4}	33.1 (Chickos and Acree, 2003)	6.74 (Lide, 2008)	2.52 (Lide, 2008)	13.0 (Dovbeshko et al., 2015)	0.33
ethyl formate	74.08	GAC	TG-DSC	52 (Giraudet et al., 2006)	1.9×10^{-4}	42.3 (Chickos and Acree, 2003)	6.88 (Lide, 2008)	1.9 (Lide, 2008)	13.0 (Dovbeshko et al., 2015)	0.67
cyclohexane	84.16	GAC	TG-DSC	55.7 (Giraudet et al., 2006)	8.5×10^{-4}	34.5 (Chickos and Acree, 2003)	10.87 (Lide, 2008)	0.61 (Yaws, 2014)	13.0 (Dovbeshko et al., 2015)	0
benzene	78.11	GAC	TG-DSC	56.7 (Giraudet et al., 2006)	1.3×10^{-3}	34.7 (Chickos and Acree, 2003)	10.53 (Lide, 2008)	0 (Yaws, 2014)	13.0 (Dovbeshko et al., 2015)	0
fluorobenzene	96.10	GAC	TG-DSC	57.4 (Giraudet et al., 2006)	1.7×10^{-3}	36.9 (Chickos and Acree, 2003)	10.3 (Lide, 2008)	1.6 (Lide, 2008)	13.0 (Dovbeshko et al., 2015)	0
methylethylketone	72.11	GAC	TG-DSC	58 (Giraudet et al., 2006)	2.2×10^{-3}	30.6 (Chickos and Acree, 2003)	8.19 (Nist, 2018)	2.78 (Lide, 2008)	13.0 (Dovbeshko et al., 2015)	0.25
3-methylbutane-2-one	86.13	GAC	TG-DSC	60.7 (Giraudet et al., 2006)	6.6×10^{-3}	31.5 (Chickos and Acree, 2003)	10.02 (Bosque and Sales, 2002)	2.77 (Lide, 2008)	13.0 (Dovbeshko et al., 2015)	0.2
hex-1-ene	84.16	GAC	TG-DSC	62.9 (Giraudet et al., 2006)	1.6×10^{-2}	32.1 (Chickos and Acree, 2003)	11.65 (Lide, 2008)	0.4	13.0 (Dovbeshko et al., 2015)	0

hexane	86.18	GAC	TG-DSC	63.4 (Giraudet et al., 2006)	2.0×10^{-2}	34.9 (Chickos and Acree, 2003)	11.9 (Lide, 2008)	0 (Yaws, 2014)	13.0 (Dovbeshko et al., 2015)	0
isopropylether	102.18	GAC	TG-DSC	65.9 (Giraudet et al., 2006)	5.6×10^{-2}	42.4 (Chickos and Acree, 2003)	12.65 (Bosque and Sales, 2002)	1.13 (Lide, 2008)	13.0 (Dovbeshko et al., 2015)	0.17
triethylamine	101.19	GAC	TG-DSC	74.1 (Giraudet et al., 2006)	1.6	31.6 (Chickos and Acree, 2003)	7.97 (Lide, 2008)	0.66 (Lide, 2008)	13.0 (Dovbeshko et al., 2015)	0
phenanthrene	178.23	kerosene soot	KU	85.6 (Guilloteau et al., 2010)	1.8×10^2	78.7 (Chickos and Acree, 2003)	30.75 (Lide, 2008)	0 (Yaws, 2014)	13.0 (Dovbeshko et al., 2015)	0
anthracene	178.23	kerosene soot	KU	88.1 (Guilloteau et al., 2010)	5.1×10^2	79.6 (Chickos and Acree, 2003)	25.67 (Lide, 2008)	0 (Yaws, 2014)	13.0 (Dovbeshko et al., 2015)	0
fluoranthene	202.26	kerosene soot	KU	93.9 (Guilloteau et al., 2008)	5.5×10^3	79.3 (Chickos and Acree, 2003)	23.23	0.23 (Yaws, 2014)	13.0 (Dovbeshko et al., 2015)	0
pyrene	202.26	kerosene soot	KU	95.2 (Guilloteau et al., 2008)	9.4×10^3	78.6 (Chickos and Acree, 2003)	28.22 (Lide, 2008)	0 (Yaws, 2014)	13.0 (Dovbeshko et al., 2015)	0
benzo(ghi)fluoranthene	226.28	kerosene soot	KU	112.1 (Guilloteau et al., 2010)	9.6×10^6	88.5 (Chickos and Acree, 2003)	32.9 (Mceachran et al., 2018)	0 (Yaws, 2014)	13.0 (Dovbeshko et al., 2015)	0
acepyrene	226.27	kerosene soot	KU	107.1 (Guilloteau et al., 2010)	1.2×10^6		31.6 (Mceachran et al., 2018)	0 (Yaws, 2014)	13.0 (Dovbeshko et al., 2015)	0
benzo(a)anthracene	228.29	kerosene soot	KU	113.9 (Guilloteau et al., 2010)	2.0×10^7	91 (Chickos and Acree, 2003)	32.86 (Lide, 2008)	0 (Yaws, 2014)	13.0 (Dovbeshko et al., 2015)	0
chrysene	228.29	kerosene soot	KU	114.9 (Guilloteau et al., 2010)	3.0×10^7	89.6 (Chickos and Acree, 2003)	33.06 (Lide, 2008)	0 (Yaws, 2014)	13.0 (Dovbeshko et al., 2015)	0
benzo(e)pyrene	252.32	kerosene soot	KU	119.9 (Guilloteau et al., 2010)	2.4×10^8	92 (Chickos and Acree, 2003)	35.8 (Mceachran et al., 2018)	0 (Yaws, 2014)	13.0 (Dovbeshko et al., 2015)	0
benzo(b)fluoranthene	252.31	kerosene soot	KU	118.7 (Guilloteau et al., 2010)	1.4×10^8	89.7 (Chickos and Acree, 2003)	35.8 (Mceachran et al., 2018)	0 (Yaws, 2014)	13.0 (Dovbeshko et al., 2015)	0
benzo(k)fluoranthene	252.32	kerosene soot	KU	120.8 (Guilloteau et al., 2010)	3.4×10^8	88.5 (Chickos and Acree, 2003)	35.8 (Mceachran et al., 2018)	0 (Yaws, 2014)	13.0 (Dovbeshko et al., 2015)	0
benzo(a)pyrene	252.32	kerosene soot	KU	121.8 (Guilloteau et al., 2010)	5.2×10^8	91 (Chickos and Acree, 2003)	35.8 (Mceachran et al., 2018)	0 (Yaws, 2014)	13.0 (Dovbeshko et al., 2015)	0

1222 **Table A6.** Compiled adsorbate-substrate interaction energies of volatile organic compounds
1223 (VOCs) on MgO(100), Pt(111), Ni(111), and Pd(111). Gas species, gas species' molar mass,
1224 substrate, experimental or theoretical method, desorption energy (E_{des}^0), and desorption lifetimes
1225 (τ_{des}) evaluated at 293 K using $A_{des} = 10^{13} \text{ s}^{-1}$, enthalpy of vaporization (ΔH_{vap}), gas species'
1226 polarizability (α), gas species' dipole moment (μ), substrate's relative permittivity (ϵ_r), and gas
1227 species' oxygen to carbon ration ($O:C$) are given.

Gas Species	Molar Mass / g mol ⁻¹	Substrate	Method	E_{des}^0 / kJ mol ⁻¹	$\tau_{des}^{293 K}$ / s	ΔH_{vap} (T) / kJ mol ⁻¹	α / 10 ⁻²⁴ cm ³	μ / D	ϵ_r	O:C
methane	16.04	MgO(100)	TPD	12.1 (Tait et al., 2006)	1.4×10^{-11}	8.5 (Chickos and Acree, 2003)	2.59 (Lide, 2008)	0 (Yaws, 2014)	9.65 (Lide, 2008)	0
ethane	30.07	MgO(100)	TPD	22.2 (Tait et al., 2006)	9.1×10^{-10}	15.3 (Chickos and Acree, 2003)	4.45 (Lide, 2008)	0 (Yaws, 2014)	9.65 (Lide, 2008)	0
propane	44.10	MgO(100)	TPD	29 (Tait et al., 2006)	1.5×10^{-8}	18.8 (Chickos and Acree, 2003)	6.33 (Lide, 2008)	0 (Yaws, 2014)	9.65 (Lide, 2008)	0
butane	58.12	MgO(100)	TPD	34.9 (Tait et al., 2006)	1.7×10^{-7}	22.4 (Chickos and Acree, 2003)	8.2 (Lide, 2008)	0 (Yaws, 2014)	9.65 (Lide, 2008)	0
hexane	86.18	MgO(100)	TPD	46.4 (Tait et al., 2006)	1.9×10^{-5}	31.5 (Chickos and Acree, 2003)	11.9 (Lide, 2008)	0 (Yaws, 2014)	9.65 (Lide, 2008)	0
octane	114.23	MgO(100)	TPD	62.9 (Tait et al., 2006)	1.6×10^{-2}	41.6 (Chickos and Acree, 2003)	15.9 (Lide, 2008)	0 (Yaws, 2014)	9.65 (Lide, 2008)	0
decane	142.29	MgO(100)	TPD	77.9 (Tait et al., 2006)	7.7	51.4 (Chickos and Acree, 2003)	19.1 (Lide, 2008)	0 (Yaws, 2014)	9.65 (Lide, 2008)	0
methane	16.04	Pt(111)	TPD	15.2 (Tait et al., 2006)	5.1×10^{-11}	8.5 (Chickos and Acree, 2003)	2.59 (Lide, 2008)	0 (Yaws, 2014)		0
methane	16.04	Pt(111)	TPD	16.1 (Weaver et al., 2003)	7.4×10^{-11}	8.5 (Chickos and Acree, 2003)	2.59 (Lide, 2008)	0 (Yaws, 2014)		0
ethane	30.07	Pt(111)	TPD	28.9 (Tait et al., 2006)	1.4×10^{-8}	15.3 (Chickos and Acree, 2003)	4.45 (Lide, 2008)	0 (Yaws, 2014)		0
ethane	30.07	Pt(111)	TPD	36.8 (Weaver et al., 2003)	3.6×10^{-7}	15.3 (Chickos and Acree, 2003)	4.45 (Lide, 2008)	0 (Yaws, 2014)		0
propane	44.10	Pt(111)	TPD	41.5 (Tait et al., 2006)	2.5×10^{-6}	18.8 (Chickos and Acree, 2003)	6.33 (Lide, 2008)	0 (Yaws, 2014)		0

propane	44.10	Pt(111)	TPD	41.2 (Weaver et al., 2003)	2.2×10^{-6}	18.8 (Chickos and Acree, 2003)	6.33 (Lide, 2008)	0 (Yaws, 2014)		0
butane	58.12	Pt(111)	TPD	50.9 (Tait et al., 2006)	1.2×10^{-4}	22.4 (Chickos and Acree, 2003)	8.2 (Lide, 2008)	0 (Yaws, 2014)		0
butane	58.12	Pt(111)	TPD	60.2 (Weaver et al., 2003)	5.4×10^{-3}	22.4 (Chickos and Acree, 2003)	8.2 (Lide, 2008)	0 (Yaws, 2014)		0
butane	58.12	Pt(111)	TPD	34.3 (Salmeron and Somorjai, 1981)	1.3×10^{-7}	22.4 (Chickos and Acree, 2003)	8.2 (Lide, 2008)	0 (Yaws, 2014)		0
pentane	72.15	Pt(111)	TPD	42.7 (Salmeron and Somorjai, 1981)	4.1×10^{-6}	25 (Chickos and Acree, 2003)	9.99 (Lide, 2008)	0 (Yaws, 2014)		0
hexane	86.18	Pt(111)	TPD	79.8 (Tait et al., 2006)	1.7×10^1	31.5 (Chickos and Acree, 2003)	11.9 (Lide, 2008)	0 (Yaws, 2014)		0
hexane	86.18	Pt(111)	TPD	61.9 (Bishop et al., 2000)	1.1×10^{-2}	31.5 (Chickos and Acree, 2003)	11.9 (Lide, 2008)	0 (Yaws, 2014)		0
heptane	100.21	Pt(111)	TPD	66.4 (Bishop et al., 2000)	6.9×10^{-2}	36.6 (Chickos and Acree, 2003)	13.61 (Lide, 2008)	0 (Yaws, 2014)		0
octane	114.23	Pt(111)	TPD	72 (Bishop et al., 2000)	6.8×10^{-1}	41.6 (Chickos and Acree, 2003)	15.9 (Lide, 2008)	0 (Yaws, 2014)		0
nonane	128.20	Pt(111)	TPD	74.2 (Bishop et al., 2000)	1.7	46.55 (Chickos and Acree, 2003)	17.36 (Lide, 2008)	0 (Yaws, 2014)		0
decane	142.29	Pt(111)	TPD	76.1 (Bishop et al., 2000)	3.7	51.4 (Chickos and Acree, 2003)	19.1 (Lide, 2008)	0 (Yaws, 2014)		0
propane	44.10	Ni(111)	DFT	57.9 (Mendes et al., 2019)	1.4×10^8	18.8 (Chickos and Acree, 2003)	6.33 (Lide, 2008)	0 (Yaws, 2014)		0
1-propanol	60.09	Ni(111)	DFT	92.6 (Mendes et al., 2019)	3.3×10^3	47.45 (Chickos and Acree, 2003)	6.74 (Lide, 2008)	1.58 (Lide, 2008)		0.33
2-propanol	60.09	Ni(111)	DFT	89.7 (Mendes et al., 2019)	9.9×10^2	47.45 (Chickos and Acree, 2003)	6.74 (Lide, 2008)	1.58 (Lide, 2008)		0.33
1,2-propanediol	76.09	Ni(111)	DFT	111.0 (Mendes et al., 2019)	6.0×10^6	60.0 (Chickos)	7.55 (Bosque)	2.25 (Lide, 2008)		0.66

						and Acree, 2003)	and Sales, 2002)			
1,3-propanediol	76.09	Ni(111)	DFT	111.0 (Mendes et al., 2019)	6.0×10^6	72.4 (Chickos and Acree, 2003)	7.55 (Bosque and Sales, 2002)	2.55 (Lide, 2008)		0.66
glycerol	92.09	Ni(111)	DFT	118.7 (Mendes et al., 2019)	1.4×10^8	91.7 (Chickos and Acree, 2003)	8.14 (Bosque and Sales, 2002)	2.56 (Lide, 2008)		1
propane	44.10	Pd(111)	DFT	57.9 (Mendes et al., 2019)	2.1×10^{-3}	18.8 (Chickos and Acree, 2003)	6.33 (Lide, 2008)	0 (Yaws, 2014)		0
1-propanol	60.09	Pd(111)	DFT	84.9 (Mendes et al., 2019)	1.4×10^2	47.45 (Chickos and Acree, 2003)	6.74 (Lide, 2008)	1.58 (Lide, 2008)		0.33
2-propanol	60.09	Pd(111)	DFT	85.9 (Mendes et al., 2019)	2.0×10^2	47.45 (Chickos and Acree, 2003)	6.74 (Lide, 2008)	1.58 (Lide, 2008)		0.33
1,2-propanediol	76.09	Pd(111)	DFT	101.3 (Mendes et al., 2019)	1.1×10^5	60.0 (Chickos and Acree, 2003)	7.55 (Bosque and Sales, 2002)	2.25 (Lide, 2008)		0.66
1,3-propanediol	76.09	Pd(111)	DFT	102.3 (Mendes et al., 2019)	1.7×10^5	72.4 (Chickos and Acree, 2003)	7.55 (Bosque and Sales, 2002)	2.55 (Lide, 2008)		0.66
glycerol	92.09	Pd(111)	DFT	116.7 (Mendes et al., 2019)	6.5×10^7	91.7 (Chickos and Acree, 2003)	8.14 (Bosque and Sales, 2002)	2.56 (Lide, 2008)		1
propane	44.10	Pt(111)	DFT	65.6 (Mendes et al., 2019)	5.0×10^{-2}	18.8 (Chickos and Acree, 2003)	6.33 (Lide, 2008)	0 (Yaws, 2014)		0
1-propanol	60.09	Pt(111)	DFT	100.3 (Mendes et al., 2019)	7.7×10^4	47.45 (Chickos and Acree, 2003)	6.74 (Lide, 2008)	1.58 (Lide, 2008)		0.33
2-propanol	60.09	Pt(111)	DFT	99.4 (Mendes et al., 2019)	5.2×10^4	47.45 (Chickos and Acree, 2003)	6.74 (Lide, 2008)	1.58 (Lide, 2008)		0.33
1,2-propanediol	76.09	Pt(111)	DFT	114.8 (Mendes et al., 2019)	2.9×10^7	60.0 (Chickos and Acree, 2003)	7.55 (Bosque and Sales, 2002)	2.25 (Lide, 2008)		0.66
1,3-propanediol	76.09	Pt(111)	DFT	119.6 (Mendes et al., 2019)	2.1×10^8	72.4 (Chickos and Acree, 2003)	7.55 (Bosque and Sales, 2002)	2.55 (Lide, 2008)		0.66
glycerol	92.09	Pt(111)	DFT	133.1 (Mendes et al., 2019)	5.5×10^{10}	91.7 (Chickos and Acree, 2003)	8.14 (Bosque and Sales, 2002)	2.56 (Lide, 2008)		1

1228

1229

1230 **Table A7.** Compiled adsorbate-substrate interaction energies of volatile organic compounds
 1231 (VOCs) on mineral surrogates and minerals and clays. Gas species, gas species' molar mass,
 1232 substrate, experimental or theoretical method, desorption energy (E_{des}^0), and desorption lifetimes
 1233 (τ_{des}) evaluated at 293 K using $A_{des} = 10^{13} \text{ s}^{-1}$, enthalpy of vaporization (ΔH_{vap}), gas species'
 1234 polarizability (α), gas species' dipole moment (μ), substrate's relative permittivity (ϵ_r), and gas
 1235 species' oxygen to carbon ration ($O:C$) are given.

Gas Species	Molar Mass / g mol ⁻¹	Substrate	Method	E_{des}^0 / kJ mol ⁻¹	$\tau_{des}^{293 K}$ / s	ΔH_{vap} (T) / kJ mol ⁻¹	α / 10 ⁻²⁴ cm ³	μ / D	ϵ_r	O:C
n-decane	142.29	α -Al ₂ O ₃	IGC	28.5 (Goss and Eisenreich, 1996)	1.2×10 ⁻⁸	51.4 (Chickos and Acree, 2003)	19.1 (Lide, 2008)	0 (Yaws, 2014)	9.34 (Lide, 2008)	0
o-xylene	106.17	α -Al ₂ O ₃	IGC	26.6 (Goss and Eisenreich, 1996)	5.5×10 ⁻⁹	42.9 (Chickos and Acree, 2003)	14.25 (Bosque and Sales, 2002)	0.64 (Lide, 2008)	9.34 (Lide, 2008)	0
propylbenzene	120.19	α -Al ₂ O ₃	IGC	30.3 (Goss and Eisenreich, 1996)	2.5×10 ⁻⁸	46.2 (Chickos and Acree, 2003)	16 (Mceachra n et al., 2018)	0.369 (Yaws, 2014)	9.34 (Lide, 2008)	0
1,2-dichlorobenzene	147.01	α -Al ₂ O ₃	IGC	28.0 (Goss and Eisenreich, 1996)	9.7×10 ⁻⁹	49.9 (Chickos and Acree, 2003)	14.3 (Bosque and Sales, 2002)	2.5 (Lide, 2008)	9.34 (Lide, 2008)	0
1,4-dichlorobenzene	147.01	α -Al ₂ O ₃	IGC	26.6 (Goss and Eisenreich, 1996)	5.5×10 ⁻⁹	54.8 (Chickos and Acree, 2003)	14.3 (Mceachra n et al., 2018)	1.72 (Lide, 2008)	9.34 (Lide, 2008)	0
1,2,3,4-tetrachlorobenzene	215.89	α -Al ₂ O ₃	IGC	42.7 (Goss and Eisenreich, 1996)	4.0×10 ⁻⁶	60.1 (Chickos and Acree, 2003)	18.2 (Mceachra n et al., 2018)	2.42 (Lide, 2008)	9.34 (Lide, 2008)	0
naphthalene	128.17	α -Al ₂ O ₃	IGC	38.0 (Goss and Eisenreich, 1996)	5.9×10 ⁻⁷	53.4 (Chickos and Acree, 2003)	17 (Lide, 2008)	0 (Yaws, 2014)	9.34 (Lide, 2008)	0
anisole	108.14	α -Al ₂ O ₃	IGC	37.7 (Goss and Eisenreich, 1996)	5.2×10 ⁻⁷	45.3 (Chickos and Acree, 2003)	13.1 (Lide, 2008)	1.38 (Lide, 2008)	9.34 (Lide, 2008)	0.14
pyridine	79.10	α -Al ₂ O ₃	IGC	47.0 (Goss and Eisenreich, 1996)	2.4×10 ⁻⁵	40.2 (Chickos and Acree, 2003)	9.34 (Lide, 2008)	2.215 (Lide, 2008)	9.34 (Lide, 2008)	0
ethanol	46.07	α -Al ₂ O ₃	IGC	48.4 (Goss and Eisenreich, 1996)	4.2×10 ⁻⁵	42.4 (Chickos and Acree, 2003)	5.41 (Lide, 2008)	1.69 (Lide, 2008)	9.34 (Lide, 2008)	0.5
ethyl acetate	88.11	α -Al ₂ O ₃	IGC	40.2 (Goss and Eisenreich, 1996)	1.5×10 ⁻⁶	35 (Chickos and Acree, 2003)	8.62 (Lide, 2008)	1.78 (Lide, 2008)	9.34 (Lide, 2008)	0.5
acetone	58.08	α -Al ₂ O ₃	IGC	38.0 (Goss and Eisenreich, 1996)	5.9×10 ⁻⁷	31.3 (Chickos and Acree, 2003)	6.37 (Lide, 2008)	2.88 (Lide, 2008)	9.34 (Lide, 2008)	0.33

n-nonane	128.26	CaCO ₃	IGC	30.4 (Goss and Eisenreich, 1996)	2.7×10 ⁻⁸	46.55 (Chickos and Acree, 2003)	17.36 (Lide, 2008)	0 (Yaws, 2014)	8.67 (Lide, 2008)	0
p-xylene	106.17	CaCO ₃	IGC	35.5 (Goss and Eisenreich, 1996)	2.2×10 ⁻⁷	42.3 (Chickos and Acree, 2003)	14.35 (Bosque and Sales, 2002)	0 (Yaws, 2014)	8.67 (Lide, 2008)	0
ethylbenzene	106.17	CaCO ₃	IGC	34.1 (Goss and Eisenreich, 1996)	1.2×10 ⁻⁷	42.3 (Chickos and Acree, 2003)	14.2 (Lide, 2008)	0.59 (Lide, 2008)	8.67 (Lide, 2008)	0
chlorobenzene	112.56	CaCO ₃	IGC	28.1 (Goss and Eisenreich, 1996)	1.0×10 ⁻⁸	40.3 (Chickos and Acree, 2003)	13.2 (Lide, 2008)	1.69 (Lide, 2008)	8.67 (Lide, 2008)	0
1,2-dichlorobenzene	147.01	CaCO ₃	IGC	36.8 (Goss and Eisenreich, 1996)	3.7×10 ⁻⁷	49.9 (Chickos and Acree, 2003)	14.3 (Bosque and Sales, 2002)	2.5 (Lide, 2008)	8.67 (Lide, 2008)	0
anisole	108.14	CaCO ₃	IGC	38.8 (Goss and Eisenreich, 1996)	8.4×10 ⁻⁷	45.3 (Chickos and Acree, 2003)	13.1 (Lide, 2008)	1.38 (Lide, 2008)	8.67 (Lide, 2008)	0.14
diethyl ether	74.12	CaCO ₃	IGC	39.3 (Goss and Eisenreich, 1996)	1.0×10 ⁻⁶	27.1 (Chickos and Acree, 2003)	9.47 (Lide, 2008)	1.098 (Lide, 2008)	8.67 (Lide, 2008)	0.25
methanol	32.04	CaCO ₃	DFT	77.2 (Budi et al., 2018)	5.8	37.8 (Chickos and Acree, 2003)	3.28 (Lide, 2008)	1.7 (Lide, 2008)	8.67 (Lide, 2008)	1
ethanol	46.07	CaCO ₃	DFT	80.1 (Budi et al., 2018)	19	42.4 (Chickos and Acree, 2003)	5.41 (Lide, 2008)	1.69 (Lide, 2008)	8.67 (Lide, 2008)	0.5
ethanol	46.07	CaCO ₃	TPD	83.9 (Dickbreder et al., 2023)	91	42.4 (Chickos and Acree, 2003)	5.41 (Lide, 2008)	1.69 (Lide, 2008)	8.67 (Lide, 2008)	0.5
ethanol	46.07	CaCO ₃	TPD	100.3 (Dickbreder et al., 2023)	7.6×10 ⁴	42.4 (Chickos and Acree, 2003)	5.41 (Lide, 2008)	1.69 (Lide, 2008)	8.67 (Lide, 2008)	0.5
formic acid	46.03	CaCO ₃	DFT	94.6 (Budi et al., 2018)	7.3×10 ³	36 (Chickos and Acree, 2003)	3.4 (Lide, 2008)	1.425 (Lide, 2008)	8.67 (Lide, 2008)	2
acetic acid	60.05	CaCO ₃	DFT	95.5 (Budi et al., 2018)	1.1×10 ⁴	41.6 (Chickos and Acree, 2003)	5.1 (Lide, 2008)	1.7 (Lide, 2008)	8.67 (Lide, 2008)	1
methane	16.04	CaCO ₃	DFT	12.5 (Budi et al., 2018)	1.7×10 ⁻¹¹	8.5 (Chickos and Acree, 2003)	2.59 (Lide, 2008)	0 (Yaws, 2014)	8.67 (Lide, 2008)	0
ethane	30.07	CaCO ₃	DFT	17.4 (Budi et al., 2018)	1.3×10 ⁻¹⁰	15.3 (Chickos and Acree, 2003)	4.45 (Lide, 2008)	0 (Yaws, 2014)	8.67 (Lide, 2008)	0

benzene	78.11	CaCO ₃	DFT	30.9 (Budi et al., 2018)	3.2×10 ⁻⁸	42.3 (Chickos and Acree, 2003)	10 (Lide, 2008)	0 (Yaws, 2014)	8.67 (Lide, 2008)	0
n-octane	114.23	α-Fe ₂ O ₃	IGC	25.0 (Goss and Eisenreich, 1996)	2.9×10 ⁻⁹	41.6 (Chickos and Acree, 2003)	15.9 (Lide, 2008)	0 (Yaws, 2014)	12.00 (Lide, 2008)	0
n-nonane	128.26	α-Fe ₂ O ₃	IGC	31.3 (Goss and Eisenreich, 1996)	3.9×10 ⁻⁸	46.55 (Chickos and Acree, 2003)	17.36 (Lide, 2008)	0 (Yaws, 2014)	12.00 (Lide, 2008)	0
toluene	92.14	α-Fe ₂ O ₃	IGC	27.5 (Goss and Eisenreich, 1996)	8.1×10 ⁻⁹	38.9 (Chickos and Acree, 2003)	11.8 (Lide, 2008)	0.375 (Lide, 2008)	12.00 (Lide, 2008)	0
p-xylene	106.17	α-Fe ₂ O ₃	IGC	32.7 (Goss and Eisenreich, 1996)	6.9×10 ⁻⁸	42.3 (Chickos and Acree, 2003)	14.35 (Bosque and Sales, 2002)	0 (Yaws, 2014)	12.00 (Lide, 2008)	0
o-xylene	106.17	α-Fe ₂ O ₃	IGC	33.6 (Goss and Eisenreich, 1996)	1.0×10 ⁻⁷	42.9 (Chickos and Acree, 2003)	14.25 (Bosque and Sales, 2002)	0.64 (Lide, 2008)	12.00 (Lide, 2008)	0
ethylbenzene	106.17	α-Fe ₂ O ₃	IGC	32.4 (Goss and Eisenreich, 1996)	6.1×10 ⁻⁸	42.3 (Chickos and Acree, 2003)	14.2 (Lide, 2008)	0.59 (Lide, 2008)	12.00 (Lide, 2008)	0
chlorobenzene	112.56	α-Fe ₂ O ₃	IGC	26.4 (Goss and Eisenreich, 1996)	5.2×10 ⁻⁹	40.3 (Chickos and Acree, 2003)	13.2 (Lide, 2008)	1.69 (Lide, 2008)	12.00 (Lide, 2008)	0
1,2-dichlorobenzene	147.01	α-Fe ₂ O ₃	IGC	35.5 (Goss and Eisenreich, 1996)	2.2×10 ⁻⁷	49.9 (Chickos and Acree, 2003)	14.3 (Bosque and Sales, 2002)	2.5 (Lide, 2008)	12.00 (Lide, 2008)	0
1,4-dichlorobenzene	147.01	α-Fe ₂ O ₃	IGC	32.5 (Goss and Eisenreich, 1996)	6.3×10 ⁻⁸	54.8 (Chickos and Acree, 2003)	14.3 (Mceachran et al., 2018)	1.72 (Lide, 2008)	12.00 (Lide, 2008)	0
anisole	108.14	α-Fe ₂ O ₃	IGC	41.0 (Goss and Eisenreich, 1996)	2.1×10 ⁻⁶	45.3 (Chickos and Acree, 2003)	13.1 (Lide, 2008)	1.38 (Lide, 2008)	12.00 (Lide, 2008)	0.143
acetone	58.08	α-Fe ₂ O ₃	IGC	39.3 (Goss and Eisenreich, 1996)	1.0×10 ⁻⁶	31.3 (Chickos and Acree, 2003)	6.37 (Lide, 2008)	2.88 (Lide, 2008)	12.00 (Lide, 2008)	0.33
diethyl ether	74.12	α-Fe ₂ O ₃	IGC	38.2 (Goss and Eisenreich, 1996)	6.6×10 ⁻⁷	27.1 (Chickos and Acree, 2003)	9.47 (Lide, 2008)	1.098 (Lide, 2008)	12.00 (Lide, 2008)	0.25
n-octane	114.23	quartz/kaolinite	IGC	27.9 (Goss and Eisenreich, 1996)	9.5×10 ⁻⁹	41.6 (Chickos and Acree, 2003)	15.9 (Lide, 2008)	0 (Yaws, 2014)	~4.0 (Leluk et al., 2010)	0
n-nonane	128.26	quartz/kaolinite	IGC	31.6 (Goss and Eisenreich, 1996)	4.3×10 ⁻⁸	46.55 (Chickos and Acree, 2003)	17.36 (Lide, 2008)	0 (Yaws, 2014)	~4.0 (Leluk et al., 2010)	0

n-decane	142.29	quartz/kaolinite	IGC	35.6 (Goss and Eisenreich, 1996)	2.2×10^{-7}	51.4 (Chickos and Acree, 2003)	19.1 (Lide, 2008)	0 (Yaws, 2014)	~4.0 (Leluk et al., 2010)	0
toluene	92.14	quartz/kaolinite	IGC	31.3 (Goss and Eisenreich, 1996)	3.8×10^{-8}	38.9 (Chickos and Acree, 2003)	11.8 (Lide, 2008)	0.375 (Lide, 2008)	~4.0 (Leluk et al., 2010)	0
p-xylene	106.17	quartz/kaolinite	IGC	35.6 (Goss and Eisenreich, 1996)	2.2×10^{-7}	42.3 (Chickos and Acree, 2003)	14.35 (Bosque and Sales, 2002)	0 (Yaws, 2014)	~4.0 (Leluk et al., 2010)	0
o-xylene	106.17	quartz/kaolinite	IGC	36.5 (Goss and Eisenreich, 1996)	3.2×10^{-7}	42.9 (Chickos and Acree, 2003)	14.25 (Bosque and Sales, 2002)	0.64 (Lide, 2008)	~4.0 (Leluk et al., 2010)	0
ethylbenzene	106.17	quartz/kaolinite	IGC	35.4 (Goss and Eisenreich, 1996)	2.1×10^{-7}	42.3 (Chickos and Acree, 2003)	14.2 (Lide, 2008)	0.59 (Lide, 2008)	~4.0 (Leluk et al., 2010)	0
propylbenzene	120.19	quartz/kaolinite	IGC	40.2 (Goss and Eisenreich, 1996)	1.5×10^{-6}	46.2 (Chickos and Acree, 2003)	16 (Mceachran et al., 2018)	0.369 (Yaws, 2014)	~4.0 (Leluk et al., 2010)	0
chlorobenzene	112.56	quartz/kaolinite	IGC	32.1 (Goss and Eisenreich, 1996)	5.3×10^{-8}	40.3 (Chickos and Acree, 2003)	13.2 (Lide, 2008)	1.69 (Lide, 2008)	~4.0 (Leluk et al., 2010)	0
1,2-dichlorobenzene	147.01	quartz/kaolinite	IGC	36.6 (Goss and Eisenreich, 1996)	3.4×10^{-7}	49.9 (Chickos and Acree, 2003)	14.3 (Bosque and Sales, 2002)	2.5 (Lide, 2008)	~4.0 (Leluk et al., 2010)	0
1,4-dichlorobenzene	147.01	quartz/kaolinite	IGC	37.2 (Goss and Eisenreich, 1996)	4.3×10^{-7}	54.8 (Chickos and Acree, 2003)	14.3 (Mceachran et al., 2018)	1.72 (Lide, 2008)	~4.0 (Leluk et al., 2010)	0
1,2,3,4-tetrachlorobenzene	215.89	quartz/kaolinite	IGC	45.3 (Goss and Eisenreich, 1996)	1.2×10^{-5}	60.1 (Chickos and Acree, 2003)	18.2 (Mceachran et al., 2018)	2.42 (Lide, 2008)	~4.0 (Leluk et al., 2010)	0
naphthalene	128.17	quartz/kaolinite	IGC	46.9 (Goss and Eisenreich, 1996)	2.3×10^{-5}	53.4 (Chickos and Acree, 2003)	17 (Lide, 2008)	0 (Yaws, 2014)	~4.0 (Leluk et al., 2010)	0
anisole	108.14	quartz/kaolinite	IGC	44.2 (Goss and Eisenreich, 1996)	7.7×10^{-6}	45.3 (Chickos and Acree, 2003)	13.1 (Lide, 2008)	1.38 (Lide, 2008)	~4.0 (Leluk et al., 2010)	0.143
pyridine	79.10	quartz/kaolinite	IGC	48.6 (Goss and Eisenreich, 1996)	4.7×10^{-5}	40.2 (Chickos and Acree, 2003)	9.34 (Lide, 2008)	2.215 (Lide, 2008)	~4.0 (Leluk et al., 2010)	0
ethanol	46.07	quartz/kaolinite	IGC	46.6 (Goss and Eisenreich, 1996)	2.1×10^{-5}	42.4 (Chickos and Acree, 2003)	5.41 (Lide, 2008)	1.38 (Lide, 2008)	~4.0 (Leluk et al., 2010)	0.5
ethyl acetate	88.11	quartz/kaolinite	IGC	45.0 (Goss and Eisenreich, 1996)	1.1×10^{-5}	35 (Chickos and Acree, 2003)	8.62 (Lide, 2008)	2.215	~4.0 (Leluk et al., 2010)	0.5

acetone	58.08	quartz/kaolinite	IGC	43.6 (Goss and Eisenreich, 1996)	6.0×10^{-6}	31.3 (Chickos and Acree, 2003)	6.37 (Lide, 2008)	2.88 (Lide, 2008)	~4.0 (Leluk et al., 2010)	0.33
diethyl ether	74.12	quartz/kaolinite	IGC	40.0 (Goss and Eisenreich, 1996)	1.4×10^{-6}	27.1 (Chickos and Acree, 2003)	9.47 (Lide, 2008)	1.098 (Lide, 2008)	~4.0 (Leluk et al., 2010)	0.25
methanol	32.04	quartz	DFT	60.8 (Budi et al., 2018)	6.9×10^{-3}	37.8 (Chickos and Acree, 2003)	3.28 (Lide, 2008)	1.7 (Lide, 2008)	3.75 (Lide, 2008)	1
ethanol	46.07	quartz	DFT	64.6 (Budi et al., 2018)	3.3×10^{-2}	42.4 (Chickos and Acree, 2003)	5.41 (Lide, 2008)	1.69 (Lide, 2008)	3.75 (Lide, 2008)	0.5
formic acid	46.03	quartz	DFT	57.9 (Budi et al., 2018)	2.1×10^{-3}	36 (Chickos and Acree, 2003)	3.4 (Lide, 2008)	1.425 (Lide, 2008)	3.75 (Lide, 2008)	2
acetic acid	60.05	quartz	DFT	60.8 (Budi et al., 2018)	6.9×10^{-3}	41.6 (Chickos and Acree, 2003)	5.1 (Lide, 2008)	1.7 (Lide, 2008)	3.75 (Lide, 2008)	1
methane	16.04	quartz	DFT	6.8 (Budi et al., 2018)	1.6×10^{-12}	8.5 (Chickos and Acree, 2003)	2.59 (Lide, 2008)	0 (Yaws, 2014)	3.75 (Lide, 2008)	0
ethane	30.07	quartz	DFT	12.5 (Budi et al., 2018)	1.7×10^{-11}	15.3 (Chickos and Acree, 2003)	4.45 (Lide, 2008)	0 (Yaws, 2014)	3.75 (Lide, 2008)	0
benzene	78.11	quartz	DFT	33.8 (Budi et al., 2018)	1.1×10^{-7}	42.3 (Chickos and Acree, 2003)	10 (Lide, 2008)	0 (Yaws, 2014)	3.75 (Lide, 2008)	0
methanol	32.04	kaolinite (Al)	DFT	61.8 (Budi et al., 2018)	1.0×10^{-2}	37.8 (Chickos and Acree, 2003)	3.28 (Lide, 2008)	1.7 (Lide, 2008)	5.10 (Leluk et al., 2010)	1
ethanol	46.07	kaolinite (Al)	DFT	64.6 (Budi et al., 2018)	3.3×10^{-2}	42.4 (Chickos and Acree, 2003)	5.41 (Lide, 2008)	1.69 (Lide, 2008)	5.10 (Leluk et al., 2010)	0.5
formic acid	46.03	kaolinite (Al)	DFT	79.1 (Budi et al., 2018)	1.3×10^1	36 (Chickos and Acree, 2003)	3.4 (Lide, 2008)	1.425 (Lide, 2008)	5.10 (Leluk et al., 2010)	2
acetic acid	60.05	kaolinite (Al)	DFT	82.0 (Budi et al., 2018)	4.2×10^1	41.6 (Chickos and Acree, 2003)	5.1 (Lide, 2008)	1.7 (Lide, 2008)	5.10 (Leluk et al., 2010)	1
methane	16.04	kaolinite (Al)	DFT	16.4 (Budi et al., 2018)	8.4×10^{-11}	8.5 (Chickos and Acree, 2003)	2.59 (Lide, 2008)	0 (Yaws, 2014)	5.10 (Leluk et al., 2010)	0
ethane	30.07	kaolinite (Al)	DFT	22.2 (Budi et al., 2018)	9.1×10^{-10}	15.3 (Chickos and Acree, 2003)	4.45 (Lide, 2008)	0 (Yaws, 2014)	5.10 (Leluk et al., 2010)	0
benzene	78.11	kaolinite (Al)	DFT	37.6 (Budi et al., 2018)	5.0×10^{-7}	42.3 (Chickos and Acree, 2003)	10 (Lide, 2008)	0 (Yaws, 2014)	5.10 (Leluk et al., 2010)	0

						and Acree, 2003)			et al., 2010)	
methanol	32.04	kaolinite (Si)	DFT	21.2 (Budi et al., 2018)	6.0×10^{-10}	37.8 (Chickos and Acree, 2003)	3.28 (Lide, 2008)	1.7 (Lide, 2008)	5.10 (Leluk et al., 2010)	1
ethanol	46.07	kaolinite (Si)	DFT	23.2 (Budi et al., 2018)	1.4×10^{-9}	42.4 (Chickos and Acree, 2003)	5.41 (Lide, 2008)	1.69 (Lide, 2008)	5.10 (Leluk et al., 2010)	0.5
formic acid	46.03	kaolinite (Si)	DFT	21.2 (Budi et al., 2018)	6.0×10^{-10}	36 (Chickos and Acree, 2003)	3.4 (Lide, 2008)	1.425 (Lide, 2008)	5.10 (Leluk et al., 2010)	2
acetic acid	60.05	kaolinite (Si)	DFT	21.2 (Budi et al., 2018)	6.0×10^{-10}	41.6 (Chickos and Acree, 2003)	5.1 (Lide, 2008)	1.7 (Lide, 2008)	5.10 (Leluk et al., 2010)	1
methane	16.04	kaolinite (Si)	DFT	7.7 (Budi et al., 2018)	2.4×10^{-12}	8.5 (Chickos and Acree, 2003)	2.59 (Lide, 2008)	0 (Yaws, 2014)	5.10 (Leluk et al., 2010)	0
ethane	30.07	kaolinite (Si)	DFT	11.6 (Budi et al., 2018)	1.2×10^{-11}	15.3 (Chickos and Acree, 2003)	4.45 (Lide, 2008)	0 (Yaws, 2014)	5.10 (Leluk et al., 2010)	0
benzene	78.11	kaolinite (Si)	DFT	18.3 (Budi et al., 2018)	1.8×10^{-10}	42.3 (Chickos and Acree, 2003)	10 (Lide, 2008)	0 (Yaws, 2014)	5.10 (Leluk et al., 2010)	0
limonene up	136.24	SiO ₂	DFT	46.3 (Fang et al., 2019)	1.8×10^{-5}	49.6 (Chickos and Acree, 2003)	17.94 (Helburn et al., 2008)	0.7 (Svirbely et al., 1935)	4.42 (Lide, 2008)	0
limonene down	136.24	SiO ₂	DFT	41.6 (Fang et al., 2019)	2.6×10^{-6}	49.6 (Chickos and Acree, 2003)	17.94 (Helburn et al., 2008)	0.7 (Svirbely et al., 1935)	4.42 (Lide, 2008)	0
benzene	78.11	SiO ₂	DFT	27.5 (Fang et al., 2019)	8.0×10^{-9}	33.83 (Chickos and Acree, 2003)	10.44 (Bosque and Sales, 2002)	0 (Yaws, 2014)	4.42 (Lide, 2008)	0
cyclohexene	82.143	SiO ₂	DFT	29.2 (Fang et al., 2019)	1.6×10^{-8}	33.5 (Chickos and Acree, 2003)	10.79 (Bosque and Sales, 2002)	0 (Yaws, 2014)	4.42 (Lide, 2008)	0
cyclohexane	84.16	SiO ₂	DFT	24.3 (Fang et al., 2019)	2.1×10^{-9}	33 (Chickos and Acree, 2003)	11.04 (Bosque and Sales, 2002)	0 (Yaws, 2014)	4.42 (Lide, 2008)	0
limonene	136.24	Hydroxylated TiO ₂	MD	71 (Fan et al., 2022)	0.5	49.6 (Chickos and Acree, 2003)	17.94 (Helburn et al., 2008)	1.57 (Yaws, 2014)	86 (Lide, 2008)	0
carvone	150.22	Hydroxylated TiO ₂	MD	148.8 (Fan et al., 2022)	3.4×10^{13}	58.2 (Hoskovec et al., 2005)	18.25 (Yankova et al., 2019)	3.56 (Yankova et al., 2019)	86 (Lide, 2008)	0.1
toluene	92.14	Nefta dust	DRIFTS	88.8 (Romanias et al., 2016)	6.9×10^2	38.9 (Chickos)	12.12 (Lide, 2008)	0.375 (Lide, 2008)	~4.5 (Lide, 2008;	0

						and Acree, 2003)			Leluk et al., 2010)	
toluene	92.14	Touggourt dust	DRIFTS	88.9 (Romanias et al., 2016)	7.0×10 ²	38.9 (Chickos and Acree, 2003)	12.12 (Lide, 2008)	0.375 (Lide, 2008)	~4.5 (Lide, 2008; Leluk et al., 2010)	0
toluene	92.14	N'Goussa dust	DRIFTS	88.5 (Romanias et al., 2016)	6.0×10 ²	38.9 (Chickos and Acree, 2003)	12.12 (Lide, 2008)	0.375 (Lide, 2008)	~4.5 (Lide, 2008; Leluk et al., 2010)	0
toluene	92.14	Bordj dust	DRIFTS	88.6 (Romanias et al., 2016)	6.1×10 ²	38.9 (Chickos and Acree, 2003)	12.12 (Lide, 2008)	0.375 (Lide, 2008)	~4.5 (Lide, 2008; Leluk et al., 2010)	0
toluene	92.14	Laayoune dust	DRIFTS	87.9 (Romanias et al., 2016)	4.6×10 ²	38.9 (Chickos and Acree, 2003)	12.12 (Lide, 2008)	0.375 (Lide, 2008)	~4.5 (Lide, 2008; Leluk et al., 2010)	0
toluene	92.14	Tarfaya dust	DRIFTS	87.7 (Romanias et al., 2016)	4.3×10 ²	38.9 (Chickos and Acree, 2003)	12.12 (Lide, 2008)	0.375 (Lide, 2008)	~4.5 (Lide, 2008; Leluk et al., 2010)	0
limonene	136.24	Nefta dust	DRIFTS	91.4 (Romanias et al., 2016)	2.0×10 ³	49.6 (Chickos and Acree, 2003)	17.94 (Helburn et al., 2008)	1.57 (Yaws, 2014)	~4.5 (Lide, 2008; Leluk et al., 2010)	0
limonene	136.24	Touggourt dust	DRIFTS	88.5 (Romanias et al., 2016)	6.0×10 ²	49.6 (Chickos and Acree, 2003)	17.94 (Helburn et al., 2008)	1.57 (Yaws, 2014)	~4.5 (Lide, 2008; Leluk et al., 2010)	0
limonene	136.24	N'Goussa dust	DRIFTS	91.6 (Romanias et al., 2016)	2.1×10 ³	49.6 (Chickos and Acree, 2003)	17.94 (Helburn et al., 2008)	1.57 (Yaws, 2014)	~4.5 (Lide, 2008; Leluk et al., 2010)	0
limonene	136.24	Bordj dust	DRIFTS	91.8 (Romanias et al., 2016)	2.3×10 ³	49.6 (Chickos and Acree, 2003)	17.94 (Helburn et al., 2008)	1.57 (Yaws, 2014)	~4.5 (Lide, 2008; Leluk et al., 2010)	0
limonene	136.24	Laayoune dust	DRIFTS	88.7 (Romanias et al., 2016)	6.4×10 ²	49.6 (Chickos and Acree, 2003)	17.94 (Helburn et al., 2008)	1.57 (Yaws, 2014)	~4.5 (Lide, 2008; Leluk et	0

									al., 2010)	
limonene	136.24	Tarfaya dust	DRIFTS	88.1 (Romanias et al., 2016)	5.0×10^2	49.6 (Chickos and Acree, 2003)	17.94 (Helburn et al., 2008)	1.57 (Yaws, 2014)	~4.5 (Lide, 2008; Leluk et al., 2010)	0

1236

1237

1238 **Table A8.** Compiled adsorbate-substrate interaction energies of inorganic and organic gas
1239 species on ice. Gas species, gas species' molar mass, substrate, experimental or theoretical method,
1240 desorption energy (E_{des}^0), and desorption lifetimes (τ_{des}) evaluated at 293 K using $A_{des} = 10^{13} \text{ s}^{-1}$,
1241 enthalpy of vaporization (ΔH_{vap}), gas species' polarizability (α), gas species' dipole moment (μ),
1242 substrate's relative permittivity (ϵ_r), and gas species' oxygen to carbon ration ($O:C$) are given.

Gas Species	Molar Mass / g mol ⁻¹	Substrate	Method	E_{des}^0 / kJ mol ⁻¹	$\tau_{des}^{293 K}$ / s	ΔH_{vap} (T) / kJ mol ⁻¹	α / 10 ⁻²⁴ cm ³	μ / D	ϵ_r	O:C
H ₂ O	18.02	ice	MB	48.3 (Brown et al., 1996)	4.1×10^{-5}	44 (Chickos and Acree, 2003)	1.45 (Lide, 2008)	1.85 (Lide, 2008)	97.5 (Lide, 2008; Auty and Cole, 1952)	0
H ₂ O	18.02	ice (170-230 K)	VM	43.1 (Delval and Rossi, 2005; Delval et al., 2003)	4.8×10^{-6}	44 (Chickos and Acree, 2003)	1.45 (Lide, 2008)	1.85 (Lide, 2008)	119.5 (Lide, 2008; Auty and Cole, 1952)	0
H ₂ O	18.02	ice	MD	50.0 (Schlesinger et al., 2020)	8.2×10^{-5}	44 (Chickos and Acree, 2003)	1.45 (Lide, 2008)	1.85 (Lide, 2008)	97.5 (Lide, 2008; Auty and Cole, 1952)	0
D ₂ O	20.03	ice	MB	42 (Kong et al., 2014a)	3.1×10^{-6}	45.14 (Crabtree and Siman-Tov, 1993)	1.26 (Lide, 2008)	1.87 (Townes and Schawlow, 1975)	97.5 (Lide, 2008; Auty and Cole, 1952)	0
CO ₂	44.01	amorphous ice	TPD	22.5 (Kim et al., 2008)	1.0×10^{-9}	16.4 (Chickos and Acree, 2003)	2.91 (Lide, 2008)	0.0001 (Kolomiitsova et al., 2000)	97.5 (Lide, 2008; Auty and Cole, 1952)	0.5
n-hexane	86.18	ice	IGC	23.0 (Langenberg and Schurath, 2018)	1.3×10^{-9}	31.5 (Chickos and Acree, 2003)	11.9 (Lide, 2008)	0	97.5 (Lide, 2008; Auty and Cole, 1952)	0
formaldehyde	30.03	ice	GCMC	30.0 (Hantal et al., 2007)	2.2×10^{-8}	24.3 (Chickos)	2.63 (Lide, 2008)	2.33 (Lide, 2008)	97.5 (Lide, 2008;)	1

						and Acree, 2003)			Auty and Cole, 1952)	
acetaldehyde	44.05	ice	KU	29.1 (Crowley et al., 2010)	1.5×10^{-8}	27.6 (Chickos and Acree, 2003)	4.6 (Lide, 2008)	2.75 (Lide, 2008)	97.5 (Lide, 2008; Auty and Cole, 1952)	0.5
methanol	32.04	ice	KU	51.0 (Winkler et al., 2002)	1.2×10^{-4}	37.8 (Chickos and Acree, 2003)	3.28 (Lide, 2008)	1.7 (Lide, 2008)	97.5 (Lide, 2008; Auty and Cole, 1952)	0
acetone	58.08	ice	KU	48.6 (Crowley et al., 2010)	4.6×10^{-5}	31.3 (Chickos and Acree, 2003)	6.37 (Lide, 2008)	2.88 (Lide, 2008)	97.5 (Lide, 2008; Auty and Cole, 1952)	0.33
formic acid	46.03	ice	KU	48.1 (Crowley et al., 2010)	3.8×10^{-5}	36 (Chickos and Acree, 2003)	3.4 (Lide, 2008)	1.43 (Lide, 2008)	97.5 (Lide, 2008; Auty and Cole, 1952)	2
acetic acid	60.05	ice	KU	70.7 (Crowley et al., 2010)	0.4	41.6 (Chickos and Acree, 2003)	5.1 (Lide, 2008)	1.7 (Lide, 2008)	97.5 (Lide, 2008; Auty and Cole, 1952)	1
acetic acid	60.05	ice	KU	73.2 (Sokolov and Abbatt, 2002)	1.1	41.6 (Chickos and Acree, 2003)	5.1 (Lide, 2008)	1.7 (Lide, 2008)	97.5 (Lide, 2008; Auty and Cole, 1952)	1
1-pentanol	88.15	ice	KU	71.5 (Sokolov and Abbatt, 2002)	0.6	57.8 (Chickos and Acree, 2003)	10.61 (Bosque and Sales, 2002)	1.7 (liq.)(Lide, 2008)	97.5 (Lide, 2008; Auty and Cole, 1952)	0.2
1-butanol	74.12	ice	KU	67.8 (Sokolov and Abbatt, 2002)	0.1	52.5 (Chickos and Acree, 2003)	8.88 (Lide, 2008)	1.66 (Lide, 2008)	97.5 (Lide, 2008; Auty and Cole, 1952)	0.25
ethanol	46.07	ice	KU	62.4 (Crowley et al., 2010)	1.3×10^{-2}	42.4 (Chickos and Acree, 2003)	5.41 (Lide, 2008)	1.69 (Lide, 2008)	97.5 (Lide, 2008; Auty and Cole, 1952)	0.5
ethanol	46.07	ice	KU	61.9 (Sokolov and Abbatt, 2002)	1.1×10^{-2}	42.4 (Chickos and Acree, 2003)	5.41 (Lide, 2008)	1.69 (Lide, 2008)	97.5 (Lide, 2008; Auty and	0.5

									Cole, 1952)	
1-propanol	60.09	ice	GCMC	70.0 (Joliat et al.)	0.3	47.45 (Chickos and Acree, 2003)	6.74 (Lide, 2008)	1.58 (Lide, 2008)	97.5 (Lide, 2008; Auty and Cole, 1952)	0.33
2-propanol	60.09	ice	GCMC	71.5 (Joliat et al.)	0.6	47.45 (Chickos and Acree, 2003)	6.74 (Lide, 2008)	1.58 (Lide, 2008)	97.5 (Lide, 2008; Auty and Cole, 1952)	0.33
hexanal	100.16	ice	KU	64.9 (Sokolov and Abbatt, 2002)	3.7×10^{-2}	42.3 (Chickos and Acree, 2003)	11.9 (Mceachran et al., 2018)	2.6 (Wiberg and Rablen, 1993; Bak et al., 2000)	97.5 (Lide, 2008; Auty and Cole, 1952)	0
peroxyacetyl nitrate	121.05	ice	IGC	30.0 (Bartels-Rausch et al., 2002)	2.2×10^{-8}	34.6 (Stephenson and Malanowski, 1987)	8.27 (Mceachran et al., 2018)		97.5 (Lide, 2008; Auty and Cole, 1952)	2.5
acetylene	26.04	ice	VS	15.5 (Silva and Devlin, 1994)	5.8×10^{-11}	16.7	3.40 (Gussoni et al., 1998)	0	97.5 (Lide, 2008; Auty and Cole, 1952)	0
ethylene	28.05	ice	VS	15.9 (Silva and Devlin, 1994)	6.8×10^{-11}	13.8	4.09 (Gussoni et al., 1998)	0	97.5 (Lide, 2008; Auty and Cole, 1952)	
benzene	78.11	ice	VS	18.0 (Silva and Devlin, 1994)	1.6×10^{-10}	33.5	9.96 (Gussoni et al., 1998)	0	97.5 (Lide, 2008; Auty and Cole, 1952)	
HCl	36.46	ice (100-170 K)	TPD	28.0 (Isakson and Sitz, 1999)	9.8×10^{-9}	16.15 (Lide, 2008)	2.63 (Lide, 2008)	1.11 (Lide, 2008)	119.5 (Lide, 2008; Auty and Cole, 1952)	0
HOCl	52.46	ice (185-225K)	KU	39.6 (Crowley et al., 2010)	1.1×10^{-6}	36.66 (Joback and Reid, 1987)	3.31 (Hait and Head-Gordon, 2018)	1.3 (Lide, 2008)	119.5 (Lide, 2008; Auty and Cole, 1952)	0
H ₂ O ₂	34.01	ice	KU	31.6 (Pouvesle et al., 2010; Crowley et al., 2010)	4.3×10^{-8}	51.6 (Lide, 2008)	2.3 (Giguere, 1983)	1.57 (Lide, 2008)	97.5 (Lide, 2008; Auty and	0

									Cole, 1952)	
NO	30.01	ice (93-150 K)	MB	15.4 (Lejonhuth et al., 2014)	5.7×10^{-11}	13.83 (Lide, 2008)	1.7 (Lide, 2008)	0.16 (Lide, 2008)	119.5 (Lide, 2008; Auty and Cole, 1952)	0
NO ₂	46.01	ice (150-171 K)	MB	25.1 (Lejonhuth et al., 2014)	3.0×10^{-9}	18.89	3.02 (Lide, 2008)	0.32 (Lide, 2008)	119.5 (Lide, 2008; Auty and Cole, 1952)	0
NO ₂	46.01	ice	IGC	22.0 (Bartels-Rausch et al., 2002)	8.4×10^{-10}	18.89	3.02 (Lide, 2008)	0.32 (Lide, 2008)	97.5 (Lide, 2008; Auty and Cole, 1952)	0
HONO	47.01	ice	KU	43.0 (Crowley et al., 2010)	4.6×10^{-6}		2.81 (Jensen et al., 2002)	1.42 (Lide, 2008)	97.5 (Lide, 2008; Auty and Cole, 1952)	0
N ₂ O ₅	108.01	ice (135-168 K)	MB	34.7 (Lejonhuth et al., 2014)	1.6×10^{-7}	57.4 (Stull, 1947)	7.7 (Wincel et al., 1995)	0.5 (Grabow et al., 1996)	119.5 (Lide, 2008; Auty and Cole, 1952)	0
N ₂ O ₅	108.01	ice covered HNO ₃ (135-168 K)	MB	23.2 (Lejonhuth et al., 2014)	1.3×10^{-9}	57.4 (Stull, 1947)	7.7 (Wincel et al., 1995)	0.5 (Grabow et al., 1996)	119.5 (Lide, 2008; Auty and Cole, 1952)	0
HNO ₃	63.01	ice	KU	38.1 (Crowley et al., 2010)	6.2×10^{-7}	39.1 (Lide, 2008)	3.55 (Jensen et al., 2002)	2.17 (Lide, 2008)	97.5 (Lide, 2008; Auty and Cole, 1952)	0
HO ₂ NO ₂	79.01	ice	KU	59.0 (Ulrich et al., 2012)	3.3×10^{-3}			2.44 (Wei et al., 2011)	97.5 (Lide, 2008; Auty and Cole, 1952)	0
OH	17.01	ice (205-230 K)	MC	31.2 (Remorov and Bardwell, 2005)	3.6×10^{-8}		7.11 (Zen et al., 2014)	1.65 (Lide, 2008)	119.5 (Lide, 2008; Auty and Cole, 1952)	0
O ₃	48.00	amorphous ice	TPD	20.0 (Borget et al., 2001)	3.7×10^{-10}	12.2 (Stull, 1947)	3.21 (Lide, 2008)	0.53 (Lide, 2008)	97.5 (Lide, 2008; Auty and Cole, 1952)	0

SO ₂	64.07	ice	KU	17.2 (Crowley et al., 2010)	1.2×10 ⁻¹⁰	24.9 (Chickos and Acree, 2003)	4 (Lide, 2008)	1.63 (Lide, 2008)	97.5 (Lide, 2008; Auty and Cole, 1952)	0
-----------------	-------	-----	----	--------------------------------	-----------------------	-----------------------------------	----------------	----------------------	---	---

1243

1244

1245 **Table A9.** Compiled adsorbate-substrate data for water vapor and inorganic gases adsorbed on
1246 water and aqueous substrates. Gas species, gas species' molar mass, substrate, experimental or
1247 theoretical method, desorption energy (E_{des}^0), and desorption lifetimes (τ_{des}) evaluated at 293 K
1248 using $A_{des} = 10^{13} \text{ s}^{-1}$, enthalpy of vaporization (ΔH_{vap}) and solvation (ΔH_{solv}), gas species'
1249 polarizability (α), gas species' dipole moment (μ), substrate's relative permittivity (ϵ_r), and gas
1250 species' oxygen to carbon ration ($O:C$) are given.

Gas Species	Molar Mass / g mol ⁻¹	Substrate	Method	E_{des}^0 / kJ mol ⁻¹	$\tau_{des}^{293 K}$ / s	ΔH_{vap} (T) / kJ mol ⁻¹	α / 10 ⁻²⁴ cm ³	μ / D	ϵ_r	ΔH_{solv} (T) / kJ mol ⁻¹	O:C
H ₂ O	18.02	H ₂ O	MD	9.2 (Vieceli et al., 2004)	4.4×10 ⁻¹²	44 (Chickos and Acree, 2003)	1.45 (Lide, 2008)	1.85 (Lide, 2008)	80.2 (Lide, 2008)		0
H ₂ O	18.02	H ₂ O, 1.92 nm radius	MD	10.6 (Julin et al., 2013)	7.8×10 ⁻¹²	44 (Chickos and Acree, 2003)	1.45 (Lide, 2008)	1.85 (Lide, 2008)	80.2 (Lide, 2008)		0
H ₂ O	18.02	H ₂ O, 4.14 nm radius	MD	10.9 (Julin et al., 2013)	8.8×10 ⁻¹²	44 (Chickos and Acree, 2003)	1.45 (Lide, 2008)	1.85 (Lide, 2008)	80.2 (Lide, 2008)		0
H ₂ O	18.02	H ₂ O, planar	MD	11.4 (Julin et al., 2013)	1.1×10 ⁻¹¹	44 (Chickos and Acree, 2003)	1.45 (Lide, 2008)	1.85 (Lide, 2008)	80.2 (Lide, 2008)		0
H ₂ O	18.02	H ₂ O, planar	MD	9.05 (Julin et al., 2013)	4.1×10 ⁻¹²	44 (Chickos and Acree, 2003)	1.45 (Lide, 2008)	1.85 (Lide, 2008)	80.2 (Lide, 2008)		0
H ₂ O	18.02	H ₂ O, planar	MD	10.4 (Julin et al., 2013)	7.1×10 ⁻¹²	44 (Chickos and Acree, 2003)	1.45 (Lide, 2008)	1.85 (Lide, 2008)	80.2 (Lide, 2008)		0
H ₂ O	18.02	H ₂ O, planar	MD	10.3 (Julin et al., 2013)	6.9×10 ⁻¹²	44 (Chickos and Acree, 2003)	1.45 (Lide, 2008)	1.85 (Lide, 2008)	80.2 (Lide, 2008)		0
SO ₂	64.07	H ₂ O	KU	44.2 (Ammann et al., 2013; Jayne et al., 1990)	7.6×10 ⁻⁶	24.9 (Chickos and Acree, 2003)	4 (Lide, 2008)	1.633 (Lide, 2008)	80.2 (Lide, 2008)	24.11 (Sander et al., 2011)	0

						Acree, 2003)					
NH ₃	17.03	H ₂ O	ST	41 (Donaldson, 1999)	2.0×10^{-6}	22.7 (Chickos and Acree, 2003)	2.35 (Lide, 2008)	1.472 (Lide, 2008)	80.2 (Lide, 2008)	34.92 (Sander et al., 2011)	0
O ₃	48.00	H ₂ O	MD	14.7 (Vieceli et al., 2005)	4.2×10^{-11}	12.2 (Stull, 1947)	3.21 (Lide, 2008)	0.533 (Lide, 2008)	80.2 (Lide, 2008)	23.28 (Sander et al., 2011)	0
H ₂ O ₂	34.01	H ₂ O	KU	26 (Worsnop et al., 1989)	4.3×10^{-9}	51.16	2.3 (Giguere, 1983)	1.573 (Lide, 2008)	80.2 (Lide, 2008)	63.19 (Sander et al., 2011)	0
HCl	36.46	H ₂ SO ₄	KU	14.1 (Ammann et al., 2013; Behr et al., 2009; Robinson et al., 1998)	3.3×10^{-11}	16.15	2.63 (Lide, 2008)	1.11 (Lide, 2008)	95 (Hall and Cole, 1981)	19.12 (Marsh and Mcelroy, 1985)	0
O ₃	48.00	shikimic acid (aqueous)	KU	20 (Berkemeier et al., 2016; Steimer et al., 2015)	3.7×10^{-10}	12.2 (Stull, 1947)	3.21 (Lide, 2008)	0.533 (Lide, 2008)		23.28 (Sander et al., 2011)	0
N ₂ O ₅	108.01	H ₂ O	MD	15.4 (Cruzeiro et al., 2022)	5.6×10^{-11}	57.4 (Stull, 1947)	7.7 (Wincel et al., 1995)	0.5 (Grabow et al., 1996)	80.2 (Lide, 2008)		0

1251

1252

1253 **Table A10.** Compiled adsorbate-substrate data for volatile aromatic gases adsorbed on water. Gas
1254 species, gas species' molar mass, substrate, experimental or theoretical method, desorption energy
1255 (E_{des}^0), and desorption lifetimes (τ_{des}) evaluated at 293 K using $A_{des} = 10^{13} \text{ s}^{-1}$, enthalpy of
1256 vaporization (ΔH_{vap}) and solvation (ΔH_{solv}), gas species' polarizability (α), gas species' dipole
1257 moment (μ), substrate's relative permittivity (ϵ_r), and gas species' oxygen to carbon ration (O:C)
1258 are given.

Gas Species	Molar Mass / g mol ⁻¹	Substrate	Method	E_{des}^0 / kJ mol ⁻¹	$\tau_{des}^{293 K}$ / s	ΔH_{vap} (T) / kJ mol ⁻¹	α / 10 ⁻²⁴ cm ³	μ / D	ϵ_r	ΔH_{solv} (T) / kJ mol ⁻¹	O:C
toluene	92.14	H ₂ O	ST	31 (Blank and Ottewill, 1964)	3.4×10^{-8}	38.9 (Chickos and Acree, 2003)	11.8 (Lide, 2008)	0.375 (Lide, 2008)	80.2 (Lide, 2008)	35.75 (Staudinger and Roberts, 2001; Sander, 2015)	0
toluene	92.14	H ₂ O	IGC	37.2 (Hartkopf and Karger, 1973)	4.3×10^{-7}	38.9 (Chickos and Acree, 2003)	11.8 (Lide, 2008)	0.375 (Lide, 2008)	80.2 (Lide, 2008)	35.75 (Staudinger and Roberts, 2001; Sander, 2015)	0

toluene	92.14	H ₂ O	ST	43.4 (Hauxwell and Ottewill, 1968)	5.5×10 ⁻⁶	38.9 (Chickos and Acree, 2003) (Chickos and Acree, 2003)	11.8 (Lide, 2008)	0.375 (Lide, 2008)	80.2 (Lide, 2008)	35.75 (Staudinger and Roberts, 2001; Sander, 2015)	0
toluene	92.14	H ₂ O	IGC	28.8 (Goss, 2009)	1.4×10 ⁻⁸	38.9 (Chickos and Acree, 2003)	11.8 (Lide, 2008)	0.375 (Lide, 2008)	80.2 (Lide, 2008)	35.75 (Staudinger and Roberts, 2001; Sander, 2015)	0
toluene	92.14	H ₂ O	ST	47.1 (Bruant and Conklin, 2002)	2.5×10 ⁻⁵	38 (Chickos and Acree, 2003)	11.8 (Lide, 2008)	0.375 (Lide, 2008)	80.2 (Lide, 2008)	35.75 (Staudinger and Roberts, 2001; Sander, 2015)	0
benzene	78.11	H ₂ O	ST	41 (Bruant and Conklin, 2002)	2.0×10 ⁻⁶	42.3 (Chickos and Acree, 2003)	10.53 (Lide, 2008)	0 (Yaws, 2014)	80.2 (Lide, 2008)	34.92 (Staudinger and Roberts, 2001; Sander, 2015)	0
benzene	78.11	H ₂ O	ST	25.8 (Blank and Ottewill, 1964)	4.0×10 ⁻⁹	42.3 (Chickos and Acree, 2003)	10.53 (Lide, 2008)	0 (Yaws, 2014)	80.2 (Lide, 2008)	34.92 (Staudinger and Roberts, 2001; Sander, 2015)	0
benzene	78.11	H ₂ O	IGC	31.4 (Hartkopf and Karger, 1973)	4.0×10 ⁻⁸	42.3 (Chickos and Acree, 2003)	10.53 (Lide, 2008)	0 (Yaws, 2014)	80.2 (Lide, 2008)	34.92 (Staudinger and Roberts, 2001; Sander, 2015)	0
benzene	78.11	H ₂ O	IGC	41 (Rajaset al., 2002)	2.0×10 ⁻⁶	42.3 (Chickos and Acree, 2003)	10.53 (Lide, 2008) (Lide, 2008)	0 (Yaws, 2014)	80.2 (Lide, 2008)	34.92 (Staudinger and Roberts, 2001; Sander, 2015)	0
1,2-dimethylbenzene	106.17	H ₂ O	ST	45.9 (Bruant and Conklin, 2002)	1.5×10 ⁻⁵	43.4 (Chickos and Acree, 2003)	14.5 (Lide, 2008)	0.63 (Yaws, 2014)	80.2 (Lide, 2008)	34.92 (Staudinger and Roberts, 2001; Sander, 2015)	0
1,3-dimethylbenzene	106.17	H ₂ O	ST	51.6 (Bruant and	1.6×10 ⁻⁴	42.7 (Chickos and	14.2 (Lide, 2008)	0.3 (Yaws, 2014)	80.2 (Lide, 2008)	34.92 (Staudinger and Roberts,	0

				Conklin, 2002)		Acree, 2003)				2001; Sander, 2015)	
1,4- dimethylbenz ene	106.17	H ₂ O	ST	46.5 (Bruant and Conklin, 2002)	1.9x1 0 ⁻⁵	42.3 (Chicko s and Acree, 2003)	14.27 (Lide, 2008)	0 (Yaws, 2014)	80.2 (Lide, 2008)	34.92 (Stauding er and Roberts, 2001; Sander, 2015)	0
1,3,5- trimethylbenz ene	120.20	H ₂ O	ST	56.2 (Bruant and Conklin, 2002)	1.0x1 0 ⁻³	47.6 (Chicko s and Acree, 2003)	15.82 (Lide, 2008)	0.6 (Yaws, 2014)	80.2 (Lide, 2008)	34.92 (Sander, 2015)	0
ethylbenzene	106.17	H ₂ O	IGC	41.4 (Hartkop f and Karger, 1973)	2.4x1 0 ⁻⁶	42.3 (Chicko s and Acree, 2003)	14.2 (Lide, 2008)	0.59 (Lide, 2008)	80.2 (Lide, 2008)	42.40 (Stauding er and Roberts, 2001; Sander, 2015)	0
fuorobenzene	96.10	H ₂ O	IGC	32.6 (Hartkop f and Karger, 1973)	6.5x1 0 ⁻⁸	34.5 (Chicko s and Acree, 2003)	10.3 (Lide, 2008)	1.6 (Lide, 2008)	80.2 (Lide, 2008)	34.92 (Stauding er and Roberts, 2001; Sander, 2015)	0
chlorobenzene	112.56	H ₂ O	IGC	36.4 (Arp et al., 2006)	3.1x1 0 ⁻⁷	46.2 (Chicko s and Acree, 2003)	13.2 (Lide, 2008)	1.69 (Yaws, 2014)	80.2 (Lide, 2008)	31.59 (Stauding er and Roberts, 2001; Sander, 2015)	0
chlorobenzene	112.56	H ₂ O	IGC	35.1 (Hartkop f and Karger, 1973)	1.8x1 0 ⁻⁷	46.2 (Chicko s and Acree, 2003)	13.2 (Lide, 2008)	1.69 (Yaws, 2014)	80.2 (Lide, 2008)	31.59 (Stauding er and Roberts, 2001; Sander, 2015)	0
naphthalene	128.17	H ₂ O	IGC	67 (Raja et al., 2002)	8.8x1 0 ⁻²	53.4 (Chicko s and Acree, 2003)	16.99 (Lide, 2008)	0 (Yaws, 2014)	80.2 (Lide, 2008)	44.07 (Fogg and Sangster, 2003; Sander, 2015)	0
naphthalene	128.17	H ₂ O	IGC	50.4 (Arp et al., 2006)	9.7x1 0 ⁻⁵	53.4 (Chicko s and Acree, 2003)	16.99 (Lide, 2008)	0 (Yaws, 2014)	80.2 (Lide, 2008)	44.07 (Fogg and Sangster, 2003; Sander, 2015)	0
phenanthrene	178.23	H ₂ O	IGC	104 (Raja et al., 2002)	3.5x1 0 ⁵	78.7 (Chicko s and Acree, 2003)	30.75 (Lide, 2008)	0 (Yaws, 2014)	80.2 (Lide, 2008)	34.92 (Fogg and Sangster, 2003; Sander, 2015)	0

1,2,3,4-tetrachlorobenzene	215.88	H ₂ O	IGC	54.5 (Arp et al., 2006)	5.2×10 ⁻⁴	60.1 (Chickos and Acree, 2003)	18.2 (Mceachran et al., 2018)	2.42 (Lide, 2008)	80.2 (Lide, 2008)	39.91 (Sander, 2015; Tenhulshaker et al., 1992)	0
1,2,3,5-tetrachlorobenzene	215.88	H ₂ O	IGC	50.7 (Arp et al., 2006)	1.1×10 ⁻⁴	60.7 (Chickos and Acree, 2003)	18.2 (Mceachran et al., 2018)	1.46 (Lide, 2008)	80.2 (Lide, 2008)		0
1,2,4,5-tetrachlorobenzene	215.88	H ₂ O	IGC	64.7 (Arp et al., 2006)	3.4×10 ⁻²	60.7 (Chickos and Acree, 2003)	18.2 (Mceachran et al., 2018)	0.06 (Baron and Arevalo, 1988)	80.2 (Lide, 2008)		0
1,2,4-trichlorobenzene	181.44	H ₂ O	IGC	57.2 (Arp et al., 2006)	1.6×10 ⁻³	55.5 (Chickos and Acree, 2003)	16.32 (Bosque and Sales, 2002)	1.26 (in benzene) (Yaws, 2014)	80.2 (Lide, 2008)	37.62 (Sander, 2015)	0
1,2-dinitrobenzene	168.11	H ₂ O	IGC	69.2 (Goss, 2009)	2.2×10 ⁻¹	60 (Chickos and Acree, 2003)	15.6 (Mceachran et al., 2018)	6.3 (in benzene) (Yaws, 2014)	80.2 (Lide, 2008)		0.67
1,3-dinitrobenzene	168.11	H ₂ O	IGC	59.2 (Goss, 2009)	3.6×10 ⁻³	96.7 (Chickos and Acree, 2003)	15.6 (Mceachran et al., 2018)	3.84 (in benzene) (Yaws, 2014)	80.2 (Lide, 2008)		0.67
2,4-dinitrotoluene	168.11	H ₂ O	IGC	78.1 (Goss, 2009)	8.4	76.9 (Chickos and Acree, 2003)	17.5 (Mceachran et al., 2018)	4.32 (in benzene) (Yaws, 2014)	80.2 (Lide, 2008)	24.11 (Sander, 2015; Goldstein, 1982)	0.67
1-methylnaphthalene	142.20	H ₂ O	IGC	48.4 (Arp et al., 2006)	4.2×10 ⁻⁵	62.4 (Chickos and Acree, 2003)	19.35 (Lide, 2008)	0.51 (in benzene) (Yaws, 2014)	80.2 (Lide, 2008)	50.72 (Fogg and Sangster, 2003; Sander, 2015)	0
2,3-dichlorophenol	163.0	H ₂ O	IGC	75.6 (Arp et al., 2006)	3.0	60.8 (Chickos and Acree, 2003)	15 (Mceachran et al., 2018)		80.2 (Lide, 2008)		0.17
2,6-dichlorophenol	163.0	H ₂ O	IGC	65.4 (Arp et al., 2006)	4.6×10 ⁻²	57.9 (Chickos and Acree, 2003)	15 (Mceachran et al., 2018)	5.03 (in benzene) (Oszust and Ratajczak, 1981)	80.2 (Lide, 2008)		0.17
2-chlorophenol	128.56	H ₂ O	IGC	57.9 (Arp et al., 2006)	2.1×10 ⁻³	47 (Chickos and Acree, 2003)	13.1 (Mceachran et al., 2018)	1.33 (in benzene) (Yaws, 2014)	80.2 (Lide, 2008)	47.39 (Tabai et al., 1997; Sander, 2015)	0.17
2,4,5-trichlorophenol	197.44	H ₂ O	IGC	85.4 (Arp et al., 2006)	1.7×10 ²	54.5 (Chickos and Acree, 2003)	17 (Mceachran et al., 2018)	2.4 (Baron and Acree, 1988)	80.2 (Lide, 2008)		0.17

				al., 2006)		Acree, 2003)	n et al., 2018)	Arevalo, 1988)			
2-nitroanisole	153.14	H ₂ O	IGC	65.4 (Arp et al., 2006)	4.6×10 ⁻²	58.6 (Chickos and Acree, 2003)	15.7 (Lide, 2008)	5 (liq.) (Lide, 2008)	80.2 (Lide, 2008)		0.43
2-nitrotoluene	137.14	H ₂ O	IGC	50.1 (Arp et al., 2006)	8.5×10 ⁻⁵	59.1 (Chickos and Acree, 2003)	14.9 (Mceachran et al., 2018)	3.75 (in benzene) (Yaws, 2014)	80.2 (Lide, 2008)	24.11 (Sander, 2015; Baron and Arevalo, 1988)	0.29
2-phenylethyl acetate	164.20	H ₂ O	IGC	77.4 (Goss, 2009)	6.3	64.5 (Chickos and Acree, 2003)	18.6 (Mceachran et al., 2018)	1.85 (in benzene) (Rajyam and Murty, 1966; Mopsik, 1967)	80.2 (Lide, 2008)		0.2
3(m)-nitroanisole	153.14	H ₂ O	IGC	55.6 (Arp et al., 2006)	8.2×10 ⁻⁴	49.8 (Chickos and Acree, 2003)	15.7 (Lide, 2008)	4.51 (Groves and Sudden, 1937)	80.2 (Lide, 2008)		0.43
4(p)-nitroanisole	153.14	H ₂ O	IGC	69.7 (Arp et al., 2006)	2.7×10 ⁻¹	54.2 (Chickos and Acree, 2003)	15.7 (Lide, 2008)	5.22 (Groves and Sudden, 1937)	80.2 (Lide, 2008)		0.43
acenaphthene	154.21	H ₂ O	IGC	60.8 (Arp et al., 2006)	6.9×10 ⁻³	66.2 (Chickos and Acree, 2003)	20.61 (Lide, 2008)	~0.85 (Lide, 2008)	80.2 (Lide, 2008)	54.04 (Fogg and Sangster, 2003; Sander, 2015)	0
acetophenone	120.15	H ₂ O	IGC	52.2 (Arp et al., 2006)	2.0×10 ⁻⁴	55.4 (Chickos and Acree, 2003)	15 (Lide, 2008)	3.02 (Lide, 2008)	80.2 (Lide, 2008)	64.02 (Staudinger and Roberts, 2001; Sander, 2015)	0
α-HCH	290.81	H ₂ O	IGC	85.5 (Goss, 2009)	1.7×10 ²		22.5 (Mceachran et al., 2018)	2.2	80.2 (Lide, 2008)	54.04 (Sander, 2015)	0
anthracene	178.23	H ₂ O	IGC	64 (Arp et al., 2006)	2.6×10 ⁻²	79.6 (Chickos and Acree, 2003)	25.67 (Lide, 2008)	0 (Yaws, 2014)	80.2 (Lide, 2008)	47.39 (Fogg and Sangster, 2003; Sander, 2015)	0
azobenzene	182.23	H ₂ O	IGC	74.4 (Arp et al., 2006)	1.8	72.8 (Chickos and Acree, 2003)	23.3 (Mceachran et al., 2018)	0 (Merino and Ribagorda, 2012)	80.2 (Lide, 2008)		0

benzaldehyde	106.12	H ₂ O	IGC	53.9 (Goss, 2009)	4.1×10 ⁻⁴	49.1 (Chickos and Acree, 2003)	12.7 (Bosque and Sales, 2002)	3 (liq.) (Lide, 2008)	80.2 (Lide, 2008)	45.73 (Fogg and Sangster, 2003; Sander, 2015)	0.14
benzyl acetate	150.18	H ₂ O	IGC	70.5 (Goss, 2009)	3.7×10 ⁻¹	55.5 (Chickos and Acree, 2003)	16.7 (Mceachra n et al., 2018)	1.22 (liq.) (Lide, 2008)	80.2 (Lide, 2008)		0.22
biphenyl	154.21	H ₂ O	IGC	59.5 (Arp et al., 2006)	4.0×10 ⁻³	64.5 (Chickos and Acree, 2003)	20.2 (Mceachra n et al., 2018)	0 (Yaws, 2014)	80.2 (Lide, 2008)	38.80 (Sander, 2015)	0
bromobenzene	157.01	H ₂ O	IGC	31.2 (Arp et al., 2006)	3.6×10 ⁻⁸	44.5 (Chickos and Acree, 2003)	13.62 (Lide, 2008)	1.7 (Lide, 2008)	80.2 (Lide, 2008)	34.92 (Fogg and Sangster, 2003; Sander, 2015)	0
dibenzofurane	168.20	H ₂ O	IGC	61.5 (Arp et al., 2006)	9.2×10 ⁻³	66.2 (Chickos and Acree, 2003)	21.5	0.88 (in benzene) (Yaws, 2014)	80.2 (Lide, 2008)		0.08
ethylbenzene	106.17	H ₂ O	IGC	35.9 (Goss, 2009)	2.5×10 ⁻⁷	42.3 (Chickos and Acree, 2003)	14.2 (Lide, 2008)	0.6 (Yaws, 2014)	80.2 (Lide, 2008)	41.16 (Sander, 2015)	0
<i>m</i> -cresol	108.14	H ₂ O	IGC	64.8 (Arp et al., 2006)	3.6×10 ⁻²	62.5 (Chickos and Acree, 2003)	13.1 (Mceachra n et al., 2018)	1.48 (liq.) (Lide, 2008)	80.2 (Lide, 2008)	62.36 (Sander, 2015)	0.14
methylbenzoate	136.15	H ₂ O	IGC	54.8 (Goss, 2009)	5.9×10 ⁻⁴	55.6 (Chickos and Acree, 2003)	15.06 (Bosque and Sales, 2002)	1.94 (liq.) (Lide, 2008)	80.2 (Lide, 2008)		0.25
<i>p</i> -cresol	108.14	H ₂ O	IGC	66.6 (Arp et al., 2006)	7.5×10 ⁻²	62 (Chickos and Acree, 2003)	13.2 (Bosque and Sales, 2002)	1.48 (liq.) (Lide, 2008)	80.2 (Lide, 2008)	62.63 (Sander, 2015)	0.14
phenanthrene	178.23	H ₂ O	IGC	66.5 (Arp et al., 2006)	7.2×10 ⁻²	78.7 (Chickos and Acree, 2003)	30.75 (Lide, 2008)	0 (Yaws, 2014)	80.2 (Lide, 2008)	34.92 (Fogg and Sangster, 2003; Sander, 2015)	0
phenol	94.11	H ₂ O	IGC	63 (Arp et al., 2006)	1.7×10 ⁻²	58.8 (Chickos and Acree, 2003)	10.52 (Lide, 2008)	1.224 (Lide, 2008)	80.2 (Lide, 2008)	49.61 (Sander, 2015)	0.17
propylbenzene	120.20	H ₂ O	IGC	47.2 (Goss, 2009)	2.6×10 ⁻⁵	46.2 (Chickos and Acree, 2003)	16 (Mceachra n et al., 2018)	0.37 (in benzene)	80.2 (Lide, 2008)	34.75 (Sander, 2015)	0

						Acree, 2003)	n et al., 2018)	(Yaws, 2014)			
<i>p</i> -xylene	106.17	H ₂ O	IGC	35.5 (Goss, 2009)	2.1×10 ⁻⁷	42.3 (Chickos and Acree, 2003)	14.35 (Bosque and Sales, 2002)	0 (Yaws, 2014)	80.2 (Lide, 2008)	34.92 (Fogg and Sangster, 2003; Sander, 2015)	0
tetrahydrofuran	72.11	H ₂ O	IGC	42.6 (Arp et al., 2006)	3.9×10 ⁻⁶	32 (Chickos and Acree, 2003)	7.97 (Bosque and Sales, 2002)	1.75 (Lide, 2008)	80.2 (Lide, 2008)	35.75 (Sander, 2015)	0.25

1259

1260

1261 **Table A11.** Compiled adsorbate-substrate data for volatile amine and alcohol compounds
1262 adsorbed on water. Gas species, gas species' molar mass, substrate, experimental or theoretical
1263 method, desorption energy (E_{des}^0), and desorption lifetimes (τ_{des}) evaluated at 293 K using A_{des}
1264 = 10^{13} s^{-1} , enthalpy of vaporization (ΔH_{vap}) and solvation (ΔH_{solv}), gas species' polarizability (α),
1265 gas species' dipole moment (μ), substrate's relative permittivity (ϵ_r), and gas species' oxygen to
1266 carbon ration ($O:C$) are given.

Gas Species	Molar Mass / g mol ⁻¹	Substrate	Method	E_{des}^0 / kJ mol ⁻¹	$\tau_{des}^{293 K}$ / s	ΔH_{vap} (T) / kJ mol ⁻¹	α / 10 ⁻²⁴ cm ³	μ / D	ϵ_r	ΔH_{solv} (T) / kJ mol ⁻¹	O:C
methylamine	31.06	H ₂ O	ST	28 (Mmerek i et al., 2000)	9.8×10 ⁻⁹	26.1 (Chickos and Acree, 2003)	4.24 (Lide, 2008)	1.31 (Lide, 2008)	80.2 (Lide, 2008)	33.67 (Sander, 2015)	0
dimethylamine	45.09	H ₂ O	ST	37 (Mmerek i et al., 2000)	3.9×10 ⁻⁷	27 (Chickos and Acree, 2003)	6.37 (Hickey and Rowley, 2014)	1.01 (Lide, 2008)	80.2 (Lide, 2008)	43.23 (Sander, 2015)	0
trimethylamine	59.11	H ₂ O	ST	34 (Mmerek i et al., 2000)	1.2×10 ⁻⁷	24.1 (Chickos and Acree, 2003)	8.15 (Hickey and Rowley, 2014)	0.612 (Lide, 2008)	80.2 (Lide, 2008)	49.6 (Leng et al., 2015)	0
methanol	32.04	H ₂ O	ST	39.2 (Donald son and Anderson, 1999)	9.7×10 ⁻⁷	37.8 (Chickos and Acree, 2003)	3.28 (Lide, 2008)	1.7 (Lide, 2008)	80.2 (Lide, 2008)	46.56 (Sander, 2015; Sander et al., 2011)	0
1-propanol	60.09	H ₂ O	ST	68.2 (Donald son and Anderson, 1999)	1.4×10 ⁻¹	47.45 (Chickos and Acree, 2003)	6.74 (Lide, 2008)	1.58 (Lide, 2008)	80.2 (Lide, 2008)	57.37 (Sander, 2015; Sander et al., 2011)	0.33
2-propanol	60.09	H ₂ O	ST	68.9 (Donald son and Anderson, 1999)	1.9×10 ⁻¹	45.34 (Chickos and Acree, 2003)	7.29 (Lide, 2008)	1.58 (Lide, 2008)	80.2 (Lide, 2008)	62.36 (Sander, 2015; Sander et al., 2011)	0.33
1-propanol	60.09	H ₂ O	ST	58.8 (Demou and Donalds)	3.0×10 ⁻³	47.45 (Chickos and Acree, 2003)	6.74 (Lide, 2008)	1.58 (Lide, 2008)	80.2 (Lide, 2008)	57.37 (Sander, 2015; Sander et al., 2011)	0.33

				on, 2002)							
1-propanol	60.09	H ₂ O	ST	56.7 (Goss, 2009)	1.3×10 ⁻³	47.45 (Chickos and Acree, 2003)	6.74 (Lide, 2008)	1.58 (Lide, 2008)	80.2 (Lide, 2008)	57.37 (Sander, 2015; Sander et al., 2011)	0.33
1-butanol	74.12	H ₂ O	ST	62.8 (Donald son and Anderson, 1999)	1.6×10 ⁻²	52.34 (Chickos and Acree, 2003)	8.88 (Lide, 2008)	1.66 (Lide, 2008)	80.2 (Lide, 2008)	62.36 (Sander, 2015; Sander et al., 2011)	0.25
2-butanol	74.12	H ₂ O	ST	63.5 (Donald son and Anderson, 1999)	2.1×10 ⁻²	49.74 (Chickos and Acree, 2003)	8.77 (Bosque and Sales, 2002)	1.66 (Yaws, 2014)	80.2 (Lide, 2008)	60.70 (Sander, 2015; Sander et al., 2011)	0.25
1-butanol	74.12	H ₂ O	IGC	56.1 (Goss, 2009)	1.0×10 ⁻³	52.34 (Chickos and Acree, 2003)	8.88 (Lide, 2008)	1.66 (Lide, 2008)	80.2 (Lide, 2008)	62.36 (Sander, 2015; Sander et al., 2011)	0.25
ethanediol	62.07	H ₂ O	IGC	84.8 (Goss, 2009)	1.3×10 ²	65.6 (Chickos and Acree, 2003)	5.72 (Bosque and Sales, 2002)	2.36 (Lide, 2008)	80.2 (Lide, 2008)	73.17 (Comperno lle and Muller, 2014; Sander, 2015)	1
ethanol	46.07	H ₂ O	IGC	51.1 (Goss, 2009)	1.3×10 ⁻⁴	42.4 (Chickos and Acree, 2003)	5.41 (Lide, 2008)	1.69 (Lide, 2008)	80.2 (Lide, 2008)	53.21 (Sander, 2015; Sander et al., 2011)	0.5
cyclohexanol	100.16	H ₂ O	IGC	79.5 (Goss, 2009)	1.5×10 ¹	62 (Chickos and Acree, 2003)	11.56 (Lide, 2008)	1.86 (in CCl ₄) (Yaws, 2014)	80.2 (Lide, 2008)	66.51 (Sander, 2015)	0.17
cyclopentanol	86.13	H ₂ O	IGC	62.7 (Goss, 2009)	1.5×10 ⁻²	57.5 (Chickos and Acree, 2003)	9.72 (Lide, 2008)		80.2 (Lide, 2008)	63.19 (Sander, 2015)	0.2
3-methylbutan-1-ol	88.15	H ₂ O	IGC	61.6 (Goss, 2009)	9.6×10 ⁻³	54.3 (Chickos and Acree, 2003)	10.61 (Lide, 2008)	1.88 (2- Methylbuta n-1-ol) (Lide, 2008)	80.2 (Lide, 2008)	63.19 (Kuhne et al., 2005)	0.2
1,2-propanediol	76.10	H ₂ O	IGC	64.5 (Goss, 2009)	3.2×10 ⁻²	58.6 (Chickos and Acree, 2003)	7.55 (Bosque and Sales, 2002)	2.25 (liq.) (Lide, 2008)	80.2 (Lide, 2008)	78.99 (Comperno lle and Muller, 2014; Sander, 2015)	0.67
1,3-propanediol	76.10	H ₂ O	IGC	75 (Goss, 2009)	2.3	72.4 (Chickos and Acree, 2003)	7.54 (Mceachran et al., 2018)	2.55 (liq.) (Lide, 2008)	80.2 (Lide, 2008)	78.99 (Comperno lle and Muller, 2014; Sander, 2015)	0.67

1,4-butanediol	90.12	H ₂ O	IGC	105.1 (Goss, 2009)	5.4×10 ⁵	79.3 (Chickos and Acree, 2003)	9.35 (Bosque and Sales, 2002)	2.48 (liq.) (Lide, 2008)	80.2 (Lide, 2008)	91.46 (Comperno Ile and Muller, 2014; Sander, 2015)	0.5
1-decanol	158.29	H ₂ O	IGC	94.8 (Goss, 2009)	7.9×10 ³	81.5 (Chickos and Acree, 2003)	19.83 (Bosque and Sales, 2002)	1.70 (Crossley, 1971)	80.2 (Lide, 2008)	49.47 (Sander, 2015)	0.1
1-heptanol	116.20	H ₂ O	IGC	75.7 (Goss, 2009)	3.1	66.5 (Chickos and Acree, 2003)	14.3 (Bosque and Sales, 2002)	1.74 (in benzene) (Yaws, 2014)	80.2 (Lide, 2008)	56.12 (Sander, 2015)	0.14
1-hexanol	102.18	H ₂ O	IGC	66.2 (Goss, 2009)	6.3×10 ⁻²	61.6 (Chickos and Acree, 2003)	12.46 (Bosque and Sales, 2002)	1.55 (Speight, 2017)	80.2 (Lide, 2008)	51.96 (Sander, 2015)	0.17
1-nonanol	144.26	H ₂ O	IGC	86.3 (Goss, 2009)	2.4×10 ²	76.9 (Chickos and Acree, 2003)	18 (Mceachran et al., 2018)	1.61 (in benzene) (Yaws, 2014)	80.2 (Lide, 2008)	51.96 (Sander, 2015)	0.11
1-octanol	130.23	H ₂ O	IGC	75.7 (Goss, 2009)	3.1	71 (Chickos and Acree, 2003)	16.14 (Bosque and Sales, 2002)	1.76 (liq.) (Lide, 2008)	80.2 (Lide, 2008)	53.63 (Sander, 2015)	0.13
1-pentanol	88.15	H ₂ O	IGC	68.9 (Goss, 2009)	1.9×10 ⁻¹	57.8 (Chickos and Acree, 2003)	10.61 (Bosque and Sales, 2002)	1.7 (liq.) (Lide, 2008)	80.2 (Lide, 2008)	55.91 (Sander, 2015)	0.2
1-undecanol	172.31	H ₂ O	IGC	88 (Goss, 2009)	4.9×10 ²	83.5 (Chickos and Acree, 2003)	21.6 (Mceachran et al., 2018)	1.67 (Yaws, 2014)	80.2 (Lide, 2008)		0.09
2-methylpropan-1-ol	74.12	H ₂ O	IGC	50.7 (Goss, 2009)	1.1×10 ⁻⁴	54.1 (Chickos and Acree, 2003)	8.92 (Lide, 2008)	1.64 (Lide, 2008)	80.2 (Lide, 2008)	59.86 (Kuhne et al., 2005)	0.25

1267

1268

1269 **Table A12.** Compiled adsorbate-substrate data for alkene and ketone compounds adsorbed on
1270 water. Gas species, gas species' molar mass, substrate, experimental or theoretical method,
1271 desorption energy (E_{des}^0), and desorption lifetimes (τ_{des}) evaluated at 293 K using $A_{des} = 10^{13} \text{ s}^{-1}$,
1272 enthalpy of vaporization (ΔH_{vap}) and solvation (ΔH_{solv}), gas species' polarizability (α), gas
1273 species' dipole moment (μ), substrate's relative permittivity (ϵ_r), and gas species' oxygen to
1274 carbon ration (O:C) are given.

Gas Species	Molar Mass / g mol ⁻¹	Substrate	Method	E_{des}^0 / kJ mol ⁻¹	$\tau_{des}^{293 K}$ / s	ΔH_{vap} (T) / kJ mol ⁻¹	α / 10 ⁻²⁴ cm ³	μ / D	ϵ_r	ΔH_{solv} (T) / kJ mol ⁻¹	O:C
1-decene	140.27	H ₂ O	IGC	47.5 (Goss, 2009)	2.9×10 ⁻⁵	50.4 (Chickos and Acree, 2003)	19.1 (Mceachran et al., 2018)	0.42 (in benzene) (Yaws, 2014)	80.2 (Lide, 2008)		0

1-dodecene	168.32	H ₂ O	IGC	49 (Goss, 2009)	5.4×10 ⁻⁵	60.8 (Chickos and Acree, 2003)	22.7 (Mceachran et al., 2018)	0.52 (in benzene) (Yaws, 2014)	80.2 (Lide, 2008)		0
1-tridecene	182.35	H ₂ O	IGC	52.7 (Goss, 2009)	2.5×10 ⁻⁴	65.3 (Chickos and Acree, 2003)	24.6 (Mceachran et al., 2018)	0 (Yaws, 2014)	80.2 (Lide, 2008)		0
cis-2-octene	112.22	H ₂ O	IGC	36 (Hartkop f and Karger, 1973)	2.6×10 ⁻⁷	40.2 (Chickos and Acree, 2003)	15.5 (Mceachran et al., 2018)	0.31 (Yaws, 2014)	80.2 (Lide, 2008)		0
trans-2-octene	112.22	H ₂ O	IGC	36 (Hartkop f and Karger, 1973)	2.6×10 ⁻⁷	40.2 (Chickos and Acree, 2003)	15.5 (Mceachran et al., 2018)	0 (Yaws, 2014)	80.2 (Lide, 2008)		0
1-nonene	126.24	H ₂ O	IGC	44.3 (Goss, 2009)	7.9×10 ⁻⁶	44.7 (Chickos and Acree, 2003)	17.2 (Mceachran et al., 2018)	0.36 (Yaws, 2014)	80.2 (Lide, 2008)		0
1-undecene	154.30	H ₂ O	IGC	54.1 (Goss, 2009)	4.4×10 ⁻⁴	54.3 (Chickos and Acree, 2003)	20.9 (Mceachran et al., 2018)	0.53 (in benzene) (Yaws, 2014)	80.2 (Lide, 2008)		0
acetone	58.08	H ₂ O	ST	50.3 (Donald son and Anderso n, 1999)	9.3×10 ⁻⁵	31.3 (Chickos and Acree, 2003)	6.37 (Lide, 2008)	2.88 (Lide, 2008)	80.2 (Lide, 2008)	44.27 (Sander, 2015)	0.33
propanone	58.08	H ₂ O	IGC	42.9 (Arp et al., 2006)	4.4×10 ⁻⁶	31.3 (Chickos and Acree, 2003)	6.37 (Lide, 2008)	2.88 (=acetone) (Yaws, 2014)	80.2 (Lide, 2008)	44.27 (Sander, 2015)	0.33
pentanal	86.13	H ₂ O	IGC	46.7 (Goss, 2009)	2.1×10 ⁻⁵	38.3 (Chickos and Acree, 2003)	10.1 (Mceachran et al., 2018)	2.57 (in benzene) (Yaws, 2014)	80.2 (Lide, 2008)	51.55 (Sander, 2015)	0.2
2,3-butanedione	86.09	H ₂ O	IGC	46.9 (Goss, 2009)	2.3×10 ⁻⁵	38.5 (Chickos and Acree, 2003)	8.2 (Lide, 2008)	1.03 (Henderson and Meyer, 1976)	80.2 (Lide, 2008)	51.55 (Sander, 2015)	0.5
2,5-hexanedione	114.14	H ₂ O	IGC	64.1 (Goss, 2009)	2.7×10 ⁻²	50.1 (Chickos and Acree, 2003)	11.9 (Mceachran et al., 2018)	2.5 (in dioxane) (Wittwer et al., 1988)	80.2 (Lide, 2008)		0.33
2-butanone	72.11	H ₂ O	IGC	49.3 (Arp et al., 2006)	6.1×10 ⁻⁵	34.8 (Chickos and Acree, 2003)	8.25 (Bosque and Sales, 2002)	2.78 (Lide, 2008)	80.2 (Lide, 2008)	99.77	0.25
2-heptanone	114.19	H ₂ O	IGC	59.7 (Arp et al., 2006)	4.4×10 ⁻³	47.4 (Chickos and Acree, 2003)	13.7 (Mceachran et al., 2018)	2.59 (liq.) (Lide, 2008)	80.2 (Lide, 2008)	46.56 (Sander, 2015)	0.14
2-hexanone	100.16	H ₂ O	IGC	47 (Arp et al., 2006)	2.4×10 ⁻⁵	43.1 (Chickos and Acree, 2003)	11.95 (Bosque and Sales, 2002)	2.66 (liq.) (Lide, 2008)	80.2 (Lide, 2008)	52.05 (Sander, 2015)	0.17

2-octanone	128.22	H ₂ O	IGC	63.2 (Arp et al., 2006)	1.8×10 ⁻²	52.6 (Chickos and Acree, 2003)	15.5 (Mceachran et al., 2018)	2.7 (liq.) (Lide, 2008)	80.2 (Lide, 2008)	60.69 (Kuhne et al., 2005; Sander, 2015)	0.13
2-pentanone	86.13	H ₂ O	IGC	43.2 (Arp et al., 2006)	5.0×10 ⁻⁶	38.3 (Chickos and Acree, 2003)	9.93 (Lide, 2008)	2.7 (liq.) (Lide, 2008)	80.2 (Lide, 2008)	41.85 (Sander, 2015)	0.2
cyclopentanone	84.19	H ₂ O	IGC	54.1 (Arp et al., 2006)	4.4×10 ⁻⁴	42.7 (Chickos and Acree, 2003)	9.19 (Mceachran et al., 2018)	3.3 (liq.) (Lide, 2008)	80.2 (Lide, 2008)	48.22 (Kuhne et al., 2005; Sander, 2015)	0.2

1275

1276

1277 **Table A13.** Compiled adsorbate-substrate data for volatile acid and ether compounds adsorbed on
1278 water. Gas species, gas species' molar mass, substrate, experimental or theoretical method,
1279 desorption energy (E_{des}^0), and desorption lifetimes (τ_{des}) evaluated at 293 K using $A_{des} = 10^{13} \text{ s}^{-1}$,
1280 enthalpy of vaporization (ΔH_{vap}) and solvation (ΔH_{solv}), gas species' polarizability (α), gas
1281 species' dipole moment (μ), substrate's relative permittivity (ϵ_r), and gas species' oxygen to
1282 carbon ration (O:C) are given.

Gas Species	Molar Mass / g mol ⁻¹	Substrate	Method	E_{des}^0 / kJ mol ⁻¹	$\tau_{des}^{293 K}$ / s	ΔH_{vap} (T) / kJ mol ⁻¹	α / 10 ⁻²⁴ cm ³	μ / D	ϵ_r	ΔH_{solv} (T) / kJ mol ⁻¹	O:C
acetic acid	60.05	H ₂ O	ST	58.8 (Donaldson and Anderson, 1999)	3.0×10 ⁻³	41.6 (Chickos and Acree, 2003)	5.1 (Lide, 2008)	1.7 (Lide, 2008)	80.2 (Lide, 2008)	51.96 (Sander, 2015)	1
propionic acid	74.08	H ₂ O	ST	61.4 (Donaldson and Anderson, 1999)	8.8×10 ⁻³	31.1 (Chickos and Acree, 2003)	6.9 (Lide, 2008)	1.75 (Lide, 2008)	80.2 (Lide, 2008)	56.54 (Abraham, 1984; Sander, 2015)	0.67
butanoic acid	88.11	H ₂ O	ST	58.6 (Donaldson and Anderson, 1999)	2.8×10 ⁻³	40.5 (Chickos and Acree, 2003)	8.58 (Lide, 2008)	1.65 (liq.) (Lide, 2008)	80.2 (Lide, 2008)	59.86 (Abraham, 1984; Sander, 2015)	0.5
hexanoic acid	116.16	H ₂ O	ST	57.6 (Demou and Donaldson, 2002)	1.9×10 ⁻³	69.2 (Chickos and Acree, 2003)	12.5	1.13 (liq.) (Lide, 2008)	80.2 (Lide, 2008)	50.72 (Staudinger and Roberts, 2001; Sander, 2015)	0.33
methyl formate	60.05	H ₂ O	IGC	32.6 (Hartkopf and Karger, 1973)	6.5×10 ⁻⁸	31.6 (Chickos and Acree, 2003)	5.05 (Lide, 2008)	1.77 (Lide, 2008)	80.2 (Lide, 2008)	33.26 (Sander, 2015; Sander et al., 2011)	1
ethyl formate	74.08	H ₂ O	IGC	28.9 (Hartkopf and Karger, 1973)	1.4×10 ⁻⁸	31.6 (Chickos and Acree, 2003)	6.88 (Lide, 2008)	1.93 (Lide, 2008)	80.2 (Lide, 2008)	38.25 (Sander, 2015; Sander et al., 2011)	0.67

				Karger, 1973)						Sander et al., 2011)	
butyl acetate	116.16	H ₂ O	IGC	60.4 (Goss, 2009)	5.9×10 ⁻³	41.3 (Chickos and Acree, 2003)	12.57 (Bosque and Sales, 2002)	1.87 (liq.) (Lide, 2008)	80.2 (Lide, 2008)	46.01 (Sander, 2015)	0.33
Diethyl phthalate	222.24	H ₂ O	IGC	94.6 (Goss, 2009)	7.3×10 ³	81.8 (Chickos and Acree, 2003)	23.4 (Mceachran et al., 2018)	2.73 (in benzene) (Yaws, 2014)	80.2 (Lide, 2008)	100.7 (Kuhne et al., 2005)	0.33
dimethyl oxalate	118.09	H ₂ O	IGC	48.2 (Goss, 2009)	3.9×10 ⁻⁵	48.8 (Chickos and Acree, 2003)	9.57 (Mceachran et al., 2018)	2 (in m-xylene) (Aihara and Davies, 1956)	80.2 (Lide, 2008)		1
dimethyl phthalate	194.19	H ₂ O	IGC	84 (Goss, 2009)	9.4×10 ¹	77.2 (Chickos and Acree, 2003)	19.7 (Mceachran et al., 2018)	2.78 (in benzene) (Yaws, 2014)	80.2 (Lide, 2008)		0.4
dimethyl succinate	146.14	H ₂ O	IGC	63.3 (Goss, 2009)	1.9×10 ⁻²	49.3 (Chickos and Acree, 2003)	13.2 (Mceachran et al., 2018)	2.16 (in benzene) (Yaws, 2014)	80.2 (Lide, 2008)	64.85 (Sander, 2015)	0.5
pentyl acetate	130.19	H ₂ O	IGC	58.3 (Goss, 2009)	2.5×10 ⁻³	48.6 (Chickos and Acree, 2003)	14.9 (Lide, 2008)	1.75 (Lide, 2008)	80.2 (Lide, 2008)	54.04 (Kieckbusch and King, 1979; Sander, 2015)	0.29
ethyl acetate	88.11	H ₂ O	IGC	47 (Goss, 2009)	2.4×10 ⁻⁵	35.1 (Chickos and Acree, 2003)	8.62 (Lide, 2008)	1.78 (Lide, 2008)	80.2 (Lide, 2008)	49.05 (Sander, 2015; Sander et al., 2011)	0.5
di-n-butyl ether	130.23	H ₂ O	IGC	57.4 (Arp et al., 2006)	1.7×10 ⁻³	45 (Chickos and Acree, 2003)	16.31 (Bosque and Sales, 2002)	~1.17 (Lide, 2008)	80.2 (Lide, 2008)	54.87 (Kuhne et al., 2005; Sander, 2015)	0.125
di-n-pentyl ether	158.28	H ₂ O	IGC	59.6 (Arp et al., 2006)	4.2×10 ⁻³	46.2 (Chickos and Acree, 2003)	19.9 (Mceachran et al., 2018)	~1.2 (liq.) (Lide, 2008)	80.2 (Lide, 2008)		0.1
ethyl-t-butyl ether	102.18	H ₂ O	IGC	47.9 (Arp et al., 2006)	3.5×10 ⁻⁵	33.5 (Chickos and Acree, 2003)	12.5 (Mceachran et al., 2018)	1.22 (in benzene) (Yaws, 2014)	80.2 (Lide, 2008)	39.2 (Kuhne et al., 2005)	0.17
methyl tert-butyl ether	88.15	H ₂ O	IGC	38.7 (Arp et al., 2006)	7.9×10 ⁻⁷	30.4 (Chickos and Acree, 2003)	10.7 (Mceachran et al., 2018)	1.36 (in benzene) (Yaws, 2014)	80.2 (Lide, 2008)	45.97 (Sander, 2015)	0.2
n-propyl ether	102.18	H ₂ O	IGC	53.6 (Hartkopf and Karger, 1973)	3.6×10 ⁻⁴	35.7 (Chickos and Acree, 2003)	12.5 (Mceachran et al., 2018)	1.21 (Yaws, 2014)	80.2 (Lide, 2008)	61.80 (Sander, 2015)	0.17

1283

1284

1285 **Table A14.** Compiled adsorbate-substrate data for volatile alkane compounds adsorbed on water.
 1286 Gas species, gas species' molar mass, substrate, experimental or theoretical method, desorption
 1287 energy (E_{des}^0), and desorption lifetimes (τ_{des}) evaluated at 293 K using $A_{des} = 10^{13} \text{ s}^{-1}$, enthalpy
 1288 of vaporization (ΔH_{vap}) and solvation (ΔH_{solv}), gas species' polarizability (α), gas species' dipole
 1289 moment (μ), substrate's relative permittivity (ϵ_r), and gas species' oxygen to carbon ration ($O:C$)
 1290 are given.

Gas Species	Molar Mass / g mol^{-1}	Substrate	Method	$E_{des}^0 / \text{kJ mol}^{-1}$	$\tau_{des}^{293 \text{ K}} / \text{s}$	$\Delta H_{vap} (\text{T}) / \text{kJ mol}^{-1}$	$\alpha / 10^{-24} \text{ cm}^3$	μ / D	ϵ_r	$\Delta H_{solv} (\text{T}) / \text{kJ mol}^{-1}$	O:C
decane	142.29	H ₂ O	IGC	46.5 (Goss, 2009)	1.9×10^{-5}	51.4 (Chickos and Acree, 2003)	19.1 (Lide, 2008)	0 (Yaws, 2014)	80.2 (Lide, 2008)		0
dodecane	170.34	H ₂ O	IGC	58.1 (Goss, 2009)	2.3×10^{-3}	62.1 (Chickos and Acree, 2003)	22.75 (Laib and Mittleman, 2010)	0 (Yaws, 2014)	80.2 (Lide, 2008)		0
nonane	128.26	H ₂ O	IGC	34.6 (Goss, 2009)	1.5×10^{-7}	46.55 (Chickos and Acree, 2003)	17.36 (Laib and Mittleman, 2010)	0 (Yaws, 2014)	80.2 (Lide, 2008)	34.50 (Sander et al., 2011)	0
tetradecane	198.39	H ₂ O	IGC	67.6 (Goss, 2009)	1.1×10^{-1}	71.73 (Chickos and Acree, 2003)	26.22 (Laib and Mittleman, 2010)	0 (Yaws, 2014)	80.2 (Lide, 2008)		0
tridecane	184.37	H ₂ O	IGC	58.2 (Goss, 2009)	2.4×10^{-3}	66.68 (Chickos and Acree, 2003)	24.41 (Laib and Mittleman, 2010)	0 (Yaws, 2014)	80.2 (Lide, 2008)		0
trimethyl phosphite	124.08	H ₂ O	IGC	77.4 (Arp et al., 2006)	6.3	42.5 (Chickos and Acree, 2003)	28.6 (Aroney et al., 1964)		80.2 (Lide, 2008)		1
undecane	156.31	H ₂ O	IGC	52.8 (Goss, 2009)	2.6×10^{-4}	56.58 (Chickos and Acree, 2003)	21.03 (Lide, 2008)	0 (Yaws, 2014)	80.2 (Lide, 2008)		0
n-pentane	72.15	H ₂ O	IGC	23.8 (Hartkopf and Karger, 1973)	1.7×10^{-9}	25 (Chickos and Acree, 2003)	9.99 (Lide, 2008)	0 (Yaws, 2014)	80.2 (Lide, 2008)	25.77 (Sander et al., 2011)	0
n-hexane	86.18	H ₂ O	IGC	27.6 (Hartkopf and Karger, 1973)	8.3×10^{-9}	31.5 (Chickos and Acree, 2003)	11.9 (Lide, 2008)	0 (Yaws, 2014)	80.2 (Lide, 2008)	46.89 (Sander et al., 2011)	0
n-heptane	100.21	H ₂ O	IGC	31.4 (Hartkopf and Karger, 1973)	4.0×10^{-8}	36.6 (Chickos and Acree, 2003)	13.61 (Lide, 2008)	0 (Yaws, 2014)	80.2 (Lide, 2008)	34.64 (Sander et al., 2011)	0
n-octane	114.23	H ₂ O	IGC	35.6 (Hartkopf and Karger, 1973)	2.2×10^{-7}	41.6 (Chickos and Acree, 2003)	15.9 (Lide, 2008)	0 (Yaws, 2014)	80.2 (Lide, 2008)	45.31 (Sander et al., 2011)	0

n-nonane	128.26	H ₂ O	IGC	39.7 (Hartkopf and Karger, 1973)	1.2×10 ⁻⁶	46.55 (Chickos and Acree, 2003)	17.36 (Lide, 2008)	0 (Yaws, 2014)	80.2 (Lide, 2008)	34.50 (Sander et al., 2011)	0
n-decane	142.29	H ₂ O	IGC	44.8 (Hartkopf and Karger, 1973)	9.7×10 ⁻⁶	51.4 (Chickos and Acree, 2003)	19.1 (Lide, 2008)	0 (Yaws, 2014)	80.2 (Lide, 2008)		0
2-methylheptane	114.23	H ₂ O	IGC	34.7 (Hartkopf and Karger, 1973)	1.5×10 ⁻⁷	46.55 (Chickos and Acree, 2003)	15.5 (Mceachran et al., 2018)	0 (Yaws, 2014)	80.2 (Lide, 2008)		0
2,4-dimethylhexane	114.23	H ₂ O	IGC	33.5 (Hartkopf and Karger, 1973)	9.4×10 ⁻⁸	71.73 (Chickos and Acree, 2003)	15.5 (Mceachran et al., 2018)	0 (Yaws, 2014)	80.2 (Lide, 2008)	38.5 (2,5-dimethylhexane) (Kuhne et al., 2005)	0
2,2,4-trimethylpentane	114.23	H ₂ O	IGC	32.2 (Hartkopf and Karger, 1973)	5.5×10 ⁻⁸	66.68 (Chickos and Acree, 2003)	15.44 (Lide, 2008)	0 (Yaws, 2014)	80.2 (Lide, 2008)	36.17 (Sander et al., 2011)	0
cycloheptane	98.19	H ₂ O	IGC	31.4 (Hartkopf and Karger, 1973)	4.0×10 ⁻⁸	42.5 (Chickos and Acree, 2003)	12.84 (Bosque and Sales, 2002)	0 (Yaws, 2014)	80.2 (Lide, 2008)		0
cyclooctane	112.22	H ₂ O	IGC	35.6 (Hartkopf and Karger, 1973)	2.2×10 ⁻⁷	56.58 (Chickos and Acree, 2003)	14.62 (Bosque and Sales, 2002)	0 (Yaws, 2014)	80.2 (Lide, 2008)	39.63 (Sander et al., 2011)	0
trichloroethane	133.40	H ₂ O	ST	26.3 (Bruant and Conklin, 2001)	4.9×10 ⁻⁹	32.5 (Chickos and Acree, 2003)	10.7 (Lide, 2008)	1.78 (Yaws, 2014)	80.2 (Lide, 2008)	32.15 (Sander et al., 2011)	0
dichloromethane	84.93	H ₂ O	IGC	23.4 (Hartkopf and Karger, 1973)	1.5×10 ⁻⁹	30.6 (Chickos and Acree, 2003)	6.49 (Mceachran et al., 2018)	1.60 (Yaws, 2014)	80.2 (Lide, 2008)	33.26 (Sander et al., 2011)	0
chloroform	119.37	H ₂ O	IGC	26.8 (Hartkopf and Karger, 1973)	6.0×10 ⁻⁹	31.1 (Chickos and Acree, 2003)	8.87 (Lide, 2008)	1.01 (Yaws, 2014)	80.2 (Lide, 2008)	37.00 (Sander et al., 2011)	0
carbon tetrachloride	153.81	H ₂ O	IGC	23.4 (Hartkopf and Karger, 1973)	1.5×10 ⁻⁹	32.4 (Chickos and Acree, 2003)	10.85 (Lide, 2008)	0 (Yaws, 2014)	80.2 (Lide, 2008)	35.13 (Sander et al., 2011)	0

1,2-dichloroethane	98.95	H ₂ O	IGC	32.6 (Hartkopf and Karger, 1973)	6.5×10 ⁻⁸	35.2 (Chickos and Acree, 2003)	8 (Lide, 2008)	1.83 (Lide, 2008)	80.2 (Lide, 2008)	35.47 (Sander et al., 2011)	0
--------------------	-------	------------------	-----	-------------------------------------	----------------------	-----------------------------------	----------------	----------------------	----------------------	--------------------------------	---

1291

1292

1293 **Table A15.** Compiled adsorbate-substrate data for volatile acid and alcohol compounds adsorbed
1294 on aqueous solutions. Gas species, gas species' molar mass, substrate, experimental or theoretical
1295 method, desorption energy (E_{des}^0), and desorption lifetimes (τ_{des}) evaluated at 293 K using A_{des}
1296 = 10^{13} s^{-1} , enthalpy of vaporization (ΔH_{vap}) and solvation (ΔH_{solv}), gas species' polarizability (α),
1297 gas species' dipole moment (μ), substrate's relative permittivity (ϵ_r), and gas species' oxygen to
1298 carbon ratio ($O:C$) are given.

Gas Species	Molar Mass / g mol ⁻¹	Substrate	Method	E_{des}^0 / kJ mol ⁻¹	$\tau_{des}^{293 K}$ / s	ΔH_{vap} (T) / kJ mol ⁻¹	α / 10 ⁻²⁴ cm ³	μ / D	ϵ_r	ΔH_{solv} (T) / kJ mol ⁻¹	O:C
hexanoic acid	116.16	4 M NaCl (aq)	ST	54.2 (Demou and Donaldson, 2002)	4.6×10 ⁻⁴	69.2 (Chickos and Acree, 2003)	12.5 (Mceachran et al., 2018)	1.13 (liq.) (Lide, 2008)	40 (Maribomogensen et al., 2013)	50.72 (Staudinger and Roberts, 2001; Sander, 2015)	0.33
hexanoic acid	116.16	4 M (NH ₄) ₂ SO ₄ (aq)	ST	55.4 (Demou and Donaldson, 2002)	7.5×10 ⁻⁴	69.2 (Chickos and Acree, 2003)	12.5 (Mceachran et al., 2018)	1.13 (liq.) (Lide, 2008)	42 (Lileev and Lyashchenko, 2009)	50.72 (Staudinger and Roberts, 2001; Sander, 2015)	0.33
1-propanol	60.09	4 M NaCl (aq)	ST	58.7 (Demou and Donaldson, 2002)	2.9×10 ⁻³	47.45 (Chickos and Acree, 2003)	6.74 (Lide, 2008)	1.58 (Lide, 2008)	40 (Maribomogensen et al., 2013)	57.37 (Sander, 2015; Sander et al., 2011)	0.33
1-propanol	60.09	4 M (NH ₄) ₂ SO ₄ (aq)	ST	58.9 (Demou and Donaldson, 2002)	3.2×10 ⁻³	47.45 (Chickos and Acree, 2003)	6.74 (Lide, 2008)	1.58 (Lide, 2008)	42 (Lileev and Lyashchenko, 2009)	57.37 (Sander, 2015; Sander et al., 2011)	0.33

1299

1300 **Data availability.** Data needed to draw the conclusions in the present study are given in the paper
1301 and in the Supplement. In addition, the datasets required to reproduce the results and corresponding
1302 figures are available on Zenodo (Knopf et al., 2023).

1303

1304 **Supplement.** The supplement related to this article is available online at: XYZ

1305

1306 **Author contributions.** DAK and MS envisioned the project. DAK supervised project, performed
1307 correlation analyses, and wrote first draft of manuscript. MS performed kinetic flux modeling.
1308 MA, TB, and UP critically discussed analyses and results and were involved in representation of
1309 data. All authors discussed interpretation of the data and contributed to the writing of the paper.

1310

1311 **Competing interests.** At least one of the (co-)authors is a member of the editorial board of
1312 Atmospheric Chemistry and Physics. The peer-review process was guided by an independent
1313 editor, and the authors also have no other competing interests to declare.

1314

1315 **Disclaimer.** Publisher's note: Copernicus Publications remains neutral with regard to
1316 jurisdictional claims in published maps and institutional affiliations.

1317

1318 **Acknowledgments.** D.K. acknowledges support by the U.S. National Science Foundation (grant
1319 no. AGS-1446286) and the Max-Planck Society to support a sabbatical stay in 2014 that initiated
1320 this project. M.S. acknowledges support by the U.S. National Science Foundation (grant no. AGS-
1321 1654104) and the U.S. Department of Energy (grant no DE-SC0022139). M. A. acknowledges
1322 support by the Swiss National Science Foundation (grant no. 188662).

1323

1324 **Financial support.** This research has been supported by the U.S. National Science Foundation
1325 (grant nos. AGS-1446286 and AGS-1654104), the U.S. Department of Energy (DE-SC0022139),
1326 and the Swiss National Science Foundation (grant no. 188662).

1327
1328

Table 1. Intermolecular forces for selected functional groups and gases (Jeffrey, 1997; Jeffrey and Saenger, 1991; Vinogradov and Linnell, 1971; Iupac, 1997).

Functional Group	London dispersion force	Keesom force	Hydrogen Bonding
Alkane	Increases with chain length	none	None with itself.
Ether	Increases with chain length	Slightly polar, 1 O	None with itself. H-bond acceptor (max. 2) of other molecules
Ester	Increases with chain length	More polar than ether, 1 O	None with itself. H-bond acceptor (max. 2) of other molecules
Amine	Increases with chain length	Polar, 1 N	0-2 H-bonds with itself. <i>Primary:</i> H-bond donor (max. 2) and acceptor (max. 1). <i>Secondary:</i> H-bond donor (max. 1) and acceptor (max. 1). <i>Tertiary:</i> H-bond acceptor (max. 1).
Imine	Increases with chain length	Polar, 1 N	1-2 H-bonds with itself. <i>Primary:</i> H-bond donor (max. 1) and acceptor (max. 1). <i>Secondary:</i> H-bond acceptor (max. 1). <i>Tertiary:</i> H-bond acceptor (max. 1).
Aldehyde / Ketone	Increases with chain length	Polar C=O manifest strong dipole	None with itself. H-bond acceptor (max. 2) of other molecules
Alcohol	Increases with chain length	Polar, 1 O	2 H-bonds with itself. H-bond donor (max. 1) and acceptor (max. 2).
Acid	Increases with chain length	Polar, 2 O	2 H-bonds with itself forming dimer increasing molecule size. H-bond donor (max. 1) and acceptor (max. 4).
Amide	Increases with chain length	Polar, strong dipole 1 N & 1 O	2 H-bonds with itself. H-bond donor (max. 2) and acceptor (max. 3).
Other Species	Vapor pressure	Polar	
N ₂ O ₅	100 hPa @ 3.9 °C	Yes	None with itself. H-bond acceptor (max. 12).
HONO		Yes	2 H-bonds with itself. H-bond donor (max. 1) and acceptor (max. 5).
NH ₃	100 hPa @ -71.3 °C	Yes	2 H-bonds with itself.

			H-bond donor (max. 3) and acceptor (max. 1).
HNO ₃	100 hPa @ 28.4 °C	Yes	2 H-bonds with itself. H-bond donor (max. 1) and acceptor (max. 7).
H ₂ SO ₄	100 hPa @ 248 °C	Yes	4 H-bonds with itself. H-bond donor (max. 2) and acceptor (max. 8).
H ₂ O	100 hPa @ 45.8 °C	Yes	4 H-bonds with itself. H-bond donor (max. 2) and acceptor (max. 2).

1329

1330

1331 **Table 2.** Characteristic estimates of desorption energies (E_{des}^0) and desorption lifetimes (τ_{des} , at
 1332 298 K) for widely used categories of secondary organic aerosol volatility basis sets (SOA-VBS):
 1333 volatile organic compounds (VOC), intermediate-volatile (IVOC), semi-volatile (SVOC), low-
 1334 volatile (LVOC), and extremely/ultra-low volatile (ELVOC/ULVOC).

Category	Volatility p^0 (atm)	Desorption Energy E_{des}^0 (kJ mol ⁻¹)	Desorption Lifetime τ_{des} (298 K)
VOC	$\geq 10^{-3}$	$\lesssim 60$	nanoseconds to milliseconds
IVOC	$\sim 10^{-5}$	~ 80	milliseconds to hours
SVOC	$\sim 10^{-9}$	~ 100	seconds to months
LVOC	$\sim 10^{-12}$	~ 120	minutes to centuries
ELVOC/ULVOC	$\lesssim 10^{-14}$	≥ 140	days to millennia

1340

1341

1342

1343

1344

1345

1346

1347

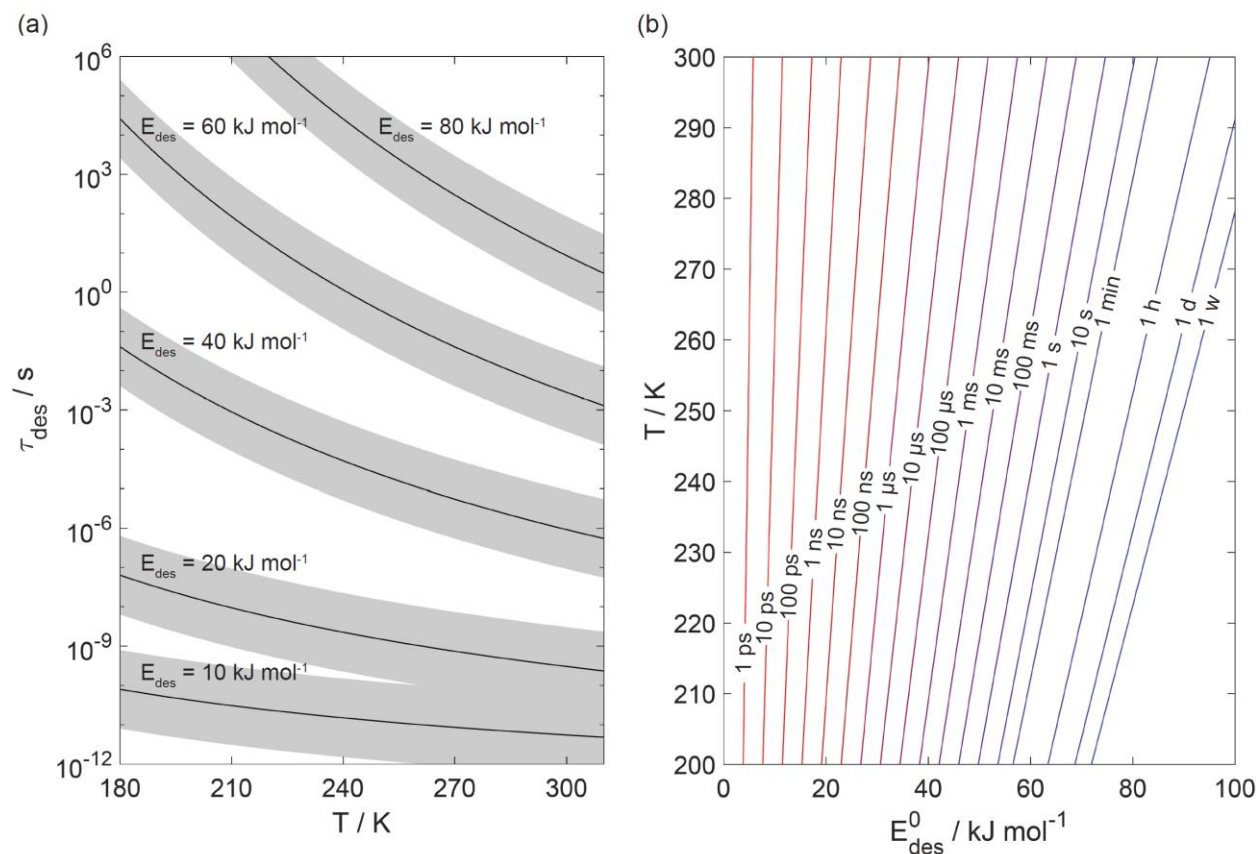
1348

1349

1350

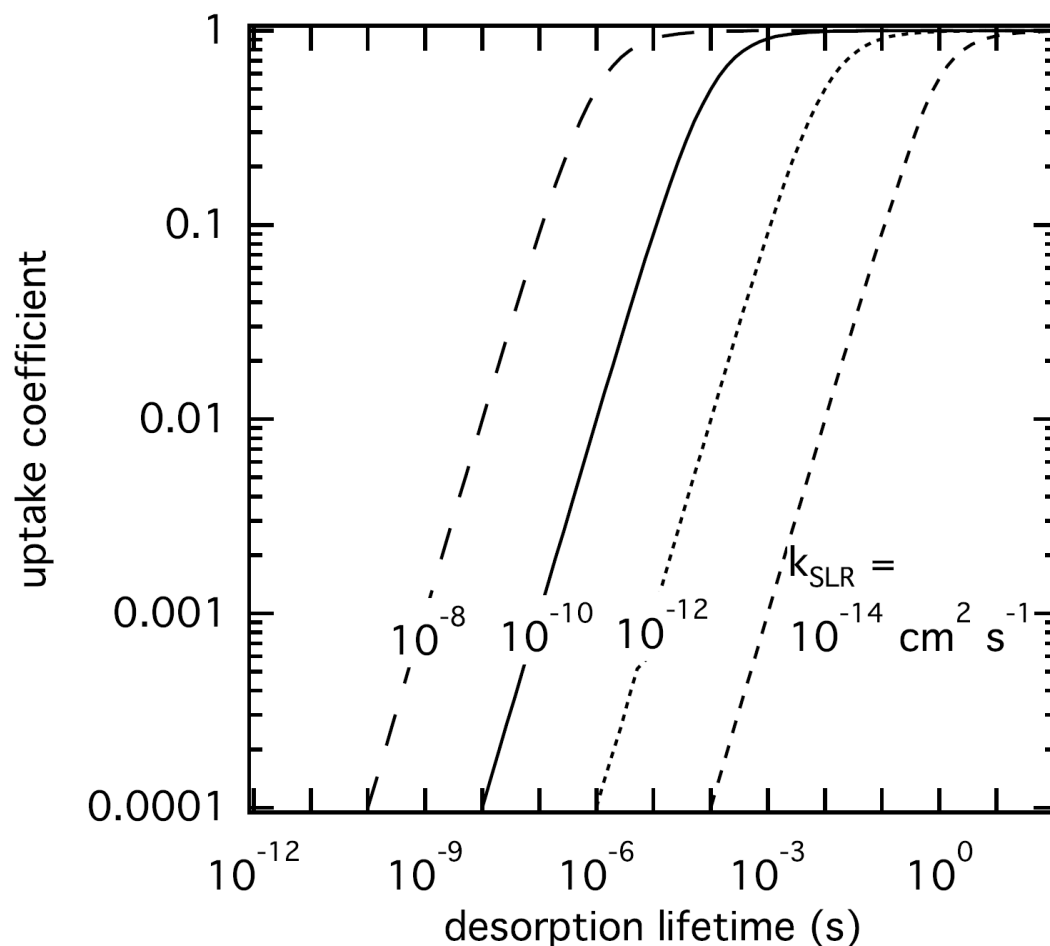
1351

1352



1353
 1354 **Figure 1.** The dependence of the desorption lifetime (τ_{des}) on temperature (T) and desorption
 1355 energy (E_{des}^0). (a) τ_{des} as a function of T for various E_{des}^0 values. The shaded area covers the range
 1356 of the pre-exponential factor (A_{des}) varied by ± 1 order of magnitude. (b) Iso- τ_{des} lines for various
 1357 combination of T and E_{des}^0 . All presented data calculated applying Eq. (1) and using $A_{\text{des}} = 1 \times 10^{13}$
 1358 s^{-1} .

1359
 1360
 1361
 1362
 1363
 1364
 1365
 1366
 1367
 1368



1370

1371 **Figure 2.** The response in reactive uptake coefficient of a reactive gas species X with a condensed-
 1372 phase species Y when varying the desorption lifetime and second-order rate coefficients derived
 1373 by the numerical diffusion model K2-SURF. The gas phase concentration of X and the surface
 1374 concentration of Y remained fixed during the calculations. The surface accommodation coefficient
 1375 is assumed to be equal to one.

1376

1377

1378

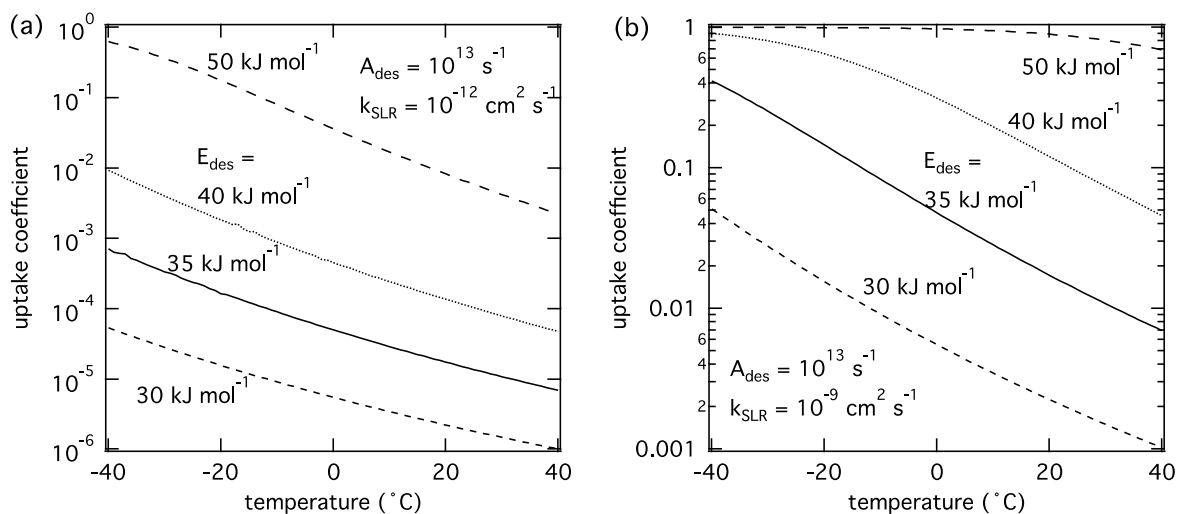
1379

1380

1381

1382

1383



1384

1385 **Figure 3.** The response of the reactive uptake coefficient as temperature and adsorption energy are
1386 varied for two different second-order rate coefficients derived by K2-SURF. The gas phase
1387 concentration of X remained fixed during the calculations. The pre-exponential factor A_{des} is fixed
1388 for both cases. The surface accommodation coefficient is assumed to be one.

1389

1390

1391

1392

1393

1394

1395

1396

1397

1398

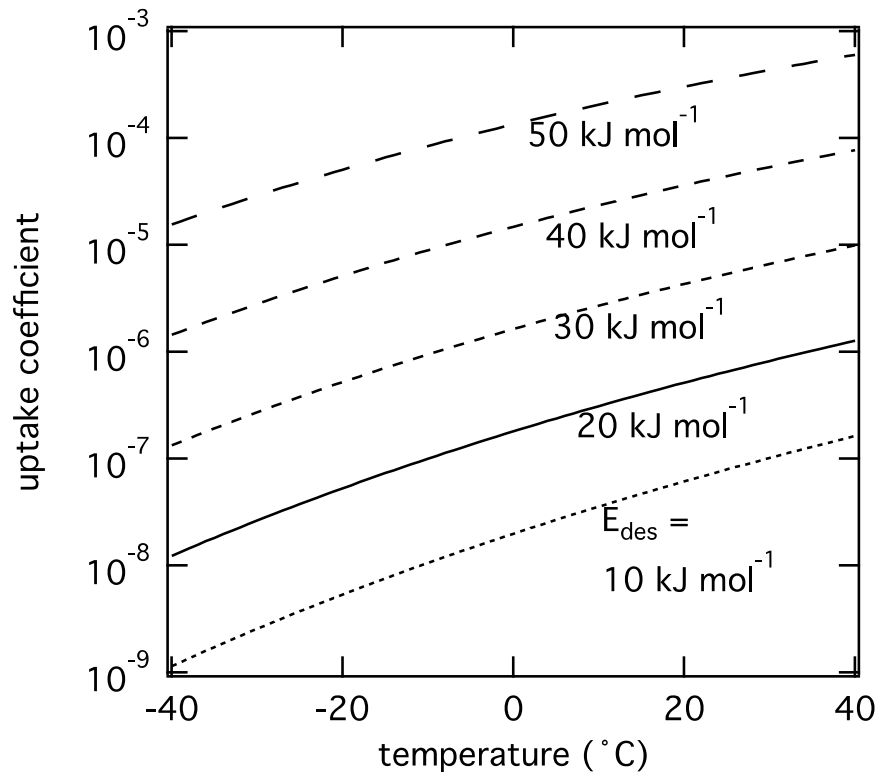
1399

1400

1401

1402

1403



1404

1405 **Figure 4.** The response of the reactive uptake coefficient of O₃ by PAH coated on soot including
1406 formation of reactive oxygen intermediates (ROIs) following Shiraiwa et al. (2011) as temperature
1407 and adsorption energy are varied using the numerical diffusion model K2-SURF. ROI formation
1408 and oxidation reaction rates are adjusted using an Arrhenius-based temperature scaling. The pre-
1409 exponential factor A_{des} is fixed at 10^{13} s^{-1} .

1410

1411

1412

1413

1414

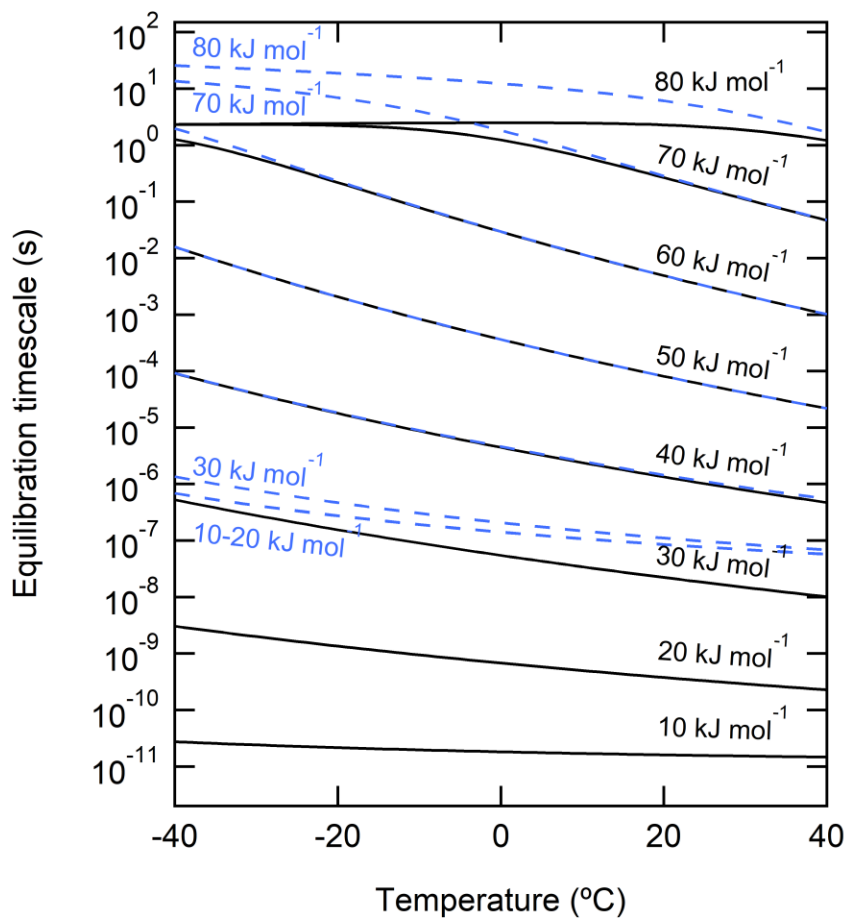
1415

1416

1417

1418

1419



1420

1421 **Figure 5.** Equilibration timescale of non-reactive uptake of gas molecules onto the surface (solid
 1422 black lines) and into the particle phase (blue dashed lines) of liquid particles with a diameter of
 1423 100 nm for different desorption energies. Gas-phase mixing ratio is fixed to be 1 ppb.

1424

1425

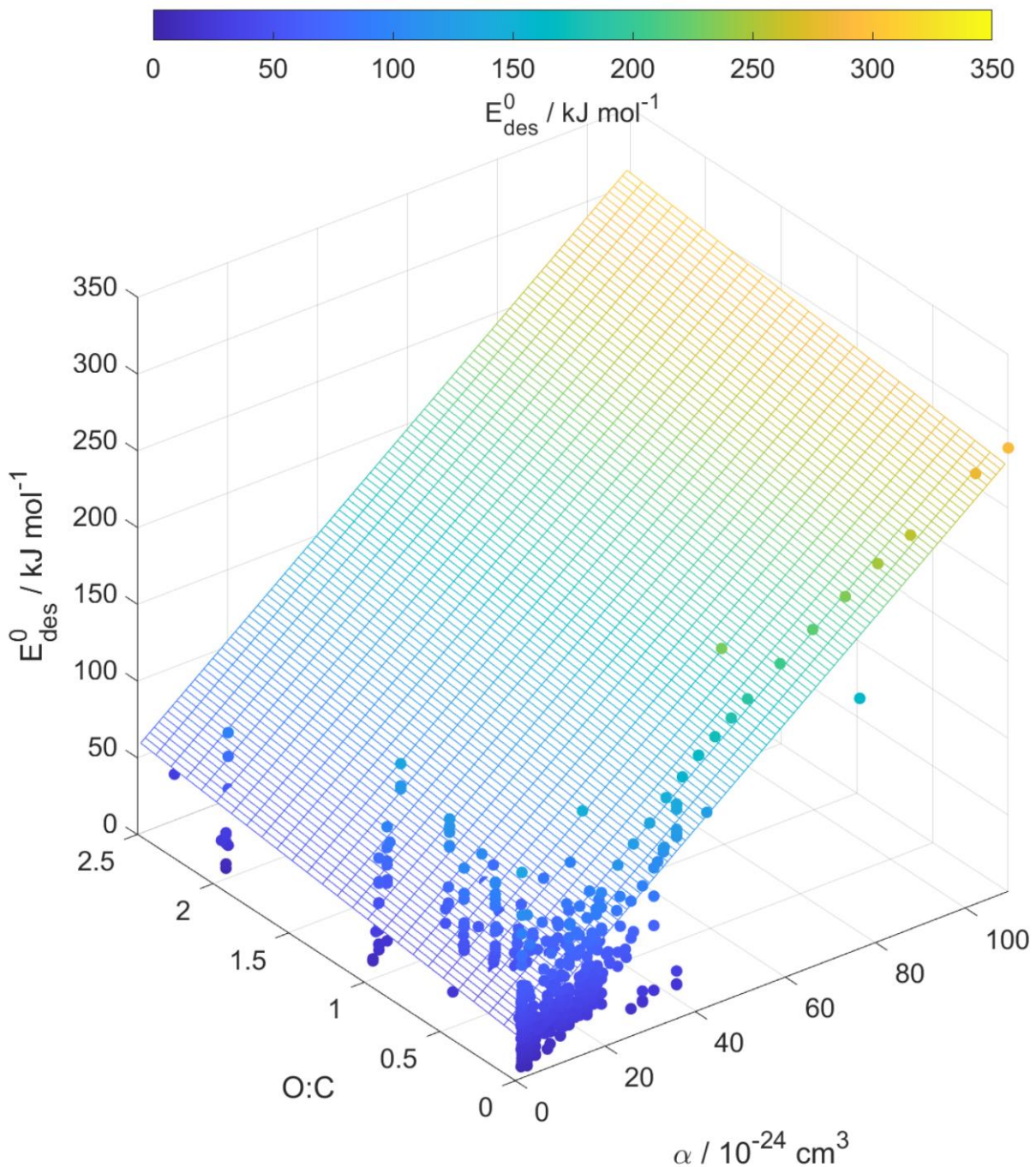
1426

1427

1428

1429

1430



1431

1432

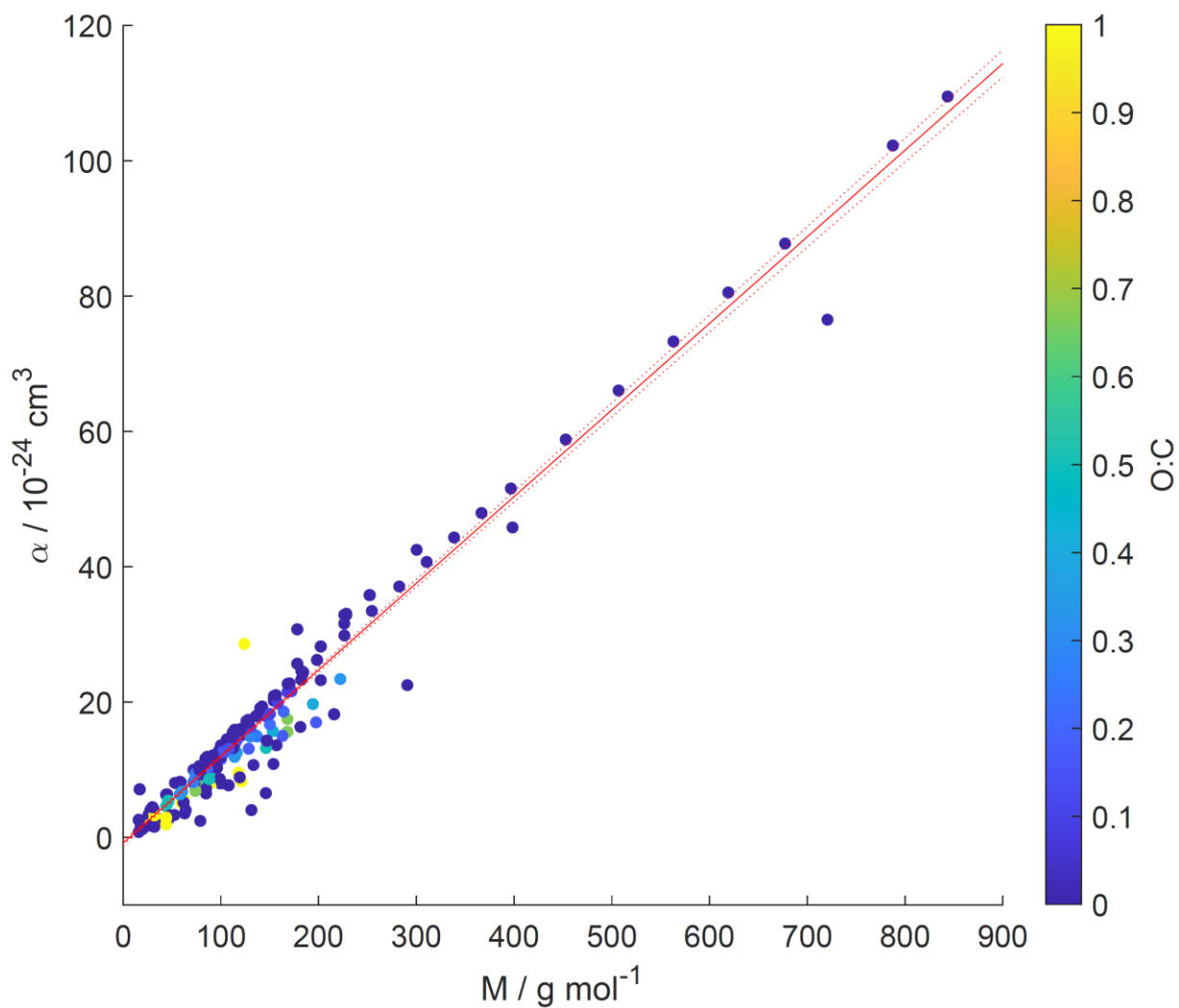
1433 **Figure 6.** Multilinear regression analysis of E_{des}^0 , oxygen to carbon ratio of gas species expressed
 1434 as $O:C$, and gas species polarizability (α) using data from Tables A1-A15. Gridded surface shows
 1435 regression model and color shading indicates changes in E_{des}^0 .

1436

1437

1438

1439



1440

1441 **Figure 7.** Gas species polarizability (α) as a function of molar mass (M) and its dependence on
1442 oxygen to carbon ratio expressed as $O:C$. $O:C$ is given as color shading. Red solid and dotted lines
1443 represent a linear fit to the data and its 95% prediction bands, respectively. Note that three gas
1444 species with $O:C > 1$ (CO_2 , formic acid, and peroxyacetyl nitrate) are included in this plot as
1445 having $O:C = 1$ to allow for better visualization of entire data set.

1446

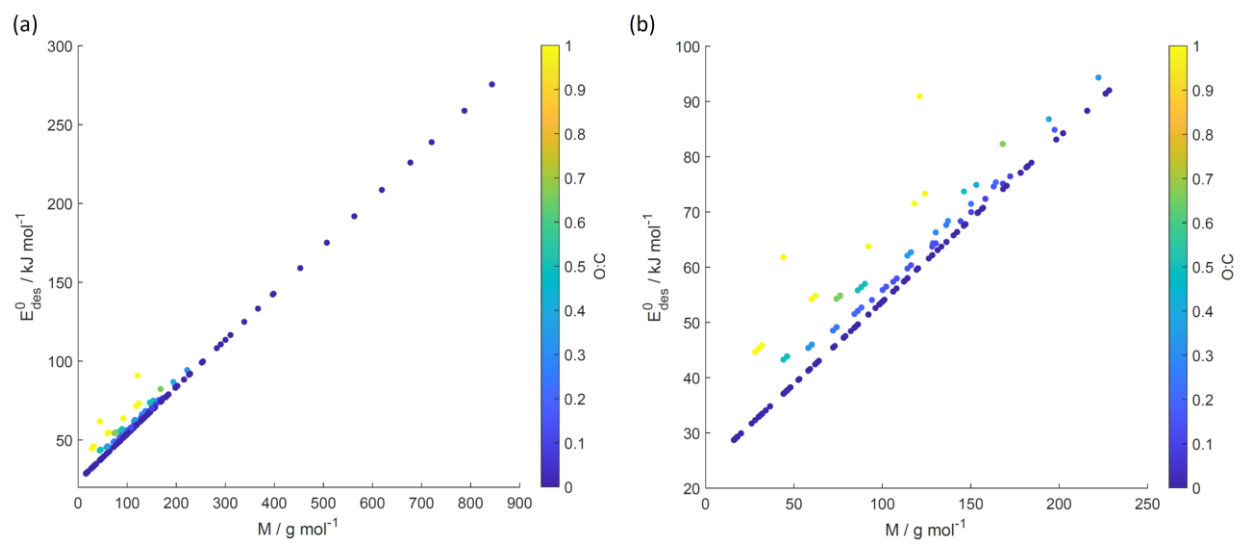
1447

1448

1449

1450

1451



1452

1453 **Figure 8.** E_{des}^0 values derived from the new parameterization (Eq. (16)) applying the training
1454 dataset of gas species with molar mass (M) and $O:C$, the latter coded as symbol color described
1455 by the color bar. (b) is an enlarged view of (a). Note that three gas species with $O:C > 1$ (CO_2 ,
1456 formic acid, and peroxyacetyl nitrate) are included in these plots as having $O:C = 1$ to allow for
1457 better visualization of entire data set.

1458

1459

1460

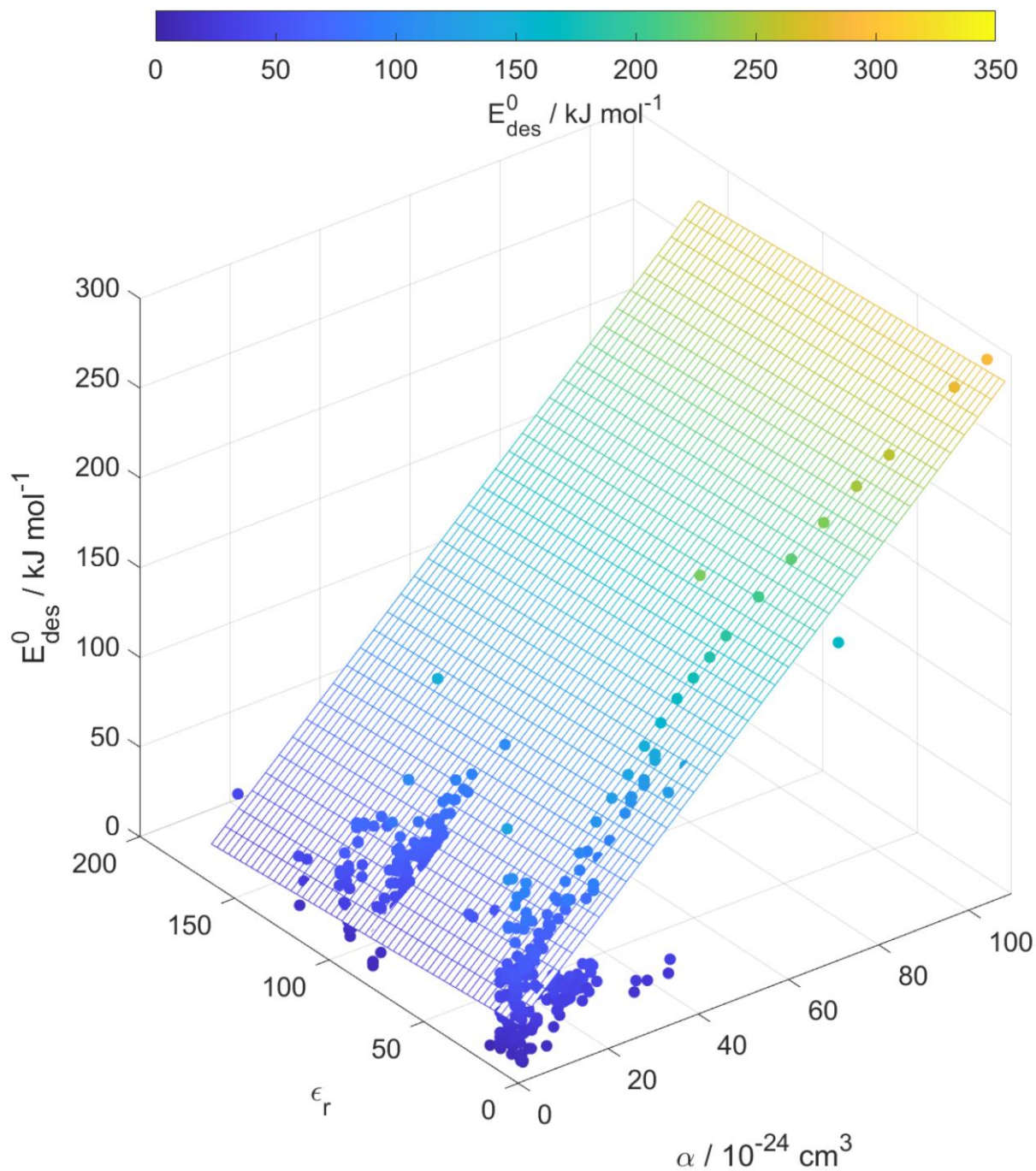
1461

1462

1463

1464

1465



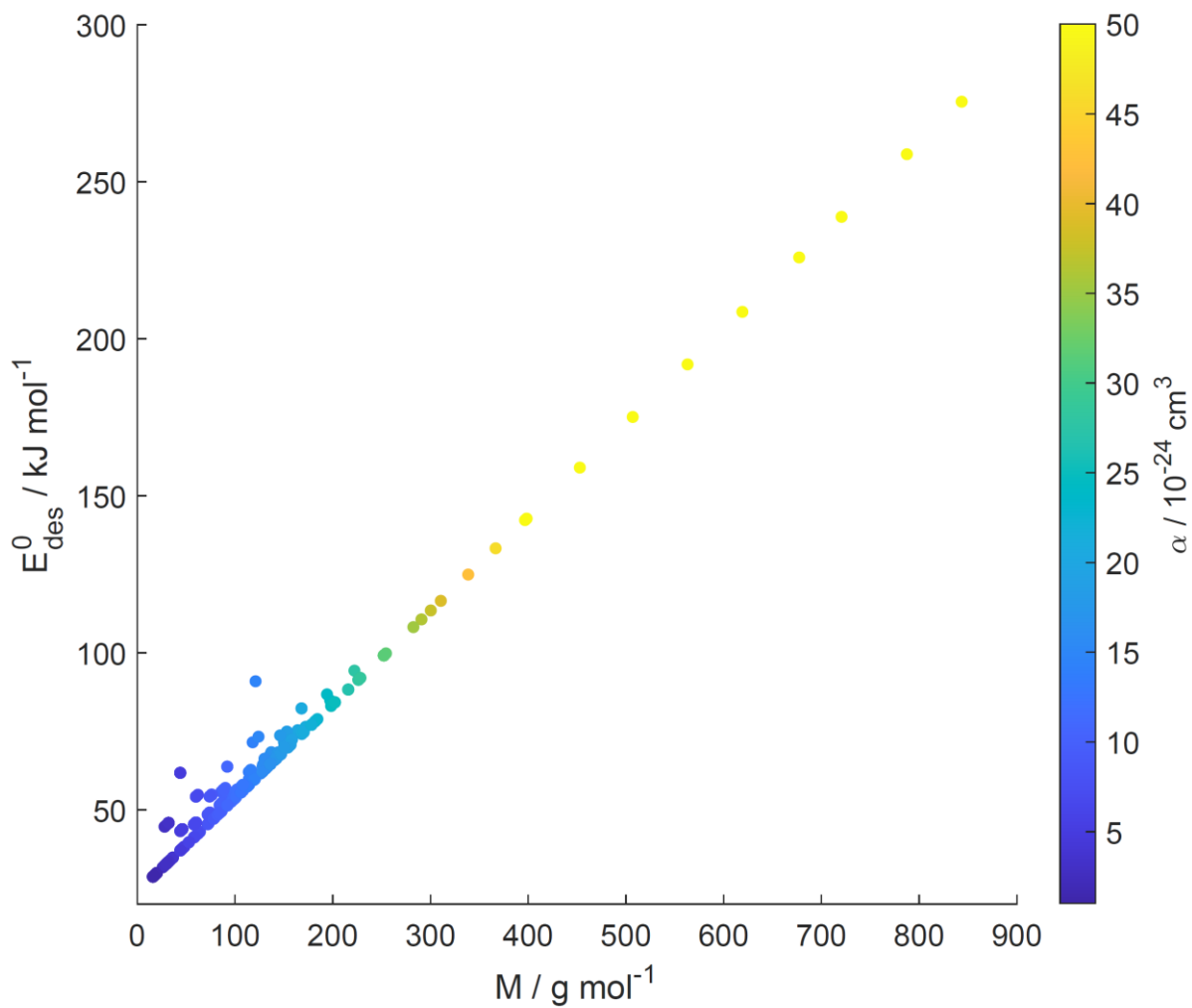
1466

1467 **Figure 9.** Multilinear regression analysis of E_{des}^0 , substrate relative permittivity (ϵ_r), and gas
 1468 species polarizability (α) using data from Tables A1-A15. Gridded surface shows regression
 1469 model and color shading indicates changes in E_{des}^0 .

1470

1471

1472



1473

1474 **Figure 10.** Parameterized E_{des}^0 values as a function of gas species molar mass (M) and
1475 polarizability (α) given as color bar following Eq. (16).

1476

1477

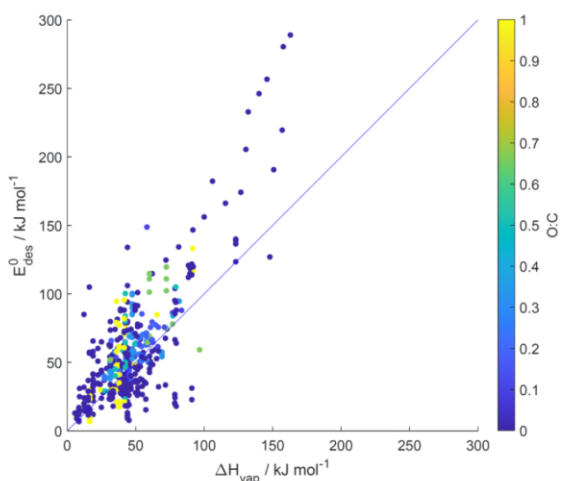
1478

1479

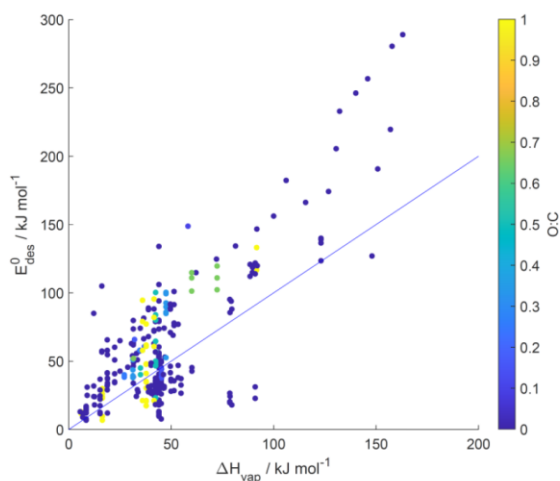
1480

1481

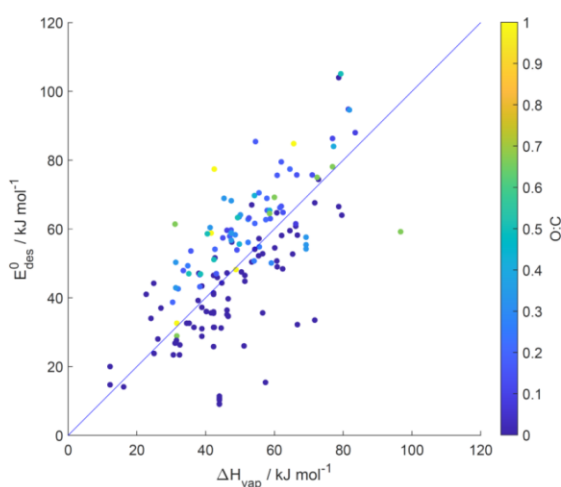
(a): all substrates



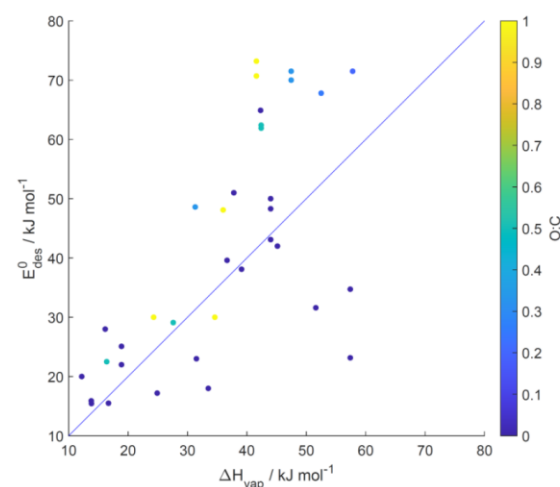
(b): solid substrates



(c): liquid substrates



(d): ice substrates



1482

1483 **Figure 11.** Desorption energy (E_{des}^0) as a function of enthalpy of vaporization (ΔH_{vap}) and its
1484 dependence on $O:C$ for all (a), solid (b), liquid (c), and ice (d) substrates. Blue lines indicate 1:1
1485 lines.

1486

1487

1488

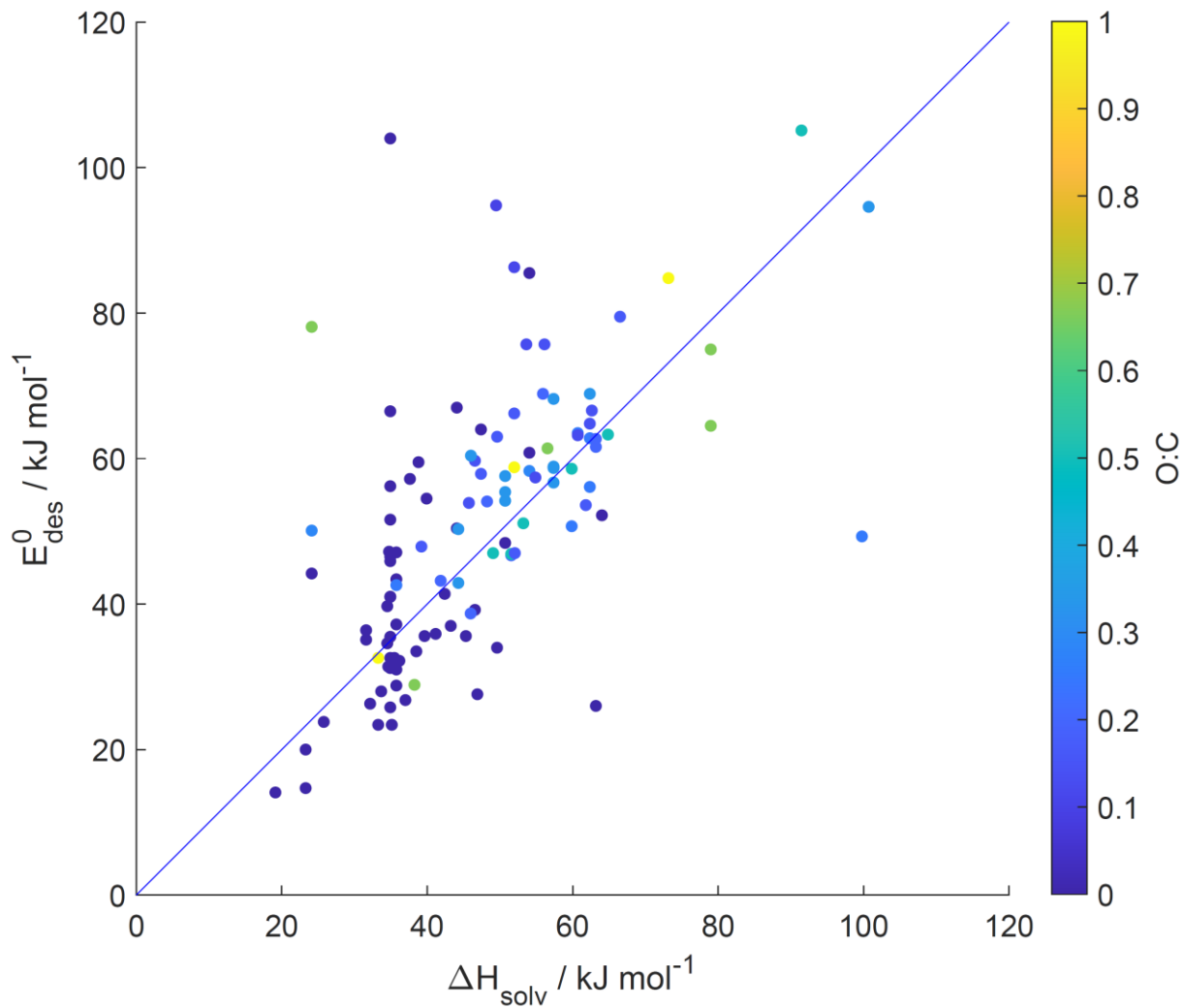
1489

1490

1491

1492

1493



1494

1495 **Figure 12.** Desorption energy (E_{des}^0) as a function of enthalpy of solvation (ΔH_{solv}) and its
1496 dependence on $O:C$ for liquid substrates. Blue line indicates 1:1 line.

1497

1498

1499

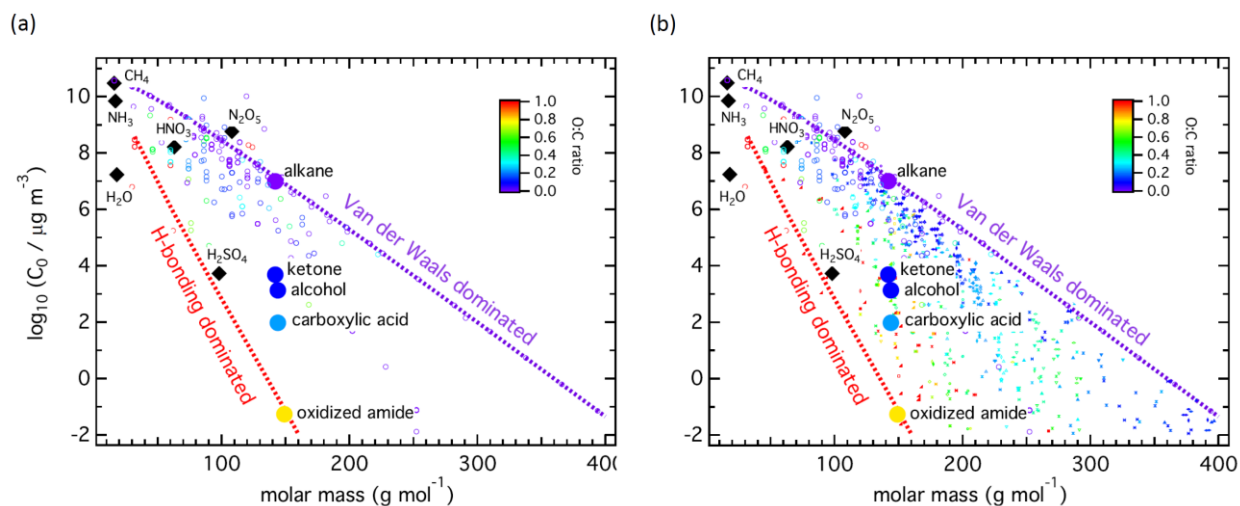
1500

1501

1502

1503

1504



1505

1506 **Figure 13.** Molecular corridors of SOA formation showing saturation mass concentration (C_0) as
 1507 a function of molar mass (M). The small markers represent individual gas species color-coded by
 1508 $O:C$ ratio. (a) displays data from Tables S1-S15. (b) includes SOA precursor gases and oxidation
 1509 products data discussed in (Shiraiwa et al., 2014). The dotted lines represent linear alkanes C_nH_{2n+2}
 1510 (purple with $O:C = 0$) and sugar alcohols $C_nH_{2n+2}O_n$ (red with $O:C = 1$). Inorganic species
 1511 (diamonds) and organic species with similar molar mass but with different functional groups
 1512 (circles) are plotted.

1513

1514

1515

1516

1517

1518

1519

1520

1521

1522

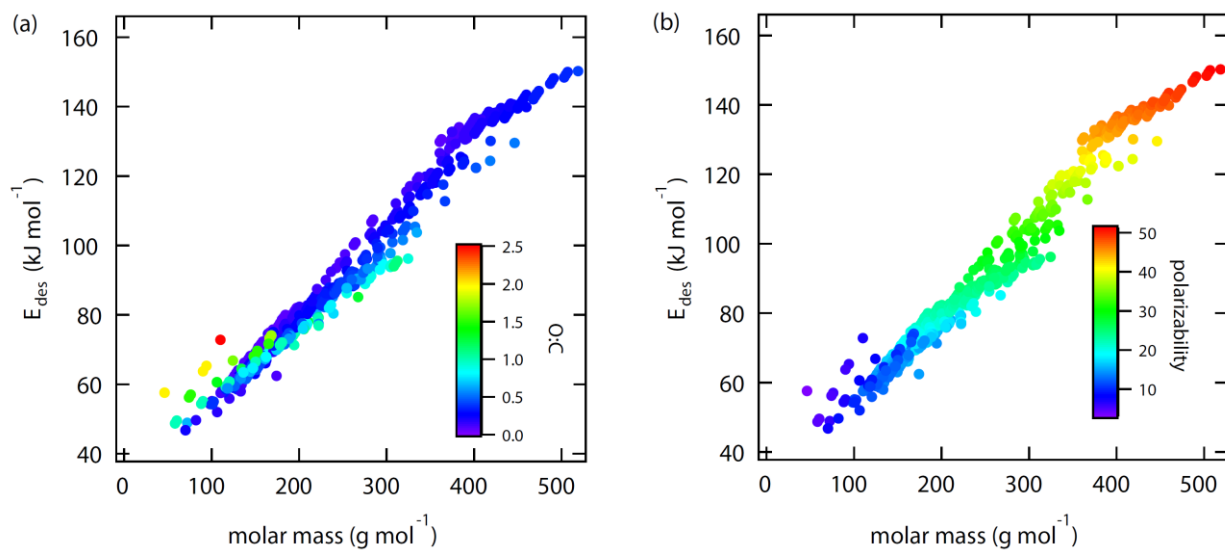
1523

1524

1525

1526

1527



1528

1529 **Figure 14.** Desorption energies (E_{des}^0) calculated for molecular corridor data of SOA precursor
1530 gases and oxidation products from Fig. 13. (Shiraiwa et al., 2014) as a function of molar mass and
1531 its dependence on $O:C$ (a) and polarizability (b). This analysis applies the parameterizations given
1532 in Eqs. (14) and (20).

1533

1534

1535

1536

1537

1538

1539

1540

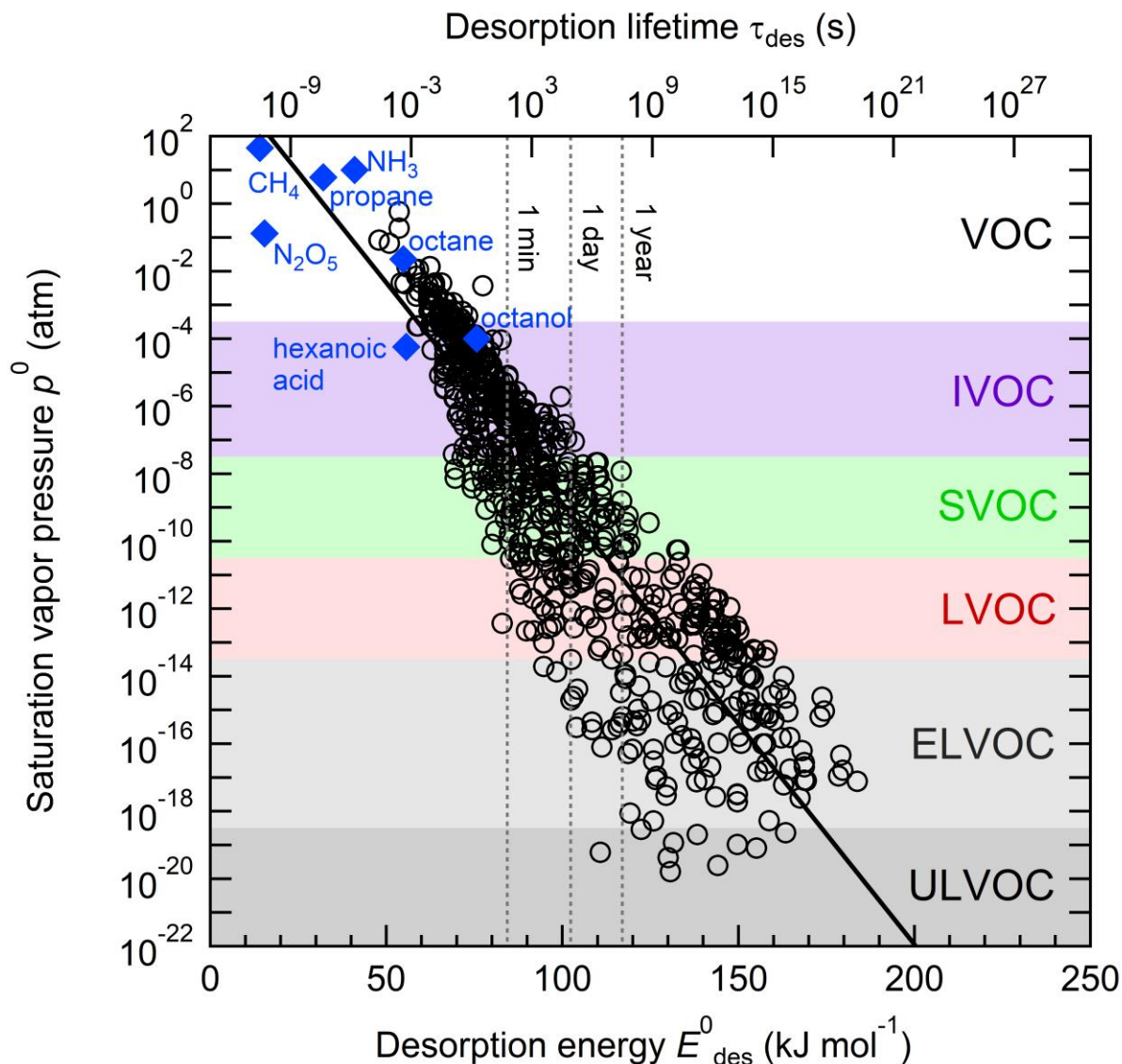
1541

1542

1543

1544

1545



1546 **Figure 15.** Characteristic desorption energies (E_{des}^0), desorption lifetimes (τ_{des}), and saturation
 1547 vapor pressures (p^0) at 298 K for secondary organic aerosol (SOA) components and other selected
 1548 compounds of atmospheric relevance. The blue markers show experimental literature data of E_{des}^0
 1549 and p^0 . The black markers correspond to the molecular corridor data of SOA formation displayed
 1550 in Fig. 13 (Shiraiwa et al., 2014), for which p^0 was estimated with the EVAPORATION model
 1551 (Compernelle et al., 2011) and E_{des}^0 was estimated using Eq. 14. The black solid line represents an
 1552 exponential fit to the SOA molecular corridor data. Blue markers show experimental data for
 1553 selected other compounds of atmospheric relevance. Color shadings indicate widely used
 1554 categories of SOA volatility basis set (VBS): volatile organic compounds (VOC), semi-volatile
 1555 organic compounds (SVOC), low volatility organic compounds (LVOC), extremely-low volatility
 1556 organic compounds (ELVOC) and ultra-low volatility organic compounds (ULVOC) (Schervish
 1557 and Donahue, 2020; Donahue et al., 2009).

1558

1559 **References**

- 1560 Abbatt, J. P. D. and Ravishankara, A. R.: Opinion: Atmospheric multiphase chemistry – past,
1561 present, and future, *Atmos. Chem. Phys.*, 23, 9765–9785, 10.5194/acp-23-9765-2023, 2023.
- 1562 Abbatt, J. P. D., Lee, A. K. Y., and Thornton, J. A.: Quantifying trace gas uptake to tropospheric
1563 aerosol: recent advances and remaining challenges, *Chem. Soc. Rev.*, 41, 6555-6581,
1564 10.1039/C2cs35052a, 2012.
- 1565 Abraham, M. H.: Measurement of Enthalpies of Solution of Electrolytes, in: *Thermochemistry
1566 and Its Applications to Chemical and Biochemical Systems*. NATO ASI Series (Series C:
1567 Mathematical and Physical Sciences), edited by: Ribeiro da Silva, M. A. V., 119, Springer,
1568 Dordrecht, 10.1007/978-94-009-6312-2_20, 1984.
- 1569 Ahmed, M., Blum, M., Crumlin, E. J., Geissler, P. L., Head-Gordon, T., Limmer, D. T.,
1570 Mandadapu, K. K., Saykally, R. J., and Wilson, K. R.: Molecular Properties and Chemical
1571 Transformations Near Interfaces, *J. Phys. Chem. B*, 125, 9037-9051, 10.1021/acs.jpcc.1c03756,
1572 2021.
- 1573 Aihara, A. and Davies, M.: Dielectric relaxation times of some nonrigid polar molecules, *J. Coll.
1574 Sci. Imp. U. Tok.*, 11, 671-687, 10.1016/0095-8522(56)90182-9, 1956.
- 1575 Akkerman, H. B., Naber, R. C. G., Jongbloed, B., van Hal, P. A., Blom, P. W. M., de Leeuw, D.
1576 M., and de Boer, B.: Electron tunneling through alkanedithiol self-assembled monolayers in
1577 large-area molecular junctions, *Proc. Natl. Acad. Sci. U. S. A.*, 104, 11161-11166,
1578 10.1073/pnas.0701472104, 2007.
- 1579 Alcalá-Jornod, C., van den Bergh, H., and Rossi, M. J.: Reactivity of NO₂ and H₂O on soot
1580 generated in the laboratory: a diffusion tube study at ambient temperature, *Phys. Chem. Chem.
1581 Phys.*, 2, 5584-5593, 2000.
- 1582 Alcalá-Jornod, C., van den Bergh, H., and Rossi, M. J.: Can soot particles emitted by airplane
1583 exhaust contribute to the formation of aviation contrails and cirrus clouds?, *Geophys. Res. Lett.*,
1584 29, 4, 10.1029/2001gl014115, 2002.
- 1585 Alkorta, I., Plane, J. M. C., Elguero, J., Davalos, J. Z., Acuna, A. U., and Saiz-Lopez, A.:
1586 Theoretical study of the NO₃ radical reaction with CH₂ClBr, CH₂Cl, CH₂BrI, CHCl₂Br, and
1587 CHClBr₂, *Phys. Chem. Chem. Phys.*, 24, 14365-14374, 10.1039/d2cp00021k, 2022.
- 1588 Allouche, A. and Bahr, S.: Acetic acid-water interaction in solid interfaces, *Journal of Physical
1589 Chemistry B*, 110, 8640-8648, 10.1021/jp0559736, 2006.
- 1590 Ammann, M. and Pöschl, U.: Kinetic model framework for aerosol and cloud surface chemistry
1591 and gas-particle interactions - Part 2: Exemplary practical applications and numerical
1592 simulations, *Atmos. Chem. Phys.*, 7, 6025-6045, 2007.
- 1593 Ammann, M., Pöschl, U., and Rudich, Y.: Effects of reversible adsorption and Langmuir-
1594 Hinshelwood surface reactions on gas uptake by atmospheric particles, *Phys. Chem. Chem.
1595 Phys.*, 5, 351-356, 2003.
- 1596 Ammann, M., Cox, R. A., Crowley, J. N., Jenkin, M. E., Mellouki, A., Rossi, M. J., Troe, J., and
1597 Wallington, T. J.: Evaluated kinetic and photochemical data for atmospheric chemistry: Volume
1598 VI - heterogeneous reactions with liquid substrates, *Atmos. Chem. Phys.*, 13, 8045-8228,
1599 10.5194/acp-13-8045-2013, 2013.
- 1600 Arangio, A. M., Slade, J. H., Berkemeier, T., Pöschl, U., Knopf, D. A., and Shiraiwa, M.:
1601 Multiphase Chemical Kinetics of OH Radical Uptake by Molecular Organic Markers of Biomass
1602 Burning Aerosols: Humidity and Temperature Dependence, Surface Reaction, and Bulk
1603 Diffusion, *J. Phys. Chem. A*, 119, 4533-4544, 10.1021/jp510489z, 2015.

1604 Aroney, M. J., Saxby, J. D., Lefevre, R. J. W., and Chia, L. H. L.: Molecular polarisability.
1605 Dipole moments molar Kerr constants + conformations of 11 phosphate + phosphite triesters as
1606 solutes in benzene, *J. Chem. Soc.*, 2948-2954, 10.1039/jr9640002948, 1964.
1607 Arp, H. P. H., Goss, K. U., and Schwarzenbach, R. P.: Evaluation of a predictive model for
1608 air/surface adsorption equilibrium constants and enthalpies, *Environ. Toxicol. Chem.*, 25, 45-51,
1609 10.1897/05-291r.1, 2006.
1610 Arrhenius, S. A.: Über die Dissociationswärme und den Einfluß der Temperatur auf den
1611 Dissociationsgrad der Elektrolyte, *Z. Phys. Chem.*, 4, 96-116, 1889a.
1612 Arrhenius, S. A.: Über die Reaktionsgeschwindigkeit bei der Inversion von Rohrzucker durch
1613 Säuren, *Z. Phys. Chem.*, 4, 226-248, 1889b.
1614 Artiglia, L., Edebeli, J., Orlando, F., Chen, S. Z., Lee, M. T., Arroyo, P. C., Gilgen, A., Bartels-
1615 Rausch, T., Kleibert, A., Vazdar, M., Carignano, M. A., Francisco, J. S., Shepson, P. B., Gladich,
1616 I., and Ammann, M.: A surface-stabilized ozonide triggers bromide oxidation at the aqueous
1617 solution-vapour interface, *Nat. Commun.*, 8, 8, 10.1038/s41467-017-00823-x, 2017.
1618 Asakawa, H., Sazaki, G., Nagashima, K., Nakatsubo, S., and Furukawa, Y.: Two types of quasi-
1619 liquid layers on ice crystals are formed kinetically, *Proc. Natl. Acad. Sci. U. S. A.*, 113, 1749-
1620 1753, 10.1073/pnas.1521607113, 2016.
1621 Auty, R. P. and Cole, R. H.: Dielectric properties of ice and solid D₂O, *J. Chem. Phys.*, 20,
1622 1309-1314, 10.1063/1.1700726, 1952.
1623 Bak, K. L., Gauss, J., Helgaker, T., Jorgensen, P., and Olsen, J.: The accuracy of molecular
1624 dipole moments in standard electronic structure calculations, *Chemical Physics Letters*, 319,
1625 563-568, 10.1016/s0009-2614(00)00198-6, 2000.
1626 Baron, M. and Arevalo, E. S.: Dipole-moment values from single-solution measurements, *J.*
1627 *Chem. Educ.*, 65, 644-645, 10.1021/ed065p644, 1988.
1628 Bartels-Rausch, T.: Ten things we need to know about ice and snow, *Nature*, 494, 27-29,
1629 10.1038/494027a, 2013.
1630 Bartels-Rausch, T., Huthwelker, T., Gaggeler, H. W., and Ammann, M.: Atmospheric pressure
1631 coated-wall flow-tube study of acetone adsorption on ice, *J. Phys. Chem. A*, 109, 4531-4539,
1632 10.1021/jp0451871, 2005.
1633 Bartels-Rausch, T., Eichler, B., Zimmermann, P., Gaggeler, H. W., and Ammann, M.: The
1634 adsorption enthalpy of nitrogen oxides on crystalline ice, *Atmos. Chem. Phys.*, 2, 235-247,
1635 10.5194/acp-2-235-2002, 2002.
1636 Bartels-Rausch, T., Orlando, F., Kong, X. R., Artiglia, L., and Ammann, M.: Experimental
1637 Evidence for the Formation of Solvation Shells by Soluble Species at a Nonuniform Air-Ice
1638 Interface, *ACS Earth Space Chem.*, 1, 572-579, 10.1021/acsearthspacechem.7b00077, 2017.
1639 Bartels-Rausch, T., Jacobi, H. W., Kahan, T. F., Thomas, J. L., Thomson, E. S., Abbatt, J. P. D.,
1640 Ammann, M., Blackford, J. R., Bluhm, H., Boxe, C., Domine, F., Frey, M. M., Gladich, I.,
1641 Guzman, M. I., Heger, D., Huthwelker, T., Klan, P., Kuhs, W. F., Kuo, M. H., Maus, S., Moussa,
1642 S. G., McNeill, V. F., Newberg, J. T., Pettersson, J. B. C., Roeselova, M., and Sodeau, J. R.: A
1643 review of air-ice chemical and physical interactions (AICI): liquids, quasi-liquids, and solids in
1644 snow, *Atmos. Chem. Phys.*, 14, 1587-1633, 10.5194/acp-14-1587-2014, 2014.
1645 Behr, P., Scharfenort, U., Ataya, K., and Zellner, R.: Dynamics and mass accommodation of HCl
1646 molecules on sulfuric acid-water surfaces, *Phys. Chem. Chem. Phys.*, 11, 8048-8055,
1647 10.1039/b904629a, 2009.

1648 Behr, P., Morris, J. R., Antman, M. D., Ringeisen, B. R., Splan, J. R., and Nathanson, G. M.:
1649 Reaction and desorption of HCl and HBr following collisions with supercooled sulfuric acid,
1650 *Geophys. Res. Lett.*, 28, 1961-1964, 10.1029/2000gl012716, 2001.

1651 Beller, M., Renken, A., and van Santen, R. A.: *Catalysis: From Principles to Applications*, John
1652 Wiley & Sons, Inc., Hoboken, New Jersey, USA2012.

1653 Berkemeier, T., Takeuchi, M., Eris, G., and Ng, N. L.: Kinetic modeling of formation and
1654 evaporation of secondary organic aerosol from NO₃ oxidation of pure and mixed monoterpenes,
1655 *Atmos. Chem. Phys.*, 20, 15513-15535, 10.5194/acp-20-15513-2020, 2020.

1656 Berkemeier, T., Huisman, A. J., Ammann, M., Shiraiwa, M., Koop, T., and Pöschl, U.: Kinetic
1657 regimes and limiting cases of gas uptake and heterogeneous reactions in atmospheric aerosols
1658 and clouds: a general classification scheme, *Atmos. Chem. Phys.*, 13, 6663-6686, 10.5194/acp-
1659 13-6663-2013, 2013.

1660 Berkemeier, T., Mishra, A., Mattei, C., Huisman, A. J., Krieger, U. K., and Pöschl, U.:
1661 Ozonolysis of Oleic Acid Aerosol Revisited: Multiphase Chemical Kinetics and Reaction
1662 Mechanisms, *ACS Earth Space Chem.*, 5, 3313-3323, 10.1021/acsearthspacechem.1c00232,
1663 2021.

1664 Berkemeier, T., Steimer, S. S., Krieger, U. K., Peter, T., Pöschl, U., Ammann, M., and Shiraiwa,
1665 M.: Ozone uptake on glassy, semi-solid and liquid organic matter and the role of reactive oxygen
1666 intermediates in atmospheric aerosol chemistry, *Phys. Chem. Chem. Phys.*, 18, 12662-12674,
1667 10.1039/c6cp00634e, 2016.

1668 Bertram, A. K., Martin, S. T., Hanna, S. J., Smith, M. L., Bodsworth, A., Chen, Q., Kuwata, M.,
1669 Liu, A., You, Y., and Zorn, S. R.: Predicting the relative humidities of liquid-liquid phase
1670 separation, efflorescence, and deliquescence of mixed particles of ammonium sulfate, organic
1671 material, and water using the organic-to-sulfate mass ratio of the particle and the oxygen-to-
1672 carbon elemental ratio of the organic component, *Atmos. Chem. Phys.*, 11, 10995-11006,
1673 10.5194/acp-11-10995-2011, 2011.

1674 Bishop, A. R., Girolami, G. S., and Nuzzo, R. G.: Structural models and thermal desorption
1675 energetics for multilayer assemblies of the n-alkanes on Pt(111), *J. Phys. Chem. B*, 104, 754-
1676 763, 10.1021/jp9926488, 2000.

1677 Blank, M. and Ottewill, R. H.: Adsorption of aromatic vapors on water surfaces, *J. Phys. Chem.*,
1678 68, 2206-2211, 10.1021/j100790a030, 1964.

1679 Bolis, V.: Fundamentals in Adsorption at the Solid-Gas Interface. Concepts and
1680 Thermodynamics, in: *Calorimetry and Thermal Methods in Catalysis*, edited by: Auroux, A.,
1681 154, Springer-Verlag Berlin Heidelberg, Berlin, 3-50, 10.1007/978-3-642-11954-5, 2013.

1682 Bond, T. C., Doherty, S. J., Fahey, D. W., Forster, P. M., Berntsen, T., DeAngelo, B. J., Flanner,
1683 M. G., Ghan, S., Karcher, B., Koch, D., Kinne, S., Kondo, Y., Quinn, P. K., Sarofim, M. C.,
1684 Schultz, M. G., Schulz, M., Venkataraman, C., Zhang, H., Zhang, S., Bellouin, N., Guttikunda,
1685 S. K., Hopke, P. K., Jacobson, M. Z., Kaiser, J. W., Klimont, Z., Lohmann, U., Schwarz, J. P.,
1686 Shindell, D., Storelvmo, T., Warren, S. G., and Zender, C. S.: Bounding the role of black carbon
1687 in the climate system: A scientific assessment, *J. Geophys. Res.*, 118, 5380-5552,
1688 10.1002/jgrd.50171, 2013.

1689 Borget, F., Chiavassa, T., Allouche, A., and Aycard, J. P.: Experimental and quantum study of
1690 adsorption of ozone (O₃) on amorphous water ice film, *J. Phys. Chem. B*, 105, 449-454,
1691 10.1021/jp001785y, 2001.

1692 Borodin, D., Rahinov, I., Shirhatti, P. R., Huang, M., Kandratsenka, A., Auerbach, D. J., Zhong,
1693 T. L., Guo, H., Schwarzer, D., Kitsopoulos, T. N., and Wodtke, A. M.: Following the

1694 microscopic pathway to adsorption through chemisorption and physisorption wells, *Science*, 369,
1695 1461-1465, 10.1126/science.abc9581, 2020.

1696 Borrmann, S., Solomon, S., Dye, J. E., and Luo, B. P.: The potential of cirrus clouds for
1697 heterogeneous chlorine activation, *Geophys. Res. Lett.*, 23, 2133-2136, 1996.

1698 Bosque, R. and Sales, J.: Polarizabilities of solvents from the chemical composition, *J. Chem.*
1699 *Inf. Comput. Sci.*, 42, 1154-1163, 10.1021/ci025528x, 2002.

1700 Brastad, S. M., Albert, D. R., Huang, M. W., and Nathanson, G. M.: Collisions of DCl with a
1701 Solution Covered with Hydrophobic and Hydrophilic Ions: Tetrahexylammonium Bromide in
1702 Glycerol, *J. Phys. Chem. A*, 113, 7422-7430, 10.1021/jp900232v, 2009.

1703 Brini, E., Fennell, C. J., Fernandez-Serra, M., Hribar-Lee, B., Luksic, M., and Dill, K. A.: How
1704 Water's Properties Are Encoded in Its Molecular Structure and Energies, *Chem. Rev.*, 117,
1705 12385-12414, 10.1021/acs.chemrev.7b00259, 2017.

1706 Broderick, A., Rocha, M. A., Khalifa, Y., Shiflett, M. B., and Newberg, J. T.: Mass Transfer
1707 Thermodynamics through a Gas-Liquid Interface, *J. Phys. Chem. B*, 123, 2576-2584,
1708 10.1021/acs.jpcc.9b00958, 2019.

1709 Brown, D. E., George, S. M., Huang, C., Wong, E. K. L., Rider, K. B., Smith, R. S., and Kay, B.
1710 D.: H₂O condensation coefficient and refractive index for vapor-deposited ice from molecular
1711 beam and optical interference measurements, *J. Phys. Chem.*, 100, 4988-4995,
1712 10.1021/jp952547j, 1996.

1713 Bruant, R. G. and Conklin, M. H.: Adsorption of trichloroethene at the vapor/water interface,
1714 *Environ. Sci. Technol.*, 35, 362-364, 10.1021/es000994t, 2001.

1715 Bruant, R. G. and Conklin, M. H.: Adsorption of benzene and methyl-substituted benzenes at the
1716 vapor/water interface. 2. Single-component VHOC adsorption, *J. Phys. Chem. B*, 106, 2224-
1717 2231, 10.1021/jp0029156, 2002.

1718 Bruska, M. K. and Piechota, J.: Density functional study of sulphur hexafluoride (SF₆) and its
1719 hydrogen derivatives, *Mol. Simul.*, 34, 1041-1050, 10.1080/08927020802258708, 2008.

1720 Budi, A., Stipp, S. L. S., and Andersson, M. P.: Calculation of Entropy of Adsorption for Small
1721 Molecules on Mineral Surfaces, *J. Phys. Chem. C*, 122, 8236-8243, 10.1021/acs.jpcc.7b11860,
1722 2018.

1723 Caloz, F., Fenter, F. F., Tabor, K. D., and Rossi, M. J.: Paper I: Design and construction of a
1724 Knudsen-cell reactor for the study of heterogeneous reactions over the temperature range 130-
1725 750 K: Performances and limitations, *Rev. Sci. Instrum.*, 68, 3172-3179, 1997.

1726 Cambi, R., Cappelletti, D., Liuti, G., and Pirani, F.: Generalized correlations in terms of
1727 polarizability for vanderwaals interaction potential parameter calculations, *J. Chem. Phys.*, 95,
1728 1852-1861, 10.1063/1.461035, 1991.

1729 Campbell, C. T., Sprowl, L. H., and Arnadottir, L.: Equilibrium Constants and Rate Constants
1730 for Adsorbates: Two-Dimensional (2D) Ideal Gas, 2D Ideal Lattice Gas, and Ideal Hindered
1731 Translator Models, *J. Phys. Chem. C*, 120, 10283-10297, 10.1021/acs.jpcc.6b00975, 2016.

1732 Cao, X., Liu, C. L., Zhang, T. F., Xu, Q., Zhang, D. L., Liu, X. T., Jiao, H. J., Wen, X. D., Yang,
1733 Y., Li, Y. W., Niemantsverdriet, J. W., and Zhu, J. F.: Revisiting Oxygen Adsorption on Ir(100),
1734 *J. Phys. Chem. C*, 126, 10035-10044, 10.1021/acs.jpcc.2c01237, 2022.

1735 Cappa, C. D., Onasch, T. B., Massoli, P., Worsnop, D. R., Bates, T. S., Cross, E. S., Davidovits,
1736 P., Hakala, J., Hayden, K. L., Jobson, B. T., Kolesar, K. R., Lack, D. A., Lerner, B. M., Li, S.
1737 M., Mellon, D., Nuaaman, I., Olfert, J. S., Petaja, T., Quinn, P. K., Song, C., Subramanian, R.,
1738 Williams, E. J., and Zaveri, R. A.: Radiative Absorption Enhancements Due to the Mixing State
1739 of Atmospheric Black Carbon, *Science*, 337, 1078-1081, 10.1126/science.1223447, 2012.

1740 Carslaw, K. S., Peter, T., and Muller, R.: Uncertainties in reactive uptake coefficients for solid
1741 stratospheric particles .2. Effect on ozone depletion, *Geophys. Res. Lett.*, 24, 1747-1750,
1742 10.1029/97gl01684, 1997.

1743 Chan, M. N., Zhang, H., Goldstein, A. H., and Wilson, K. R.: Role of Water and Phase in the
1744 Heterogeneous Oxidation of Solid and Aqueous Succinic Acid Aerosol by Hydroxyl Radicals, *J.*
1745 *Phys. Chem. C*, 118, 28978-28992, 10.1021/jp5012022, 2014.

1746 Chandler, D.: Interfaces and the driving force of hydrophobic assembly, *Nature*, 437, 640-647,
1747 10.1038/nature04162, 2005.

1748 Charnawskas, J. C., Alpert, P. A., Lambe, A. T., Berkemeier, T., O'Brien, R. E., Massoli, P.,
1749 Onasch, T. B., Shiraiwa, M., Moffet, R. C., Gilles, M. K., Davidovits, P., Worsnop, D. R., and
1750 Knopf, D. A.: Condensed-phase biogenic-anthropogenic interactions with implications for cold
1751 cloud formation, *Faraday Discuss.*, 200, 164-195, 10.1039/C7FD00010C, 2017.

1752 Chickos, J. S. and Acree, W. E.: Enthalpies of vaporization of organic and organometallic
1753 compounds, 1880-2002, *J. Phys. Chem. Ref. Data*, 32, 519-878, 10.1063/1.1529214, 2003.

1754 China, S., Mazzoleni, C., Gorkowski, K., Aiken, A. C., and Dubey, M. K.: Morphology and
1755 mixing state of individual freshly emitted wildfire carbonaceous particles, *Nat. Commun.*, 4,
1756 2122, 10.1038/ncomms3122, 2013.

1757 Cho, H., Shepson, P. B., Barrie, L. A., Cowin, J. P., and Zaveri, R.: NMR investigation of the
1758 quasi-brine layer in ice/brine mixtures, *J. Phys. Chem. B*, 106, 11226-11232,
1759 10.1021/jp020449+, 2002.

1760 Chorkendorff, I. and Niemantsverdriet, J. W.: *Concepts of Modern Catalysis and Kinetics*, 2nd,
1761 Wiley-VCH Verlag GmbH & Co. KGaA, Weinheim, 477 pp.2007.

1762 Chu, S. N., Sands, S., Tomasik, M. R., Lee, P. S., and McNeill, V. F.: Ozone Oxidation of
1763 Surface-Adsorbed Polycyclic Aromatic Hydrocarbons: Role of PAH-Surface Interaction, *J. Am.*
1764 *Chem. Soc.*, 132, 15968-15975, 10.1021/ja1014772, 2010.

1765 Collignon, B., Hoang, P. N. M., Picaud, S., and Rayez, J. C.: Ab initio study of the water
1766 adsorption on hydroxylated graphite surfaces, *Chemical Physics Letters*, 406, 430-435,
1767 10.1016/j.cplett.2005.03.026, 2005.

1768 Compernelle, S. and Muller, J. F.: Henry's law constants of polyols, *Atmos. Chem. Phys.*, 14,
1769 12815-12837, 10.5194/acp-14-12815-2014, 2014.

1770 Compernelle, S., Ceulemans, K., and Muller, J. F.: EVAPORATION: a new vapour pressure
1771 estimation method for organic molecules including non-additivity and intramolecular
1772 interactions, *Atmos. Chem. Phys.*, 11, 9431-9450, 10.5194/acp-11-9431-2011, 2011.

1773 Crabtree, A. and Siman-Tov, M.: Thermophysical properties of saturated light and heavy water
1774 for advanced neutron source applications, Oak Ridge National Laboratory ORNL/TM-12322,
1775 1993.

1776 Crossley, J.: Dielectric relaxation of 1-butanol and 1-decanol in several solvents, *J. Phys. Chem.*,
1777 75, 1790-&, 10.1021/j100681a005, 1971.

1778 Crossley, J.: Dielectric-relaxation of 1-alkenes, *J. Chem. Phys.*, 58, 5315-5318,
1779 10.1063/1.1679145, 1973.

1780 Croteau, T., Bertram, A. K., and Patey, G. N.: Simulation of Water Adsorption on Kaolinite
1781 under Atmospheric Conditions, *J. Phys. Chem. A*, 113, 7826-7833, 10.1021/jp902453f, 2009.

1782 Crowley, J. N., Ammann, M., Cox, R. A., Hynes, R. G., Jenkin, M. E., Mellouki, A., Rossi, M.
1783 J., Troc, J., and Wallington, T. J.: Evaluated kinetic and photochemical data for atmospheric
1784 chemistry: Volume V - heterogeneous reactions on solid substrates (vol 10, pg 9059, 2010),
1785 *Atmos. Chem. Phys.*, 13, 7359-7359, 10.5194/acp-13-7359-2013, 2013.

1786 Crowley, J. N., Ammann, M., Cox, R. A., Hynes, R. G., Jenkin, M. E., Mellouki, A., Rossi, M.
1787 J., Troe, J., and Wallington, T. J.: Evaluated kinetic and photochemical data for atmospheric
1788 chemistry: Volume V - heterogeneous reactions on solid substrates, *Atmos. Chem. Phys.*, 10,
1789 9059-9223, 10.5194/acp-10-9059-2010, 2010.

1790 Cruzeiro, V. W. D., Galib, M., Limmer, D. T., and Gotz, A. W.: Uptake of N₂O₅ by aqueous
1791 aerosol unveiled using chemically accurate many-body potentials, *Nat. Commun.*, 13, 7,
1792 10.1038/s41467-022-28697-8, 2022.

1793 Cussler, E. L.: *Diffusion - Mass Transfer in Fluid Systems*, 2009.

1794 Cwiertny, D. M., Young, M. A., and Grassian, V. H.: Chemistry and photochemistry of mineral
1795 dust aerosol, *Annu. Rev. Phys. Chem.*, 59, 27-51,
1796 10.1146/annurev.physchem.59.032607.093630, 2008.

1797 Daniels, D. J., Daniels, D. J. (Ed.): *Ground Penetrating Radar*, 2nd, The Institution of Engineering
1798 and Technology, London, United Kingdom, 726 pp.2004.

1799 Davidovits, P., Kolb, C. E., Williams, L. R., Jayne, J. T., and Worsnop, D. R.: Mass
1800 accommodation and chemical reactions at gas-liquid interfaces, *Chem. Rev.*, 106, 1323-1354,
1801 10.1021/cr040366k, 2006.

1802 Davidovits, P., Kolb, C. E., Williams, L. R., Jayne, J. T., and Worsnop, D. R.: Update 1 of: Mass
1803 Accommodation and Chemical Reactions at Gas-Liquid Interfaces, *Chem. Rev.*, 111, PR76-
1804 PR109, 10.1021/cr100360b, 2011.

1805 Davies, J. F. and Wilson, K. R.: Nanoscale interfacial gradients formed by the reactive uptake of
1806 OH radicals onto viscous aerosol surfaces, *Chem. Sci.*, 6, 7020-7027, 10.1039/c5sc02326b,
1807 2015.

1808 Delval, C. and Rossi, M. J.: Influence of monolayer amounts of HNO₃ on the evaporation rate of
1809 H₂O over ice in the range 179 to 208 K: A quartz crystal microbalance study, *J. Phys. Chem. A*,
1810 109, 7151-7165, 10.1021/jp0505072, 2005.

1811 Delval, C., Fluckiger, B., and Rossi, M. J.: The rate of water vapor evaporation from ice
1812 substrates in the presence of HCl and HBr: implications for the lifetime of atmospheric ice
1813 particles, *Atmos. Chem. Phys.*, 3, 1131-1145, 10.5194/acp-3-1131-2003, 2003.

1814 Demou, E. and Donaldson, D. J.: Adsorption of atmospheric gases at the air-water interface. 4:
1815 The influence of salts, *J. Phys. Chem. A*, 106, 982-987, 10.1021/jp0128628, 2002.

1816 Desjonqueres, M.-C. and Spanjaard, D.: *Concepts in Surface Physics*, Springer-Verlag Berlin
1817 Heidelberg, 10.1007/978-3-642-61400-2, 1996.

1818 Devlin, J. P., Joyce, C., and Buch, V.: Infrared spectra and structures of large water clusters, *J.*
1819 *Phys. Chem. A*, 104, 1974-1977, 2000.

1820 Dickbreder, T., Lautner, D., Kohler, A., Klausfering, L., Bechstein, R., and Kuhnle, A.: How
1821 water desorbs from calcite, *Phys. Chem. Chem. Phys.*, 25, 12694, 10.1039/d3cp01159c, 2023.

1822 Donahue, N. M., Robinson, A. L., and Pandis, S. N.: Atmospheric organic particulate matter:
1823 From smoke to secondary organic aerosol, *Atmos. Environ.*, 43, 94-106,
1824 10.1016/j.atmosenv.2008.09.055, 2009.

1825 Donahue, N. M., Epstein, S. A., Pandis, S. N., and Robinson, A. L.: A two-dimensional volatility
1826 basis set: 1. organic-aerosol mixing thermodynamics, *Atmos. Chem. Phys.*, 11, 3303-3318,
1827 10.5194/acp-11-3303-2011, 2011.

1828 Donahue, N. M., Kroll, J. H., Pandis, S. N., and Robinson, A. L.: A two-dimensional volatility
1829 basis set - Part 2: Diagnostics of organic-aerosol evolution, *Atmos. Chem. Phys.*, 12, 615-634,
1830 10.5194/acp-12-615-2012, 2012.

1831 Donaldson, D. J.: Adsorption of atmospheric gases at the air-water interface. I. NH₃, J. Phys.
1832 Chem. A, 103, 62-70, 1999.

1833 Donaldson, D. J. and Anderson, D.: Adsorption of atmospheric gases at the air-water interface. 2.
1834 C-1-C-4 alcohols, acids, and acetone, J. Phys. Chem. A, 103, 871-876, 1999.

1835 Donaldson, D. J., Guest, J. A., and Goh, M. C.: Evidence For Adsorbed So₂ At the Aqueous Air
1836 Interface, J. Phys. Chem., 99, 9313-9315, 1995.

1837 Donaldson, D. J., Ammann, M., Bartels-Rausch, T., and Pöschl, U.: Standard States and
1838 Thermochemical Kinetics in Heterogeneous Atmospheric Chemistry, J. Phys. Chem. A, 116,
1839 6312-6316, 10.1021/jp212015g, 2012a.

1840 Donaldson, D. J., Ammann, M., Bartels-Rausch, T., and Pöschl, U.: Standard States and
1841 Thermochemical Kinetics in Heterogeneous Atmospheric Chemistry, J. Phys. Chem. A, 116,
1842 6312-6316, 10.1021/jp212015g, 2012b.

1843 Dovbeshko, G. I., Romanyuk, V. R., Pidgirnyi, D. V., Cherepanov, V. V., Andreev, E. O., Levin,
1844 V. M., Kuzhir, P. P., Kaplas, T., and Svirko, Y. P.: Optical Properties of Pyrolytic Carbon Films
1845 Versus Graphite and Graphene, Nanoscale Res. Lett., 10, 234, 10.1186/s11671-015-0946-8,
1846 2015.

1847 Dubois, L. H., Zegarski, B. R., and Nuzzo, R. G.: Fundamental-studies of microscopic wetting
1848 on organic-surfaces .2. interaction of secondary adsorbates with chemically textured organic
1849 monolayers, J. Am. Chem. Soc., 112, 570-579, 10.1021/ja00158a013, 1990.

1850 Edebeli, J., Ammann, M., and Bartels-Rausch, T.: Microphysics of the aqueous bulk counters the
1851 water activity driven rate acceleration of bromide oxidation by ozone from 289-245 K, Environ.
1852 Sci.-Process Impacts, 21, 63-73, 10.1039/c8em00417j, 2019.

1853 Edwards, K. C., Klodt, A. L., Galeazzo, T., Schervish, M., Wei, J. L., Fang, T., Donahue, N. M.,
1854 Aumont, B., Nizkorodov, S. A., and Shiraiwa, M.: Effects of Nitrogen Oxides on the Production
1855 of Reactive Oxygen Species and Environmentally Persistent Free Radicals from alpha-Pinene
1856 and Naphthalene Secondary Organic Aerosols, J. Phys. Chem. A, 126, 7361-7372,
1857 10.1021/acs.jpca.2c05532, 2022.

1858 Ekholm, V., Caleman, C., Prytz, N. B., Walz, M. M., Werner, J., Ohrwall, G., Rubensson, J. E.,
1859 and Bjorneholm, O.: Strong enrichment of atmospherically relevant organic ions at the aqueous
1860 interface: the role of ion pairing and cooperative effects, Phys. Chem. Chem. Phys., 20, 27185-
1861 27191, 10.1039/c8cp04525a, 2018.

1862 Epstein, S. A., Riipinen, I., and Donahue, N. M.: A Semiempirical Correlation between Enthalpy
1863 of Vaporization and Saturation Concentration for Organic Aerosol, Environ. Sci. Technol., 44,
1864 743-748, 10.1021/es902497z, 2010.

1865 Fan, H. Y., Lakey, P. S. J., Frank, E. S., Tobias, D. J., Shiraiwa, M., and Grassian, V. H.:
1866 Comparison of the Adsorption-Desorption Kinetics of Limonene and Carvone on TiO₂ and SiO₂
1867 Surfaces under Different Relative Humidity Conditions, J. Phys. Chem. C, 126, 21253-21262,
1868 10.1021/acs.jpcc.2c06853, 2022.

1869 Fang, Y., Riahi, S., McDonald, A. T., Shrestha, M., Tobias, D. J., and Grassian, V. H.: What Is
1870 the Driving Force behind the Adsorption of Hydrophobic Molecules on Hydrophilic Surfaces?, J.
1871 Phys. Chem. Lett., 10, 468-473, 10.1021/acs.jpcclett.8b03484, 2019.

1872 Faust, J. A. and Nathanson, G. M.: Microjets and coated wheels: versatile tools for exploring
1873 collisions and reactions at gas-liquid interfaces, Chem. Soc. Rev., 45, 3609-3620,
1874 10.1039/c6cs00079g, 2016.

1875 Faust, J. A., Dempsey, L. P., and Nathanson, G. M.: Surfactant-Promoted Reactions of Cl₂ and
1876 Br₂ with Br⁻ in Glycerol, J. Phys. Chem. B, 117, 12602-12612, 10.1021/jp4079037, 2013.

1877 Faust, J. A., Sobyra, T. B., and Nathanson, G. M.: Gas-Microjet Reactive Scattering: Collisions
1878 of HCl and DCl with Cool Salty Water, *J. Phys. Chem. Lett.*, 7, 730-735,
1879 10.1021/acs.jpcclett.5b02848, 2016.

1880 Fichthorn, K. A. and Miron, R. A.: Thermal desorption of large molecules from solid surfaces,
1881 *Phys. Rev. Lett.*, 89, 4, 10.1103/PhysRevLett.89.196103, 2002.

1882 Finlayson-Pitts, B. J. and Pitts, J. N.: *Chemistry of the Upper and Lower Atmosphere: Theory,*
1883 *Experiments and Applications*, Academic Press, San Diego, Calif. ; London, xxii, 969 pp.2000.

1884 Fogg, P. G. T. and Sangster, J. M.: *Chemicals in the Atmosphere: Solubility, Sources and*
1885 *Reactivity*, John Wiley & Sons Inc., Hoboken, New Jersey2003.

1886 Foster, M. C. and Ewing, G. E.: Adsorption of water on the NaCl(001) surface. II. An infrared
1887 study at ambient temperatures, *J. Chem. Phys.*, 112, 6817-6826, 10.1063/1.481256, 2000.

1888 Frenkel, J.: Theory of the adsorption and related occurrences, *Z. Phys.*, 26, 117-138,
1889 10.1007/bf01327320, 1924.

1890 Fuchs, N. A.: *Mechanics of Aerosols*, Pergamon, New York1964.

1891 Fuchs, N. A. and Sutugin, A. G.: High-dispersed aerosols, in: *Topics in current aerosol research*,
1892 edited by: Hidy, G. M., and Brock, J. R., Pergamon, New York, 1971.

1893 Galeazzo, T. and Shiraiwa, M.: Predicting glass transition temperature and melting point of
1894 organic compounds <i>via</i> machine learning and molecular embeddings, *Environ. Sci. -*
1895 *Atmospheres*, 2, 362-374, 10.1039/d1ea00090j, 2022.

1896 Galib, M. and Limmer, D. T.: Reactive uptake of N2O5 by atmospheric aerosol is dominated by
1897 interfacial processes, *Science*, 371, 921-+, 10.1126/science.abd7716, 2021.

1898 Gao, X. F. and Nathanson, G. M.: Exploring Gas-Liquid Reactions with Microjets: Lessons We
1899 Are Learning, *Accounts Chem. Res.*, 55, 3294-3302, 10.1021/acs.accounts.2c00602, 2022.

1900 George, C., Ammann, M., D'Anna, B., Donaldson, D. J., and Nizkorodov, S. A.: Heterogeneous
1901 Photochemistry in the Atmosphere, *Chem. Rev.*, 115, 4218-4258, 10.1021/cr500648z, 2015.

1902 George, I. J. and Abbatt, J. P. D.: Heterogeneous oxidation of atmospheric aerosol particles by
1903 gas-phase radicals, *Nat. Chem.*, 2, 713-722, 10.1038/Nchem.806, 2010.

1904 Giguere, P. A.: Molecular association and structure of hydrogen-peroxide, *J. Chem. Educ.*, 60,
1905 399-401, 10.1021/ed060p399, 1983.

1906 Giraudet, S., Pre, P., Tezel, H., and Le Cloirec, P.: Estimation of adsorption energies using
1907 physical characteristics of activated carbons and VOCs' molecular properties, *Carbon*, 44, 1873-
1908 1883, 10.1016/j.carbon.2006.02.018, 2006.

1909 Goldstein, D. J.: Air and steam stripping of toxic pollutants, *Industrial Environmental Research*
1910 *Laboratory*, Cincinnati, OH, USAEPA-68-03-002, 1982.

1911 Goodman, A. L., Bernard, E. T., and Grassian, V. H.: Spectroscopic study of nitric acid and
1912 water adsorption on oxide particles: Enhanced nitric acid uptake kinetics in the presence of
1913 adsorbed water, *J. Phys. Chem. A*, 105, 6443-6457, 2001.

1914 Goss, K. U.: Adsorption of organic vapors on ice and quartz sand at temperatures below 0 C,
1915 *Environ. Sci. Technol.*, 27, 2826-2830, 10.1021/es00049a024, 1993.

1916 Goss, K. U.: Adsorption of organic vapors on polar mineral surfaces and on a bulk water-surface
1917 - development of an empirical predictive model, *Environ. Sci. Technol.*, 28, 640-645,
1918 10.1021/es00053a017, 1994a.

1919 Goss, K. U.: Predicting the enrichment of organic-compounds in fog caused by adsorption on the
1920 water-surface, *Atmos. Environ.*, 28, 3513-3517, 10.1016/1352-2310(94)90008-6, 1994b.

1921 Goss, K. U.: Predicting Adsorption of Organic Chemicals at the Air-Water Interface, *J. Phys.*
1922 *Chem. A*, 113, 12256-12259, 10.1021/jp907347p, 2009.

1923 Goss, K. U. and Eisenreich, S. J.: Effects of temperature and relative-humidity on the adsorption
1924 of organic vapors on hematite, corundum and lime, *Abstr. Pap. Am. Chem. Soc.*, 209, 84-ENVR,
1925 1995a.

1926 Goss, K. U. and Eisenreich, S. J.: Adsorption of organic-compounds from water to mineral
1927 surfaces - a theoretical approach, *Abstr. Pap. Am. Chem. Soc.*, 209, 157-ENVR, 1995b.

1928 Goss, K. U. and Eisenreich, S. J.: Adsorption of VOCs from the gas phase to different minerals
1929 and a mineral mixture, *Environ. Sci. Technol.*, 30, 2135-2142, 10.1021/es950508f, 1996.

1930 Grabow, J. U., Andrews, A. M., Fraser, G. T., Irikura, K. K., Suenram, R. D., Lovas, F. J.,
1931 Lafferty, W. J., and Domenech, J. L.: Microwave spectrum, large-amplitude motions, and ab
1932 initio calculations for N₂O₅, *J. Chem. Phys.*, 105, 7249-7262, 10.1063/1.472586, 1996.

1933 Grayson, J. W., Evoy, E., Song, M., Chu, Y. X., Maclean, A., Nguyen, A., Upshur, M. A.,
1934 Ebrahimi, M., Chan, C. K., Geiger, F. M., Thomson, R. J., and Bertram, A. K.: The effect of
1935 hydroxyl functional groups and molar mass on the viscosity of non-crystalline organic and
1936 organic-water particles, *Atmos. Chem. Phys.*, 17, 8509-8524, 10.5194/acp-17-8509-2017, 2017.

1937 Grimm, R. L., Barrentine, N. M., Knox, C. J. H., and Hemminger, J. C.: D₂O water interaction
1938 with mixed alkane thiol monolayers of tuned hydrophobic and hydrophilic character, *J. Phys.*
1939 *Chem. C*, 112, 890-894, 10.1021/jp710257q, 2008.

1940 Groves, L. G. and Sudden, S.: The dipole moments of vapours - Part V Aromatic compounds,
1941 *Journal of the Chemical Society*, 1782-1784, 10.1039/jr9370001782, 1937.

1942 Guilloteau, A., Bedjanian, Y., Nguyen, M. L., and Tomas, A.: Desorption of Polycyclic
1943 Aromatic Hydrocarbons from a Soot Surface: Three- to Five-Ring PAHs, *J. Phys. Chem. A*, 114,
1944 942-948, 10.1021/jp908862c, 2010.

1945 Guilloteau, A., Nguyen, M. L., Bedjanian, Y., and Le Bras, G.: Desorption of Polycyclic
1946 Aromatic Hydrocarbons from Soot Surface: Pyrene and Fluoranthene, *J. Phys. Chem. A*, 112,
1947 10552-10559, 10.1021/jp803043s, 2008.

1948 Gussoni, M., Rui, M., and Zerbi, G.: Electronic and relaxation contribution to linear molecular
1949 polarizability. An analysis of the experimental values, *J. Mol. Struct.*, 447, 163-215,
1950 10.1016/s0022-2860(97)00292-5, 1998.

1951 Gustafsson, K. and Andersson, S.: Dipole active vibrations and dipole moments of N-2 and O-2
1952 physisorbed on a metal surface, *J. Chem. Phys.*, 125, 5, 10.1063/1.2218842, 2006.

1953 Hai, P., Wu, C., Ding, X., and Li, Y.: Coverage-dependent adsorption and dissociation of H₂O
1954 on Al surfaces, *Phys. Chem. Chem. Phys.*, 25, 13041, 10.1039/d2cp04386f, 2023.

1955 Hait, D. and Head-Gordon, M.: How accurate are static polarizability predictions from density
1956 functional theory? An assessment over 132 species at equilibrium geometry, *Phys. Chem. Chem.*
1957 *Phys.*, 20, 19800-19810, 10.1039/c8cp03569e, 2018.

1958 Hakem, I. F., Boussaid, A., Benchouk-Taleb, H., and Bockstaller, M. R.: Temperature, pressure,
1959 and isotope effects on the structure and properties of liquid water: A lattice approach, *J. Chem.*
1960 *Phys.*, 127, 10, 10.1063/1.2804418, 2007.

1961 Hall, D. G. and Cole, R. H.: Dielectric polarization of sulfuric-acid-solutions, *J. Phys. Chem.*, 85,
1962 1065-1069, 10.1021/j150608a029, 1981.

1963 Hallquist, M., Wenger, J. C., Baltensperger, U., Rudich, Y., Simpson, D., Claeys, M., Dommen,
1964 J., Donahue, N. M., George, C., Goldstein, A. H., Hamilton, J. F., Herrmann, H., Hoffmann, T.,
1965 Iinuma, Y., Jang, M., Jenkin, M. E., Jimenez, J. L., Kiendler-Scharr, A., Maenhaut, W.,
1966 McFiggans, G., Mentel, T. F., Monod, A., Prevot, A. S. H., Seinfeld, J. H., Surratt, J. D.,
1967 Szmigielski, R., and Wildt, J.: The formation, properties and impact of secondary organic
1968 aerosol: current and emerging issues, *Atmos. Chem. Phys.*, 9, 5155-5236, 2009.

1969 Hanefeld, U. and Lefferts, L.: Catalysis, John Wiley & Sons, Inc., Hoboken, New Jersey, USA,
1970 384 pp.2018.

1971 Hanson, D. R.: Surface-specific reactions on liquids, *J. Phys. Chem. B*, 101, 4998-5001, 1997.

1972 Hanson, D. R. and Lovejoy, E. R.: The Reaction of ClONO₂ With Submicrometer Sulfuric-Acid
1973 Aerosol, *Science*, 267, 1326-1328, 1995.

1974 Hanson, D. R. and Ravishankara, A. R.: The Loss of CF₂O On Ice, Nat, and Sulfuric-Acid-
1975 Solutions, *Geophys. Res. Lett.*, 18, 1699-1701, 1991.

1976 Hanson, D. R., Ravishankara, A. R., and Lovejoy, E. R.: Reaction of BrONO₂ with H₂O on
1977 submicron sulfuric acid aerosol and the implications for the lower stratosphere, *J. Geophys. Res.*,
1978 101, 9063-9069, 1996.

1979 Hanson, D. R., Ravishankara, A. R., and Solomon, S.: Heterogeneous Reactions in Sulfuric-Acid
1980 Aerosols - a Framework For Model-Calculations, *J. Geophys. Res.*, 99, 3615-3629, 1994.

1981 Hantal, G., Jedlovsky, P., Hoang, P. N. M., and Picaud, S.: Calculation of the adsorption
1982 isotherm of formaldehyde on ice by grand canonical Monte Carlo simulation, *J. Phys. Chem. C*,
1983 111, 14170-14178, 10.1021/jp0742564, 2007.

1984 Hao, H. X., Leven, I., and Head-Gordon, T.: Can electric fields drive chemistry for an aqueous
1985 microdroplet?, *Nat. Commun.*, 13, 8, 10.1038/s41467-021-27941-x, 2022.

1986 Hartkopf, A. and Karger, B. L.: Study of interfacial properties of water by gas-chromatography,
1987 *Accounts Chem. Res.*, 6, 209-216, 10.1021/ar50066a006, 1973.

1988 Hauxwell, F. and Ottewill, R. H.: Adsorption of toluene vapor on water surfaces, *J. Colloid
1989 Interface Sci.*, 28, 514-&, 10.1016/0021-9797(68)90084-2, 1968.

1990 Hearn, J. D. and Smith, G. A.: Ozonolysis of mixed oleic acid/n-docosane particles: The roles of
1991 phase, morphology, and metastable states, *J. Phys. Chem. A*, 111, 11059-11065,
1992 10.1021/jp0755701, 2007.

1993 Helburn, R., Albritton, J., Howe, G., Michael, L., and Franke, D.: Henry's law constants for
1994 fragrance and organic solvent compounds in aqueous industrial surfactants, *J. Chem. Eng. Data*,
1995 53, 1071-1079, 10.1021/je700418a, 2008.

1996 Hems, R. F., Schnitzler, E. G., Liu-Kang, C., Cappa, C. D., and Abbatt, J. P. D.: Aging of
1997 Atmospheric Brown Carbon Aerosol, *ACS Earth Space Chem.*, 5, 722-748,
1998 10.1021/acsearthspacechem.0c00346, 2021.

1999 Henderson, G. L. and Meyer, G. H.: Intramolecular torsional potential and dielectric properties
2000 of 2,3-butanedione, *J. Phys. Chem.*, 80, 2422-2425, 10.1021/j100562a020, 1976.

2001 Hickey, A. L. and Rowley, C. N.: Benchmarking Quantum Chemical Methods for the
2002 Calculation of Molecular Dipole Moments and Polarizabilities, *J. Phys. Chem. A*, 118, 3678-
2003 3687, 10.1021/jp502475e, 2014.

2004 Hildebrand, J. and Scott, R.: The solubility of nonelectrolytes, 3rd ed., Dover Publications, New
2005 York1964.

2006 Hill, T. L.: An Introduction to Statistical Thermodynamics, Dover Publications, Inc., New York,
2007 501 pp.1986.

2008 Hoffmann, M. R. and Edwards, J. O.: Kinetics of oxidation of sulfite by hydrogen-peroxide in
2009 acidic solution, *J. Phys. Chem.*, 79, 2096-2098, 10.1021/j100587a005, 1975.

2010 Hoffmann, M. R., Martin, S. T., Choi, W. Y., and Bahnemann, D. W.: Environmental
2011 Applications of Semiconductor Photocatalysis, *Chem. Rev.*, 95, 69-96, 10.1021/cr00033a004,
2012 1995.

2013 Hoose, C. and Möhler, O.: Heterogeneous ice nucleation on atmospheric aerosols: a review of
2014 results from laboratory experiments, *Atmos. Chem. Phys.*, 12, 9817-9854, 10.5194/acp-12-9817-
2015 2012, 2012.

2016 Hoskovec, M., Grygarova, D., Cvacka, J., Streinz, L., Zima, J., Verevkin, S. P., and Koutek, B.:
2017 Determining the vapour pressures of plant volatiles from gas chromatographic retention data, *J.*
2018 *Chromatogr. A*, 1083, 161-172, 10.1016/j.chroma.2005.06.006, 2005.

2019 Houle, F. A., Wiegel, A. A., and Wilson, K. R.: Predicting Aerosol Reactivity Across Scales:
2020 from the Laboratory to the Atmosphere, *Environ. Sci. Technol.*, 52, 13774-13781,
2021 10.1021/acs.est.8b04688, 2018.

2022 Hu, Z. M. and Nakatsuji, H.: Adsorption and disproportionation reaction of OH on Ag surfaces:
2023 dipped adcluster model study, *Surf. Sci.*, 425, 296-312, 10.1016/s0039-6028(99)00215-0, 1999.

2024 Huang, Y. Z., Mahrt, F., Xu, S., Shiraiwa, M., Zuend, A., and Bertram, A. K.: Coexistence of
2025 three liquid phases in individual atmospheric aerosol particles, *Proc. Natl. Acad. Sci. U. S. A.*,
2026 118, 9, 10.1073/pnas.2102512118, 2021.

2027 Huthwelker, T., Ammann, M., and Peter, T.: The uptake of acidic gases on ice, *Chem. Rev.*, 106,
2028 1375-1444, 10.1021/cr020506v, 2006.

2029 Hvidt, A.: Interactions of water with non-polar solutes, *Annual Review of Biophysics and*
2030 *Bioengineering*, 12, 1-20, 10.1146/annurev.bb.12.060183.000245, 1983.

2031 Ibrahim, S., Romanias, M. N., Alleman, L. Y., Zeineddine, M. N., Angeli, G. K., Trikalitis, P.
2032 N., and Thevenet, F.: Water Interaction with Mineral Dust Aerosol: Particle Size and
2033 Hygroscopic Properties of Dust, *ACS Earth Space Chem.*, 2, 376-386,
2034 10.1021/acsearthspacechem.7b00152, 2018.

2035 Ingram, S., Rovelli, G., Song, Y. C., Topping, D., Dutcher, C. S., Liu, S. H., Nandy, L.,
2036 Shiraiwa, M., and Reid, J. P.: Accurate Prediction of Organic Aerosol Evaporation Using Kinetic
2037 Multilayer Modeling and the Stokes-Einstein Equation, *J. Phys. Chem. A*, 125, 3444-3456,
2038 10.1021/acs.jpca.1c00986, 2021.

2039 Isaacman-VanWertz, G., Massoli, P., O'Brien, R., Lim, C., Franklin, J. P., Moss, J. A., Hunter, J.
2040 F., Nowak, J. B., Canagaratna, M. R., Misztal, P. K., Arata, C., Roscioli, J. R., Herndon, S. T.,
2041 Onasch, T. B., Lambe, A. T., Jayne, J. T., Su, L., Knopf, D. A., Goldstein, A. H., Worsnop, D.
2042 R., and Kroll, J. H.: Chemical evolution of atmospheric organic carbon over multiple generations
2043 of oxidation, *Nat. Chem.*, 10.1038/s41557-018-0002-2, 2018.

2044 Isakson, M. J. and Sitz, G. O.: Adsorption and desorption of HCl on ice, *J. Phys. Chem. A*, 103,
2045 2044-2049, 10.1021/jp984106g, 1999.

2046 IUPAC, McNaught, A. D., and Wilkinson, A. (Eds.): *Compendium of Chemical Terminology*,
2047 (the "Gold Book"), 2nd, Blackwell Scientific Publications, Oxford, 10.1351/goldbook, 1997.

2048 Jayne, J. T., Davidovits, P., Worsnop, D. R., Zahniser, M. S., and Kolb, C. E.: Uptake of SO₂(G)
2049 By Aqueous Surfaces As a Function of Ph - the Effect of Chemical-Reaction At the Interface, *J.*
2050 *Phys. Chem.*, 94, 6041-6048, 1990.

2051 Jeffrey, G. A.: *An Introduction to Hydrogen Bonding*, Oxford University Press, Oxford, 303
2052 pp.1997.

2053 Jeffrey, G. A. and Saenger, W.: *Hydrogen Bonding in Biological Structures*, Springer-Verlag,
2054 Berlin, 569 pp., 10.1007/978-3-642-85135-3, 1991.

2055 Jensen, L., Astrand, P. O., Osted, A., Kongsted, J., and Mikkelsen, K. V.: Polarizability of
2056 molecular clusters as calculated by a dipole interaction model, *J. Chem. Phys.*, 116, 4001-4010,
2057 10.1063/1.1433747, 2002.

2058 Jeong, D., McNamara, S. M., Barget, A. J., Raso, A. R. W., Upchurch, L. M., Thanekar, S.,
2059 Quinn, P. K., Simpson, W. R., Fuentes, J. D., Shepson, P. B., and Pratt, K. A.: Multiphase
2060 Reactive Bromine Chemistry during Late Spring in the Arctic: Measurements of Gases, Particles,
2061 and Snow, *ACS Earth Space Chem.*, 6, 2877-2887, 10.1021/acsearthspacechem.2c00189, 2022.
2062 Jimenez, J. L., Canagaratna, M. R., Donahue, N. M., Prevot, A. S. H., Zhang, Q., Kroll, J. H.,
2063 DeCarlo, P. F., Allan, J. D., Coe, H., Ng, N. L., Aiken, A. C., Docherty, K. S., Ulbrich, I. M.,
2064 Grieshop, A. P., Robinson, A. L., Duplissy, J., Smith, J. D., Wilson, K. R., Lanz, V. A., Hueglin,
2065 C., Sun, Y. L., Tian, J., Laaksonen, A., Raatikainen, T., Rautiainen, J., Vaattovaara, P., Ehn, M.,
2066 Kulmala, M., Tomlinson, J. M., Collins, D. R., Cubison, M. J., Dunlea, E. J., Huffman, J. A.,
2067 Onasch, T. B., Alfarra, M. R., Williams, P. I., Bower, K., Kondo, Y., Schneider, J., Drewnick, F.,
2068 Borrmann, S., Weimer, S., Demerjian, K., Salcedo, D., Cottrell, L., Griffin, R., Takami, A.,
2069 Miyoshi, T., Hatakeyama, S., Shimono, A., Sun, J. Y., Zhang, Y. M., Dzepina, K., Kimmel, J.
2070 R., Sueper, D., Jayne, J. T., Herndon, S. C., Trimborn, A. M., Williams, L. R., Wood, E. C.,
2071 Middlebrook, A. M., Kolb, C. E., Baltensperger, U., and Worsnop, D. R.: Evolution of Organic
2072 Aerosols in the Atmosphere, *Science*, 326, 1525-1529, 10.1126/science.1180353, 2009.
2073 Joback, K. G. and Reid, R. C.: Estimation of pure-component properties from group-
2074 contributions, *Chem. Eng. Commun.*, 57, 233-243, 10.1080/00986448708960487, 1987.
2075 Johansson, S. M., Lovric, J., Kong, X. R., Thomson, E. S., Hallquist, M., and Pettersson, J. B.
2076 C.: Experimental and Computational Study of Molecular Water Interactions with Condensed
2077 Nopinone Surfaces Under Atmospherically Relevant Conditions, *J. Phys. Chem. A*, 124, 3652-
2078 3661, 10.1021/acs.jpca.9b10970, 2020.
2079 Johansson, S. M., Lovric, J., Kong, X. R., Thomson, E. S., Papagiannakopoulos, P., Briquez, S.,
2080 Toubin, C., and Pettersson, J. B. C.: Understanding water interactions with organic surfaces:
2081 environmental molecular beam and molecular dynamics studies of the water-butanol system,
2082 *Phys. Chem. Chem. Phys.*, 21, 1141-1151, 10.1039/c8cp04151b, 2019.
2083 Joliat, J., Lenoir, T., and Picaud, S.: Comparative Study of the Adsorption of 1-and 2-Propanol
2084 on Ice by Means of Grand Canonical Monte Carlo Simulations, *ACS Earth Space Chem.*, 13,
2085 10.1021/acsearthspacechem.2c00390, 2023.
2086 Julin, J., Shiraiwa, M., Miles, R. E. H., Reid, J. P., Pöschl, U., and Riipinen, I.: Mass
2087 Accommodation of Water: Bridging the Gap Between Molecular Dynamics Simulations and
2088 Kinetic Condensation Models, *J. Phys. Chem. A*, 117, 410-420, 10.1021/jp310594e, 2013.
2089 Jungwirth, P., Finlayson-Pitts, B. J., and Tobias, D. J.: Introduction: Structure and chemistry at
2090 aqueous interfaces, *Chem. Rev.*, 106, 1137-1139, 2006.
2091 Kahan, T. F., Kwamena, N. O. A., and Donaldson, D. J.: Heterogeneous ozonation kinetics of
2092 polycyclic aromatic hydrocarbons on organic films, *Atmos. Environ.*, 40, 3448-3459,
2093 10.1016/j.atmosenv.2006.02.004, 2006.
2094 Kaiser, J. C., Riemer, N., and Knopf, D. A.: Detailed heterogeneous oxidation of soot surfaces in
2095 a particle-resolved aerosol model, *Atmos. Chem. Phys.*, 11, 4505-4520, 2011.
2096 Kanakidou, M., Seinfeld, J. H., Pandis, S. N., Barnes, I., Dentener, F. J., Facchini, M. C., Van
2097 Dingenen, R., Ervens, B., Nenes, A., Nielsen, C. J., Swietlicki, E., Putaud, J. P., Balkanski, Y.,
2098 Fuzzi, S., Horth, J., Moortgat, G. K., Winterhalter, R., Myhre, C. E. L., Tsigaridis, K., Vignati,
2099 E., Stephanou, E. G., and Wilson, J.: Organic aerosol and global climate modelling: a review,
2100 *Atmos. Chem. Phys.*, 5, 1053-1123, 2005.
2101 Kanji, Z. A., Ladino, L. A., Wex, H., Boose, Y., Burkert-Kohn, M., Cziczo, D. J., and Krämer,
2102 M.: Overview of Ice Nucleating Particles, in: *Ice Formation and Evolution in Clouds and*

2103 Precipitation: Measurement and Modeling Challenges, Meteorological Monographs, American
2104 Meteorological Society, 1.1-1.33, DOI: 10.1175/AMSMONOGRAPHS-D-16-0006.1, 2017.
2105 Kerbrat, M., Huthwelker, T., Gaggeler, H. W., and Ammann, M.: Interaction of Nitrous Acid
2106 with Polycrystalline Ice: Adsorption on the Surface and Diffusion into the Bulk, *J. Phys. Chem.*
2107 *C*, 114, 2208-2219, 10.1021/jp909535c, 2010.
2108 Keyser, L. F., Moore, S. B., and Leu, M. T.: Surface-Reaction and Pore Diffusion in Flow-Tube
2109 Reactors, *J. Phys. Chem.*, 95, 5496-5502, 1991.
2110 Kieckbusch, T. G. and King, C. J.: Partition-coefficients for acetates in food systems, *J. Agric.*
2111 *Food Chem.*, 27, 504-507, 10.1021/jf60223a033, 1979.
2112 Kim, Y. K., Park, S. C., Kim, J. H., Lee, C. W., and Kang, H.: Interaction of Carbon Dioxide and
2113 Hydroxide Ion at the Surface of Ice Films, *J. Phys. Chem. C*, 112, 18104-18109,
2114 10.1021/jp806643e, 2008.
2115 Kisliuk, P.: The sticking probabilities of gases chemisorbed on the surfaces of solids, *J. Phys.*
2116 *Chem. Solids*, 3, 95-101, 10.1016/0022-3697(57)90054-9, 1957.
2117 Kisliuk, P.: The sticking probabilities of gases chemisorbed on the surfaces of solids. 2., *J. Phys.*
2118 *Chem. Solids*, 5, 78-84, 1958.
2119 Klassen, J. K., Fiehrer, K. M., and Nathanson, G. M.: Collisions of organic molecules with
2120 concentrated sulfuric acid: Scattering, trapping, and desorption, *J. Phys. Chem. B*, 101, 9098-
2121 9106, 10.1021/jp972329l, 1997.
2122 Klassen, J. K., Hu, Z. J., and Williams, L. R.: Diffusion coefficients for HCl and HBr in 30 wt %
2123 to 72 wt % sulfuric acid at temperatures between 220 and 300 K, *J. Geophys. Res.-Atmospheres*,
2124 103, 16197-16202, 10.1029/98jd01252, 1998.
2125 Knopf, D. A. and Alpert, P. A.: Atmospheric ice nucleation, *Nat. Rev. Phys.*, 10.1038/s42254-
2126 023-00570-7, 2023.
2127 Knopf, D. A. and Ammann, M.: Technical note: Adsorption and desorption equilibria from
2128 statistical thermodynamics and rates from transition state theory, *Atmos. Chem. Phys.*, 21,
2129 15725-15753, 10.5194/acp-21-15725-2021, 2021.
2130 Knopf, D. A. and Koop, T.: Heterogeneous nucleation of ice on surrogates of mineral dust, *J.*
2131 *Geophys. Res.*, 111, D12201, 10.1029/2005jd006894, 2006.
2132 Knopf, D. A., Alpert, P. A., and Wang, B.: The Role of Organic Aerosol in Atmospheric Ice
2133 Nucleation: A Review, *ACS Earth Space Chem.*, 2, 168-202,
2134 10.1021/acsearthspacechem.7b00120, 2018.
2135 Knopf, D. A., Anthony, L. M., and Bertram, A. K.: Reactive uptake of O₃ by multicomponent
2136 and multiphase mixtures containing oleic acid, *J. Phys. Chem. A*, 109, 5579-5589, 2005.
2137 Knopf, D. A., Forrester, S. M., and Slade, J. H.: Heterogeneous oxidation kinetics of organic
2138 biomass burning aerosol surrogates by O₃, NO₂, N₂O₅, and NO₃, *Phys. Chem. Chem. Phys.*,
2139 13, 21050-21062, 10.1039/C1cp22478f, 2011.
2140 Knopf, D. A., Pöschl, U., and Shiraiwa, M.: Radial Diffusion and Penetration of Gas Molecules
2141 and Aerosol Particles through Laminar Flow Reactors, Denuders, and Sampling Tubes, *Anal.*
2142 *Chem.*, 87, 3746-3754, 10.1021/ac5042395, 2015.
2143 Knopf, D. A., Ammann, M., Berkemeier, T., Pöschl, U., and Shiraiwa, M.: Desorption Lifetimes
2144 and Activation Energies influencing Gas-Surface Interactions and Multiphase Chemical
2145 Kinetics: Atmospheric and Environmental Implications [dataset], XYZ, 2023.
2146 Knox, C. J. H. and Phillips, L. F.: Capillary-wave model of gas-liquid exchange, *J. Phys. Chem.*
2147 *B*, 102, 8469-8472, 10.1021/jp973183t, 1998.

2148 Koch, T. G. and Rossi, M. J.: Direct measurement of surface residence times: Nitryl chloride and
2149 chlorine nitrate on alkali halides at room temperature, *J. Phys. Chem. A*, 102, 9193-9201,
2150 10.1021/jp982539d, 1998a.

2151 Koch, T. G. and Rossi, M. J.: Direct measurement of surface residence times: Nitryl chloride and
2152 chlorine nitrate on alkali halides at room temperature, *J. Phys. Chem. A*, 102, 9193-9201, 1998b.

2153 Koch, T. G., Fenter, F. F., and Rossi, M. J.: Real-time measurement of residence times of gas
2154 molecules on solid surfaces, *Chemical Physics Letters*, 275, 253-260, 1997.

2155 Kolasinski, K. W.: *Surface Science: Foundations of Catalysis and Nanoscience*, 3rd, John Wiley
2156 & Sons, Ltd., West Sussex, United Kingdom, 556 pp., 10.1002/9781119941798, 2012.

2157 Kolb, C. E., Worsnop, D. R., Zahniser, M. S., Davidovits, P., Keyser, L. F., Leu, M.-T., Molina,
2158 M. J., Hanson, D. R., Ravishankara, A. R., Williams, L. R., and Tolbert, M. A.: *Laboratory
2159 Studies of Atmospheric Heterogeneous Chemistry*, in: *Progress and Problems in Atmospheric
2160 Chemistry*, edited by: Barker, J. R., World Scientific, Singapore, 771-875, 1995.

2161 Kolb, C. E., Cox, R. A., Abbatt, J. P. D., Ammann, M., Davis, E. J., Donaldson, D. J., Garrett, B.
2162 C., George, C., Griffiths, P. T., Hanson, D. R., Kulmala, M., McFiggans, G., Pöschl, U.,
2163 Riipinen, I., Rossi, M. J., Rudich, Y., Wagner, P. E., Winkler, P. M., Worsnop, D. R., and O'
2164 Dowd, C. D.: An overview of current issues in the uptake of atmospheric trace gases by aerosols
2165 and clouds, *Atmos. Chem. Phys.*, 10, 10561-10605, 2010.

2166 Kolomiitsova, T. D., Lyaptsev, A. V., and Shchepkin, D. N.: Determination of parameters of the
2167 dipole moment of the CO₂ molecule, *Opt. Spectrosc.*, 88, 648-660, 10.1134/1.626856, 2000.

2168 Kong, X. R., Thomson, E. S., Markovic, N., and Pettersson, J. B. C.: Dynamics and Kinetics of
2169 Methanol-Graphite Interactions at Low Surface Coverage, *ChemPhysChem*, 20, 2171-2178,
2170 10.1002/cphc.201900457, 2019.

2171 Kong, X. R., Lovri, J., Johansson, S. M., Prisle, N. L., and Pettersson, J. B. C.: Dynamics and
2172 Sorption Kinetics of Methanol Monomers and Clusters on Nopinone Surfaces, *J. Phys. Chem. A*,
2173 125, 6263-6272, 10.1021/acs.jpca.1c02309, 2021.

2174 Kong, X. R., Papagiannakopoulos, P., Thomson, E. S., Markovic, N., and Pettersson, J. B. C.:
2175 Water Accommodation and Desorption Kinetics on Ice, *J. Phys. Chem. A*, 118, 3973-3979,
2176 10.1021/jp503504e, 2014a.

2177 Kong, X. R., Thomson, E. S., Papagiannakopoulos, P., Johansson, S. M., and Pettersson, J. B.
2178 C.: Water Accommodation on Ice and Organic Surfaces: Insights from Environmental Molecular
2179 Beam Experiments, *J. Phys. Chem. B*, 118, 13378-13386, 10.1021/jp5044046, 2014b.

2180 Kong, X. R., Waldner, A., Orlando, F., Artiglia, L., Huthwelker, T., Ammann, M., and Bartels-
2181 Rausch, T.: Coexistence of Physisorbed and Solvated HCl at Warm Ice Surfaces, *J. Phys. Chem.
2182 Lett.*, 8, 4757-4762, 10.1021/acs.jpcllett.7b01573, 2017.

2183 Koop, T., Carslaw, K. S., and Peter, T.: Thermodynamic stability and phase transitions of PSC
2184 particles, *Geophys. Res. Lett.*, 24, 2199-2202, 1997.

2185 Koop, T., Bookhold, J., Shiraiwa, M., and Poeschl, U.: Glass transition and phase state of
2186 organic compounds: dependency on molecular properties and implications for secondary organic
2187 aerosols in the atmosphere, *Phys. Chem. Chem. Phys.*, 13, 19238-19255, 10.1039/c1cp22617g,
2188 2011a.

2189 Koop, T., Bookhold, J., Shiraiwa, M., and Pöschl, U.: Glass transition and phase state of organic
2190 compounds: dependency on molecular properties and implications for secondary organic
2191 aerosols in the atmosphere, *Phys. Chem. Chem. Phys.*, 13, 19238-19255, 10.1039/c1cp22617g,
2192 2011b.

2193 Kroll, J. H., Donahue, N. M., Jimenez, J. L., Kessler, S. H., Canagaratna, M. R., Wilson, K. R.,
2194 Altieri, K. E., Mazzoleni, L. R., Wozniak, A. S., Bluhm, H., Mysak, E. R., Smith, J. D., Kolb, C.
2195 E., and Worsnop, D. R.: Carbon oxidation state as a metric for describing the chemistry of
2196 atmospheric organic aerosol, *Nat Chem*, 3, 133-139, 10.1038/nchem.948, 2011.
2197 Kronberg, B.: The hydrophobic effect, *Curr. Opin. Colloid Interface Sci.*, 22, 14-22,
2198 10.1016/j.cocis.2016.02.001, 2016.
2199 Kronberger, H. and Weiss, J.: Formation and structure of some organic molecular compounds.
2200 Part III. The dielectric polarisation of some solid crystalline molecular compounds, *J. Chem.*
2201 *Soc.*, 464-469, 10.1039/jr9440000464, 1944.
2202 Kuhne, R., Ebert, R. U., and Schuurmann, G.: Prediction of the temperature dependency of
2203 Henry's law constant from chemical structure, *Environ. Sci. Technol.*, 39, 6705-6711,
2204 10.1021/es050527h, 2005.
2205 Kwamena, N. O. A., Thornton, J. A., and Abbatt, J. P. D.: Kinetics of surface-bound benzo a
2206 pyrene and ozone on solid organic and salt aerosols, *J. Phys. Chem. A*, 108, 11626-11634,
2207 10.1021/jp046161x, 2004.
2208 Laib, J. P. and Mittleman, D. M.: Temperature-Dependent Terahertz Spectroscopy of Liquid n-
2209 alkanes, *J. Infrared Millim. Terahertz Waves*, 31, 1015-1021, 10.1007/s10762-010-9678-0, 2010.
2210 Laidler, K. J.: The mechanisms of some elementary surface reactions, *J. Phys. Colloid Chem.*,
2211 53, 712-732, 10.1021/j150470a010, 1949.
2212 Laidler, K. J., Glasstone, S., and Eyring, H.: Application of the Theory of Absolute Reaction
2213 Rates to Heterogeneous Processes II. Chemical Reactions on Surfaces, *J. Chem. Phys.*, 8, 667-
2214 676, 10.1063/1.1750737, 1940.
2215 Lakey, P. S. J., Cummings, B. E., Waring, M. S., Morrison, G. C., and Shiraiwa, M.: Effective
2216 mass accommodation for partitioning of organic compounds into surface films with different
2217 viscosities, *Environ. Sci.-Process Impacts*, 15, 10.1039/d3em00213f, 2023.
2218 Lakey, P. S. J., Eichler, C. M. A., Wang, C. Y., Little, J. C., and Shiraiwa, M.: Kinetic multi-
2219 layer model of film formation, growth, and chemistry (KM-FILM): Boundary layer processes,
2220 multi-layer adsorption, bulk diffusion, and heterogeneous reactions, *Indoor Air*, 31, 2070-2083,
2221 10.1111/ina.12854, 2021.
2222 Lakey, P. S. J., Berkemeier, T., Krapf, M., Dommen, J., Steimer, S. S., Whalley, L. K., Ingham,
2223 T., Baeza-Romero, M. T., Pöschl, U., Shiraiwa, M., Ammann, M., and Heard, D. E.: The effect
2224 of viscosity and diffusion on the HO₂ uptake by sucrose and secondary organic aerosol particles,
2225 *Atmos. Chem. Phys.*, 16, 13035-13047, 10.5194/acp-16-13035-2016, 2016.
2226 Langenberg, S. and Schurath, U.: Gas chromatography using ice-coated fused silica columns:
2227 study of adsorption of sulfur dioxide on water ice, *Atmos. Chem. Phys.*, 18, 7527-7537,
2228 10.5194/acp-18-7527-2018, 2018.
2229 Langmuir, I.: A theory of adsorption, *Phys. Rev.*, 6, 79-80, 1915.
2230 Langmuir, I.: The evaporation, condensation and reflection of molecules and the mechanism of
2231 adsorption, *Phys. Rev.*, 8, 149-176, 10.1103/PhysRev.8.149, 1916.
2232 Langmuir, I.: The adsorption of gases on plane surfaces of glass, mica and platinum, *J. Am.*
2233 *Chem. Soc.*, 40, 1361-1403, 10.1021/ja02242a004, 1918.
2234 Laskin, A., Laskin, J., and Nizkorodov, S. A.: Chemistry of Atmospheric Brown Carbon, *Chem.*
2235 *Rev.*, 115, 4335-4382, 10.1021/cr5006167, 2015.
2236 Lee, G., Lee, B., Kim, J., and Cho, K.: Ozone Adsorption on Graphene: Ab Initio Study and
2237 Experimental Validation, *J. Phys. Chem. C*, 113, 14225-14229, 10.1021/jp904321n, 2009.

2238 Lee, M. T., Orlando, F., Artiglia, L., Chen, S. Z., and Ammann, M.: Chemical Composition and
2239 Properties of the Liquid-Vapor Interface of Aqueous C1 to C4 Monofunctional Acid and Alcohol
2240 Solutions, *J. Phys. Chem. A*, 120, 9749-9758, 10.1021/acs.jpca.6b09261, 2016.
2241 Lee, M. T., Orlando, F., Khabiri, M., Roeselova, M., Brown, M. A., and Ammann, M.: The
2242 opposing effect of butanol and butyric acid on the abundance of bromide and iodide at the
2243 aqueous solution-air interface, *Phys. Chem. Chem. Phys.*, 21, 8418-8427, 10.1039/c8cp07448h,
2244 2019.
2245 Lee, W. M. G. and Chen, J. C.: Partitioning coefficients of polycyclic aromatic-hydrocarbons in
2246 stack gas from a municipal incinerator, *Environ. Int.*, 21, 827-831, 10.1016/0160-
2247 4120(95)00092-4, 1995.
2248 Lejonthun, L., Andersson, P. U., Hallquist, M., Thomson, E. S., and Pettersson, J. B. C.:
2249 Interactions of N₂O₅ and Related Nitrogen Oxides with Ice Surfaces: Desorption Kinetics and
2250 Collision Dynamics, *J. Phys. Chem. B*, 118, 13427-13434, 10.1021/jp5053826, 2014.
2251 Leluk, K., Orzechowski, K., Jerie, K., Baranowski, A., Slonka, T., and Glowinski, J.: Dielectric
2252 permittivity of kaolinite heated to high temperatures, *J. Phys. Chem. Solids*, 71, 827-831,
2253 10.1016/j.jpcs.2010.02.008, 2010.
2254 Leng, C. B., Kish, J. D., Roberts, J. E., Dwebi, I., Chon, N., and Liu, Y.: Temperature-Dependent
2255 Henry's Law Constants of Atmospheric Amines, *J. Phys. Chem. A*, 119, 8884-8891,
2256 10.1021/acs.jpca.5b05174, 2015.
2257 Li, G., Su, H., Kuhn, U., Meusel, H., Ammann, M., Shao, M., Poschl, U., and Cheng, Y. F.:
2258 Technical note: Influence of surface roughness and local turbulence on coated-wall flow tube
2259 experiments for gas uptake and kinetic studies, *Atmos. Chem. Phys.*, 18, 2669-2686,
2260 10.5194/acp-18-2669-2018, 2018.
2261 Li, J. and Knopf, D. A.: Representation of Multiphase OH Oxidation of Amorphous Organic
2262 Aerosol for Tropospheric Conditions, *Environ. Sci. Technol.*, 55, 7266-7275,
2263 10.1021/acs.est.0c07668, 2021.
2264 Li, J. N., Forrester, S. M., and Knopf, D. A.: Heterogeneous oxidation of amorphous organic
2265 aerosol surrogates by O₃, NO₃, and OH at typical tropospheric temperatures, *Atmos. Chem.*
2266 *Phys.*, 20, 6055-6080, 10.5194/acp-20-6055-2020, 2020.
2267 Li, Y. and Shiraiwa, M.: Timescales of secondary organic aerosols to reach equilibrium at
2268 various temperatures and relative humidities, *Atmos. Chem. Phys.*, 19, 5959-5971, 10.5194/acp-
2269 19-5959-2019, 2019.
2270 Li, Y., Pöschl, U., and Shiraiwa, M.: Molecular corridors and parameterizations of volatility in
2271 the chemical evolution of organic aerosols, *Atmos. Chem. Phys.*, 16, 3327-3344, 10.5194/acp-
2272 16-3327-2016, 2016.
2273 Liang, Z., Li, K. J., Wang, Z. M., Bu, Y. S., and Zhang, J. L.: Adsorption and reaction
2274 mechanisms of single and double H₂O molecules on graphene surfaces with defects: a density
2275 functional theory study, *Phys. Chem. Chem. Phys.*, 23, 19071-19082, 10.1039/d1cp02595c,
2276 2021.
2277 Lide, D. R.: *CRC Handbook of Chemistry and Physics*, 82nd, CRC Press., Boca Raton 2008.
2278 Lileev, A. and Lyashchenko, A.: Dielectric properties of ammonium salt aqueous solutions, *J.*
2279 *Mol. Liq.*, 150, 4-8, 10.1016/j.molliq.2009.08.008, 2009.
2280 Longfellow, C. A., Imamura, T., Ravishankara, A. R., and Hanson, D. R.: HONO solubility and
2281 heterogeneous reactivity on sulfuric acid surfaces, *J. Phys. Chem. A*, 102, 3323-3332, 1998.
2282 Mack, K. M. and Muentner, J. S.: Stark and Zeeman properties of ozone from molecular-beam
2283 spectroscopy, *J. Chem. Phys.*, 66, 5278-5283, 10.1063/1.433909, 1977.

2284 Mader, B. T., Goss, K. U., and Eisenreich, S. J.: Sorption of nonionic, hydrophobic organic
2285 chemicals to mineral surfaces, *Environ. Sci. Technol.*, 31, 1079-1086, 10.1021/es960606g, 1997.
2286 Maribo-Mogensen, B., Kontogeorgis, G. M., and Thomsen, K.: Modeling of Dielectric
2287 Properties of Aqueous Salt Solutions with an Equation of State, *J. Phys. Chem. B*, 117, 10523-
2288 10533, 10.1021/jp403375t, 2013.
2289 Marsh, A. R. W. and McElroy, W. J.: The dissociation-constant and Henry law constant of HCl
2290 in aqueous-solution, *Atmos. Environ.*, 19, 1075-1080, 10.1016/0004-6981(85)90192-1, 1985.
2291 Marshall, F. H., Berkemeier, T., Shiraiwa, M., Nandy, L., Ohm, P. B., Dutcher, C. S., and Reid,
2292 J. P.: Influence of particle viscosity on mass transfer and heterogeneous ozonolysis kinetics in
2293 aqueous-sucrose-maleic acid aerosol, *Phys. Chem. Chem. Phys.*, 20, 15560-15573,
2294 10.1039/c8cp01666f, 2018.
2295 Marshall, F. H., Miles, R. E. H., Song, Y. C., Ohm, P. B., Power, R. M., Reid, J. P., and Dutcher,
2296 C. S.: Diffusion and reactivity in ultraviscous aerosol and the correlation with particle viscosity,
2297 *Chem. Sci.*, 7, 1298-1308, 10.1039/c5sc03223g, 2016.
2298 Masel, R. I.: Principles of Adsorption and Reaction on Solid Surfaces, Wiley Series in Chemical
2299 Engineering 1996.
2300 McEachran, A. D., Mansouri, K., Grulke, C., Schymanski, E. L., Ruttkies, C., and Williams, A.
2301 J.: "MS-Ready" structures for non-targeted high-resolution mass spectrometry screening studies,
2302 *J. Cheminformatics*, 10, 16, 10.1186/s13321-018-0299-2, 2018.
2303 McNamara, S. M., Chen, Q. J., Edebeli, J., Kulju, K. D., Mumpfield, J., Fuentes, J. D., Bertman,
2304 S. B., and Pratt, K. A.: Observation of N₂O₅ Deposition and ClNO₂ Production on the Saline
2305 Snowpack, *ACS Earth Space Chem.*, 5, 1020-1031, 10.1021/acsearthspacechem.0c00317, 2021.
2306 McNeill, V. F., Loerting, T., Geiger, F. M., Trout, B. L., and Molina, M. J.: Hydrogen chloride-
2307 induced surface disordering on ice, *Proc. Natl. Acad. Sci. U. S. A.*, 103, 9422-9427,
2308 10.1073/pnas.0603494103, 2006.
2309 McNeill, V. F., Geiger, F. M., Loerting, T., Trout, B. L., Molina, L. T., and Molina, M. J.:
2310 Interaction of hydrogen chloride with ice surfaces: The effects of grain size, surface roughness,
2311 and surface disorder, *J. Phys. Chem. A*, 111, 6274-6284, 10.1021/jp068914g, 2007.
2312 McNeill, V. F., Grannas, A. M., Abbatt, J. P. D., Ammann, M., Ariya, P., Bartels-Rausch, T.,
2313 Domine, F., Donaldson, D. J., Guzman, M. I., Heger, D., Kahan, T. F., Klan, P., Masclin, S.,
2314 Toubin, C., and Voisin, D.: Organics in environmental ices: sources, chemistry, and impacts,
2315 *Atmos. Chem. Phys.*, 12, 9653-9678, 10.5194/acp-12-9653-2012, 2012.
2316 Mendes, P. C. D., Costa-Amaral, R., Gomes, J. F., and Da Silva, J. L. F.: The influence of
2317 hydroxy groups on the adsorption of three-carbon alcohols on Ni(111), Pd(111) and Pt(111)
2318 surfaces: a density functional theory study within the D3 dispersion correction, *Phys. Chem.*
2319 *Chem. Phys.*, 21, 8434, 10.1039/c9cp00752k, 2019.
2320 Meng, S., Wang, E. G., and Gao, S. W.: Water adsorption on metal surfaces: A general picture
2321 from density functional theory studies, *Phys. Rev. B*, 69, 13, 10.1103/PhysRevB.69.195404,
2322 2004.
2323 Merino, E. and Ribagorda, M.: Control over molecular motion using the cis-trans
2324 photoisomerization of the azo group, *Beilstein J. Org. Chem.*, 8, 1071-1090, 10.3762/bjoc.8.119,
2325 2012.
2326 Messerer, A., Niessner, R., and Pöschl, U.: Comprehensive kinetic characterization of the
2327 oxidation and gasification of model and real diesel soot by nitrogen oxides and oxygen under
2328 engine exhaust conditions: Measurement, Langmuir-Hinshelwood, and Arrhenius parameters,
2329 *Carbon*, 44, 307-324, 10.1016/j.carbon.2005.07.017, 2006.

2330 Messerer, A., Schmatloch, V., Pöschl, U., and Niessner, R.: Combined particle emission
2331 reduction and heat recovery from combustion exhaust - A novel approach for small wood-fired
2332 appliances, *Biomass & Bioenergy*, 31, 512-521, 10.1016/j.biombioe.2007.01.022, 2007.

2333 Meyer, H., Entel, P., and Hafner, J.: Physisorption of water on salt surfaces, *Surf. Sci.*, 488, 177-
2334 192, 10.1016/s0039-6028(01)01136-0, 2001.

2335 Mikhailov, E., Vlasenko, S., Martin, S. T., Koop, T., and Poschl, U.: Amorphous and crystalline
2336 aerosol particles interacting with water vapor: conceptual framework and experimental evidence
2337 for restructuring, phase transitions and kinetic limitations, *Atmos. Chem. Phys.*, 9, 9491-9522,
2338 2009.

2339 Millany, H. M. and Jonscher, A. K.: Dielectric-properties of stearic-acid multilayers, *Thin Solid*
2340 *Films*, 68, 257-273, 10.1016/0040-6090(80)90151-0, 1980.

2341 Mmerek, B. T., Hicks, J. M., and Donaldson, D. J.: Adsorption of atmospheric gases at the air-
2342 water interface. 3: Methylamines, *J. Phys. Chem. A*, 104, 10789-10793, 10.1021/jp0023258,
2343 2000.

2344 Moise, T., Flores, J. M., and Rudich, Y.: Optical properties of secondary organic aerosols and
2345 their changes by chemical processes, *Chem. Rev.*, 115, 4400-4439, 10.1021/cr5005259, 2015.

2346 Mopsik, F. I.: *Digest of Literature on Dielectrics: National Academy of Sciences, National*
2347 *Research Council Washington, D. C.*, 1967.

2348 Morris, J. R., Behr, P., Antman, M. D., Ringeisen, B. R., Splan, J., and Nathanson, G. M.:
2349 Molecular beam scattering from supercooled sulfuric acid: Collisions of HCl, HBr, and HNO₃
2350 with 70 wt % D₂SO₄, *J. Phys. Chem. A*, 104, 6738-6751, 10.1021/jp000105o, 2000.

2351 Moussa, S. G., McIntire, T. M., Szori, M., Roeselova, M., Tobias, D. J., Grimm, R. L.,
2352 Hemminger, J. C., and Finlayson-Pitts, B. J.: Experimental and Theoretical Characterization of
2353 Adsorbed Water on Self-Assembled Monolayers: Understanding the Interaction of Water with
2354 Atmospherically Relevant Surfaces, *J. Phys. Chem. A*, 113, 2060-2069, 10.1021/jp808710n,
2355 2009.

2356 Mu, Q., Shiraiwa, M., Octaviani, M., Ma, N., Ding, A. J., Su, H., Lammel, G., Poschl, U., and
2357 Cheng, Y. F.: Temperature effect on phase state and reactivity controls atmospheric multiphase
2358 chemistry and transport of PAHs, *Sci. Adv.*, 4, 8, 10.1126/sciadv.aap7314, 2018.

2359 Muller, R., Crutzen, P. J., Gross, J. U., Bruhl, C., Russell, J. M., Gernandt, H., McKenna, D. S.,
2360 and Tuck, A. F.: Severe chemical ozone loss in the Arctic during the winter of 1995-96, *Nature*,
2361 389, 709-712, 1997.

2362 Nakanishi, M. and Nozaki, R.: Systematic study of the glass transition in polyhydric alcohols,
2363 *Phys. Rev. E*, 83, 5, 10.1103/PhysRevE.83.051503, 2011.

2364 Nakatsuji, H.: Dipped adcluster model for chemisorptions and catalytic reactions on a metal-
2365 surface, *J. Chem. Phys.*, 87, 4995-5001, 10.1063/1.452814, 1987.

2366 Nathanson, G. M.: Molecular beam studies of gas-liquid interfaces, *Annu. Rev. Phys. Chem.*, 55,
2367 231-255, 10.1146/annurev.physchem.55.091602.094357, 2004.

2368 Nathanson, G. M., Davidovits, P., Worsnop, D. R., and Kolb, C. E.: Dynamics and kinetics at the
2369 gas-liquid interface, *J. Phys. Chem.*, 100, 13007-13020, 1996.

2370 Nelson, C. E., Elam, J. W., Tolbert, M. A., and George, S. M.: H₂O and HCl adsorption on
2371 single crystal alpha-Al₂O₃(0001) at stratospheric temperatures, *Appl. Surf. Sci.*, 171, 21-33,
2372 2001.

2373 Nelson, C. E., Elam, J. W., Cameron, M. A., Tolbert, M. A., and George, S. M.: Desorption of
2374 H₂O from a hydroxylated single-crystal alpha-Al₂O₃(0001) surface, *Surf. Sci.*, 416, 341-353,
2375 10.1016/s0039-6028(98)00439-7, 1998.

2376 NIST: NIST Computational Chemistry Comparison and Benchmark Database,
2377 10.18434/T47C7Z, 2018.

2378 Nizkorodov, S. A., Laskin, J., and Laskin, A.: Molecular chemistry of organic aerosols through
2379 the application of high resolution mass spectrometry, *Phys. Chem. Chem. Phys.*, 13, 3612-3629,
2380 10.1039/c0cp02032j, 2011.

2381 Ohrwall, G., Prisle, N. L., Ottosson, N., Werner, J., Ekholm, V., Walz, M. M., and Bjorneholm,
2382 O.: Acid-Base Speciation of Carboxylate Ions in the Surface Region of Aqueous Solutions in the
2383 Presence of Ammonium and Aminium Ions, *J. Phys. Chem. B*, 119, 4033-4040,
2384 10.1021/jp509945g, 2015.

2385 Oszust, J. and Ratajczak, H.: Dipole-moments and spectral features of some phenol-diethylamine
2386 complexes, *J. Chem. Soc. Farad. T* 1, 77, 1215-1221, 10.1039/f19817701215, 1981.

2387 Pankow, J. F.: Common gamma-intercept and single compound regressions of gas particle
2388 partitioning data vs $1/t$, *Atmos. Environ. A-Gen.*, 25, 2229-2239, 10.1016/0960-1686(91)90098-
2389 r, 1991.

2390 Paserba, K. R. and Gellman, A. J.: Effects of conformational isomerism on the desorption
2391 kinetics of n-alkanes from graphite, *J. Chem. Phys.*, 115, 6737-6751, 10.1063/1.1398574, 2001.

2392 Penkett, S. A., Jones, B. M. R., Brice, K. A., and Eggleton, A. E. J.: Importance of atmospheric
2393 ozone and hydrogen-peroxide in oxidizing sulfur-dioxide in cloud and rainwater, *Atmos.*
2394 *Environ.*, 13, 123-137, 10.1016/0004-6981(79)90251-8, 1979.

2395 Perraud, V., Bruns, E. A., Ezell, M. J., Johnson, S. N., Yu, Y., Alexander, M. L., Zelenyuk, A.,
2396 Imre, D., Chang, W. L., Dabdub, D., Pankow, J. F., and Finlayson-Pitts, B. J.: Nonequilibrium
2397 atmospheric secondary organic aerosol formation and growth, *P. Natl. Acad. Sci. USA*, 109,
2398 2836-2841, 10.1073/pnas.1119909109, 2012.

2399 Peter, T.: Microphysics and heterogeneous chemistry of polar stratospheric clouds, *Annu. Rev.*
2400 *Phys. Chem.*, 48, 785-822, 1997.

2401 Petters, M. D., Prenni, A. J., Kreidenweis, S. M., DeMott, P. J., Matsunaga, A., Lim, Y. B., and
2402 Ziemann, P. J.: Chemical aging and the hydrophobic-to-hydrophilic conversion of carbonaceous
2403 aerosol, *Geophys. Res. Lett.*, 33, 10.1029/2006gl027249, 2006.

2404 Poe, S. H., Valsaraj, K. T., Thibodeaux, L. J., and Springer, C.: Equilibrium vapor-phase
2405 adsorption of volatile organic-chemicals on dry soils, *J. Hazard. Mater.*, 19, 17-32,
2406 10.1016/0304-3894(88)85071-4, 1988.

2407 Pöschl, U. and Shiraiwa, M.: Multiphase Chemistry at the Atmosphere-Biosphere Interface
2408 Influencing Climate and Public Health in the Anthropocene, *Chem. Rev.*, 115, 4440-4475,
2409 10.1021/cr500487s, 2015.

2410 Pöschl, U., Rudich, Y., and Ammann, M.: Kinetic model framework for aerosol and cloud
2411 surface chemistry and gas-particle interactions - Part 1: General equations, parameters, and
2412 terminology, *Atmos. Chem. Phys.*, 7, 5989-6023, 2007.

2413 Pöschl, U., Letzel, T., Schauer, C., and Niessner, R.: Interaction of ozone and water vapor with
2414 spark discharge soot aerosol particles coated with benzo a pyrene: O₃ and H₂O adsorption,
2415 benzo a pyrene degradation, and atmospheric implications, *J. Phys. Chem. A*, 105, 4029-4041,
2416 2001.

2417 Pouvesle, N., Kippenberger, M., Schuster, G., and Crowley, J. N.: The interaction of H₂O₂ with
2418 ice surfaces between 203 and 233 K, *Phys. Chem. Chem. Phys.*, 12, 15544-15550,
2419 10.1039/c0cp01656j, 2010.

2420 Raja, S., Yacone, F. S., Ravikrishna, R., and Valsaraj, K. T.: Thermodynamic parameters for
2421 the adsorption of aromatic hydrocarbon vapors at the gas-water interface, *J. Chem. Eng. Data*,
2422 47, 1213-1219, 10.1021/je025520j, 2002.

2423 Rajyam, B. S. and Murty, C. R. K.: Dipole moments of some alkyl phenylacetates, *Indian J. Pure*
2424 *Appl. Phys.*, 4, 327-&, 1966.

2425 Rampi, M. A., Schueller, O. J. A., and Whitesides, G. M.: Alkanethiol self-assembled
2426 monolayers as the dielectric of capacitors with nanoscale thickness, *Appl. Phys. Lett.*, 72, 1781-
2427 1783, 10.1063/1.121183, 1998.

2428 Raso, A. R. W., Custard, K. D., May, N. W., Tanner, D., Newburn, M. K., Walker, L., Moore, R.
2429 J., Huey, L. G., Alexander, L., Shepson, P. B., and Pratt, K. A.: Active molecular iodine
2430 photochemistry in the Arctic, *Proc. Natl. Acad. Sci. U. S. A.*, 114, 10053-10058,
2431 10.1073/pnas.1702803114, 2017.

2432 Ravishankara, A. R.: Heterogeneous and multiphase chemistry in the troposphere, *Science*, 276,
2433 1058-1065, 1997.

2434 Redhead, P. A.: Thermal desorption of gases, *Vacuum*, 12, 203-211, 10.1016/0042-
2435 207X(62)90978-8, 1962.

2436 Remorov, R. G. and Bardwell, M. W.: Model of uptake of OH radicals on nonreactive solids, *J.*
2437 *Phys. Chem. B*, 109, 20036-20043, 2005.

2438 Rettner, C. T., Auerbach, D. J., Tully, J. C., and Kleyn, A. W.: Chemical dynamics at the gas-
2439 surface interface, *J. Phys. Chem.*, 100, 13021-13033, 10.1021/jp9536007, 1996.

2440 Ringeisen, B. R., Muentner, A. H., and Nathanson, G. M.: Collisions of DCl with liquid glycerol:
2441 Evidence for rapid, near-interfacial D \rightarrow H exchange and desorption, *J. Phys. Chem. B*, 106,
2442 4999-5010, 10.1021/jp013959x, 2002a.

2443 Ringeisen, B. R., Muentner, A. H., and Nathanson, G. M.: Collisions of HCl, DCl, and HBr with
2444 liquid glycerol: Gas uptake, D \rightarrow H exchange, and solution thermodynamics, *J. Phys. Chem. B*,
2445 106, 4988-4998, 10.1021/jp013960w, 2002b.

2446 Robinson, D. A., Cooper, J. D., and Gardner, C. M. K.: Modelling the relative permittivity of
2447 soils using soil hygroscopic water content, *J. Hydrol.*, 255, 39-49, 10.1016/s0022-
2448 1694(01)00508-x, 2002.

2449 Robinson, G. N., Worsnop, D. R., Jayne, J. T., Kolb, C. E., Swartz, E., and Davidovits, P.:
2450 Heterogeneous uptake of HCl by sulfuric acid solutions, *J. Geophys. Res.*, 103, 25371-25381,
2451 1998.

2452 Romaner, L., Heimel, G., Ambrosch-Draxl, C., and Zojer, E.: The Dielectric Constant of Self-
2453 Assembled Monolayers, *Adv. Funct. Mater.*, 18, 3999-4006, 10.1002/adfm.200800876, 2008.

2454 Romanias, M. N., Ourrad, H., Thevenet, F., and Riffault, V.: Investigating the Heterogeneous
2455 Interaction of VOCs with Natural Atmospheric Particles: Adsorption of Limonene and Toluene
2456 on Saharan Mineral Dusts, *J. Phys. Chem. A*, 120, 1197-1212, 10.1021/acs.jpca.5b10323, 2016.

2457 Rothfuss, N. E. and Petters, M. D.: Influence of Functional Groups on the Viscosity of Organic
2458 Aerosol, *Environ. Sci. Technol.*, 51, 271-279, 10.1021/acs.est.6b04478, 2017.

2459 Rouquerol, J. and Davy, L.: Automatic gravimetric apparatus for recording adsorption-isotherms
2460 of gases or vapors onto solids, *Thermochim. Acta*, 24, 391-397, 10.1016/0040-6031(78)80027-6,
2461 1978.

2462 Rowland, F. S.: Stratospheric ozone depletion, *Annu. Rev. Phys. Chem.*, 42, 731-768,
2463 10.1146/annurev.physchem.42.1.731, 1991.

2464 Rudich, Y., Donahue, N. M., and Mentel, T. F.: Aging of organic aerosol: Bridging the gap
2465 between laboratory and field studies, *Annu. Rev. Phys. Chem.*, 58, 321-352,
2466 10.1146/annurev.physchem.58.032806.104432, 2007.

2467 Salmeron, M. and Somorjai, G. A.: Adsorption and bonding of butane and pentane on the
2468 Pt(111) crystal-surfaces - effects of oxygen treatments and deuterium pre-adsorption, *J. Phys.*
2469 *Chem.*, 85, 3835-3840, 10.1021/j150625a025, 1981.

2470 Sander, R.: Compilation of Henry's law constants (version 4.0) for water as solvent, *Atmos.*
2471 *Chem. Phys.*, 15, 4399-4981, 10.5194/acp-15-4399-2015, 2015.

2472 Sander, R.: Compilation of Henry's law constants (version 5.0.0) for water as solvent, *Atmos.*
2473 *Chem. Phys.*, 23, 10901–12440, 10.5194/acp-23-10901-2023, 2023.

2474 Sander, S. P., Abbatt, J., Barker, J. R., Burkholder, J. B., Friedl, R. R., Golden, D. M., Huie, R.
2475 E., Kolb, C. E., Kurylo, M. J., Moortgat, G. K., Orkin, V. L., and Wine, P. H.: *Chemical Kinetics*
2476 *and Photochemical Data for Use in Atmospheric Studies*, Evaluation No. 17, NASA Jet
2477 Propulsion Laboratory, Pasadena 2011.

2478 Savara, A.: Standard States for Adsorption on Solid Surfaces: 2D Gases, Surface Liquids, and
2479 Langmuir Adsorbates, *J. Phys. Chem. C*, 117, 15710-15715, 10.1021/jp404398z, 2013.

2480 Savara, A., Schmidt, C. M., Geiger, F. M., and Weitz, E.: Adsorption Entropies and Enthalpies
2481 and Their Implications for Adsorbate Dynamics, *J. Phys. Chem. C*, 113, 2806-2815,
2482 10.1021/jp806221j, 2009.

2483 Schervish, M. and Donahue, N. M.: Peroxy radical chemistry and the volatility basis set, *Atmos.*
2484 *Chem. Phys.*, 20, 1183-1199, 10.5194/acp-20-1183-2020, 2020.

2485 Schervish, M. and Shiraiwa, M.: Impact of phase state and non-ideal mixing on equilibration
2486 timescales of secondary organic aerosol partitioning, *Atmos. Chem. Phys.*, 23, 221-233,
2487 10.5194/acp-23-221-2023, 2023.

2488 Schervish, M., Donahue, N. M., and Shiraiwa, M.: Effects of volatility, viscosity, and non-
2489 ideality on particle-particle mixing timescales of secondary organic aerosols, *Aerosol Sci.*
2490 *Technol.*, 16, 10.1080/02786826.2023.2256827, 2023.

2491 Schlesinger, D., Lowe, S. J., Olenius, T., Kong, X. R., Pettersson, J. B. C., and Riipinen, I.:
2492 Molecular Perspective on Water Vapor Accommodation into Ice and Its Dependence on
2493 Temperature, *J. Phys. Chem. A*, 124, 10879-10889, 10.1021/acs.jpca.0c09357, 2020.

2494 Schroder, E.: Methanol Adsorption on Graphene, *J. Nanomater.*, 2013, 6, 10.1155/2013/871706,
2495 2013.

2496 Schwartz, S. E.: Mass-transport considerations pertinent to aqueous phase reactions of gases in
2497 liquid-water clouds, in: *Chemistry of multiphase atmospheric systems*, edited by: Jaeschke, W.,
2498 NATO ASI Series, G6, Springer, New York, 1986.

2499 Sebastiani, F., Campbell, R. A., Rastogi, K., and Pfrang, C.: Nighttime oxidation of surfactants at
2500 the air-water interface: effects of chain length, head group and saturation, *Atmos. Chem. Phys.*,
2501 18, 3249-3268, 10.5194/acp-18-3249-2018, 2018.

2502 Seinfeld, J. H. and Pandis, S. N.: *Atmospheric Chemistry and Physics. From Air Pollution to*
2503 *Climate Change*, John Wiley, New York, 1326 pp. 1998.

2504 Shalowski, M. A., Gord, J. R., Staudt, S., Quinn, S. L., Bertram, T. H., and Nathanson, G. M.:
2505 Reactions of N₂O₅ with Salty and Surfactant-Coated Glycerol: Interfacial Conversion of Br⁻ to
2506 Br₂ Mediated by Alkylammonium Cations, *J. Phys. Chem. A*, 121, 3708-3719,
2507 10.1021/acs.jpca.7b02040, 2017.

2508 Sharif, S.: Chemical and mineral-composition of dust and its effect on the dielectric-constant,
2509 *IEEE Trans. Geosci. Remote Sensing*, 33, 353-359, 10.1109/36.377935, 1995.

2510 Shen, C. Y., Zhang, W., Choczynski, J., Davies, J. F., and Zhang, H. F.: Phase State and Relative
2511 Humidity Regulate the Heterogeneous Oxidation Kinetics and Pathways of Organic-Inorganic
2512 Mixed Aerosols, *Environ. Sci. Technol.*, 56, 15398-15407, 10.1021/acs.est.2c04670, 2022.
2513 Shi, Q., Jayne, J. T., Kolb, C. E., Worsnop, D. R., and Davidovits, P.: Kinetic model for reaction
2514 of ClONO₂ with H₂O and HCl and HOCl with HCl in sulfuric acid solutions, *J. Geophys. Res.*,
2515 106, 24259-24274, 2001.
2516 Shinoda, K.: Iceberg formation and solubility, *J. Phys. Chem.*, 81, 1300-1302,
2517 10.1021/j100528a016, 1977.
2518 Shinoda, K.: Characteristic property in aqueous-solutions - effect of iceberg formation of water
2519 surrounding solute on the solubility (or cmc) and its peculiar temperature-dependence, *Adv.*
2520 *Colloid Interface Sci.*, 41, 81-100, 10.1016/0001-8686(92)80008-1, 1992.
2521 Shiraiwa, M. and Pöschl, U.: Mass accommodation and gas-particle partitioning in secondary
2522 organic aerosols: dependence on diffusivity, volatility, particle-phase reactions, and penetration
2523 depth, *Atmos. Chem. Phys.*, 21, 1565-1580, 10.5194/acp-21-1565-2021, 2021.
2524 Shiraiwa, M. and Seinfeld, J. H.: Equilibration timescale of atmospheric secondary organic
2525 aerosol partitioning, *Geophys. Res. Lett.*, 39, L24801, 10.1029/2012gl054008, 2012.
2526 Shiraiwa, M., Garland, R. M., and Pöschl, U.: Kinetic double-layer model of aerosol surface
2527 chemistry and gas-particle interactions (K2-SURF): Degradation of polycyclic aromatic
2528 hydrocarbons exposed to O₃, NO₂, H₂O, OH and NO₃, *Atmos. Chem. Phys.*, 9, 9571-9586,
2529 2009.
2530 Shiraiwa, M., Pfrang, C., and Pöschl, U.: Kinetic multi-layer model of aerosol surface and bulk
2531 chemistry (KM-SUB): the influence of interfacial transport and bulk diffusion on the oxidation
2532 of oleic acid by ozone, *Atmos. Chem. Phys.*, 10, 3673-3691, 2010.
2533 Shiraiwa, M., Ammann, M., Koop, T., and Pöschl, U.: Gas uptake and chemical aging of
2534 semisolid organic aerosol particles, *P. Natl. Acad. Sci. USA*, 108, 11003-11008, 2011a.
2535 Shiraiwa, M., Pfrang, C., Koop, T., and Pöschl, U.: Kinetic multi-layer model of gas-particle
2536 interactions in aerosols and clouds (KM-GAP): linking condensation, evaporation and chemical
2537 reactions of organics, oxidants and water, *Atmos. Chem. Phys.*, 12, 2777-2794, 2012.
2538 Shiraiwa, M., Zuend, A., Bertram, A. K., and Seinfeld, J. H.: Gas-particle partitioning of
2539 atmospheric aerosols: interplay of physical state, non-ideal mixing and morphology, *Phys.*
2540 *Chem. Chem. Phys.*, 15, 11441-11453, 10.1039/c3cp51595h, 2013a.
2541 Shiraiwa, M., Berkemeier, T., Schilling-Fahnestock, K. A., Seinfeld, J. H., and Pöschl, U.:
2542 Molecular corridors and kinetic regimes in the multiphase chemical evolution of secondary
2543 organic aerosol, *Atmos. Chem. Phys.*, 14, 8323-8341, 10.5194/acp-14-8323-2014, 2014.
2544 Shiraiwa, M., Sosedova, Y., Rouviere, A., Yang, H., Zhang, Y. Y., Abbatt, J. P. D., Ammann,
2545 M., and Pöschl, U.: The role of long-lived reactive oxygen intermediates in the reaction of ozone
2546 with aerosol particles, *Nature Chemistry*, 3, 291-295, 2011b.
2547 Shiraiwa, M., Yee, L. D., Schilling, K. A., Loza, C. L., Craven, J. S., Zuend, A., Ziemann, P. J.,
2548 and Seinfeld, J. H.: Size distribution dynamics reveal particle-phase chemistry in organic aerosol
2549 formation, *Proc. Natl. Acad. Sci. U. S. A.*, 110, 11746-11750, 10.1073/pnas.1307501110, 2013b.
2550 Shiraiwa, M., Li, Y., Tsimpidi, A. P., Karydis, V. A., Berkemeier, T., Pandis, S. N., Lelieveld, J.,
2551 Koop, T., and Pöschl, U.: Global distribution of particle phase state in atmospheric secondary
2552 organic aerosols, *Nat. Commun.*, 8, 15002, 10.1038/ncomms15002, 2017a.
2553 Shiraiwa, M., Ueda, K., Pozzer, A., Lammel, G., Kampf, C. J., Fushimi, A., Enami, S., Arangio,
2554 A. M., Frohlich-Nowoisky, J., Fujitani, Y., Furuyama, A., Lakey, P. S. J., Lelieveld, J., Lucas,
2555 K., Morino, Y., Pöschl, U., Takaharna, S., Takami, A., Tong, H. J., Weber, B., Yoshino, A., and

2556 Sato, K.: Aerosol Health Effects from Molecular to Global Scales, *Environ. Sci. Technol.*, 51,
2557 13545-13567, 10.1021/acs.est.7b04417, 2017b.

2558 Shklyarevskii, I. N. and Pakhomov, P. L.: Separation of contributions from free and coupled
2559 electrons into real and imaginary parts of a dielectric-constant of gold, *Opt. Spektrosk.*, 34, 163-
2560 166, 1973.

2561 Shrivastava, M., Lou, S. J., Zelenyuk, A., Easter, R. C., Corley, R. A., Thrall, B. D., Rasch, P. J.,
2562 Fast, J. D., Simonich, S. L. M., Shen, H. Z., and Tao, S.: Global long-range transport and lung
2563 cancer risk from polycyclic aromatic hydrocarbons shielded by coatings of organic aerosol (vol
2564 114, pg 1246, 2017), *Proc. Natl. Acad. Sci. U. S. A.*, 114, E2263-E2263,
2565 10.1073/pnas.1702221114, 2017a.

2566 Shrivastava, M., Cappa, C. D., Fan, J. W., Goldstein, A. H., Guenther, A. B., Jimenez, J. L.,
2567 Kuang, C., Laskin, A., Martin, S. T., Ng, N. L., Petaja, T., Pierce, J. R., Rasch, P. J., Roldin, P.,
2568 Seinfeld, J. H., Shilling, J., Smith, J. N., Thornton, J. A., Volkamer, R., Wang, J., Worsnop, D.
2569 R., Zaveri, R. A., Zelenyuk, A., and Zhang, Q.: Recent advances in understanding secondary
2570 organic aerosol: Implications for global climate forcing, *Rev. Geophys.*, 55, 509-559,
2571 10.1002/2016rg000540, 2017b.

2572 Sikorski, M., Gutt, C., Chushkin, Y., Lippmann, M., and Franz, H.: Dynamics at the Liquid-
2573 Vapor Interface of a Supercooled Organic Glass Former, *Phys. Rev. Lett.*, 105, 4,
2574 10.1103/PhysRevLett.105.215701, 2010.

2575 Silva, S. C. and Devlin, J. P.: Interaction of acetylene, ethylene, and benzene with ice surfaces, *J.*
2576 *Phys. Chem.*, 98, 10847-10852, 10.1021/j100093a027, 1994.

2577 Slade, J. H. and Knopf, D. A.: Heterogeneous OH oxidation of biomass burning organic aerosol
2578 surrogate compounds: assessment of volatilisation products and the role of OH concentration on
2579 the reactive uptake kinetics, *Phys. Chem. Chem. Phys.*, 15, 5898-5915, 10.1039/c3cp44695f,
2580 2013.

2581 Slade, J. H. and Knopf, D. A.: Multiphase OH oxidation kinetics of organic aerosol: The role of
2582 particle phase state and relative humidity, *Geophys. Res. Lett.*, 41, 5297-5306,
2583 10.1002/2014gl060582, 2014.

2584 Slade, J. H., Thalman, R., Wang, J., and Knopf, D. A.: Chemical aging of single and
2585 multicomponent biomass burning aerosol surrogate particles by OH: implications for cloud
2586 condensation nucleus activity, *Atmos. Chem. Phys.*, 15, 10183-10201, 10.5194/acp-15-10183-
2587 2015, 2015.

2588 Slade, J. H., Shiraiwa, M., Arangio, A., Su, H., Pöschl, U., Wang, J., and Knopf, D. A.: Cloud
2589 droplet activation through oxidation of organic aerosol influenced by temperature and particle
2590 phase state, *Geophys. Res. Lett.*, 44, 1583-1591, 10.1002/2016gl072424, 2017.

2591 Slater, B. and Michaelides, A.: Surface premelting of water ice, *Nat. Rev. Chem.*, 3, 172-188,
2592 10.1038/s41570-019-0080-8, 2019.

2593 Smith, R. S. and Kay, B. D.: Desorption Kinetics of Carbon Dioxide from a Graphene-Covered
2594 Pt(111) Surface, *J. Phys. Chem. A*, 123, 3248-3254 10.1021/acs.jpca.9b00674, 2019.

2595 Sokolov, O. and Abbatt, J. P. D.: Adsorption to ice of n-alcohols (ethanol to 1-hexanol), acetic
2596 acid, and hexanal, *J. Phys. Chem. A*, 106, 775-782, 2002.

2597 Sokolowska, Z., Jozefaciuk, G., Sokolowski, S., and Ourumovapesheva, A.: Adsorption of
2598 water-vapor by soils - investigations of the influence of organic-matter, iron, and aluminum on
2599 energetic heterogeneity of soil clays, *Clay Clay Min.*, 41, 346-352, 10.1346/ccmn.1993.0410310,
2600 1993.

2601 Solomon, S.: Stratospheric ozone depletion: A review of concepts and history, *Rev. Geophys.*,
2602 37, 275-316, 1999.

2603 Speight, J. G.: in: *Lange's Handbook of Chemistry*, 17th ed., McGraw-Hill Education, New
2604 York, 2017.

2605 Springmann, M., Knopf, D. A., and Riemer, N.: Detailed heterogeneous chemistry in an urban
2606 plume box model: reversible co-adsorption of O₃, NO₂, and H₂O on soot coated with benzo a
2607 pyrene, *Atmos. Chem. Phys.*, 9, 7461-7479, 2009.

2608 Sprowl, L. H., Campbell, C. T., and Arnadottir, L.: Hindered Translator and Hindered Rotor
2609 Models for Adsorbates: Partition Functions and Entropies, *J. Phys. Chem. C*, 120, 9719-9731,
2610 10.1021/acs.jpcc.5b11616, 2016.

2611 Staudinger, J. and Roberts, P. V.: A critical compilation of Henry's law constant temperature
2612 dependence relations for organic compounds in dilute aqueous solutions, *Chemosphere*, 44, 561-
2613 576, 10.1016/s0045-6535(00)00505-1, 2001.

2614 Steimer, S. S., Berkemeier, T., Gilgen, A., Krieger, U. K., Peter, T., Shiraiwa, M., and Ammann,
2615 M.: Shikimic acid ozonolysis kinetics of the transition from liquid aqueous solution to highly
2616 viscous glass, *Phys. Chem. Chem. Phys.*, 17, 31101-31109, 10.1039/c5cp04544d, 2015.

2617 Steiner, D. and Burtscher, H. K.: Desorption of perylene from combustion, nacl, and carbon
2618 particles, *Environ. Sci. Technol.*, 28, 1254-1259, 10.1021/es00056a012, 1994.

2619 Steiner, T.: The hydrogen bond in the solid state, *Angew. Chem.-Int. Edit.*, 41, 48-76,
2620 10.1002/1521-3773(20020104)41:1<48::Aid-anie48>3.0.Co;2-u, 2002.

2621 Stephenson, R. M. and Malanowski, S.: *Handbook of the Thermodynamics of Organic*
2622 *Compounds*, Elsevier Science Publishing Co., Inc., Dordrecht, 10.1007/978-94-009-3173-2,
2623 1987.

2624 Stolzenburg, D., Fischer, L., Vogel, A. L., Heinritzi, M., Schervish, M., Simon, M., Wagner, A.
2625 C., Dada, L., Ahonen, L. R., Amorim, A., Baccharini, A., Bauer, P. S., Baumgartner, B., Bergen,
2626 A., Bianchi, F., Breitenlechner, M., Brilke, S., Mazon, S. B., Chen, D. X., Dias, A., Draper, D.
2627 C., Duplissy, J., Haddad, I., Finkenzeller, H., Frege, C., Fuchs, C., Garmash, O., Gordon, H., He,
2628 X., Helm, J., Hofbauer, V., Hoyle, C. R., Kim, C., Kirkby, J., Kontkanen, J., Kuerten, A.,
2629 Lampilahti, J., Lawler, M., Lehtipalo, K., Leiminger, M., Mai, H., Mathot, S., Mentler, B.,
2630 Molteni, U., Nie, W., Nieminen, T., Nowak, J. B., Ojdanic, A., Onnela, A., Passananti, M.,
2631 Petaja, T., Quelever, L. L. J., Rissanen, M. P., Sarnela, N., Schallhart, S., Tauber, C., Tome, A.,
2632 Wagner, R., Wang, M., Weitz, L., Wimmer, D., Xiao, M., Yan, C., Ye, P., Zha, Q.,
2633 Baltensperger, U., Curtius, J., Dommen, J., Flagan, R. C., Kulmala, M., Smith, J. N., Worsnop,
2634 D. R., Hansel, A., Donahue, N. M., and Winkler, P. M.: Rapid growth of organic aerosol
2635 nanoparticles over a wide tropospheric temperature range, *Proc. Natl. Acad. Sci. U. S. A.*, 115,
2636 9122-9127, 10.1073/pnas.1807604115, 2018.

2637 Stull, D. R.: Vapor pressure of pure substances - inorganic compounds, *Industrial and*
2638 *Engineering Chemistry*, 4, 540-550, 10.1021/ie50448a023, 1947.

2639 Su, H., Cheng, Y. F., and Poschl, U.: New Multiphase Chemical Processes Influencing
2640 Atmospheric Aerosols, Air Quality, and Climate in the Anthropocene, *Accounts Chem. Res.*, 53,
2641 2034-2043, 10.1021/acs.accounts.0c00246, 2020.

2642 Svrbely, W. J., Ablard, J. E., and Warner, J. C.: Molar polarizations in extremely dilute
2643 solutions. The dipole moments of d-limonene, d-pinene, methyl benzoate and ethyl benzoate, *J.*
2644 *Am. Chem. Soc.*, 57, 652-655, 10.1021/ja01307a015, 1935.

2645 Tabai, S., Rogalski, M., Solimando, R., and Malanowski, S. K.: Activity coefficients of
2646 chlorophenols in water at infinite dilution, *J. Chem. Eng. Data*, 42, 1147-1150,
2647 10.1021/je960336h, 1997.

2648 Tabazadeh, A., Turco, R. P., and Jacobson, M. Z.: A Model for Studying the Composition and
2649 Chemical Effects of Stratospheric Aerosols, *J. Geophys. Res.*, 99, 12897-12914, 1994.

2650 Tait, S. L., Dohnalek, Z., Campbell, C. T., and Kay, B. D.: n-alkanes on Pt(111) and on
2651 C(0001)/Pt(111): Chain length dependence of kinetic desorption parameters, *J. Chem. Phys.*,
2652 125, 15, 10.1063/1.2400235, 2006.

2653 Takenaka, N. and Rossi, M. J.: The heterogeneous reaction of NO₂ with NH₄Cl: A molecular
2654 diffusion tube study, *J. Atmos. Chem.*, 50, 171-194, 10.1007/s10874-005-5898-4, 2005.

2655 Tang, M. J., Cziczo, D. J., and Grassian, V. H.: Interactions of Water with Mineral Dust Aerosol:
2656 Water Adsorption, Hygroscopicity, Cloud Condensation, and Ice Nucleation, *Chem. Rev.*, 116,
2657 4205-4259, 10.1021/acs.chemrev.5b00529, 2016.

2658 Tenhulscher, T. E. M., Vandervelde, L. E., and Bruggeman, W. A.: Temperature-dependence of
2659 henry law constants for selected chlorobenzenes, polychlorinated-biphenyls and polycyclic
2660 aromatic-hydrocarbons, *Environ. Toxicol. Chem.*, 11, 1595-1603, 10.1897/1552-
2661 8618(1992)11[1595:Tdohlc]2.0.Co;2, 1992.

2662 Thomas, J. M. and Williams, B. R.: Theory and applications of vacuum microbalance
2663 techniques, *Quarterly Reviews*, 19, 231-+, 10.1039/qr9651900231, 1965.

2664 Thomson, E. S., Kong, X., Papagiannakopoulos, P., and Pettersson, J. B. C.: Deposition-mode
2665 ice nucleation reexamined at temperatures below 200 K, *Atmos. Chem. Phys.*, 15, 1621-1632,
2666 10.5194/acp-15-1621-2015, 2015.

2667 Thomson, E. S., Kong, X. R., Andersson, P. U., Markovic, N., and Pettersson, J. B. C.: Collision
2668 Dynamics and Solvation of Water Molecules in a Liquid Methanol Film, *J. Phys. Chem. Lett.*, 2,
2669 2174-2178, 10.1021/jz200929y, 2011.

2670 Tian, H. K., Xu, Q. Y., Zhang, H. Y., Priestley, R. D., and Zuo, B.: Surface dynamics of glasses,
2671 *Appl. Phys. Rev.*, 9, 25, 10.1063/5.0083726, 2022.

2672 Tolbert, M. A., Rossi, M. J., Malhotra, R., and Golden, D. M.: Reaction of chlorine nitrate with
2673 hydrogen-chloride and water at antarctic stratospheric temperatures, *Science*, 238, 1258-1260,
2674 10.1126/science.238.4831.1258, 1987.

2675 Townes, C. H. and Schawlow, A. L.: *Microwave Spectroscopy*, Dover Publications, Inc., New
2676 York 1975.

2677 Tully, J. C.: The dynamics of adsorption and desorption, *Surf. Sci.*, 299, 667-677, 10.1016/0039-
2678 6028(94)90688-2, 1994.

2679 Ulbricht, H., Zacharia, R., Cindir, N., and Hertel, T.: Thermal desorption of gases and solvents
2680 from graphite and carbon nanotube surfaces, *Carbon*, 44, 2931-2942,
2681 10.1016/j.carbon.2006.05.040, 2006.

2682 Ulrich, T., Ammann, M., Leutwyler, S., and Bartels-Rausch, T.: The adsorption of peroxyntic
2683 acid on ice between 230 K and 253 K, *Atmos. Chem. Phys.*, 12, 1833-1845, 10.5194/acp-12-
2684 1833-2012, 2012.

2685 Usher, C. R., Michel, A. E., and Grassian, V. H.: Reactions on mineral dust, *Chem. Rev.*, 103,
2686 4883-4939, 2003.

2687 Valsaraj, K. T.: On the physicochemical aspects of partitioning of non-polar hydrophobic
2688 organics at the air-water-interface, *Chemosphere*, 17, 875-887, 10.1016/0045-6535(88)90060-4,
2689 1988a.

2690 Valsaraj, K. T.: Binding constants for non-polar hydrophobic organics at the air-water-interface -
2691 comparison of experimental and predicted values, *Chemosphere*, 17, 2049-2053, 10.1016/0045-
2692 6535(88)90015-x, 1988b.

2693 Valsaraj, K. T.: Hydrophobic compounds in the environment - adsorption equilibrium at the air-
2694 water-interface, *Water Res.*, 28, 819-830, 10.1016/0043-1354(94)90088-4, 1994.

2695 Valsaraj, K. T.: Trace gas adsorption thermodynamics at the air-water interface: Implications in
2696 atmospheric chemistry, *Pure Appl. Chem.*, 81, 1889-1901, 10.1351/pac-con-08-07-06, 2009.

2697 Valsaraj, K. T. and Thibodeaux, L. J.: Equilibrium adsorption of chemical vapors on surface
2698 soils, landfills and landfarms - a review, *J. Hazard. Mater.*, 19, 79-99, 10.1016/0304-
2699 3894(88)85075-1, 1988.

2700 Valsaraj, K. T., Thoma, G. J., Reible, D. D., and Thibodeaux, L. J.: On the enrichment of
2701 hydrophobic organic-compounds in fog droplets, *Atmospheric Environment Part a-General
2702 Topics*, 27, 203-210, 10.1016/0960-1686(93)90351-x, 1993.

2703 van der Sman, R. G. M.: Predictions of Glass Transition Temperature for Hydrogen Bonding
2704 Biomaterials, *J. Phys. Chem. B*, 117, 16303-16313, 10.1021/jp408184u, 2013.

2705 van Duijnen, P. T. and Swart, M.: Molecular and atomic polarizabilities: Thole's model revisited,
2706 *J. Phys. Chem. A*, 102, 2399-2407, 10.1021/jp980221f, 1998.

2707 Vega, C. P., Pohjola, V. A., Samyn, D., Pettersson, R., Isaksson, E., Bjorkman, M. P., Martma,
2708 T., Marca, A., and Kaiser, J.: First ice core records of NO₃- stable isotopes from
2709 Lomonosovfonna, Svalbard, *J. Geophys. Res.-Atmos.*, 120, 313-330, 10.1002/2013jd020930,
2710 2015.

2711 Vieceli, J., Roeselova, M., and Tobias, D. J.: Accommodation coefficients for water vapor at the
2712 air/water interface, *Chemical Physics Letters*, 393, 249-255, 10.1016/j.cplett.2004.06.038, 2004.

2713 Vieceli, J., Roeselova, M., Potter, N., Dang, L. X., Garrett, B. C., and Tobias, D. J.: Molecular
2714 dynamics simulations of atmospheric oxidants at the air-water interface: Solvation and
2715 accommodation of OH and O₃, *J. Phys. Chem. B*, 109, 15876-15892, 10.1021/jp051361+, 2005.

2716 Vinogradov, S. N. and Linnell, R. H.: *Hydrogen Bonding*, Van Nostrand Reinhold Company,
2717 London, 319 pp.1971.

2718 Virtanen, A., Joutsensaari, J., Koop, T., Kannosto, J., Yli-Pirila, P., Leskinen, J., Makela, J. M.,
2719 Holopainen, J. K., Pöschl, U., Kulmala, M., Worsnop, D. R., and Laaksonen, A.: An amorphous
2720 solid state of biogenic secondary organic aerosol particles, *Nature*, 467, 824-827,
2721 10.1038/nature09455, 2010.

2722 Vlasenko, A., Huthwelker, T., Gaggeler, H. W., and Ammann, M.: Kinetics of the heterogeneous
2723 reaction of nitric acid with mineral dust particles: an aerosol flowtube study, *Phys. Chem. Chem.
2724 Phys.*, 11, 7921-7930, 10.1039/b904290n, 2009.

2725 Voigt, C., Schlager, H., Ziereis, H., Karcher, B., Luo, B. P., Schiller, C., Kramer, M., Popp, P. J.,
2726 Irie, H., and Kondo, Y.: Nitric acid in cirrus clouds, *Geophys. Res. Lett.*, 33, L05803,
2727 10.1029/2005gl025159, 2006.

2728 Voloshina, E., Usvyat, D., Schutz, M., Dedkov, Y., and Paulus, B.: On the physisorption of
2729 water on graphene: a CCSD(T) study, *Phys. Chem. Chem. Phys.*, 13, 12041-12047,
2730 10.1039/c1cp20609e, 2011.

2731 von Domaros, M., Lakey, P. S. J., Shiraiwa, M., and Tobias, D. J.: Multiscale Modeling of
2732 Human Skin Oil-Induced Indoor Air Chemistry: Combining Kinetic Models and Molecular
2733 Dynamics, *J. Phys. Chem. B*, 124, 3836-3843, 10.1021/acs.jpcc.0c02818, 2020.

2734 von Hessberg, P., Pouvesle, N., Winkler, A. K., Schuster, G., and Crowley, J. N.: Interaction of
2735 formic and acetic acid with ice surfaces between 187 and 227 K. Investigation of single species-
2736 and competitive adsorption, *Phys. Chem. Chem. Phys.*, 10, 2345-2355, 10.1039/b800831k, 2008.
2737 Wang, B. and Knopf, D. A.: Heterogeneous ice nucleation on particles composed of humic-like
2738 substances impacted by O₃, *J. Geophys. Res.*, 116, D03205, 10.1029/2010jd014964, 2011.
2739 Wang, B., Lambe, A. T., Massoli, P., Onasch, T. B., Davidovits, P., Worsnop, D. R., and Knopf,
2740 D. A.: The deposition ice nucleation and immersion freezing potential of amorphous secondary
2741 organic aerosol: Pathways for ice and mixed-phase cloud formation, *J. Geophys. Res.*, 117,
2742 D16209, 10.1029/2012jd018063, 2012.
2743 Wang, C., Collins, D. B., Arata, C., Goldstein, A. H., Mattila, J. M., Farmer, D. K., Ampollini,
2744 L., DeCarlo, P. F., Novoselac, A., Vance, M. E., Nazaroff, W. W., and Abbatt, J. P. D.: Surface
2745 reservoirs dominate dynamic gas-surface partitioning of many indoor air constituents, *Sci. Adv.*,
2746 6, 11, 10.1126/sciadv.aay8973, 2020.
2747 Wang, X. F., Qiao, L., Deng, C. B., Chu, G., Li, X. F., Zhao, Q., and Wang, G. L.: Study on the
2748 characteristics of nitrogen dioxide adsorption and storage of coal residue in coal-fired power
2749 plants in goaf, *Sci Rep*, 11, 11, 10.1038/s41598-021-87855-y, 2021.
2750 Weaver, J. F., Carlsson, A. F., and Madix, R. J.: The adsorption and reaction of low molecular
2751 weight alkanes on metallic single crystal surfaces, *Surf. Sci. Rep.*, 50, 107-199, 10.1016/s0167-
2752 5729(03)00031-1, 2003.
2753 Wei, W. M., Zheng, R. H., Jing, Y. Y., Liu, Y. T., Hu, J. C., Ye, Y., and Shi, Q.: Theoretical
2754 Study on Raman Spectra of Aqueous Peroxynitric Acid, *Chin. J. Chem. Phys.*, 24, 625-630,
2755 10.1088/1674-0068/24/05/625-630, 2011.
2756 Weschler, C. J. and Nazaroff, W. W.: Growth of organic films on indoor surfaces, *Indoor Air*,
2757 27, 1101-1112, 10.1111/ina.12396, 2017.
2758 Whitten, J. L.: Theoretical-studies of surface-reactions - Embedded-cluster theory, *Chemical*
2759 *Physics*, 177, 387-397, 10.1016/0301-0104(93)80020-a, 1993.
2760 Wiberg, K. B. and Rablen, P. R.: Comparison of atomic charges derived via different procedures,
2761 *J. Comput. Chem.*, 14, 1504-1518, 10.1002/jcc.540141213, 1993.
2762 Wiegel, A. A., Liu, M. J., Hinsberg, W. D., Wilson, K. R., and Houle, F. A.: Diffusive
2763 confinement of free radical intermediates in the OH radical oxidation of semisolid aerosols,
2764 *Phys. Chem. Chem. Phys.*, 19, 6814-6830, 10.1039/c7cp00696a, 2017.
2765 Willis, M. D. and Wilson, K. R.: Coupled Interfacial and Bulk Kinetics Govern the Timescales
2766 of Multiphase Ozonolysis Reactions, *J. Phys. Chem. A*, 126, 4991-5010,
2767 10.1021/acs.jpca.2c03059, 2022.
2768 Wilson, J., Poschl, U., Shiraiwa, M., and Berkemeier, T.: Non-equilibrium interplay between
2769 gas-particle partitioning and multiphase chemical reactions of semi-volatile compounds:
2770 mechanistic insights and practical implications for atmospheric modeling of polycyclic aromatic
2771 hydrocarbons, *Atmos. Chem. Phys.*, 21, 6175-6198, 10.5194/acp-21-6175-2021, 2021.
2772 Wilson, K. R., Prophet, A. M., and Willis, M. D.: A Kinetic Model for Predicting Trace Gas
2773 Uptake and Reaction, *J. Phys. Chem. A*, 126, 7291-7308, 10.1021/acs.jpca.2c03559, 2022.
2774 Wincel, H., Mereand, E., and Castleman, A. W.: Gas-Phase Reactions of N₂O₅ with NO₂-
2775 (H₂O)(N=0-2), NO₃-(H₂O)(N=1,2), and NON=2,3-HNO₂, *J. Chem. Phys.*, 102, 9228-9234,
2776 10.1063/1.468872, 1995.
2777 Winkler, A. K., Holmes, N. S., and Crowley, J. N.: Interaction of methanol, acetone and
2778 formaldehyde with ice surfaces between 198 and 223 K, *Phys. Chem. Chem. Phys.*, 4, 5270-
2779 5275, 10.1039/b206258e, 2002.

2780 Wittwer, H., Pino, P., and Suter, U. W.: Dipole-moments and conformational-analysis of
2781 copolymers of ethylene and carbon-monoxide, *Macromolecules*, 21, 1262-1269,
2782 10.1021/ma00183a015, 1988.

2783 Woodill, L. A., O'Neill, E. M., and Hinrichs, R. Z.: Impacts of Surface Adsorbed Catechol on
2784 Tropospheric Aerosol Surrogates: Heterogeneous Ozonolysis and Its Effects on Water Uptake, *J.*
2785 *Phys. Chem. A*, 117, 5620-5631, 10.1021/jp400748r, 2013.

2786 Worsnop, D. R., Morris, J. W., Shi, Q., Davidovits, P., and Kolb, C. E.: A chemical kinetic
2787 model for reactive transformations of aerosol particles, *Geophys. Res. Lett.*, 29, 2002.

2788 Worsnop, D. R., Zahniser, M. S., Kolb, C. E., Gardner, J. A., Watson, L. R., Vandoren, J. M.,
2789 Jayne, J. T., and Davidovits, P.: Temperature-Dependence of Mass Accommodation of SO₂ and
2790 H₂O₂ On Aqueous Surfaces, *J. Phys. Chem.*, 93, 1159-1172, 1989.

2791 Yamasaki, H., Kuwata, K., and Miyamoto, H.: Effects of ambient-temperature on aspects of
2792 airborne polycyclic aromatic-hydrocarbons, *Environ. Sci. Technol.*, 16, 189-194,
2793 10.1021/es00098a003, 1982.

2794 Yang, H. and Whitten, J. L.: Energetics of hydroxyl and influence of coadsorbed oxygen on
2795 metal surfaces, *J. Phys. Chem. B*, 101, 4090-4096, 10.1021/jp9702311, 1997.

2796 Yankova, R., Dimov, M., Dobрева, K., and Stoyanova, A.: Electronic structure, reactivity, and
2797 Hirshfeld surface analysis of carvone, *J. Chem. Res*, 43, 319-329, 10.1177/1747519819863957,
2798 2019.

2799 Yaws, C. L.: *Thermophysical Properties of Chemicals and Hydrocarbons 2nd*, Elsevier, Oxford,
2800 1000 pp.2014.

2801 You, Y. and Bertram, A. K.: Effects of molecular weight and temperature on liquid-liquid phase
2802 separation in particles containing organic species and inorganic salts, *Atmos. Chem. Phys.*, 15,
2803 1351-1365, 10.5194/acp-15-1351-2015, 2015.

2804 You, Y., Smith, M. L., Song, M. J., Martin, S. T., and Bertram, A. K.: Liquid-liquid phase
2805 separation in atmospherically relevant particles consisting of organic species and inorganic salts,
2806 *Int. Rev. Phys. Chem.*, 33, 43-77, 10.1080/0144235x.2014.890786, 2014.

2807 You, Y., Renbaum-Wolff, L., Carreras-Sospedra, M., Hanna, S. J., Hiranuma, N., Kamal, S.,
2808 Smith, M. L., Zhang, X. L., Weber, R. J., Shilling, J. E., Dabdub, D., Martin, S. T., and Bertram,
2809 A. K.: Images reveal that atmospheric particles can undergo liquid-liquid phase separations, *P.*
2810 *Natl. Acad. Sci. USA*, 109, 13188-13193, 10.1073/pnas.1206414109, 2012.

2811 Zen, A., Trout, B. L., and Guidoni, L.: Properties of reactive oxygen species by quantum Monte
2812 Carlo, *J. Chem. Phys.*, 141, 14, 10.1063/1.4885144, 2014.

2813 Zhang, Y. and Fakhraai, Z.: Decoupling of surface diffusion and relaxation dynamics of
2814 molecular glasses, *Proc. Natl. Acad. Sci. U. S. A.*, 114, 4915-4919, 10.1073/pnas.1701400114,
2815 2017.

2816 Zhao, X. Y., Nathanson, G. M., and Andersson, G. G.: Experimental Depth Profiles of
2817 Surfactants, Ions, and Solvent at the Angstrom Scale: Studies of Cationic and Anionic
2818 Surfactants and Their Salting Out, *J. Phys. Chem. B*, 124, 2218-2229, 10.1021/acs.jpcc.9b11686,
2819 2020.

2820 Zheng, G. J., Su, H., Wang, S. W., Andreae, M. O., Poschl, U., and Cheng, Y. F.: Multiphase
2821 buffer theory explains contrasts in atmospheric aerosol acidity, *Science*, 369, 1374-+,
2822 10.1126/science.aba3719, 2020.

2823 Zhou, S., Shiraiwa, M., McWhinney, R. D., Pöschl, U., and Abbatt, J. P. D.: Kinetic limitations
2824 in gas-particle reactions arising from slow diffusion in secondary organic aerosol, *Faraday*
2825 *Discuss.*, 165, 391-406, 10.1039/c3fd00030c, 2013.

2826 Zimmermann, S., Kippenberger, M., Schuster, G., and Crowley, J. N.: Adsorption isotherms for
2827 hydrogen chloride (HCl) on ice surfaces between 190 and 220 K, *Phys. Chem. Chem. Phys.*, 18,
2828 13799-13810, 10.1039/c6cp01962e, 2016.

2829 Zobrist, B., Marcolli, C., Pedernera, D. A., and Koop, T.: Do atmospheric aerosols form
2830 glasses?, *Atmos. Chem. Phys.*, 8, 5221-5244, 2008.

2831 Zobrist, B., Soonsin, V., Luo, B. P., Krieger, B. P., Marcolli, C., Peter, T., and Koop, T.: Ultra-
2832 slow water diffusion in aqueous sucrose glasses, *Phys. Chem. Chem. Phys.*, 13, 3514–3526,
2833 2011.

2834